EFFECTS OF RADIATION QUALITY
ON THE RADIOLYSIS OF WATER

by

LAURENCE FREDERICK MILLER

B. S., Kansas State University, 1964

A MASTER'S THESIS

submitted in partial fulfillment of the

requirements for the degree

MASTER OF SCIENCE

Department of Nuclear Engineering

KANSAS STATE UNIVERSITY
Manhattan, Kansas

1966

Approved by:

Richard E. Faw

Major Professor

TABLE OF CONTENTS

1.0 INTRODUCTION.. 1

2.0 DEVELOPMENT OF THE THEORY... 4

2.1 Development of the Diffusion Kinetics Model for Application to Spur Coalescence................................ 4

2.2 Development of the Electron Energy Spectrum Resulting from Electron Slowing Down....................... 19

2.3 Electron Slowing-Down Spectrum Resulting from Co^{60} Gamma Irradiation of Water...................... 30

2.4 Electron Spectra Resulting from Fast Neutron Irradiation of Water.. 33

2.5 Determination of the Stopping Power of Water for Low Energy Electrons.................................. 37

2.6 Spur Size Distribution.. 40

2.7 Spur Separation Distance...................................... 42

2.8 Energy Balance.. 44

2.9 Comparison of Experimental and Theoretical $G(Fe^{+3})$ Values, Using a One-Radical Model for an Oxygen Free Solution...... 46

2.10 Error Analysis Methods....................................... 48

3.0 RESULTS, DISCUSSIONS AND CONCLUSIONS................................ 52

3.1 Results, Discussion and Conclusions of the Chemical Yield Calculations................................. 52

3.2 Results, Discussion and Conclusions of Calculations for the Electron Energy Spectra Resulting from Monoenergetic Electron Sources................................ 72

3.3 Results, Discussion and Conclusions of the Electron Spectrum Resulting from Co^{60} Irradiation.................. 78

3.4 Results, Discussion and Conclusions of the Determination of the Electron Energy Spectra Resulting from Fast Neutron Irradiation.. 85

3.5 Results, Discussion and Conclusions of the Determination of a Low Energy Cross Section and Low Energy Stopping Power for Water... 95

3.6 Results, Discussion and Conclusions Concerning the Determination of the Weighted Average Spur Size............103

3.7 Results, Discussion and Conclusions Concerning the Determination of the Average Spur Separation Distance......116

3.8 Results, Discussion and Conclusions Concerning the Energy Balance..124

3.9 Results, Discussion and Conclusions of Prediction of G-Values....................................129

3.10 Suggestions for Further Work...............................138

4.0 ACKNOWLEDGMENT..140

5.0 REFERENCES...141

6.0 EXPLANATION OF THE COMPUTER PROGRAMS USED IN THIS WORK..........143

6.1 Integration of the Chemical Yield Expression..............143

6.1.2 Method Using Gaussian Quadrature...................151

6.1.3 Method Using a Combination of Laguerre and Gaussian Quadrature Integration....................157

6.2 Explanation of the Computer Program Which Calculates the Electron Spectrum Resulting from a Monoenergetic Electron Source....164

6.3 Program to Calculate the Electron Spectrum Resulting from Co^{60} Irradiation of Water....171

6.4 Explanation of the Computer Programs Which Calculate the Electron Spectra Resulting from Fast Neutron Irradiation....177

6.5 Explanation of Programs Used to Synthesize an Electron-Electron Cross Section and a Program to Calculate the Stopping Power of Water Using the Synthesized Cross Section....190

6.5.1 Program for Evaluating the Parameters a, b and AKT in the Energy Region Where the Moller Formula is Valid....190

6.5.2 Explanation of the Program Used to Investigate the Behavior of a and b by Assuming AKT to be Proportional to a Constant Power of E....194

6.5.3 Explanation of the Program Used to Calculate the Stopping Power of Water from the Synthesized Cross Section....197

6.6 Explanation of the Program Used to Calculate the Weighted Average Spur Size....200

6.7 Explanation of the Program Used to Calculate the Weighted Average Spur Separation Distance....209

6.8 Explanation of Subprograms Used in More Than One Code......218

6.8.1 Explanation of SUBROUTINE BATES......................218

6.8.2 Explanation of Subprogram Y(T)......................223

6.8.3 Explanation of Subprogram ZEE(TI,T)................226

6.8.4 Explanation of Subprogram INTER(M,N,X,Y,CHECK)......229

6.8.5 Explanation of Subprogram AINEXD(T,BLIMIT,TAU)......233

6.8.6 Explanation of Subprogram SMALL(TAU)................234

6.8.7 Explanation of Subprogram AINGS(T,DELTA1,TAU).......236

6.8.8 Explanation of FUNCTION PROBT(T,TAU)................237

6.8.9 Explanation of FUNCTION AMOLIN(T,DELTA).............238

6.8.10 Explanation of FUNCTION AINEX(DELTA)'...............239

6.8.11 Explanation of FUNCTION SPRS(E,DELTA2).............240

LIST OF TABLES

I. Chemical Yield Results for Various Values of A, B, n and ℓ... 56

II. Chemical Yield Results for Various Values of A, B, n, ℓ and θ. 62

III. Calculated Results for $z(E_o,E)((m_oc^2)^{-1}cm^{-1})$ for Various Values of E_o and E in m_oc^2 Units.......................... 75

IV. Differential Cross Section, $d_e\sigma(E)/dE$, for the Number of Electrons with Kinetic Energies Between E and E + dE Scattered per Electron for Monoenergetic Photon Sources of 1.17 and 1.33 Mev.. 81

V. Electron Energy Spectra Resulting from Co^{60} Irradiation Calculated by the Method of Spencer and Fano $y_g(E)$ and by the Method of Continuous Slowing-Down Theory $y_g^{SP}(E)$ Listed with the Electron Energy E in m_oc^2 Units.................... 82

VI. Comparison of y(E) Calculated in This Work and y(E) Obtained by Harder With the Spectra Normalized to a Photon Absorbed Dose Rate of 1 rad/sec...................... 84

VII. Initial Electron Sources Resulting from Alpha and Proton Irradiation.. 90

VIII. Energy Spectra of Electrons Resulting from Alpha Irradiation Calculated by the Method of Spencer and Fano $y_a(E)$, and by the Method of Continuous Slowing-Down Theory $y_a^{SP}(E)$, Listed with the Electron Energy E in m_oc^2 Units.. 93

IX. Energy Spectra of Electrons Resulting from Proton Irradiation Calculated by the Method of Spencer and Fano $y_p(E)$, and by the Method of Continuous Slowing-Down Theory $y_p^{SP}(E)$, Listed with the Electron Energy E in m_oc^2 Units.. 94

X. Results for AKT, a and b at Various Electron Energies.........101

XI. Results for the Weighted Average Energy Loss at Various E_{min} and δ_c Considering the Electron Spectrum Resulting from the Gamma Source...113

XII. Results for the Weighted Average Energy Loss at Various E_{min} and δ_c Considering the Electron Spectrum Resulting from the Proton Source..114

XIII. Results for the Weighted Average Energy Loss at Various E_{min} and δ_c Considering the Electron Spectrum Resulting from the Alpha Source...115

XIV. Input Data and Selected Variables..............................166

XV. Explanation of Computer Program Variables.....................172

XVI. Explanation of Computer Program Variables.....................178

XVII. Listing of Q(E) and V(E) Chosen at Equally Spaced Logarithmic Intervals of Energy E in Figs. 37 and 38..........181

XVIII. Explanation of Computer Program Variables.....................201

XIX. Explanation of Computer Program Variables.....................212

XX. Explanation of Subprogram Variables............................223

XXI. Explanation of Subprogram Variables............................226

LIST OF FIGURES

1. Chemical Yield vs. A for Various Values of B and ℓ for n = 1000. 54

2. Chemical Yield vs. A for Various Values of n With B = .001 and ℓ = 1.0 55

3. Plot of $z(E_o,E)$ vs. E for Various Source Energies E_o 73

4. Percent Uncertainty in $z(E_o,E)$ and $y(E)$ vs. E 74

5. Plot of the Total Differential Cross Section for the Production of Electrons of Energy E vs. Electron Energy for Co^{60} Irradiation 79

6. Differential Electron Flux $(cm^{-2}sec^{-1}(m_oc^2)^{-1}$ vs. Electron Energy (m_oc^2) Resulting From Co^{60} Irradiation 80

7. Plot of the Electron Energy in m_oc^2 Units vs. the Electron Source Resulting From a Given Proton Flux 86

8. Plot of the Electron Energy in Units of m_oc^2 vs. the Electron Source Resulting From a Given Alpha Particle Flux 87

9. Plot of the Electron Energy Spectrum $y_p(E)(cm^{-2}sec^{-1}(m_oc^2)^{-1})$... Resulting from Proton Irradiation vs. Electron Energy in m_oc^2 Units 88

10. Plot of the Electron Energy Spectrum $y_a(E)(cm^{-2}sec^{-1}(m_oc^2)^{-1})$ Resulting from Alpha Particle Irradiation vs. Electron Energy in m_oc^2 Units 89

11. Plot of AKT vs. Electron Energy 96

12. Plot of a Parameter a vs. Electron Energy 97

13. Plot of Parameter b vs. Electron Energy 98

14. Plot of $\frac{b}{a}$ vs. Electron Energy 99

15. Stopping Power Calculated From the Synthesized Cross Section Compared to Results Obtained From a Formula Given by Berger and Seltzer....100

16. Plot of $\langle\bar{\tau}\rangle$ (ev) vs. δ_c(ev)....106

17. Plot of $\langle\bar{\tau}\rangle$ (m_oc^2) vs. $\delta_c(m_oc^2)$ for the Electron Spectra Resulting From Co^{60} Irradiation for Various E_{min}....107

18. Plot of $\langle\bar{\tau}\rangle$ vs. $\delta_c(m_oc^2)$ for the Electron Spectra Resulting From the Proton Source for Various E_{min}....108

19. Plot of $\langle\bar{\tau}\rangle$ vs. $\delta_c(m_oc^2)$ for the Electron Spectra Resulting From the Alpha Particle Source for Various E_{min}....109

20. Plot of the Spur Size $\tau(m_oc^2)$ vs. $G(\tau)(cm^{-3}sec^{-1})$ for the Electron Spectrum Resulting from Co^{60} Irradiation for E_{min} = 400 ev....110

21. Plot of the Spur Size $\tau(m_oc^2)$ vs. $G(\tau)(cm^{-3}sec^{-1})$ for the Electron Spectrum Resulting From the Proton Source for E_{min} = 400 ev....111

22. Plot of the Spur Size $\tau(m_oc^2)$ vs. $G(\tau)(cm^{-3}sec^{-1})$ for the Electron Spectrum Resulting From the Alpha Particle Source for E_{min} = 400 ev....112

23. Plot of the Spectrum of Spur Separation Distances in Å vs. Electron Energy E(Mev) as Determined From the Synthesized Cross Section Compared to Data Given by Hochanadel....119

24. Plot of the Spur Separation Distance in Å vs. LET(mev/cm)....120

25. Plot of the Weighted Average Spur Separation Distance vs. E_{min}(ev) for the Electron Spectrum Resulting From Co^{60} Irradiation with $\langle\bar{\tau}\rangle$ = 43.5 ev....121

26. Plot of the Weighted Average Spur Separation Distance vs. E_{min}(ev) for the Electron Spectrum Resulting From the Proton Source....122

27. Plot of the Weighted Average Spur Separation Distance vs. E_{min} (ev) for the Electron Spectrum Resulting From the Alpha Particle Source With $\langle\bar{\tau}\rangle$ = 43.5 ev....123

28. Plot of Several Electron Spectrum Dose Rates vs. E_{min} for the Electron Spectrum Resulting From Co^{60} Irradiation....126

29. Plot of Several Electron Spectrum Dose Rates vs. E_{min} for the Electron Spectrum Resulting From the Proton Source....127

30. Plot of Several Electron Spectrum Dose Rates vs. E_{min} for the Electron Spectrum Resulting From the Alpha Particle Source....128

31. Plot of the Fractional Chemical Yield $Y_{RS}(\ell)$ vs. ℓ for A = .0995, B = .00325 in Which $\ell = \ell'/2r_o$....132

32. Plot of the Fractional Chemical Yield Y_{RS} vs. the Solute Concentration C_S With the Number of Radicals Produced per Centimeter Along Cylindrical Tracks (N_o') as a Parameter....133

33. Plot of the Fractional Chemical Yield Y_{RS} for Cylindrical Tracks vs. the Number of Radicals Produced per Centimeter (N_o') With C_S = .0005....134

34. Plot of the Fractional Chemical Yield Y_{RS} vs. Electron Energy Making Use of Both the Spur and Cylindrical Track Models....135

35. Plot of the Average Chemical Yield vs. Initial LET ($\frac{ev}{\text{Å}}$)....136

36. Plot of Experimental and Theoretical G Values (Normalized to 1.0) vs. Initial LET....137

37. Plot of V(E) vs. E..179

38. Plot of Q(E) vs. E..180

39. Plot of the Straight Line Approximation for the Inelastic Collision Cross Section Data (Intensity vs. Energy Loss)........235

NOMENCLATURE

a	Parameter for calculating the synthesized cross section and also used as a spur separation distance
b	Parameter for calculating the synthesized cross section
AKT	Parameter for calculating the synthesized cross section
A	Combination of several spur theory parameters and used as atomic mass
Å	Denotes angstrom units
B	Combination of several spur theory parameters
c	Velocity of light
$\bar{c}$	Anistropy factor
C	1/2 the Moller formula coefficient
$C_R'(r,t')$	Free radical concentration for diffusion only
$C_R(r,t)$	Free radical concentration with chemical reaction
C_S	Solute concentration
D	Diffusion constant and also denotes a dose rate
e	Electronic charge
E'_p	Maximum proton energy
E'_a	Maximum alpha particle energy
e^-	Denotes an electron
e^-_{aq}	Solvated electron
E_o	Electron source energy
E,E',E''	Dummy variables for energy
E_{max}	Maximum energy to which the integral should be carried
E_{min}	Arbitrary lower energy limit for an integral

E_m	Maximum energy a particle can transfer to an electron
$\bar{E}_o$	Neutron source energy
$f(x)$	General one-dimensional function
$f(E)$	Alpha particle energy distribution
$F(E_o,E)$	Defined by Eq. (101)
$g(E)$	Proton energy distribution
G	Number of a certain type of molecules produced per 100 ev of energy absorbed
$G(\tau)$	Spur size distribution
h	Planck's constant
I_o	Mean ionization potential
$K(\tau,B,n,\ell)$	Defined by Eq. (74)
k_{RR}	Recombination rate constant for the free radicals
k_{RS}	Rate constant for the radical-solute reaction
$k(E,\tau)$	Electron collision cross section
$k_m(E,\tau)$	Moller formula
$k_H(E,\tau)$	Synthesized cross section
$k_{ex}(\tau)$	Experimental data on inelastic collision cross section
$K_c(E',E)$	Probability of a primary electron of energy E' dropping below E
$K_s(E',E)$	Probability of a primary electron of energy E' creating a secondary of energy E
$\bar{K}_c(E',E)$	A function which approximates $K_c(E',E)$ which was introduced for numerical treatment
$\ell'(E,\delta_c)$	Spur separation distance in units of centimeters

$\langle \ell' \rangle$	Weighted average spur separation distance
ℓ	$\ell'/2r_o$
$\bar{\ell}$	$\langle \ell' \rangle /2r_o$
$L(E)$	Total stopping power
$L(E,\delta_c)$	Stopping power restricted to energy losses less than δ_c
$L_a(E)$	Total stopping power for alpha particles
$L_p(E)$	Total stopping power for protons
LET	Linear energy transfer
$L_s(E)$	Total stopping power as obtained from the synthesized cross section
$L_s(E,\delta_c)$	Stopping power restricted to energy losses less than δ_c as obtained from the synthesized cross section
ℓ_{max}	Maximum ℓ corresponding to E_{max}
ℓ_{min}	Minimum ℓ corresponding to E_{min}
m_o	Electron rest mass
m_e	Electron mass
m_a	Alpha particle mass
m_p	Proton mass
m	Proportional to the spur separation distance and used as an index
n	Number of spurs in a chain and used as an index
N_o	Initial number of free radicals in a spur
$N_R(t)$	Free radicals in a spur as a function of time
N_A	Avogadro's number
N_H	Hydrogen atom density

$\bar{N}_0$	Oxygen atom density
NWT	Number of points chosen to perform a numerical integration
N_e	Electron density
p	Number of points required to reduce the energy scale by 1/2 with a geometric progression
$\bar{Q}$	Defined by Eq. (81)
Q(E)	Proton flux divided by energy (defined by Eq. (220))
r_o	Spur radius beginning the chemical stage
$\bar{r}_o$	Classical electron radius
r_c	Track axis in cylindrical coordinates
$S(E_o)$	Electron source
$S_e^g(E_o)$	Electron source resulting from Co^{60} irradiation
$S_e^p(E_o)$	Electron source resulting from proton irradiation
$S_e^a(E_o)$	Electron source resulting from alpha particle irradiation
$S_a(E)$	Alpha particle source
$S_s(E)$	Secondary electron source
$S_p(E)$	Proton source
$U(\ell')$	Spectrum of spur separation distances
V(E)	Alpha particle flux divided by energy (defined by Eq. (221))
w	Weight factor for numerical integration
y(E)	Electron spectrum determined by the method of Spencer and Fano
$y_g(E)$	Electron spectrum resulting from Co^{60} irradiation determined by the method of Spencer and Fano
$y_g^{SP}(E)$	Electron spectrum resulting from Co^{60} irradiation determined by continuous slowing-down theory

$y_p(E)$	Electron spectrum resulting from proton irradiation determined by the method of Spencer and Fano
$y_p^{SP}(E)$	Electron spectrum resulting from proton irradiation determined by continuous slowing-down theory
$y_a(E)$	Electron spectrum resulting from alpha particle irradiation determined by the method of Spencer and Fano
$y_a^{SP}(E)$	Electron spectrum resulting from alpha particle irradiation determined by continuous slowing-down theory
$\overline{Y}_{RS}$	Fractional radical-solute chemical yield averaged over the electron energy spectrum
$Y_{RS}(\infty)$	Fractional radical-solute chemical yield for infinite time
$\overline{Y}(Fe^{+3})$	Fractional Fe^{+3} chemical yield
$z(E_o,E)$	Electron slowing-down spectrum resulting from a monoenergetic source
Z	Atomic number
α	Photon energy in m_oc^2 units
β	Ratio of electron velocity to the velocity of light
β_a	Ratio of alpha particle velocity to the velocity of light
β_p	Ratio of proton velocity to the velocity of light
$\delta(x)$	Dirac delta function
δ_c	Arbitrary maximum spur size
δ_{min}	Minimum spur size
$\overline{\varepsilon}$	Energy required to create a radical pair
$\kappa(E)$	Energy dependent coefficient for the synthesized cross section
λ	Electron wave length
υ	Electron wave frequency
ϕ_0	Neutron flux

$\phi_p(E)$	Proton flux
$\phi_a(E)$	Alpha particle flux
$\sigma_p(E',E)$	Cross section for a proton of energy E' creating an electron of energy E
$\sigma_a(E',E)$	Cross section for an alpha particle of energy E' creating an electron of energy E
σ_I	Total cross section for the H(n,n)H reaction
σ_{II}	Total cross section for the $O^{16}(n,\ )O^{13}$ reaction
τ	Dummy variable for energy loss
$\langle \bar{\tau} \rangle$	Weighted average spur size in units of energy

1.0 INTRODUCTION

This thesis touches briefly on several phases of Radiation Chemistry; however, most of the attention is given to computation of electron energy spectra arising from several types of radiation. These spectra are necessary for accurate determination of the chemical yield induced by these electrons. The purpose of this work is to accurately predict the chemical yield of a reaction induced by ionizing radiation and thereby predict the molecular yield of a certain chemical species per 100 ev of radiation absorbed (G values). From the electron spectra and the electron cross section, $k(E,\tau)$, the chemical yield for a simple chemical reaction is determined. By treating a set of complex reactions as a simple reaction, G values are predicted for the oxygen-free Fricke dosimeter.

This work considers a very simple but typical reaction mechanism. It is assumed that the medium being irradiated breaks into free radicals to provide the mechanism for the chemical stage, which is justified by Kupperman (16). Specifically, the reaction mechanism is:

$$R_2 \rightarrow 2R \qquad \text{i}$$

$$R + R \rightarrow R_2 \qquad \text{ii}$$

$$R + S \rightarrow RS \qquad \text{iii}$$

in which R is the free radical and S is a reactive solute.

To predict the chemical yield over a wide range of linear energy transfer (LET), both a track model and a spur model are used. For radiation of low LET, energy is transferred to the medium in discrete bundles and the spur theory is valid. If the radiation has a high LET, the R species are generated continuously along a cylindrical track and the cylindrical track model must be used. An extensive example is presented in section 2.1 for a radical diffusion kinetics spur model. No development is given for the cylindrical track model. The necessary information from the track model is taken from a paper by Faw and Miller (10).

Usually, theoretical formulations of a problem involve several unknown parameters, and there are a number of parameters associated with the theoretical prediction of the chemical yield. If the LET of the radiation is such that the spur theory is valid, one must know, determine or assume: (a) D, the diffusion constant of the medium, (b) r_o, the spur radius, (c) $\ell'(E,\delta_c)$, a spectrum of spur separation distances, (d) $\langle\bar{\tau}\rangle$, a weighted average spur size, and (e) δ_c, an effective maximum spur size. Other uncertainties are involved but the above is the extent of those considered in this work. The parameters of D, r_o and δ_c are chosen from a previous work by Faw and Miller (10) while $\langle\bar{\tau}\rangle$ and $\ell'(E,\delta_c)$ are obtained herein. Problems associated with predicting the chemical yield from the cylindrical track model are not considered in this work.

The uncertainty in $\langle\bar{\tau}\rangle$ and $\ell'(E,\delta_c)$ stems from the lack of knowledge of the electron-electron collision cross section, $k(E,\tau)$, for low energy E as well as for small energy losses τ. A reasonably good approximation of the cross section for small energy losses is obtained from a synthesized cross section utilizing inelastic collision cross section data. It is necessary to know the electron-electron collision cross section for low energy electrons to obtain accurate results for the average spur size and for the spectrum of spur separation distances. An extrapolation is performed for E below 2 Kev, which may or may not be accurate. Both $\langle\bar{\tau}\rangle$ and $\ell'(E,\delta_c)$ are fairly strong functions of δ_c.

The theory is given in section 2.0 and is broken into 10 subsections. The results are presented and discussed in section 3.0. Likewise, the computer programs are explained in corresponding subsections of section 6.0. Remaining sections are adequately described in the Table of Contents.

2.0 DEVELOPMENT OF THE THEORY

2.1 Development of the Diffusion Kinetics Model for Application to Spur Coalescence

Chemical yields of reactions induced by ionizing radiation may be estimated within the accuracy of the mathematical model. Results are obtained by the solution of the partial differential equations describing simultaneous chemical reaction and diffusion along the tracks of the particles. For simple reactions, various approximate analytical solutions to the equations have been published as well as have some solutions obtained by direct numerical integration of the equations. An approximate analytic solution for the chemical yield is presented in this work.

The theoretical development of the diffusion kinetics model utilizes the prescribed diffusion hypothesis (which will be explained later) to obtain an approximate analytic solution to the diffusion kinetics equation. A comparison between results obtained by prescribed diffusion and numerical integration is given by Kupperman (16).

The radiation-chemical process is conveniently separated into three distinct stages. The first stage is the physical interaction of the radiation with the medium and may be described by the following expression:

$$\text{(Medium + Radiation = Highly Excited Ions and Molecules + Energetic Electrons).} \tag{1}$$

This physical stage, consisting of the dissipation of radiant energy in the system, has a duration on the order of 10^{-15} seconds or less.

The second stage is the physiochemical stage and consists of those processes which lead to the establishment of thermal equilibrium in the system.

According to Kupperman (16), its duration is on the order of 10^{-11} seconds for aqueous solutions. During this stage, highly excited ions and molecules lost most of their excitation energy, and it is assumed that the radiation-produced electrons and ions interact with the surrounding medium. Using water for an example, the following expression for the loss of excitation energy could be written:

$$\left.\begin{array}{l} H_2O^* \rightarrow H_2O \text{ (internal conversion)} \\ H_2O^* \rightarrow H + OH \\ (H_2O^+)^* \rightarrow H_2O^+ \text{ (internal conversion)} \end{array}\right\rangle \quad (2)$$

$$H_2O^+ + H_2O \rightarrow H_3O^+ + OH \quad (3)$$

$$e^- \rightarrow e^-_{aq} \quad (4)$$

$$H_3O^+ + e^-_{aq} \rightarrow H + H_2O \text{ (acid solution)} \quad (5)$$

It is usually assumed that the atom and the free radical[1] H and OH, are produced during the second stage in or near the region in which the energy is released by the radiation. According to Magee (18), "It is possible to think of the excitation produced by a primary particle as a wave packet formed as a superposition of excited states of the constituent molecules. The un-

---

[1]Free Radical according to Longuet-Higgins, H. C., "Reactions of Free Radicals in the Gas Phase", Sugden, ed., The Chemical Society (London), 1957, p. 5.

> We . . . restrict the term to molecular species in which there is at least one unpaired electron associated with an atom . . . of a non-metallic element whose valency shell normally comprises an even number of electrons, all paired.

certainty principle limits the extent to which we can localize such a wave packet. The wave length associated with momentum change (ΔP) of the particle is

$$\lambda(\Delta P) = \frac{h}{\Delta P} = \frac{hv}{\varepsilon} \tag{6}$$

where ε is the energy loss, h is Plank's constant and v is the particle velocity. If $v = 10^{10}$ cm/sec and $\varepsilon = 5$ ev, then $\lambda = 100$ Å and it is evident that such excitation cannot in any reasonable approximation be considered as localized in a molecule." This localized energy loss initiates a spur[1].

The third or chemical stage consists of diffusion and chemical reaction of the reactive species and leads to the establishment of chemical equilibrium. Its duration ranges from 10^{-8} seconds and upwards according to Kupperman (16). During this final stage, diffusion, occurring simultaneously with chemical reaction, causes expansion of the spur to radii exceeding the initial value r_o. For the one radical model the following three reactions denote those considered to be occurring during the third stage:

$$R_2 \rightarrow 2R \tag{7}$$

$$R + R \rightarrow R_2 \tag{8}$$

$$R + S \rightarrow RS, \tag{9}$$

in which (R) denotes a free radical and (S) denotes a reactive solute molecule.

If the order of these reactions is known, the diffusion kinetics equation, which describes the chemical action during the third stage, can easily

---

[1]<u>Spur</u> This localized region maintains its identity as a Spur but increases in size as a result of diffusion.

be written by performing a simple material balance. For the one radical model Eqs. (8) and (9) describe the chemical action. Since Eq. (8) describes a second order reaction and Eq. (9) a first order reaction, the production terms are $k_{RR}C_R{}^2(\vec{r},t)$ and $k_{RS}C_SC_R(\vec{r},t)$, respectively. Diffusion loss terms are, in general, $-D\nabla^2C_R(\vec{r},t)$. The rate balance for component R is:

$$D\nabla^2C_R(\vec{r},t) - k_{RR}C_R{}^2(\vec{r},t) - k_{RS}C_SC_R(\vec{r},t) = \frac{\partial C_R(\vec{r},t)}{\partial t} \tag{10}$$

in which D = diffusion constant

$\vec{r}$ = generalized space vector

$C_R(\vec{r},t)$ = free radical concentration

k_{RR} = rate constant for radical recombination

k_{RS} = rate constant for radical-solute reaction

∇^2 = Laplacian Operator.

For angularly independent cylindrical coordinates, the Laplacian operator is $\nabla_c{}^2 = \frac{\partial^2}{\partial r^2} + \frac{1}{r}\frac{\partial}{\partial r} + \frac{\partial^2}{\partial z^2}$. For angularly independent spherical coordinates, it is $\nabla_s{}^2 = \frac{\partial^2}{\partial r^2} + \frac{2}{r}\frac{\partial}{\partial r}$. This type of non-linear partial differential equation is of second order in space, first order in time, and probably has no exact analytical solution. The approximate analytical solution will be for equally-spaced, equally-sized spherical spurs which obey the following three major assumptions given by Kupperman (16): (a) the initial distribution of radicals in a spur is Gaussian; (b) the Gaussian form is preserved as the spur expands in spite of the reactions that go on; and (c) the variation of the radius of the Gaussian distribution with time is the same as it would be if only diffusion were occurring. The basic underlying motivation of the three assumptions seems to have been the mathematical tractability of the problem. Assumptions (b) and (c) have been called the "prescribed diffusion hypothesis" and this terminology will be used.

The first step of the mathematical development will be to present the basis for the prescribed diffusion hypothesis by solving the time dependent diffusion equation for one spur. The equation to be solved is:

$$D\nabla_s^2 C'_R(r,t') = \frac{\partial}{\partial t'} C'_R(r,t') \qquad (11)$$

with the following initial and boundary conditions for spherical coordinates:

1) $C'_R(r,0) = N_o \dfrac{\delta(r)}{4\pi r^2}$

2) $C'_R(\infty,t') = 0$

3) $\left.\dfrac{\partial C'_R(r,t)}{\partial r}\right|_{r=0} = 0.$

For Eq. (11), the following variables are defined:

N_o = initial number of free radicals

t' = time scale considering a point source

$\delta(r)$ = Dirac delta function

$C'_R(r,t')$ = radical concentration for diffusion from a point source.

This equation is solved by first solving the infinite one-dimensional case for plane geometry and then differentiating to obtain the point source expression. For the one-dimensional case, let $\nabla^2_{pl} = \dfrac{\partial^2}{\partial x^2}$. Then Eq. (11) becomes:

$$D\nabla^2_{pl} C'_R(x,t') = \frac{\partial}{\partial t'} C'_R(x,t'). \qquad (12)$$

The solution is obtained by taking the Fourier transform of the space variable, the Laplace transform of the time variable, the inverse Laplace transform of the time variable, and finally the inverse Fourier transform of the space variable. The definitions of the transforms are:

Fourier

$$\mathscr{F}(\omega,t') = \frac{1}{\sqrt{2\pi}} \int_{-\infty}^{\infty} f(x,t')e^{i\omega x}dx \tag{13}$$

in which ω is the transform variable.

Inverse Fourier

$$f(x,t') = \mathscr{F}^{-1}(\omega,t') = \frac{1}{\sqrt{2\pi}} \int_{-\infty}^{\infty} \mathscr{F}(\omega,t')e^{-i\omega x}d\omega. \tag{14}$$

Laplace

$$F(x,s) = \int_{0}^{\infty} e^{-st'} f(x,t')dt' \tag{15}$$

in which s is the transform variable.

Inverse Laplace

$$f(x,t') = F^{-1}(x,s) = \frac{1}{2\pi i} \int_{c - i\infty}^{c + i\infty} F(x,s)e^{st'}ds. \tag{16}$$

Taking the Fourier transform of Eq. (12) gives:

$$\frac{1}{\sqrt{2\pi}} \int_{-\infty}^{\infty} D\nabla^2_{pl} C'_R(x,t')e^{i\omega x}dx = \frac{1}{\sqrt{2\pi}} \int_{-\infty}^{\infty} \frac{\partial}{\partial t'} C'_R(x,t')e^{i\omega x}dx \tag{17}$$

$$D(i\omega)^2 C'_R(\omega,t') = \frac{\partial}{\partial t'} C'_R(\omega,t') \tag{18}$$

$$-D\omega^2 C'_R(\omega,t) = \frac{\partial}{\partial t'} C'_R(\omega,t'). \tag{19}$$

Taking the Laplace transform gives:

$$-D\omega^2 C'_R(\omega,s) = sC'_R(\omega,s) - C'_R(\omega,0) \tag{20}$$

in which

$$C'_R(\omega,0) = \frac{1}{\sqrt{2\pi}} \int_{-\infty}^{\infty} \delta(x) N_o e^{i\omega x} dx \tag{21}$$

$$C'_R(\omega,0) = \frac{N_o}{\sqrt{2\pi}} . \tag{22}$$

Substitution of Eq. (22) into Eq. (20) gives:

$$C'_R(\omega,s) = \frac{N_o}{\sqrt{2\pi}} \frac{1}{s + D\omega^2} . \tag{23}$$

Taking the inverse Laplace of Eq. (23) gives:

$$C'_R(\omega,t') = \frac{N_o}{\sqrt{2\pi}} e^{-D\omega^2 t'} . \tag{24}$$

Finally, one needs to find the inverse Fourier transform of Eq. (24) which reads:

$$C'_R(x,t') = \frac{1}{\sqrt{2\pi}} \int_{-\infty}^{\infty} \frac{N_o}{\sqrt{2\pi}} e^{-D\omega^2 t'} e^{-i\omega x} d\omega \tag{25}$$

$$C'_R(x,t') = \frac{1}{\sqrt{2\pi}} \int_{-\infty}^{\infty} \frac{N_o}{\sqrt{2\pi}} e^{-D\omega^2 t'} \left[\cos(\omega x) + i \sin(\omega x)\right] d\omega . \tag{26}$$

Since $e^{-D\omega^2 t'}$ is an even function in ω, it is necessary only to find the cosine transform:

$$C'_R(x,t') = \frac{2N_o}{2\pi} \int_{0}^{\infty} e^{-D\omega^2 t'} \cos(\omega x) dx \tag{27}$$

$$C'_R(x,t') = \frac{N_o}{2\sqrt{\pi}} \frac{1}{\sqrt{Dt'}} e^{-x^2/4Dt'} . \tag{28}$$

Since

$$\frac{\partial}{\partial x} C'_R(x,t')\bigg|_{x=r} = -2\pi C'_R(r,t), \tag{29}$$

Eq. (28) is differentiated and Eq. (29) is utilized, thus obtaining:

$$C'_R(r,t') = \frac{N_o e^{-r^2/(4Dt')}}{(4\pi Dt')^{3/2}} \tag{30}$$

in which r is the distance from the center of the spherical spur.

Shifting the time scale[1] to $t' = t + T$ and defining $T = \frac{r_o^2}{2D}$, results in:

$$C'_R(r,t) = \frac{N_o e^{-r^2/(4Dt + 2r_o^2)}}{\{\pi(4Dt + 2\,r_o^2)\}^{3/2}} . \tag{31}$$

By utilizing the prescribed diffusion hypothesis, the following equations result:

$$C_R(r,t) = \frac{N_R(t) e^{-r^2/(4Dt + 2r_o^2)}}{\{\pi(4Dt + 2r_o^2)\}^{3/2}} \tag{32}$$

or

$$C_R(r,t) = N_R(t)\phi(r,t). \tag{33}$$

where $C_R(r,t)$ is the free radical concentration corresponding to the shifted time scale and $N_R(t)$ is the number of free radicals per spur.

Substituting Eq. (33) into Eq. (10) gives:

---

[1]The fictitious time T is the time that the radicals would require to diffuse to a radius r_o if they came from a point source.

$$DN_R(t)\nabla^2_s\{\phi(r,t)\} - k_{RR}N_R^{\;2}(t)\phi^2(r,t)$$

$$- k_{RS}N_R(t)\phi(r,t)C_S = \frac{\partial}{\partial t} N_R(t)\phi(r,t). \tag{34}$$

The diffusion kinetics equation may be simplified by the following redefinition of functions:

$$C_R(r,t) = \psi_R(r,t)e^{-k_{RS}C_S t} \tag{35}$$

$$\psi_R(r,t) = N_R(t)\phi(r,t)e^{k_{RS}C_S t}. \tag{36}$$

Substitution of Eq. (35) into Eq. (10) gives:

$$D\nabla_s^{\;2}\psi_R(r,t) - k_{RR}\psi_R^{\;2}(r,t)e^{-k_{RS}C_S t} = \frac{\partial\psi_R(r,t)}{\partial t}. \tag{37}$$

With the definition

$$M_R(t) = N_R(t)e^{k_{RS}C_S t}, \tag{38}$$

substitution of Eq. (38) into Eq. (36) and Eq. (36) into Eq. (37) gives:

$$DM_R(t)\nabla_s^{\;2}\phi(r,t) - k_{RR}M_R^{\;2}e^{-k_{RS}C_S t}\phi^2(r,t) = \frac{\partial}{\partial t}\{M_R(t)\phi(r,t)\}. \tag{39}$$

For the case of one spur and solute competition, one needs to solve Eq. (39).

For the case of n spurs with centers aligned and solute competition, Eq. (39) may be rewritten as:

$$DM_R(t)\nabla_c^{\;2}\phi(r_c,z,t) - k_{RR}M_R^{\;2}(t)e^{-k_{RS}C_S t}\phi^2(r_c,z,t)$$

$$= \frac{\partial}{\partial t}\{M_R(t)\phi(r_c,z,t)\}. \tag{40}$$

To solve the problem for n spurs equally spaced, the expression for $\phi(r_c,z,t)$ from the spherical case may be utilized.

From Eq. (32) it is evident that

$$\phi(r,t) = \frac{e^{-r^2/(4Dt + 2\, r_o^{\,2})}}{\{\pi(4Dt + 2\, r_o^{\,2})\}^{3/2}} \tag{41}$$

in spherical geometry, where r is the radius of the spur. For cylindrical geometry, the following diagram indicates that for the i^{th} spur, r must be replaced by

$$r^2 = r_c^{\,2} + (z - z_i)^2. \tag{42}$$

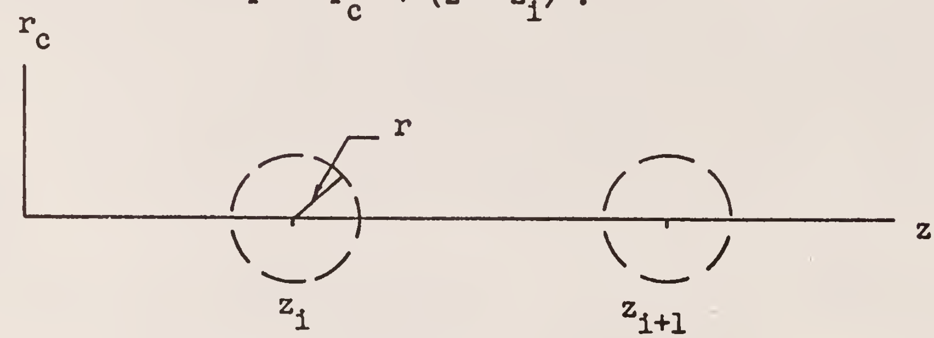

To help explain the formalism, consider a system of orthogonal cartesian axes whose origin is the center of the first spur and whose z axis is the track axis. Let r_c be the distance from the track axis and z the distance along the track axis. Due to the cylindrical symmetry of the problem, C_R has no angular dependence and is shown by:

$$C_R(r_c,z,t) = N_R(t)\phi(r_c,z,t) = \frac{N_R(t) \sum_{i=1}^{n} \exp\left[-\left[\frac{r_c^{\,2} + (z - z_i)^2}{2r_o^{\,2} + 4Dt}\right]\right]}{n\pi^{3/2}\{2r_o^{\,2} + 4Dt\}^{3/2}}. \tag{43}$$

As before, $N_R(t)$ is the total number of radicals produced and n the number of spurs.

To solve Eq. (40) for $M_R(t)$ it is necessary first to integrate over the space variables (r_c) and (z). Writing the equation in integral form gives:

$$DM_R(t)\int_V \nabla_c^{\,2}\phi(r_c,z,t)dV - k_{RR}M_R^{\,2}(t)e^{-k_{RS}C_St}\int_V \phi^2(r_c,z,t)dV$$

$$= M^R(t)\int_V \frac{\partial\phi(r_c,z,t)}{\partial t}dV + \frac{\partial M_R(t)}{\partial t}\int_V \phi(r_c,z,t)dV. \qquad (44)$$

For simplicity, each term of Eq. (44) is considered separately.

$$\underline{\text{Term 1}} = \int_V \phi^2(r_c,z,t)dV = \int_{-\infty}^{\infty} dz \int_0^{\infty} 2\pi r_c dr_c \phi^2(r_c,z,t)$$

in which

$$\phi^2(r_c,z,t) = \frac{e^{-2r_c^{\,2}/q^2}}{n^2q^{3/2}\pi^{3/2}}\sum_{i=1}^{n}\sum_{j=1}^{n} e^{-\{(z-z_i)^2+(z-z_j)^2\}/q^2} \qquad (45)$$

and

$$q^2 = (4Dt + 2r_o^{\,2})^2. \qquad (46)$$

Integration for term 1 yields:

$$\int_V \phi^2(r_c,z,t)dV = \frac{\sum_{i=1}^{n}\sum_{j=1}^{n} e^{(z_i-z_j)^2/2(4Dt+2r_o^{\,2})}}{n^2\{2\pi(4Dt+2r_o^{\,2})\}^{3/2}}. \qquad (47)$$

$$\underline{\text{Term 2}} = \int_V \nabla_c^{\,2}\phi(r_c,z,t)dV.$$

Let $R = r_c/\sqrt{q}$ and $Z_i = (z - z_i)/\sqrt{q}$; $\sqrt{q}dZ_i = dz$ and $\sqrt{q}dR = dr_c$.

$$\int_V \nabla_c^2 \phi(r_c,z,t)dV = \frac{1}{n\pi^{3/2}} \sum_{i=1}^{n} \int_{\infty}^{\infty} dZ_i \int_0^{\infty} 2\pi R dR \nabla_c^2 \{e^{-R^2} e^{-Z_i^2}\}, \tag{48}$$

in which

$$\phi_i(R,Z_i,t) = \frac{e^{-R^2} e^{-Z_i^2}}{n\pi^{3/2} q^{3/2}} = E e^{-R^2} e^{-Z_i^2} \tag{49}$$

and

$$E = \frac{1}{n(\pi q)^{3/2}} . \tag{50}$$

Note the following:

$$\frac{\partial \phi_i}{\partial R} = -\ 2R\phi_i \tag{51}$$

$$\frac{\partial^2 \phi_i}{\partial R^2} = -2R \frac{\partial \phi_i}{\partial R} - 2\phi_i = 4R^2\phi_i - 2\phi_i \tag{52}$$

$$\frac{1}{R}\frac{\partial \phi_i}{\partial R} = -\ 2\phi_i \tag{53}$$

$$\frac{\partial \phi_i}{\partial Z_i} = -\ 2Z_i\phi_i \tag{54}$$

$$\frac{\partial^2 \phi_i}{\partial Z_i^2} = 2\phi_i(2Z_i^2 - 1). \tag{55}$$

Since

$$\nabla_c^2 = \left[\frac{\partial^2}{\partial R^2} + \frac{1}{R}\frac{\partial}{\partial R} + \frac{\partial^2}{\partial Z_i^2}\right] \frac{1}{q} \tag{56}$$

$$\nabla_c^{\,2}\phi_i(R,Z_i,t) = 2\phi_i(R,Z_i,t)(2R^2 + 2\,Z_i^{\,2} - 3)\,\frac{1}{q} \tag{57}$$

$$\int_V \nabla_c^{\,2}\phi_i(R,Z_i,t) = \frac{4\pi E^{-1}}{n\pi^{3/2}}\,\left\{\frac{\sqrt{\pi}}{4} - \frac{\sqrt{\pi}}{4}\right\}\,\frac{1}{q} = 0, \tag{58a}$$

or

$$\int_V \nabla_c^{\,2}\phi(r_c,Z,t)dV = 0. \tag{58b}$$

$$\underline{\text{Term 3}} = \int_V \frac{\partial\phi_i}{\partial t}\,dV$$

$$\frac{\partial\phi_i}{\partial t} = \frac{4D\phi_i(R,Z_i,t)}{(4Dt + 2r_o^{\,2})}\,\{2(R^2 + Z_i^{\,2}) - 3\}. \tag{59}$$

Note that the spatial dependence of Eq. (59) is the same as Eq. (57). Therefore, it is evident that:

$$\int_V \frac{\partial\phi_i}{\partial t}\,dV = 0. \tag{60}$$

$$\underline{\text{Term 4}} = \int_V \phi(r_c,z,t)dV$$

$$\int_V \phi(r_c,z,t)dV = \frac{\pi\sum\limits_{i=1}^{n}}{n\pi^{3/2}\{2r_o^{\,2} + 4Dt\}^{3/2}}\left[\int_{-\infty}^{\infty} dz e^{-(z - z_i)^2/(4Dt + 2r_o^{\,2})}\right.$$

$$\left.\times \int_0^{\infty} 2r_c dr_c e^{-r_c^{\,2}/(4Dt + 2r_o^{\,2})}\right]. \tag{61}$$

Eq. (61) results in:

$$\int_V \phi(r_c,z,t)dV = \frac{1}{n}. \tag{62}$$

Substituting Eqs. (62), (60) and (58) into Eq. (44) gives:

$$k_{RR}M_R^{\,2}(t)e^{-k_{RS}C_S t}\int_V \phi^2(r_c,z,t)dV = -\frac{1}{n}\frac{dM_R(t)}{dt} \tag{63}$$

$$\int_{M_R(0)}^{M_R(t)} \frac{dM_R(t)}{M_R^{\,2}} = -nk_{RR}\int_0^t dt'\{e^{-k_{RS}C_S t'}\int_V \phi^2 dV\} \tag{64}$$

$$M_R(t) = \frac{M_R(0)}{1 + k_{RR}n\displaystyle\int_0^t dt'\{e^{-k_{RS}C_S t'}\int_V \phi^2 dV\}}. \tag{65}$$

Recalling that $M_R(t) = N_R(t)e^{k_{RS}C_S t}$ and substituting this into Eq. (65) gives:

$$N_R(t) = \frac{N_R(0)e^{-k_{RS}C_S t}}{1 + k_{RR}n\displaystyle\int_0^t dt'\{e^{-k_{RS}C_S t'}\int_V \phi^2 dV\}}. \tag{66}$$

Since there is now an expression for the total number of free radicals in a chain of n spurs, it is easy to find an expression for the yield of the RS species. The kinetics equation describing this reaction is:

$$\frac{d}{dt}C_{RS}(r,t) = k_{RS}C_S C_R(r,t). \tag{67}$$

Integrating Eq. (67) over all space gives

$$\frac{d}{dt} N_{RS}(t) = k_{RS}C_S N_R(t). \tag{68}$$

The assumption of C_S as being space and time independent constitutes the "lack of solute depletion" approximation. This approximation is valid for those cases for which C_S greatly exceeds the free radical concentration. This is the usual case in radiation-chemistry experimental work. The solution of Eq. (68) is:

$$N_{RS}(\theta) = k_{RS}C_S \int_0^{\theta} dt\; N_R(t). \tag{69}$$

Substituting Eq. (66) into Eq. (69) gives

$$Y_{RS}(\theta) \quad \frac{N_{RS}(\theta)}{N_R(0)} = \int_0^{\theta} \frac{k_{RS}C_S e^{-k_{RS}C_S\theta'}\, d\theta'}{1 + N_R(0)k_{RR}n \int_0^{\theta'} dt'\{e^{-k_{RS}C_S t'} \int_V \phi^2 dV\}} \tag{70}$$

The expression for $\int_V \phi^2 dV$, Eq. (47) can be reduced to the following single sum for equally-spaced spurs of distance a; where $z_i = ia$, $z_j = ja$

$$\int_V \phi^2 dV = \frac{1}{n^2\{2\pi(4Dt' + 2r_o^2)\}^{3/2}}$$

$$\{n + \sum_{m=1}^{n-1} 2(n - m)e^{-a^2m^2/2(4Dt' + 2r_o^2)}\}. \tag{71}$$

To simplify Eq. (70), the following changes of variables may be made:

$$t' = \frac{1}{k_{RS}C_S} t'' - \frac{r_o^2}{2D}, \ell^2 = \frac{a^2}{4r_o^2} \text{ and } \theta' = \frac{\tau}{k_{RS}C_S}. \tag{72}$$

Defining

$$A = \frac{k_{RR}N_R(0)}{8\pi^{3/2}Dr_o}$$

and

$$B = \frac{r_o^2 k_{RS}C_S}{2D} ,$$

the result is

$$Y_{RS}(\theta) = \int_0^{\theta} \frac{e^{-\tau}d\tau}{1 + Ae^{B}\sqrt{B}K(\tau,B,n,\ell)} \tag{73}$$

in which

$$K(\tau,B,n,\ell) = \int_B^{B+\tau} \frac{dt''e^{-t''}}{(t'')^{3/2}} \{\frac{1}{2} + \sum_{m=1}^{n-1} (\frac{n-m}{e})e^{-\ell^2m^2B/t''}\}. \tag{74}$$

2.2 Development of the Electron Energy Spectrum Resulting from Electron Slowing Down

This development closely follows that of Spencer and Fano (22), but their development is expanded upon and presented in a slightly different order and with different nomenclature.

When traversing a medium, electrons lose their energy through a series of inelastic collisions. The great majority of these discrete energy losses are on the order of 10 ev. However, there are a sufficient number of large energy losses so that the determination of the electron energy spectrum, $z(E_o,E)$, using a continuous slowing down model, gives an unrealistic result. The differential electron energy spectrum resulting from a monoenergetic source at E_o, $z(E_o,E)dE$ is the average track length traveled by the electrons while the electrons have energy between E and E + dE. Spencer and Fano (22) have developed a numerical scheme which includes the effect of statistical fluctuations of the energy loss on the electron energy spectrum.

For the development presented in this section, energy losses by bremsstrahlung have been omitted since this paper concerns source energies near 1 Mev, at a maximum. Bremsstrahlung does not play an important role as a mechanism for electron energy losses in this energy range. Another point that has not been considered is the effect of the density of the medium on the electron stopping power. When a high energy charged particle passes through a condensed medium, a polarization of the medium takes place. As a result long distance interactions are less probable and the stopping power of the medium is lowered. For low-Z materials, the density effect increases so that for water the correction is of the order of 2% at 1 Mev and 10% at 8 Mev, according to McGinnies (20). The most serious limitation of the numerical scheme is the inadequacy of the collision cross section at low energies.

The resulting electron energy spectrum depends primarily on the mean rate of energy loss in all collisions. This mean rate is taken into account within the uncertainty of the value of the mean ionization potential. The probability distribution of the energy losses in individual collisions has a subsidiary and appreciable effect on the energy spectrum. This effect stems particularly from collisions in which an electron loses a substantial amount (>10%) of its energy. The probability of these collisions is taken into account through the relativistic Moller formula which gives the probability of knock-on collisions with unbound electrons. This probability is estimated accurately only for collisions with an energy loss much larger than the binding energy of the electron ejected. As a result, the error incurred has a severe influence on the results of those calculations which pertain to electrons of energies comparable to the binding energies of the electron which is ejected.

The highest binding energy of atomic electrons is of the order of 100 Kev for K-shell electrons of heavy elements. However, these K-shell electrons constitute only a small fraction of the orbital electrons. For this reason, the error incurred by the use of inaccurate probabilities of energy losses is estimated to be small until the energy of the electrons being slowed down falls below half of the binding energy of the L-shell electrons in heavy elements. In light elements, the binding energies are low and the error is expected to be small down to the lower limit of 0.404 Kev, according to McGinnies (20).

It is essential to derive a statistical balance for the electrons being slowed down past an energy E in terms of a differential electron energy spectrum. For simplicity, a monoenergetic source of electrons is assumed, yielding $N_o(E_o)$ electrons per unit time per unit volume at energy E_o. Let $N(E)dE$ be defined as the number of electrons about energy E in dE which traverse a small spherical probe of cross sectional area $\pi\bar{R}^2$ per unit time. Since a normalized function is a more desirable quantity to formulate, let $\phi(E)dE = N(E)dE/\pi\bar{R}^2$, where $\phi(E)$ is the differential electron flux as viewed from a small spherical probe at the point of observation. Note that $\phi(E)dE$ has units of electrons per unit area per unit time. To put the differential spectrum in an even more convenient form, $\phi(E)dE$ is normalized as follows:

$$z(E_o,E)dE = \frac{\phi(E)dE}{N_o(E_o)} . \tag{75}$$

(The above equation has units of cm, and E_o is the monoenergetic source energy.) The physical significance of the differential energy spectrum is mentioned in the opening paragraph of this section.

Let $K(E',\tau)d\tau$ be defined as the probability per unit distance that an electron of energy E' in dE' has a collision which results in an energy loss of $\tau \pm \frac{1}{2} d$. The probability that a primary electron of energy E' drops below E, $(K_c(E',E))$ is the integral over $K(E',\tau)d\tau$ for all energy losses between (E' - E) and $\frac{1}{2}$ E'. Since a primary electron must lose less than $\frac{1}{2}$ of its energy to remain a primary, the upper limit is $\frac{1}{2}$ E'. An electron must experience an energy loss of E' - E for it to fall below E.

The function $K(E',\tau)d\tau$ is given accurately for a wide range of E' and τ, by the relativistic Moller formula, $k_m(E',\tau)$, which reads:

$$k_m(E',\tau) = \frac{2\pi N_e \bar{r}_o^{\,2}}{(\beta')^2} \left[\frac{1}{\tau^2} + \frac{1}{(E' - \tau)^2} - \left[\frac{(2 + \frac{1}{E'})}{(E' + 1)^2} \right] \left[\frac{1}{\tau} + \frac{1}{(E' - \tau)} \right] + \frac{1}{(E' + 1)^2} \right] \tag{76}$$

in which N_e is the number of electrons per cm^3; $\bar{r}_o$ is the classical electron radius; and β' is the ratio of the velocity of the electron to the velocity of light, given by $\beta' = \sqrt{\frac{E'(E' + 2)}{(E' + 1)}}$. The ratio β' can be derived directly from the relativistic expression for the kinetic energy of an electron in units of the rest energy.

$$E' = \left[\frac{1}{\sqrt{1 - (v/c)^2}} - 1 \right] \tag{77}$$

$$\beta' = \frac{v'}{c} = \frac{\sqrt{E'(E' + 2)}}{(E' + 1)}. \tag{78}$$

The expression for $K_c(E',E)$ is

$$K_c(E',E) = \int_{E' - E}^{\frac{1}{2} E'} d\tau k_m(E',\tau), \tag{79}$$

or making the change of variable $\tau = E' - s$, one obtains

$$K_c(E',E) = \int_{\frac{1}{2} E'}^{E} ds k_m(E',E - s) \tag{80}$$

where $E' - E$ must be greater than $\bar{Q}$. $\bar{Q}$ is a term given by Spencer and Fano (22), as follows:

$$\bar{Q} = \frac{1}{2} (ZI_o/m_o{}^2)\{E'(E' + 2)\}^{-1}e^{-(\beta')^2}. \tag{81}$$

Note further that $\bar{Q}$ is defined such that

$$\int_{\bar{Q}}^{\delta} d\tau k_m(E,\tau) = L(E,\delta), \tag{82}$$

in which $L(E,\delta)$ is the restricted stopping power and $\int_0^{\bar{Q}} d\tau k_m(E,\tau)$ is taken to be zero. With these criteria in mind, it becomes evident that

$$K_c(E',E) = K_c(E + \bar{Q},E) \quad \text{for } E' \leq E + \bar{Q}. \tag{83}$$

From the definition of primary electrons, it is known that $K_c(E',E) = 0$ for $E' \leq 2E$.

There is now sufficient information to write the electron balance as follows:

(Primary electrons slowed down past E = Electrons created above E)(84)

or

$$\int_{E}^{E_o} z(E_o,E')K_c(E',E)dE' = S_o(E_o) + \int_{E}^{E_o} S_s(E')dE' \tag{85}$$

in which $S_s(E')$ is the secondary electron source term for secondary electrons created about E' in dE' and $z(E_o,E')K_c(E',E)dE'$ is the mean number of electrons about E' in dE dropping below E per unit time. The Moller expression may also be used to determine the probability of the production of secondary electrons in dE' about E'. Since the secondary electron must carry less than $\frac{1}{2}$ of the incident electron energy away from a collision, the lower limit for incident electron energies must be 2E'. However, the upper limit is limited only to the most energetic electron available. The differential secondary source term is:

$$S_s(E')dE' = dE' \int_{2E'}^{E_o} dE''z(E_o,E'')k_m(E',E'' - E'). \tag{86}$$

Substituting Eq. (86) into Eq. (84) and defining $S_o(E_o)$ as equal to 1 for $2E<E_o$, one obtains

$$\int_{E}^{2E} z(E_o,E')K_c(E',E)dE' = 1 + \int_{E}^{E_o} dE' \int_{2E'}^{E_o} dE''z(E_o,E'')k_m(E',E'' - E'). \tag{87}$$

Changing the order of integration of the double integral results in

$$\int_{E}^{2E} z(E_o,E')K_c(E',E)dE' = 1 + \int_{2E}^{E_o} dE''z(E_o,E'') \int_{E}^{\frac{1}{2}E''} dE'k_m(E'',E'' - E'). \tag{88}$$

Defining

$$K_s(E'',E) = \int_{E''/2}^{E'' - E} d\tau\, k_m(E'',\tau) \tag{89}$$

and letting $E' = E'' - \tau$, Eq. (88) becomes:

$$\int_{E}^{2E} dE'z(E_o,E')K_c(E',E) = 1 + \int_{2E}^{E_o} dE''z(E_o,E'')K_s(E'',E) \tag{90}$$

in which $K_c(E',E)$ and $K_s(E'',E)$ are:

$$K_c(E',E) = 0 \quad \text{for } E'\leq 2E, \tag{91}$$

$$K_c(E',E) = \frac{2\pi N_e r_o^2}{(\beta')^2}\left[\frac{1}{E'-E} - \frac{1}{E} + \left[\frac{(2 + 1/E')}{(E'+1)^2}\right] \ln\left(\frac{1}{E'-E}\right) + \left(\frac{E - E'/2}{(E'+1)^2}\right)\right] \tag{92}$$

for $E + \overline{Q}\leq E'\leq 2E$,

$$K_c(E',E) = K_c(E + \overline{Q},E) \quad \text{for } E\leq E'\leq E + \overline{Q}, \tag{93}$$

and

$$K_s(E'',E) = \frac{2\pi N_e r_o^2}{(\beta'')^2}\left[\frac{1}{E} - \frac{1}{E''-E} - \left[\frac{2 + 1/E''}{(E''+1)^2}\right] \ln\left(\frac{E''-E}{E}\right) + \frac{E''/2 - E}{(E''-1)^2}\right] . \tag{94}$$

Since $K_c(E',E)$ is a strongly varying function over E' when E' is near E, it is convenient to lower and smooth the integrand of Eq. (90) which contains $K_c(E',E)$. This is accomplished by introducing a function $\overline{K}_c(E',E)$ which will satisfy certain requirements. By adding and subtracting $z(E_o,E)\overline{K}_c(E',E)$ from the integrand and substituting into Eq. (90) the following is obtained:

$$z(E_o,E)\int_E^{2E}\overline{K}_c(E',E)dE' = 1 + \int_{2E}^{E_o} dE''z(E_o,E'')K_s(E'',E)$$

$$-\int_E^{2E} dE'\left[z(E_o,E')K_c(E',E) - z(E_o,E)\overline{K}_c(E',E)\right] . \qquad (95)$$

If it is assumed that $z(E_o,E')$ is a continuous function, $z(E_o,E')$ will approach $z(E_o,E)$ when E' approaches E. As a result, $z(E_o,E')K_c(E',E) - z(E_o,E)\overline{K}_c(E',E)$ will tend to be small and finite as E' approaches E if $\overline{K}_c(E',E)$ is approximately equal to $K_c(E',E)$ when E' is near E. For these assumptions to be valid the following condition should prevail:

$$\int_E^{E+\delta} dE'\{K_c(E',E) - \overline{K}_c(E',E)\} = 0 \qquad (96)$$

and $\delta<<I$, $\delta<<E$ and $\delta<<mc^2$ in which I is the mean ionization potential and m_oc^2 is the rest energy of the electron. Too, it is convenient that $\overline{K}_c(E',E)$ remain rather close to $K_c(E',E)$ for $E'>>E$ and that $\overline{K}_c(E',E)$ be integrable analytically. Spencer and Fano (22) have chosen:

$$\overline{K}_c(E',E) = 0 \quad \text{for } E'\geq 2E, \qquad (97)$$

$$\overline{K}_c(E',E) = \frac{2\pi N_e r_o^2}{\beta^2}\left[\frac{1}{E'-E} - \frac{1}{E} - \left[\frac{(2+1/E)}{(E+1)^2}\right]\ln\left[\frac{1}{E'-E}\right] + \frac{E - E'/2}{(E+1)^2}\right] \quad \text{for } E+\overline{Q}\leq E'\leq 2E, \qquad (98)$$

and

$$\overline{K}_c(E',E) = \overline{K}_c(E+\overline{Q},E) \qquad \text{for } E'\leq E+\overline{Q}, \qquad (99)$$

From Eq. (78) it is evident that in Eq. (98)

$$\beta = \frac{\sqrt{E(E + 2)}}{(E + 1)} . \tag{100}$$

One now defines

$$F(E_o,E) = \int_{E}^{E + \Delta} dE'\bar{K}_c(E',E), \tag{101}$$

or

$$F(E_o,E) = \frac{2\pi N_e \bar{r}_o^{\,2}}{\beta^2} \left[1 + \ln\left(\frac{\Delta}{\bar{Q}}\right) - \frac{\Delta}{E} - \frac{(2E + 1)}{E(E + 1)^2} \Delta \left(1 + \ln E/\Delta\right) \right.$$

$$\left. + \frac{1}{4} \Delta \frac{(2E - \Delta)}{(E + 1)^2} \right], \tag{102}$$

in which

$$\Delta = \begin{cases} E, & \text{for } 2E \leq E_o \\ E_o - E, & \text{for } 2E > E_o \end{cases}$$

and all terms of the order of $\bar{Q}$ have been disregarded. According to McGinnies (20), it is possible to show that $F(E_o,E)$, when limited to small energy losses, approximates the restricted stopping power.

Equation (95) now may be written in its final form:

$$z(E_o,E) = \frac{1}{F(E_o,E)} \left[1 + \int_{E + \Delta}^{E_o} dE''z(E_o,E'')K_s(E'',E) \right.$$

$$\left. - \int_{E + \Delta}^{E + \Delta} dE'\{z(E_o,E')K_c(E',E) - z(E_o,E)\bar{K}_c(E',E)\} \right] . \tag{103}$$

A variety of numerical integration schemes to evaluate Eq. (103) could be used. After much consideration it was decided to choose the integration points on an exponential scale and use subroutine BATES (explained in section 6.8)to generate their respective weight factors. It should be noted that $1/F(E_o,E)$ is approximately equal to $z(E_o,E)$ near E_o.

As a result one can begin the iteration for $z(E_o,E_i)$ by first approximating $z(E_o,E_i)$ by $1/F(E_o,E_i)$. It is important to note that one cannot evaluate $F(E_o,E)$ at $E = E_o$. This is due to the peak in $\frac{1}{F(E_o,E)}$ as E nears E_o. According to McGinnies (20), $E = 0.95E_o$ can be used since the peak contributes very little to the integral. For this calculation an approximation by McGinnies (20) can be used to evaluate $z(E_o,0.95E_o)$. This value is then used for the first point in the iteration. The abscissa points are chosen as follows:

$$E_i = E_o \xi^{i-1}, \tag{104}$$

in which $\xi = (.5)^{1/p}$. Calculations for the cases of $p = 3$ and $p = 6$ are compared. For the computer program explained in section 6.4 the following recurrence relation is used:

$$E_i = E_{i-1}\xi. \tag{105}$$

Rewriting Eq. (103) and replacing the integrals with finite sums, results in:

$$\begin{aligned} z(E_o,E_n) = 1/F(E_o,E)\{1 &+ \sum_{i=1}^{n-p} z(E_o,E_i)K_s(E_i,E_n)W_i \\ &- \sum_{i=n-p}^{n-1} W_i \left[z(E_o,E_i)K_c(E_i,E_n) - z(E_o,E_n)\bar{K}_c(E_i,E_n)\right] \\ &- W_n \left[z(E_o,E_n)K_c(E_n,E_n) - z(E_o,E_n)\bar{K}_c(E_n,E_n)\right] \}. \end{aligned} \tag{106}$$

McGinnies (20) evaluated the last term in Eq. (106) by approximating it with a parabola and extrapolating analytically. However, the author of this paper found that the n^{th} term in Eq. (106) has a limit when the following approximations are made for $K_c(E',E)$ and $\overline{K}_c(E',E)$ when E' nears E:

$$K_c(E',E) = \frac{2C}{(\beta')^2}\frac{1}{E' - E} \tag{107}$$

$$\overline{K}_c(E',E) = \frac{2C}{\beta^2}\frac{1}{E' - E} . \tag{108}$$

From Eq. (78) one knows that

$$(\beta')^2 = E'(E' + 2)/(E' + 1)^2 \tag{109}$$

$$\beta^2 = E(E + 2)/(E + 1)^2 \tag{110}$$

and

$$C = N_A \pi \bar{r}_o Z/A = .15Z/A. \tag{111}$$

(N_A is Avogadro's number, Z is the atomic number and A is the atomic weight.) The last term of Eq. (106), $W_n H$, can now be written with

$$H = 2C \lim_{E' \to E} \left[\frac{z(E_o,E')}{(\beta')^2} \frac{1}{E' - E} - \frac{z(E_o,E)}{\beta^2} \frac{1}{E' - E} \right] . \tag{112}$$

Applying l'Hospital's rule, simplifying, one obtains:

$$H = 2C \lim_{E' \to E} \left[\frac{z(E_o,E')(E)(E + 2)(E' + 1)^2 - z(E_o,E)(E')(E' + 2)(E + 1)^2}{E(E + 2)E(E' + 2)E' - E)} \right] \tag{113}$$

Since the limit of a product is equal to the product of the limits, one can factor $z(E_o,E)$, with the final result of

$$H = - 2C \left[\frac{(2)(E + 1)}{[E(E + 2)]^2} \right] . \tag{114}$$

Substituting Eq. (114) into Eq. (106) gives:

$$z(E_o,E_n) = \frac{1}{F(E_o,E_n)}\left[1 + \sum_{j=1}^{n-p} W_j z(E_o,E_j)K_s(E_j,E_n) - \sum_{i=n-p}^{n-1}\left[z(E_o,E_n)\right.\right.$$

$$\left.\left. -z(E_o,E_n)\bar{K}_c(E_i,E_n)\right] + \frac{z(E_o,E_n)4C(E_n + 1)W_n}{\left[E_n(E_n + 2)\right]^2}\right] . \qquad (115)$$

Collecting and rearranging terms in Eq. (115) results in

$$z(E_o,E_n) = \left[\frac{1 + \sum_{j=1}^{n-p} W_j z(E_o,E_j)K_s(E_j,E_n) - \sum_{i=n-p}^{n-1} W_i z(E_o,E_i)K_c(E_i,E_n)}{F(E_o,E_n) - \left[\frac{4C(E_n + 1)W_n}{\left[E_n(E_n + 2)\right]^2} + \sum_{i=n-p}^{n-1} W_i\bar{K}_c(E_i,E_n)\right]}\right] . \qquad (116)$$

2.3 Electron Slowing-Down Spectrum Resulting From Co^{60} Gamma Irradiation of Water

Due to the complexity of other developments, only one interaction per photon will be considered in the production of electrons from Co^{60} gamma-rays. Even though there are a number of ways in which radiation interacts with matter, the only ones of interest when dealing with photons are: the photoelectric effect, pair-production and Compton scattering. Since Co^{60} irradiation is being considered, cross sections for 1.17 and 1.33 Mev gamma-rays must be obtained. Gladys White Grodstein (11) has tabulated sufficient cross sections to permit the conclusion that the photoelectric effect and pair-production contribute negligibly to the dose when Co^{60} gamma-rays interact with water. Therefore, one assumes the source electrons to be produced by first collision Compton scattering of the photons.

The Compton process must occur with a free or loosely-bound electron.

By quantum mechanical calculations, Klein and Nishina have shown that the differential cross section for the number of photons scattered into a unit solid angle at polar angle ρ per electron of material is given by

$$\frac{d_e\sigma_t}{d\Omega} = \frac{e^4}{2m_o{}^2c^4}\left[\left[\frac{1}{1 + \alpha\mathrm{Vers}(\rho)}\right]^2 \frac{1 + \cos^2(\rho) + \alpha^2\mathrm{Vers}^2(\rho)}{1 + \alpha\mathrm{Vers}(\rho)}\right] , \quad (117)$$

in which $\alpha = h\nu/m_oc^2$ are $\mathrm{Vers}(\rho) = 1-\cos(\rho)$, e is the electron's charge. The collision process may be represented by the following diagram:

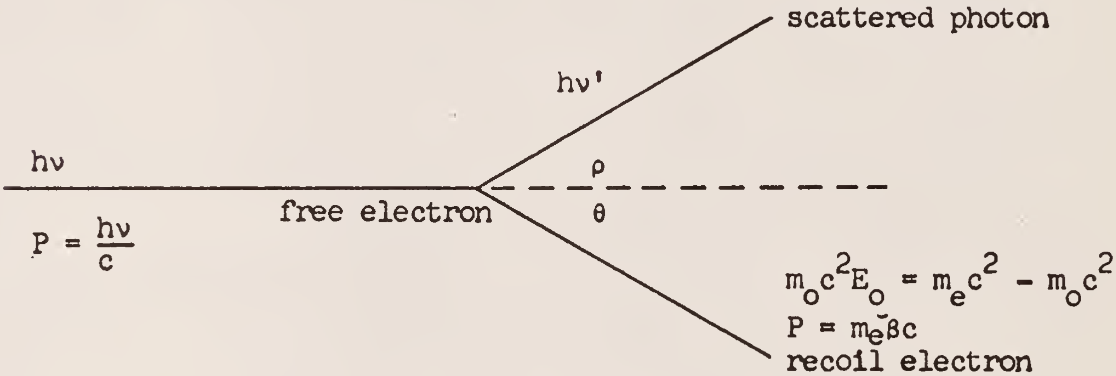

In the above diagram P represents momentum.

To determine the differential cross section for electron energy distribution the relation between the scattering angle ρ and the recoil electron energy T is used and is given by

$$E_o = \frac{h\nu\ \mathrm{Vers}(\rho)}{1 + \alpha\mathrm{Vers}(\rho)} , \quad (118)$$

and Eq. (117). According to Johns and Laughlin (14), the differential cross section $d_e\sigma(E_o)/dE_o$, for the number of electrons, with kinetic energies between E_o and $E_o + dE_o$, scattered per electron is given by

$$\frac{d_e\sigma(E_o)}{dE_o} = \frac{\pi r_o^{\,2}}{.51097\alpha^2}\left[1 + E_o\cos^2(\rho) - E_o\cos(\rho)\right] \tag{119}$$

in which $m_oc^2 = .51097$ Mev.

Note further that

$$\cos(\rho) = \frac{(\alpha^2 - \alpha E_o - E_o)}{(\alpha^2 - \alpha E_o)} \quad . \tag{120}$$

The combination of Eqs. (119) and (120) gives:

$$\frac{d_e\sigma(E_o)}{dE_o} = \frac{\pi r_o^{\,2}}{.51097\alpha^2}\left[1 + \frac{E_o(\alpha^2 - \alpha E_o - E_o)^2}{(\alpha^2 - \alpha E_o)^2} - \frac{E_o(\alpha^2 - \alpha E_o - E_o)}{(\alpha^2 - \alpha E_o)}\right] \quad . \tag{121}$$

Equation (121) is utilized as a FUNCTION statement to calculate the electron source term at any energy E_o. The resulting electron energy spectrum $y_g(E)$ is calculated by utilizing the electron energy spectrum resulting from a monoenergetic source in combination with Eq. (121). Specifically it is necessary to evaluate the following integral:

$$y_g(E) = \int_E^{E_{max}} z(E_o,E)S_e^{\,g}(E_o). \tag{122}$$

Taking into account the two equal intensity gamma rays from Co^{60} and the electron density (N_e), the following expression for $S_e^{\,g}(E_o)$ is obtained:

$$S_e^{\,g}(E_o) = \frac{\pi r_o^{\,2}N_e}{.51097}\left[\sum_{i=1}^{NQ}\frac{1}{\alpha_i^{\,2}}\left[1 + \frac{E_o(\alpha_i^{\,2} - \alpha_iE_o - E_o)^2}{(\alpha_i^{\,2} - \alpha_iE_o)^2} - \frac{E_o(\alpha_i^{\,2} - \alpha_iE_o - E_o)}{(\alpha_i^{\,2} - \alpha_iE_o)}\right]\right] \tag{123}$$

in which

$$NQ = \begin{cases} 2 \text{ if } E_o < \alpha_2^{\,2}/(1 + 2\alpha_2) \\ 1 \text{ if } E_o > \alpha^2_{\,2}/(1 + 2\alpha_2) \end{cases}$$

and

$$\alpha_2 = (1.33/.51097)\ m_oc^2.$$

2.4 Electron Spectra Resulting From Fast Neutron Irradiation of Water

This development closely follows that by Faw (8) and Faw and Miller (7). To determine the charged particle slowing down spectra resulting from fast neutron (14.6 Mev) irradiation of water, two neutron reactions are considered. They are: I, the production of protons H(n,n)H and II, the production of alpha particles $O^{16}(n,\alpha)C^{13}$. Neutrons of 14.6 Mev are considered since they are easily obtained by the $H^3(d,n)De^4$ reaction. The proton and alpha particle fluxes used were obtained from Faw (8). This information is then used to calculate the resulting electron slowing down spectra.

Continuous slowing down theory is used to determine the proton and alpha particle fluxes from their source terms as determined from reactions I and II, respectively. Electron spectra are calculated from the slowing down of the protons and alpha particles. Spatial dependence of the charged particles is assumed to be negligible.

The total cross section for reaction I, σ_I, is taken to be .668 barns, as given in reference (2). The distribution function g(E) is defined such that $\sigma_I g(E)dE$ is the cross section presented by hydrogen atoms for creation of knock-on protons of energy E in dE. The proton source term, $S_p(E)$, can be written as follows:

$$S_p(E) = N_H \sigma_I g(E) \phi_0. \tag{124}$$

in which N_H is the hydrogen atom density and ϕ_0 is the 14.6 Mev neutron flux. The distribution function, g(E), used by Faw (8) is

$$g(E) = \frac{1}{\bar{E}_o\left[1 + \frac{\bar{c}}{3}\right]}\left[1 + \bar{c}\left[1 - \frac{2E}{\bar{E}_o}\right]^2\right], \tag{125}$$

in which $\bar{c}$ is the anisotropy factor characteristic of the neutron energy $\bar{E}_o$ and has a value of 0.06. Substituting Eq. (125) into Eq. (124) yields

$$S_p(E) = N_H\sigma_I \frac{1}{E_o\left[1 + \frac{\bar{c}}{3}\right]}\left[1 + \bar{c}(1 - \frac{2E}{E_o})^2\right]. \tag{126}$$

From continuous slowing-down theory, the following expression for the proton flux can be written:

$$\phi_p(E) = \frac{1}{L_p(E)}\int_E^{E'_p} dE' S_p(E'). \tag{127}$$

in which $L_p(E)$ is the total stopping power of the medium for protons.

Computation of the alpha particle source strength and flux proceeds in a similar fashion:

$$S_a(E) = \bar{N}_0\sigma_{II}f(E)\phi_0 \tag{128}$$

$$\phi_a(E) = \frac{1}{L_a(E)}\int_E^{E'_a} dE' S_a(E'). \tag{129}$$

in which $\bar{N}_0$ is the oxygen atom density, σ_{II} is the total cross section for reaction II and is reported to be .312 barns by Kalos, Goldstein and Ray (15), f(E) is the energy distribution of alpha particles resulting from reaction II, E'_a is the maximum energy and $L_a(E)$ is the total stopping power for alpha particles.

Due to fragmentary information on the energy distribution of alpha particles resulting from the $O^{16}(n,\alpha)C^{13}$ reaction corresponding to various excited states of the C^{13} nucleous, only a mean excitation energy of 4.8 Mev is considered. A monoenergetic source of alpha particles of 5.8 Mev is given by Faw (8). Equation (128) now becomes:

$$S_a = \bar{N}_0 \sigma_{II} \phi_0 \tag{130}$$

and Eq. (129) reduces to

$$\phi_a(E) = \frac{\bar{N}_0 \sigma_{II} \phi_0}{L_a(E)} \; . \tag{131}$$

During the slowing-down process of protons and alpha particles, electrons of sufficient energy to escape from the heavy particle track are produced. These electrons are taken to be those produced with energy greater than δ_c (200 ev) and are called delta rays. These delta rays in turn produce chemical effects and must be treated as a separate electron source. In effect, the total dose resulting from the proton and alpha particles is divided between the energy lost locally by the heavy charged particles and the energy lost by delta rays away from the track. Differential electron cross sections per unit energy for creation of electrons of energy E as a result of collisions with protons or alpha particles of energy E' ($\sigma_p(E',E)$, $\sigma_a(E',E)$) are given by Rossi (21) as follows:

$$\sigma_p(E',E) = \frac{2\pi e^4}{m_e c^2 \beta_p^2 E^2} \left[1 - \beta_p \frac{E}{E_m} + \frac{1}{2} \left[\frac{E}{E' + m_p c^2} \right]^2 \right] \tag{132}$$

$$\sigma_a(E',E) = \frac{8\pi e^4}{m_e c^2 \beta_a^2 E^2} \left[1 - \beta_a \frac{E}{E_m} \right] \; . \tag{133}$$

in which β_p or β_a is the ratio of the velocity of the proton or alpha particle to the velocity of light. Explicitly:

$$\beta_p = \frac{E'(E' + 2m_pc^2)}{(E' + m_pc^2)^2} \tag{134}$$

and

$$\beta_a = \frac{E'(E' + 2m_ac^2)}{(E' + m_ac^2)^2} , \tag{135}$$

in which e is the charge on an electron, m_e, m_p, and m_a are the rest masses of the electrons, protons and alpha particles, c is the velocity of light and E_m is the maximum energy the particle under consideration can transfer to an electron.

The electron source terms, $S_e^p(E)$ and $S_e^a(E)$, from proton and alpha particle fluxes can be written as:

$$S_e^p(E) = \int_E^{E'_p} dE'\phi_p(E')N_e\sigma_p(E',E), \quad \delta_c \leq E \leq \frac{4m_eE'_p}{m_p} \tag{136}$$

and

$$S_e^a(E) = \int_E^{E'_a} dE'\phi_a(E')N_e\sigma_a(E',E), \quad \delta_c \leq E \leq \frac{4m_eE'_a}{m_a} . \tag{137}$$

in which N_e represents the electron density and the lower limit gives the lowest possible proton or alpha particle energy capable of producing an electron of energy E and δ_c is the maximum energy lost along the track (200 ev).

The electron energy spectra resulting from electron slowing down, $z(E_o,E)$, may be utilized to calculate the electron spectra resulting from the initial electron sources produced by the protons and alpha particles. The expressions for the electron spectra are:

$$y_p(E) = \int_{\frac{m_p E}{4m_e}}^{\frac{4m_e E'_p}{m_p}} dE''S_e^p(E'')z(E'',E) \tag{138}$$

$$y_a(E) = \int_{\frac{m_a E}{4m_e}}^{\frac{4m_e E'_a}{m_a}} dE''S_e^a(E'')z(E'',E). \tag{139}$$

2.5 Determination of the Stopping Power of Water for Low Energy Electrons

Accurate estimates of collision cross sections for low energy electrons are quite difficult to obtain. A literature search gave inelastic collision cross section data for small energy energy losses of 390 ev electrons. Utilizing this information and an analytic approximation, a synthesized cross section for low energy is determined. However, since the hypothesis is made without considering the physics of very low energy (below 200 ev) scattering of electrons, the relative accuracy of the synthesized cross section cannot be accurately estimated for this low energy range. This synthesized cross section is needed for calculation of the spur size distribution and the weighted average spur separation distance.

Data for the inelastic collision cross section is taken from a publication by Lassettre and Francis (17). This data, $k_{ex}(\tau)$, is then approximated by a series of straight lines (See section 6.8). Since the mean ionization potential I_0 is nearly independent of electron energy, it is assumed that the form of $k_{ex}(\tau)$ is independent of electron energy. Therefore, data for $k_{ex}(\tau)$ obtained at one energy should be sufficient.

The Moller formula is quite accurate for electron-electron collisions at high energy but neglects binding energy effects. Even for high energy incident electrons, the energy loss must be large before an interaction can be considered to be elastic. In reality, all electron-electron interactions in a condensed medium are probably inelastic (i.e., some energy is lost to excitation or ionization in every collision), unless it interacts with an entire atom or molecule. As a result it can be deduced that the inelastic collision cross section must go to zero for zero energy losses.

For small energy losses the Moller formula can be approximated by,

$$k_m(E,\tau) \simeq \frac{\kappa(E)}{\tau^2} \,. \tag{140}$$

According to a statement by L. V. Spencer, there is evidence that the Moller formula underestimates the true cross section for low energy electrons. Therefore, one should at least hypothesize a form that can become larger than $k_m(E,\tau)$ for low energies and/or small losses. After much deliberation, the following form was chosen for the hypothesized cross section:

$$k_H(E,\tau) = k_m(E,\tau), \quad \tau>150\text{ev} \quad \text{and} \quad E>2\text{Kev} \tag{141)a}$$

$$k_H(E,\tau) = \frac{\kappa(E)}{(a\tau + b)^2}, \quad \delta_1<\tau<150\text{ev} \quad \text{and} \quad E>0 \tag{141)b}$$

$$k_H(E,\tau) = \text{AKT } k_{ex}(\tau), \quad 0<\tau<\delta_1 \quad \text{and} \quad E>0 \tag{141c}$$

in which $\kappa(E) = 2C(1/E)$. The behavior of the parameters (a) and (b) is determined in regions where $k_m(E,\tau)$ is valid and their behavior is deduced for lower energies. AKT is an energy dependent term for the energy losses below δ_1.

Since the integral over the Moller cross section is a valid approximation of the stopping power for energies as low as 2 kev, the following equation can be written:

$$\text{AKT} \int_0^{\delta_1} k_{ex}(\tau)\tau d\tau + \int_{\delta_1}^{\delta_2} \frac{\kappa(E)\tau d\tau}{(a\tau + b)^2} = \int_{\bar{Q}}^{\delta_2} k_m(E,\tau)\tau d\tau. \tag{142}$$

The assumed boundary conditions are

$$\text{AKT } k_{ex}(\delta_1) = \frac{\kappa(E)}{(a\delta_1 + b)^2} \tag{143}$$

and

$$\frac{\kappa(E)}{(a\delta_2 + b)^2} = k_m(E_1\delta_2), \tag{144}$$

in which δ_1 is the high end of the experimental data (21 ev) and δ_2 is arbitrary, but must be chosen such that $k_m(E,\delta_2)$ is valid. One can solve for (a) and (b) explicitly but AKT must be obtained by iteration. Solving Eq. (143) and Eq. (144) for (a) and (b) gives

$$a = \pm \frac{\left[\sqrt{\frac{\kappa(E)}{k_m(E_1\delta_2)}} - \sqrt{\frac{\kappa(E)}{(\text{AKT})k_{ex}(\delta_1)}}\right]}{(\delta_2 - \delta_1)} \tag{145}$$

and

$$b = \pm \frac{\left[\delta_2 \sqrt{\frac{\kappa(E)}{(AKT)k_{ex}(\delta_1)}} - \delta_1 \sqrt{\frac{\kappa(E)}{k_m(E_1\delta_2)}} \right]}{(\delta_2 - \delta_1)} . \tag{146}$$

Equations (145) and (146) are substituted into Eq. (142) to carry out the iteration. Note that the definite integrals over $k_H(E,\tau)\tau d\tau$ and $k_m(E,\tau)\tau d\tau$ have the following analytical expressions:

$$\int_{\delta_1}^{\delta_2} k_H(E,\tau)\tau d\tau = \frac{\kappa(E)}{a^2} \left[\frac{b}{(a\delta_2 + b)} - \frac{b}{(a\delta_1 + b)} + \ln \left[\frac{a\delta_2 + b}{a\delta_1 + b} \right] \right] \tag{147}$$

and

$$\int_{\bar{Q}}^{\delta_2} k_m(E,\tau)\tau d\tau = 2CZ/A \left[\ln \left[\frac{\delta_2}{\bar{Q}} \right] + \left[\frac{E}{(E - \delta_2)} \right] - \left[\frac{1}{(E - \bar{Q})} \right] \right.$$

$$\left. + \ln \left[\frac{(E - \delta_2)}{(E - \bar{Q})} \right] \left[1 + \frac{E(2 + 1/E)}{(E + 1)^2} \right] + \left[\frac{1}{(E + 1)^2} \right] \left[\frac{(\delta_2^{\,2} - \bar{Q}^2)}{2} \right] \right] \tag{148}$$

The computer programs used for this calculation are explained in section 6.5.

2.6 Spur Size Distribution

For accurate determination of the radiation chemical yield (using spur theory), it is necessary to either form an average of the spur size distribution over the fractional yield expression or find a weighted average spur size to use in the yield expression. The latter approach is taken for this development.

The cross section developed in section 2.5 of the theory makes it possible to determine a weighted average spur size, considering the spur size distribution at low electron energies. Since $k_H(E,\tau)\,d\tau$ is the probability per centimeter that an electron of energy E has a collision which results in an energy loss of $\tau \pm d\tau$, $\tau k_H(E,\tau)d\tau$ is the probability per centimeter that an electron loses energy $\tau \pm d\tau$. If a spectrum y(E) of electrons is present, $\tau k_H(E,\tau)d\tau y(E)dE$ is proportional to the probability per centimeter that the electrons of differential spectrum gives up energy $\tau \pm d\tau$. A function proportional to the probability of electrons of a differential spectrum of y(E) about E in dE creating a spur with energy between τ and $\tau + d\tau$ is written as follows:

$$G(E,\tau)dEd\tau = \tau d\tau dEy(E)k_H(E,\tau). \tag{149}$$

Integrating over the energy variable gives

$$G(\tau)d\tau = \tau d\tau \int_{E_{min}}^{E_{max}} dEy(E)k_H(E,\tau). \tag{150}$$

The weighted average spur size is the first moment of τ about $G(\tau)$, which gives:

$$\langle\bar{\tau}\rangle = \frac{\int_{\delta_{Min}}^{\delta_c} \tau G(\tau)d\tau}{\int_{\delta_{Min}}^{\delta_c} G(\tau)d\tau}. \tag{151}$$

The effect of both the lower and upper limits, E_{min} and E_{max}, and δ_c are investigated.

Kupperman (16) gives a spur size distribution,

$$f(N_0) = .65e^{-N_0/4} \tag{152}$$

for even N_0. When averaged for spur sizes between 2 and 24 radicals, the result is $4.9\ \frac{\text{radicals}}{\text{spur}}$.

2.7 Spur Separation Distance

To be able to evaluate the chemical yield accurately, based on the spur model, it is necessary to average the fractional yield expression over a spectrum of spur separation distances $U(\ell')d\ell'$, where $U(\ell')d\ell'$ is the differential spectrum of spurs with separation distances between ℓ' and $\ell' + d\ell'$. Since ℓ' is a function of E, for $d\ell(E)$ corresponding to dE, the function $U\{\ell'(E)\} = U(\ell')$ is defined by:

$$U(\ell')d\ell' = y(E)dE.$$

Then the following integral averages $Y_{RS}(\ell')$

$$\bar{Y}_{RS} = \frac{\int_{\ell_{min}}^{\ell_{max}} Y_{RS}(\ell')U(\ell')d\ell'}{\int_{\ell_{min}}^{\ell_{max}} U(\ell')d\ell'} \tag{153}$$

in which ℓ_{max} would depend on the quality of the irradiation and ℓ_{min} is taken as low as information on y(E) and Y(E) permits.

However, it is assumed that a weighted average $\bar{\ell}$ can be determined from the radiation energy spectrum such that $\bar{Y}_{RS} \simeq Y_{RS}(\bar{\ell})$, in which $\bar{\ell} = \langle \ell' \rangle / 2r_o$. Therefore, several weighted averages for $\langle \ell' \rangle$, are hypothesized. The forms chosen are:

Case 1 (weighting by the electron spectrum and the relative local energy loss)

$$\langle \ell' \rangle_1 = \frac{\int_{E_{min}}^{E_{max}} y(E) \frac{L(E,\delta_c)}{L(E)} \ell'(E,\delta_c) dE}{\int_{E_{min}}^{E_{max}} y(E) \frac{L(E,\delta_c)}{L(E)} dE} \tag{154}$$

Case 2 (weighting by the local energy loss)

$$\langle \ell' \rangle_2 = \frac{\int_{E_{min}}^{E_{max}} y(E) L(E,\delta_c) \ell'(E,\delta_c) dE}{\int_{E_{min}}^{E_{max}} y(E) L(E,\delta_c) dE} \tag{155}$$

Case 3 (weighting by the electron spectrum)

$$\langle \ell' \rangle_3 = \frac{\int_{E_{min}}^{E_{max}} y(E) \ell'(E,\delta_c) dE}{\int_{E_{min}}^{E_{max}} y(E) dE} \tag{156}$$

Case 4 (The definition of the average linear energy transfer ($\overline{LET}$) is taken from a paper by Burch (6))

$$\overline{LET} = \frac{\int_{E_{min}}^{E_{max}} y(E) \frac{L(E,\delta_c)}{L(E)} L(E,\delta_c) dE}{\int_{E_{min}}^{E_{max}} y(E) \frac{L(E,\delta_c)}{L(E)} dE} \tag{157}$$

$$\langle \ell' \rangle_4 = \frac{\langle \bar{\tau} \rangle}{\text{LET}} . \tag{158}$$

The spur separation distance used in Cases 1-3 is given by

$$\ell'(E,\delta_c) = \frac{\langle \bar{\tau} \rangle}{\int_0^{\delta_c} k_H(E,\tau)\tau d\tau} \tag{159}$$

in which $\langle \bar{\tau} \rangle$ is the weighted average spur size and δ_c(200 ev) is considered to be the effective maximum local energy loss along a track. The denominator of Eq. (159)

$$\int_0^{\delta_c} k_H(E,\tau)\tau d\tau ,$$

is the stopping power, $L(E,\delta_c)$, restricted to energy losses less than δ_c, and $L(E)$ is the total stopping power. The spur separation distance $\ell'(E,\delta_c)$ has units of centimeters.

2.8 Energy Balance

For the purpose of checking the validity of a linear extrapolation for Y(E) below 200 ev on a log-log scale, several dose rates are calculated. The integrations to be performed are:

$$\underline{\text{Dose 1}} = \int_{E_{min}}^{E_{max}} S(E')(E' - E_{min})dE'' \tag{160}$$

$$\underline{\text{Dose 2}} = \int_{E_{min}}^{E_{max}} S(E')E'dE \tag{161}$$

$$\underline{\text{Dose 3}} = \int_{E_{min}}^{E_{max}} y(E')L(E')dE' \tag{162}$$

$$\underline{\text{Dose 4}} = \int_{E_{min}}^{E_{max}} y(E')L(E',\delta_c)dE'. \tag{163}$$

If the electron source results from proton or alpha irradiation, the electron source terms are zero below 200 ev. If the electron spectra resulting from fast neutron irradiation are determined by stopping power theory, $y^{SP}(E)$, Dose 1 should equal Dose 3 for all E_{min} above 200 ev. However, the results presented consider y(E) based on the theory derived in section 2.1. Therefore, the inequality, Dose 3 $\geq$ Dose 1, should be valid for all E_{min} above δ_c. With E_{min} = 200 ev, Dose 2 is the total dose rate. Dose 4 is the dose restricted to energy losses less than 200 ev.

Rather than alter the computer program explained in section 6.4, the integration for Dose 2 from the Co^{60} irradiation is performed analytically. Simplification of Eq. (121) gives:

$$S_i(E) = \frac{\pi N_e r_o^2}{\alpha_i^2} \left[\frac{\alpha_i^4 - 2\alpha_i E + (1 + \alpha_i E^3)}{(\alpha_i^2 - \alpha_i E)^2} \right] . \tag{164}$$

The expression for Dose 2 is given by

$$\underline{\text{Dose 2}} = \sum_{i=1}^{NQ} \int_{E_{min}}^{E_{max}} S_i(E)EdE, \tag{165}$$

where NQ is defined in section 2.3, and

$$\int_{E_{min}}^{E_{max}} S_1(E)EdE = \frac{\pi N_e r_o^2}{\alpha_1^2}\left[\frac{(2+\alpha_1+\alpha_1^2)(\alpha_1 - E)}{\alpha_1} + \frac{E^3(1+\alpha_1)}{3\alpha_1^2}\right.$$

$$\left.\left. - (\alpha_1 + 2)\left[\frac{\alpha_1^2}{(\alpha_1^2 - \alpha_1 E)} + (\alpha_1 + 2)\ln(\alpha_1^2 - \alpha_1 E)\right]\right]\right|_{E = E_{min}}^{E = E_{max}} . \quad (166)$$

Dose 1 is not obtained for the gamma ray source.

2.9 Comparison of Experimental and Theoretical $G(Fe^{+3})$ Values, Using a One-Radical Model for an Oxygen Free Solution

Since the one-radical model is inadequate for the oxygen-free ferrous-sulfate system, excellent results cannot be expected. However, the reaction mechanism is as simple as one can expect to find. The reactions occurring in the oxygen-free Fricke dosimeter are assumed to be:

$$H_2O \rightarrow H + OH \quad (167)$$

$$H + OH \rightarrow H_2O \quad (168)$$

$$OH + OH \rightarrow H_2O_2 \quad (169)$$

$$H + H \rightarrow H_2 \quad (170)$$

$$FE^{+2} + OH \rightarrow Fe^{+3} + OH^- \quad (171)$$

$$Fe^{+2} + H_2O_2 \rightarrow Fe^{+3} + OH^- + OH \quad (172)$$

$$Fe^{+2} \cdot HOH + H \rightarrow Fe^{+3} \cdot OH^- + H_2 \quad (173)$$

$$Fe^{+3} + H \rightarrow Fe^{+2} + H^+. \quad (174)$$

To apply the one radical model, reactions (168), (169) and (170) are considered as one radical-radical reaction and reactions (171), (172), (173) and (174) as the radical-solute reaction. One rate constant is assigned to each set of reactions (i.e., k_{RR} and k_{RS}).

For illustration, several approximations for $G(Fe^{+3})$ are considered. The following values are used for the required reaction parameters:

$$\langle\bar{\tau}\rangle = 45 \text{ ev}, \bar{\varepsilon} = 20 \frac{\text{ev}}{\text{radical pair}}, N_o = 4.5 \frac{\text{radicals}}{\text{spur}}$$

$$k_{RS} = .026\text{x}10^{10} \left(\frac{\text{moles}}{\text{liter}}\right)^{-1} \text{sec}^{-1}, k_{RR} = .4\text{x}10^{10} \left(\frac{\text{moles}}{\text{liter}}\right)^{-1} \text{sec}^{-1}$$

$$r_o = 1.5\text{x}10^{-7}\text{cm}, D = 4.5\text{x}10^{-5}\text{cm}^2/\text{sec}$$

$$C_s = 5.0\text{x}10^{-4} \frac{\text{moles}}{\text{liter}} .$$

(The above value of $\bar{\varepsilon}$ is suggested by Burch (5), $\langle\bar{\tau}\rangle$ is taken from this work, C_s is a typical value, N_o is calculated from $\langle\bar{\tau}\rangle$ and $\bar{\varepsilon}$ and those remaining are obtained from a paper by Faw and Miller (10).) Reaction (172) probably does not compete for the Fe^{+2} ions in the spur. However, according to Hochanadel (13), reaction (174) does deplete the H radicals in the spur. In effect, an attempt will be made to represent a fairly complex set of reactions by the simple hypothetical one radical model.

The first approximation will be to consider equal production of H_2O, H_2O_2 and H_2 and disregard reaction (174). For this case, the fractional yield of Fe^{+3} would be:

$$\bar{Y}(Fe^{+3}) = \bar{Y}_{RS} + \frac{2}{3}(1 - \bar{Y}_{RS}) \tag{175}$$

$$\bar{Y}(Fe^{+3}) = \frac{2}{3} + \frac{1}{3}\bar{Y}_{RS}. \tag{176}$$

Since $\langle\bar{\tau}\rangle = 45 \frac{\text{ev}}{\text{spur}}$ and $N_o = 4.5 \frac{\text{radicals}}{\text{spur}}$, the number of Fe^{+3} molecules produced per 100 ev of energy absorbed in spurs $G(Fe^{+3})$ is given by:

$$G(Fe^{+3}) = (10.)(\overline{Y}(Fe^{+3}) \tag{177}$$

$$G(Fe^{+3}) = 10.\ (\frac{2}{3} + \frac{1}{3}\,\overline{Y}_{RS}). \tag{178}$$

The second approximation is to estimate the fraction of the radical-radical reaction going to H_2O_2 from G values by Hochanadel (13). This estimate is .115 for an initial LET near .01 ev/Å. In reality, the fraction going to H_2O_2 increases with increasing LET. For this case:

$$G(Fe^{+3}) = 10.\ (.23 + .77\overline{Y}_{RS}). \tag{179}$$

The third case will be to assume that the one radical model will give the correct $G(Fe^{+3})$ at an initial LET of .01/ev/Å if, in addition to the second approximation, the contribution of the radical-solute reaction is $X_1\overline{Y}_{RS}$.

Explicitly:

$$G(Fe^{+3}) = \left[X_1\overline{Y}_{RS} + .23\ (1 - \overline{Y}_{RS})\right]\ 10. \tag{180}$$

Solving for X_1 gives $X_1 = .87$, and $G(Fe^{+3}) = .23 + .64\ \overline{Y}_{RS}$.

2.10 Error Analysis Methods

Due to the uncertainty in the mean ionization potential and the synthesized cross section, it is possible only to estimate limits of uncertainty for the results calculated. Both errors in the numerical integration and the uncertainty resulting from the lack of knowledge of physical parameters must be considered.

A standard formula is available for determining the error associated with Simpson's integration. However, no method is available to estimate the error associated with the chemical yield calculations which were performed with a combination of Gauss and Laguerre integration.

Integrations using Simpson's rule in this work are performed on a logarithmic scale. As a result, the following formula is given for Simpson's rule integration:

$$\int_{x_o}^{x_{2n}} f(x)dx = \frac{h}{3}\left[f_o + 4\sum_{i=1}^{n} x_{2i-1}\, f_{2i-1} + 2\sum_{i=1}^{n-1} x_{2i}\, f_{2i} + f_{2n}\right]$$

$$- \frac{nh^5}{90} f^{(4)}(\xi). \qquad (181)$$

In the above equation,

$$h = \frac{\ln(x_o/x_{2n})}{2n-1} . \qquad (182)$$

It is important to note that the points on the lower end of the scale are not nearly as important as those on the higher end, unless f(x) diverges for small x.

Suppose that the number of integration points is changed from n_1 to n_2. Correspondingly, the value of h is altered from h_1 to h_2, the error associated with each integration goes from E_1 to E_2 and the value of the integral changes from I_1 to I_2. From the expression for h, it is evident that an expression for the relative errors can be written as follows:

$$\frac{E_1}{E_2} = \frac{n_1}{n_2}\left[\frac{\ln(x_o/x_{2n_1})}{\ln(x_o/x_{2n_2})}\left[\frac{2n_2 - 1}{2n_1 - 1}\right]^5 \frac{f^{(4)}(\xi_1)}{f^{(4)}(\xi_2)}\right] . \qquad (183)$$

Even though ξ_1 and ξ_2 are not known, it appears reasonable to assume that $f^{(4)}(\xi_1)$ and $f^{(4)}(\xi_2)$ would not change appreciably when changing the number of integration points. Using the above assumption and simplifying, Eq. (183) becomes:

$$\frac{E_1}{E_2} = \frac{n_1}{n_2}\left[\frac{2n_2 - 1}{2n_1 - 1}\right]^5 . \qquad (184)$$

If I_∞ is the correct value of the integration,

$$I_2 - I_1 = \pm \left[(I_\infty - E_2) - (I_\infty - E_1)\right] \tag{185}$$

substitution of Eq. (184) into Eq. (185) results in

$$I_2 - I_1 = \pm E_2 \left[1 - \frac{n_1}{n_2}\left[\frac{2n_2 - 1}{2n_1 - 1}\right]^5\right] . \tag{186}$$

From Eq. (186) it is evident that changing the number of integration points from 30 to 40 or from 40 to 50 results in a smaller percent error than the percent change in the value of the integrals.

It is also possible to approximate the effect of uncertainty in I_o on the resulting electron spectra. To estimate this uncertainty, consider the following expression:

$$y(E_o,I_o) = \int_E^{E_{max}} S(E_o)z(E_o,E,I_o)dE_o . \tag{187}$$

The total derivative is given by

$$dy = dI_o \int_E^{E_{max}} S(E_o) \left[\frac{\partial z(E_o,E,I_o)}{\partial I_o}\right] dE_o . \tag{188}$$

In terms of a finite change in I_o the following expression can be written:

$$\Delta y \approx \int_E^{E_{max}} S(E_o) \left[z(E_o,E,I_o + \Delta I_o) - z(E_o,E,I_o)\right] dE_o . \tag{189}$$

For I_o = 65.1 ev and $I_o + \Delta I_o$ = 74.1 ev it can be shown that $\frac{\Delta z}{z}$ is essentially independent of E_o, where

$$\frac{\Delta z}{z} = \frac{z(E_o,E,I_o + \Delta I_o) - z(E_o,E,I_o)}{z(E_o,E,I_o)} . \tag{190}$$

The lower curve in Fig. 4 illustrates the relation between $\frac{\Delta z}{z}$ and E. Substitution of Eq. (190) into Eq. (189) results in

$$\frac{\Delta y(E)}{y(E)} \approx \frac{\Delta z(E)}{z(E)} \ . \qquad (191)$$

Therefore, from Eq. (191), it can be concluded that Fig. 4 presents a reasonable estimate of the uncertainty in the electron spectra due to the uncertainty in I_o.

3.0 RESULTS, DISCUSSIONS AND CONCLUSIONS

3.1 Results, Discussion and Conclusions of the Chemical Yield Calculations

The fractional yield for infinite time, $Y_{RS}(\infty)$, was calculated by the program described in section 6.1.3; the results for various values of A, B, n and ℓ are listed in Table I. Calculations for $Y_{RS}(\infty)$ were performed by the program explained in section 6.1.2; these results are listed in Table II for various values of A, B, n, ℓ and θ. Since $Y_{RS}(\infty)$ is the fractional radical-solute yield, $Y_{RR}(\infty) = 1 - Y_{RS}(\infty)$, in which $Y_{RR}(\infty)$ is the fractional radical-radical yield. Both sets of results were spot checked with the program explained in section 6.1.1. Due to this spot check, it is concluded that no more than 3 percent error should be considered for any result listed. Problems associated with programming the chemical yield expression for numerical integration are described in section 6.1.

The results for $Y_{RS}(\infty)$ presented in Fig. 1 should be sufficient for prediction of the chemical yield for general reaction parameters. Figure 2 is presented for illustration and should be self-explanatory.

The parameters A, B, n, ℓ are defined as follows:

$$A = \frac{k_{RR} N_R(0)}{8\pi^{3/2} D r_o}$$

$$B = \frac{r_o^2 k_{RS} C_S}{2D}$$

$$\ell = \frac{\ell'}{2r_o}$$

n = number of spurs in a chain

in which k_{RR} is the radical-radical recombination rate constant, $N_R(0)$ is the number of free radicals per spur at the beginning of the chemical stage, D is the diffusion constant of the medium for the free radicals, r_o is the spur radius, k_{RS} is the radical-solute rate constant, C_S is the solute concentration (molecules/cm^3) and ℓ' is the spur separation distance in units of centimeters.

In Fig. 1 it is apparent that as A increases, the chemical yield of the RS species decreases and as B increases, the chemical yield increases. One would expect a decrease in $Y_{RS}(\infty)$ due to an increase in k_{RR} or $N_R(0)$ since these conditions favor the radical-radical reaction. As D and r_o increase, the effective spur surface area increases and in turn the radical-solute reaction is favored. As the spur separation distance increases $Y_{RS}(\infty)$ increases due to the reduction in spur overlap. As the spurs come closer together, the effective local concentration of the free radicals is increased and the radical-radical reaction becomes more favorable. The fractional chemical yield is reduced as the number of spurs increase due to spur overlap as the spurs expand.

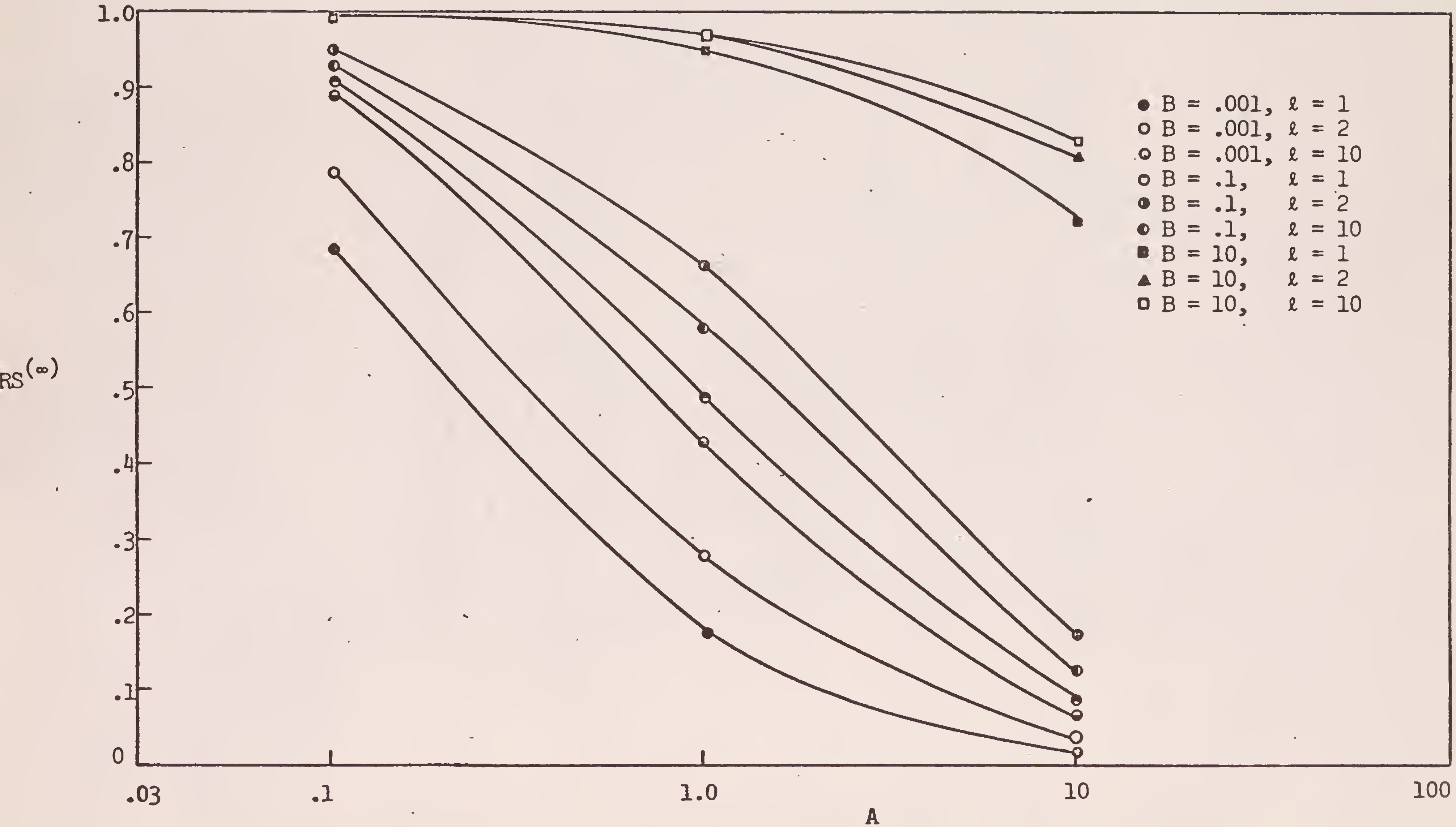

Fig. 1. Chemical Yield vs. A for Various Values of B and ℓ for n = 1000.

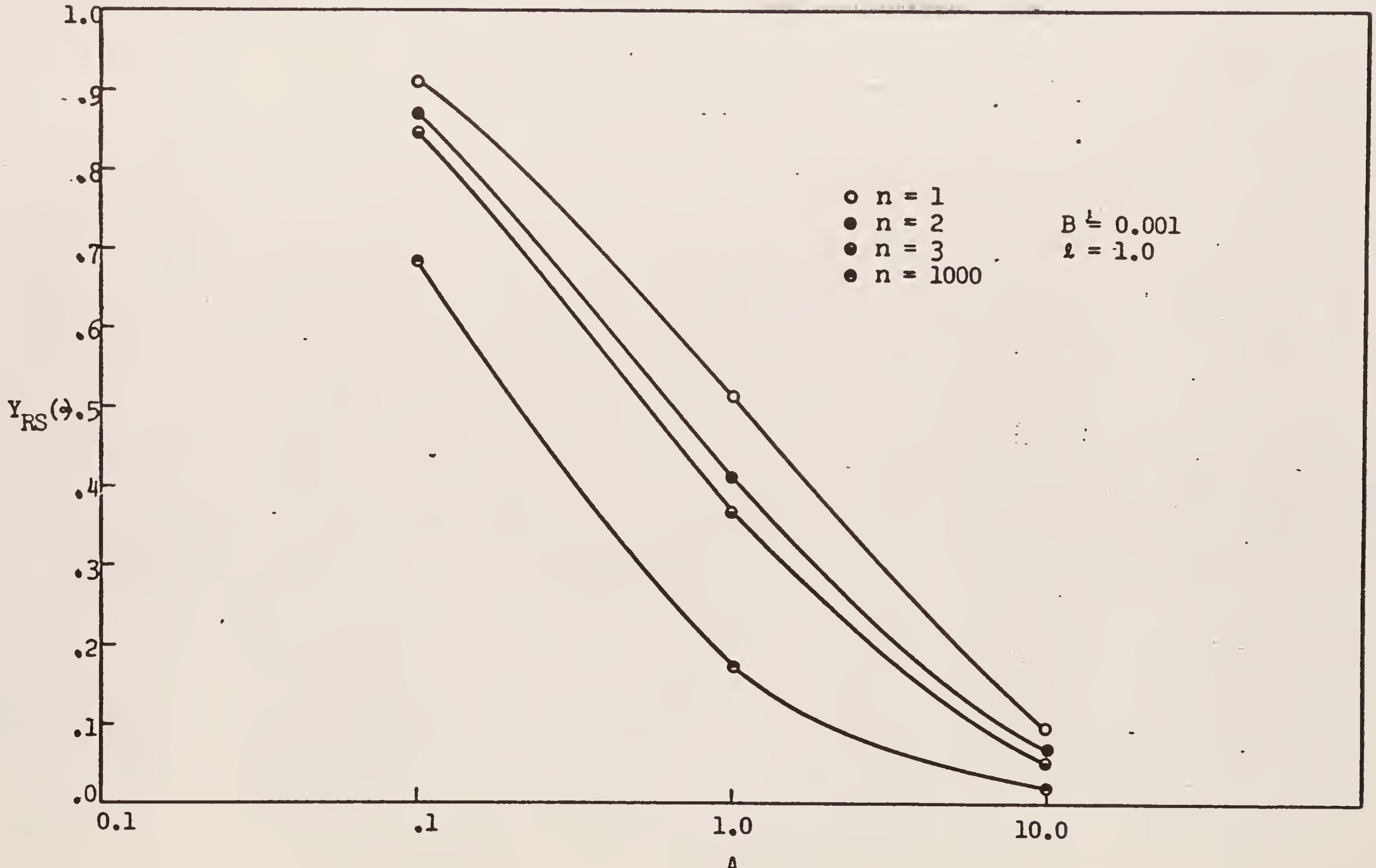

Fig. 2. Chemical Yield vs A for Various Values of n With B = .001 and ℓ = 1.0

Table I. Chemical Yield Results for Various Values of A, B, n and ℓ

Yield	A	B	n	ℓ
.9145	.1000	.0010	1.0000	1.0000
.5169	1.0000	.0010	1.0000	1.0000
.0966	10.0000	.0010	1.0000	1.0000
.8776	.1000	.0010	2.0000	1.0000
.4186	1.0000	.0010	2.0000	1.0000
.0673	10.0000	.0010	2.0000	1.0000
.8494	.1000	.0010	3.0000	1.0000
.3625	1.0000	.0010	3.0000	1.0000
.0540	10.0000	.0010	3.0000	1.0000
.6843	.1000	.0010	1000.0000	1.0000
.1782	1.0000	.0010	1000.0000	1.0000
.0213	10.0000	.0010	1000.0000	1.0000
.9145	.1000	.0010	1.0000	2.0000
.5169	1.0000	.0010	1.0000	2.0000
.0966	10.0000	.0010	1.0000	2.0000
.8770	.1000	.0010	2.0000	2.0000
.4401	1.0000	.0010	2.0000	2.0000
.0729	10.0000	.0010	2.0000	2.0000
.8697	.1000	.0010	3.0000	2.0000
.4006	1.0000	.0010	3.0000	2.0000
.0627	10.0000	.0010	3.0000	2.0000

Table I. (continued)

Yield	A	B	n	ℓ
.7989	.1000	.0010	1000.0000	2.0000
.2845	1.0000	.0010	1000.0000	2.0000
.03826	10.0000	.0010	1000.0000	2.0000
.9145	.1000	.0010	1.0000	10.0000
.5169	1.0000	.0010	1.0000	10.0000
.0966	10.0000	.0010	1.0000	10.0000
.9114	.1000	.0010	2.0000	10.0000
.5071	1.0000	.0010	2.0000	10.0000
.0933	10.0000	.0010	2.0000	10.0000
.9100	.1000	.0010	3.0000	10.0000
.5028	1.0000	.0010	3.0000	10.0000
.0918	10.0000	.0010	3.0000	10.0000
.9067	.1000	.0010	1000.0000	10.0000
.4930	1.0000	.0010	1000.0000	10.0000
.0886	10.0000	.0010	1000.0000	10.0000
.9158	.1000	.1000	1.0000	1.0000
.6653	1.0000	.1000	1.0000	1.0000
.1673	10.0000	.1000	1.0000	1.0000
.9254	.1000	.1000	2.0000	1.0000
.5564	1.0000	.1000	2.0000	1.0000

Table I. (continued)

Yield	A	B	n	ℓ
.1127	10.0000	.1000	2.0000	1.0000
.9121	.1000	.1000	3.0000	1.0000
.5129	1.0000	.1000	3.0000	1.0000
.0965	10.0000	.1000	3.0000	1.0000
.8815	.1000	.1000	1000.0000	1.0000
.4336	1.0000	.1000	1000.0000	1.0000
.0725	10.0000	.1000	1000.0000	1.0000
.9518	.1000	.1000	1.0000	2.0000
.6653	1.0000	.1000	1.0000	2.0000
.1673	10.0000	.1000	1.0000	2.0000
.9439	.1000	.1000	2.0000	2.0000
.6302	1.0000	.1000	2.0000	2.0000
.1477	10.0000	.1000	2.0000	2.0000
.9409	.1000	.1000	3.0000	2.0000
.6178	1.0000	.1000	3.0000	2.0000
.1416	10.0000	.1000	3.0000	2.0000
.9348	.1000	.1000	1000.0000	2.0000
.5942	1.0000	.1000	1000.0000	2.0000
.1307	10.0000	.1000	1000.0000	2.0000
.9518	.1000	.1000	1.0000	10.0000

Table I. (continued)

Yield	A	B	n	ℓ
.6653	1.0000	.1000	1.0000	10.0000
.1673	10.0000	.1000	1.0000	10.0000
.9518	.1000	.1000	2.0000	10.0000
.6653	1.0000	.1000	2.0000	10.0000
.1673	10.0000	.1000	2.0000	10.0000
.9518	.1000	.1000	3.0000	10.0000
.6653	1.0000	.1000	3.0000	10.0000
.1673	10.0000	.1000	3.0000	10.0000
.9518	.1000	.1000	1000.0000	10.0000
.6652	1.0000	.1000	1000.0000	10.0000
.1673	10.0000	.1000	1000.0000	10.0000
.9977	.1000	10.0000	1.0000	1.0000
.9777	1.0000	10.0000	1.0000	1.0000
.8215	10.0000	10.0000	1.0000	1.0000
.9968	.1000	10.0000	2.0000	1.0000
.9693	1.0000	10.0000	2.0000	1.0000
.7712	10.0000	10.0000	2.0000	1.0000
.9964	.1000	10.0000	3.0000	1.0000
.9662	1.0000	10.0000	3.0000	1.0000
.7544	10.0000	10.0000	3.0000	1.0000
.9958	.1000	10.0000	1000.0000	1.0000

Table I. (continued)

Yield	A	B	n	ℓ
.9602	1.0000	10.0000	1000.0000	1.0000
.7233	10.0000	10.0000	1000.0000	1.0000
.9977	.1000	10.0000	1.0000	2.0000
.9777	1.0000	10.0000	1.0000	2.0000
.8215	10.0000	10.0000	1.0000	2.0000
.9976	.1000	10.0000	2.0000	2.0000
.9772	1.0000	10.0000	2.0000	2.0000
.8185	10.0000	10.0000	2.0000	2.0000
.9976	.1000	10.0000	3.0000	2.0000
.9770	1.0000	10.0000	3.0000	2.0000
.8174	10.0000	10.0000	3.0000	2.0000
.9976	.1000	10.0000	1000.0000	2.0000
.9767	1.0000	10.0000	1000.0000	2.0000
.8154	10.0000	10.0000	1000.0000	2.0000
.9977	.1000	10.0000	1.0000	10.0000
.9777	1.0000	10.0000	1.0000	10.0000
.8215	10.0000	10.0000	1.0000	10.0000
.9977	.1000	10.0000	2.0000	10.0000
.9777	1.0000	10.0000	2.0000	10.0000
.8215	10.0000	10.0000	2.0000	10.0000

Table I. (continued)

Yield	A	B	n	ℓ
.8876	.1000	10.0000	3.0000	10.0000
.9777	1.0000	10.0000	3.0000	10.0000
.8215	10.0000	10.0000	3.0000	10.0000
.9977	.1000	10.0000	1000.0000	10.0000
.9777	1.0000	10.0000	1000.0000	10.0000
.8215	10.0000	10.0000	1000.0000	10.0000

Table II. Chemical Yield Results for Various Values of A, B, n, ℓ and θ

$Y_{RS}(\theta)$	θ	ℓ	n	B	A
.63116	1.0	1.0	1.0	10.0	.1
.86290	2.0	1.0	1.0	10.0	.1
.63116	1.0	2.0	1.0	10.0	.1
.86290	2.0	2.0	1.0	10.0	.1
.63116	1.0	10.0	1.0	10.0	.1
.86290	2.0	10.0	1.0	10.0	.1
.63079	1.0	1.0	2.0	10.0	.1
.86223	2.0	1.0	2.0	10.0	.1
.63114	1.0	2.0	2.0	10.0	.1
.86286	2.0	2.0	2.0	10.0	.1
.63116	1.0	10.0	2.0	10.0	.1
.86290	2.0	10.0	2.0	10.0	.1
.63066	1.0	1.0	3.0	10.0	.1
.86198	2.0	1.0	3.0	10.0	.1
.63113	1.0	2.0	3.0	10.0	.1
.86285	2.0	2.0	3.0	10.0	.1
.63116	1.0	10.0	3.0	10.0	.1
.86290	2.0	10.0	3.0	10.0	.1
.60593	1.0	1.0	1.0	.1	.1
.82573	2.0	1.0	1.0	.1	.1
.60593	1.0	2.0	1.0	.1	.1
.82573	2.0	2.0	1.0	.1	.1

Table II. (continued)

$Y_{RS}(\theta)$	θ	ℓ	n	B	A
.60593	1.0	10.0	1.0	.1	.1
.82573	2.0	10.0	1.0	.1	.1
.59197	1.0	1.0	2.0	.1	.1
.80447	2.0	1.0	2.0	.1	.1
.60225	1.0	2.0	2.0	.1	.1
.81948	2.0	2.0	2.0	.1	.1
.60593	1.0	10.0	2.0	.1	.1
.82573	2.0	10.0	2.0	.1	.1
.58520	1.0	1.0	3.0	.1	.1
.79379	2.0	1.0	3.0	.1	.1
.60093	1.0	2.0	3.0	.1	.1
.81713	2.0	2.0	3.0	.1	.1
.60593	1.0	10.0	3.0	.1	.1
.82573	2.0	10.0	3.0	.1	.1
.60180	1.0	1.0	1.0	.001	.1
.82848	2.0	1.0	1.0	.001	.1
.60180	1.0	2.0	1.0	.001	.1
.82848	2.0	2.0	1.0	.001	.1
.60180	1.0	10.0	1.0	.001	.1
.82848	2.0	10.0	1.0	.001	.1
.57758	1.0	1.0	2.0	.001	.1
.79889	2.0	1.0	2.0	.001	.1

Table II. (continued)

$Y_{RS}(\theta)$	θ	ℓ	n	B	A
.58364	1.0	2.0	2.0	.001	.1
.80536	2.0	2.0	2.0	.001	.1
.60006	1.0	10.0	2.0	.001	.1
.82574	2.0	10.0	2.0	.001	.1
.55898	1.0	1.0	3.0	.001	.1
.77543	2.0	1.0	3.0	.001	.1
.57230	1.0	2.0	3.0	.001	.1
.78999	2.0	2.0	3.0	.001	.1
.59929	1.0	10.0	3.0	.001	.1
.82447	2.0	10.0	3.0	.001	.1
.62268	1.0	1.0	1.0	10.0	1.0
.84744	2.0	1.0	1.0	10.0	1.0
.62268	1.0	2.0	1.0	10.0	1.0
.84744	2.0	2.0	1.0	10.0	1.0
.62268	1.0	10.0	1.0	10.0	1.0
.84744	2.0	10.0	1.0	10.0	1.0
.61922	1.0	1.0	2.0	10.0	1.0
.84111	2.0	1.0	2.0	10.0	1.0
.62249	1.0	2.0	2.0	10.0	1.0
.84709	2.0	2.0	2.0	10.0	1.0
.62268	1.0	10.0	2.0	10.0	1.0
.84744	2.0	10.0	2.0	10.0	1.0
.61796	1.0	1.0	3.0	10.0	1.0

Table II. (continued)

$Y_{RS}(\theta)$	θ	ℓ	n	B	A
.83880	2.0	1.0	3.0	10.0	1.0
.62243	1.0	2.0	3.0	10.0	1.0
.84697	2.0	2.0	3.0	10.0	1.0
.62268	1.0	10.0	3.0	10.0	1.0
.84744	2.0	10.0	3.0	10.0	1.0
.44546	1.0	1.0	1.0	.1	1.0
.59235	2.0	1.0	1.0	.1	1.0
.44546	1.0	2.0	1.0	.1	1.0
.59235	2.0	2.0	1.0	.1	1.0
.44546	1.0	10.0	1.0	.1	1.0
.59235	2.0	10.0	1.0	.1	1.0
.38419	1.0	1.0	2.0	.1	1.0
.50332	2.0	1.0	2.0	.1	1.0
.42819	1.0	2.0	2.0	.1	1.0
.56425	2.0	2.0	2.0	.1	1.0
.44546	1.0	10.0	2.0	.1	1.0
.59235	2.0	10.0	2.0	.1	1.0
.36025	1.0	1.0	3.0	.1	1.0
.46789	2.0	1.0	3.0	.1	1.0
.42237	1.0	2.0	3.0	.1	1.0
.55448	2.0	2.0	3.0	.1	1.0
.44546	1.0	10.0	3.0	.1	1.0
.59235	2.0	10.0	3.0	.1	1.0

Table II. (continued)

$Y_{RS}(\theta)$	θ	ℓ	n	B	A
.42400	1.0	1.0	1.0	.001	1.0
.60952	2.0	1.0	1.0	.001	1.0
.42400	1.0	2.0	1.0	.001	1.0
.60952	2.0	2.0	1.0	.001	1.0
.42400	1.0	10.0	1.0	.001	1.0
.60952	2.0	10.0	1.0	.001	1.0
.32948	1.0	1.0	2.0	.001	1.0
.48473	2.0	1.0	2.0	.001	1.0
.34775	1.0	2.0	2.0	.001	1.0
.50470	2.0	2.0	2.0	.001	1.0
.41494	1.0	10.0	2.0	.001	1.0
.59385	2.0	10.0	2.0	.001	1.0
.27737	1.0	1.0	3.0	.001	1.0
.41171	2.0	1.0	3.0	.001	1.0
.31055	1.0	2.0	3.0	.001	1.0
.44935	2.0	2.0	3.0	.001	1.0
.41103	1.0	10.0	3.0	.001	1.0
.58681	2.0	10.0	3.0	.001	1.0
.55170	1.0	1.0	1.0	10.0	10.0
.72449	2.0	1.0	1.0	10.0	10.0
.55170	1.0	2.0	1.0	10.0	10.0
.72449	2.0	2.0	1.0	10.0	10.0
.55170	1.0	10.0	1.0	10.0	10.0

Table II. (continued)

$Y_{RS}(\theta)$	θ	ℓ	n	B	A
.72449	2.0	10.0	1.0	10.0	10.0
.52773	1.0	1.0	2.0	10.0	10.0
.68495	2.0	1.0	2.0	10.0	10.0
.55034	1.0	2.0	2.0	10.0	10.0
.72215	2.0	2.0	2.0	10.0	10.0
.55170	1.0	10.0	2.0	10.0	10.0
.72449	2.0	10.0	2.0	10.0	10.0
.51955	1.0	1.0	3.0	10.0	10.0
.67167	2.0	1.0	3.0	10.0	10.0
.54989	1.0	2.0	3.0	10.0	10.0
.72137	2.0	2.0	3.0	10.0	10.0
.55170	1.0	10.0	3.0	10.0	10.0
.72449	2.0	10.0	3.0	10.0	10.0
.13311	1.0	1.0	1.0	.1	10.0
.16420	2.0	1.0	1.0	.1	10.0
.13311	1.0	2.0	1.0	.1	10.0
.16420	2.0	2.0	1.0	.1	10.0
.13311	1.0	10.0	1.0	.1	10.0
.16420	2.0	10.0	1.0	.1	10.0
.09558	1.0	1.0	2.0	.1	10.0
.11460	2.0	1.0	2.0	.1	10.0
.12242	1.0	2.0	2.0	.1	10.0
.14816	2.0	2.0	2.0	.1	10.0

Table II. (continued)

$Y_{RS}(\theta)$	θ	ℓ	n	B	A
.13311	1.0	10.0	2.0	.1	10.0
.16420	2.0	10.0	2.0	.1	10.0
.08464	1.0	1.0	3.0	.1	10.0
.10000	2.0	1.0	3.0	.1	10.0
.11914	1.0	2.0	3.0	.1	10.0
.14315	2.0	2.0	3.0	.1	10.0
.13311	1.0	10.0	3.0	.1	10.0
.16420	2.0	10.0	3.0	.1	10.0
.11102	1.0	1.0	1.0	.001	10.0
.17773	2.0	1.0	1.0	.001	10.0
.11102	1.0	2.0	1.0	.001	10.0
.17773	2.0	2.0	1.0	.001	10.0
.11102	1.0	10.0	1.0	.001	10.0
.17773	2.0	10.0	1.0	.001	10.0
.06373	1.0	1.0	2.0	.001	10.0
.10309	2.0	1.0	2.0	.001	10.0
.16307	2.0	10.0	2.0	.001	10.0
.04665	1.0	1.0	3.0	.001	10.0
.07491	2.0	1.0	3.0	.001	10.0
.05615	1.0	2.0	3.0	.001	10.0
.08639	2.0	2.0	3.0	.001	10.0
.10154	1.0	10.0	3.0	.001	10.0

Table II. (continued)

$Y_{RS}(\theta)$	θ	ℓ	n	B	A
.16307	2.0	10.0	2.0	.001	10.0
.505	1	1	1000	10	10
.648	2	1	1000	10	10
.549	1	2	1000	10	10
.7211	2	2	1000	10	10
.552	1	10	1000	10	10
.726	2	10	1000	10	10
.0682	1	1	1000	.1	10
.0781	2	1	1000	.1	10
.113	1	2	1000	.1	10
.134	2	2	1000	.1	10
.138	1	10	1000	.1	10
.164	2	10	1000	.1	10
.0145	1	1	1000	.001	10
.0194	2	1	1000	.001	10
.0264	1	2	1000	.001	10
.0348	2	2	1000	.001	10
.0583	1	10	1000	.001	10
.0781	2	10	1000	.001	10
.630	1	1	1000	10	.1
.861	2	1	1000	10	.1
.631	1	2	1000	10	.1

Table II. (continued)

$Y_{RS}(\theta)$	θ	ℓ	n	B	A
.862	2	2	1000	10	.1
.6311	1	10	1000	10	.1
.862	2	10	1000	10	.1
.570	1	1	1000	.1	.1
.769	2	1	1000	.1	.1
.598	1	2	1000	.1	.1
.812	2	2	1000	.1	.1
.605	1	10	1000	.1	.1
.825	2	10	1000	.1	.1
.441	1	1	1000	.001	.1
.601	2	1	1000	.001	.1
.511	1	2	1000	.001	.1
.696	2	2	1000	.001	.1
.575	1	10	1000	.001	.1
.785	2	10	1000	.001	.1
.615	1	1	1000	10	1.
.834	2	1	1000	10	1.
.622	1	2	1000	10	1.
.846	2	2	1000	10	1.
.622	1	10	1000	10	1.
.847	2	10	1000	10	1.
.317	1	1	1000	.1	1.
.403	2	1	1000	.1	1.

Table II. (continued)

$Y_{RS}(\theta)$	θ	ℓ	n	B	A
.411	1	2	1000	.1	1.
.535	2	2	1000	.1	1.
.445	1	10	1000	.1	1.
.592	2	10	1000	.1	1.
.119	1	1	1000	.001	1.
.161	2	1	1000	.001	1.
.190	1	2	1000	.001	1.
.255	2	2	1000	.001	1.
.318	1	10	1000	.001	1.
.430	2	10	1000	.001	1.

3.2 Results, Discussion and Conclusions of Calculations for the Electron Energy Spectra Resulting From Monoenergetic Electron Sources

The program used to obtain the results listed in Table III is explained in section 6.2. For illustration, several $z(E_o,E)$ spectra are plotted in Fig. 3. Calculations using the same I_o(74.1 ev) agreed with values calculated by McGinnies (20). Recent data by Berger and Seltzer (2) indicates that I_o should be 65.1 ev; therefore, the values listed in Table III were obtained with the mean ionization potential equal to 65.1 ev.

Since doubling the number of integration points only changed the results in and beyond the third place, it was assumed that less than 0.5 percent error was associated with the numerical procedure. No error estimate was given by Berger and Seltzer (2). However, comparison between the results obtained with I_o = 74.1 ev and with I_o = 65.1 ev results in the lower curve in Fig. 4 as the percent uncertainty in $z(E_o,E)$ as a function of E. Even if I_o were known accurately, the resulting spectra for source energies below 2 Kev would still be dubious since the cross section used in this work was not accurate below 2 Kev. However, no better cross section was available. Since the value of I_o given by Berger and Seltzer (2) was probably more accurate than the 65.1 ± 9 ev, the error obtained by comparison, the error estimate given by the lower curve in Fig. 4 was probably too large. Therefore, this curve was considered to be a reasonable estimate for the uncertainty of $z(E_o,E)$, including the error incurred by the numerical procedure.

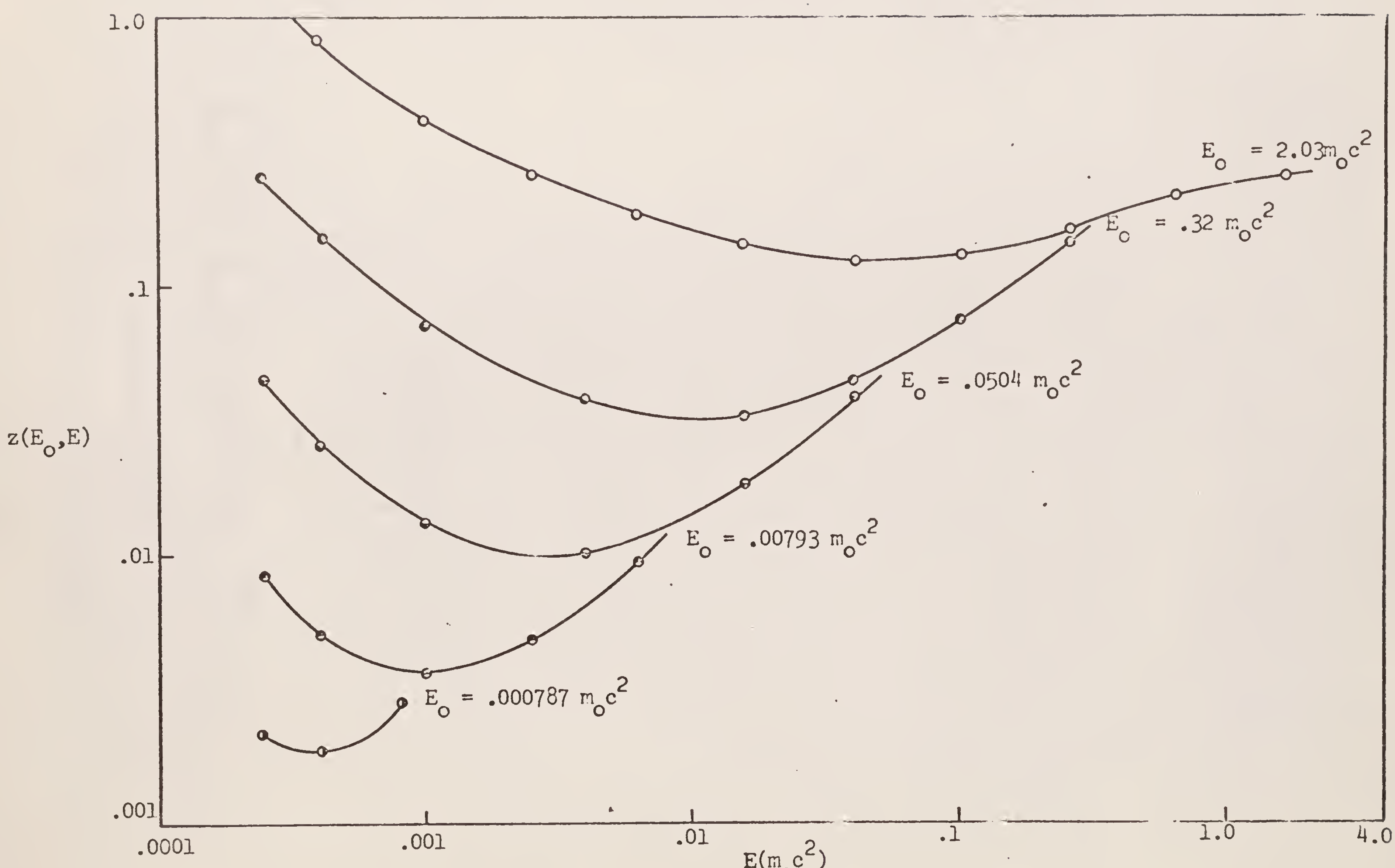

Fig. 3. Plot of $z(E_o,E)$ vs. E for Various Source Energies E_o

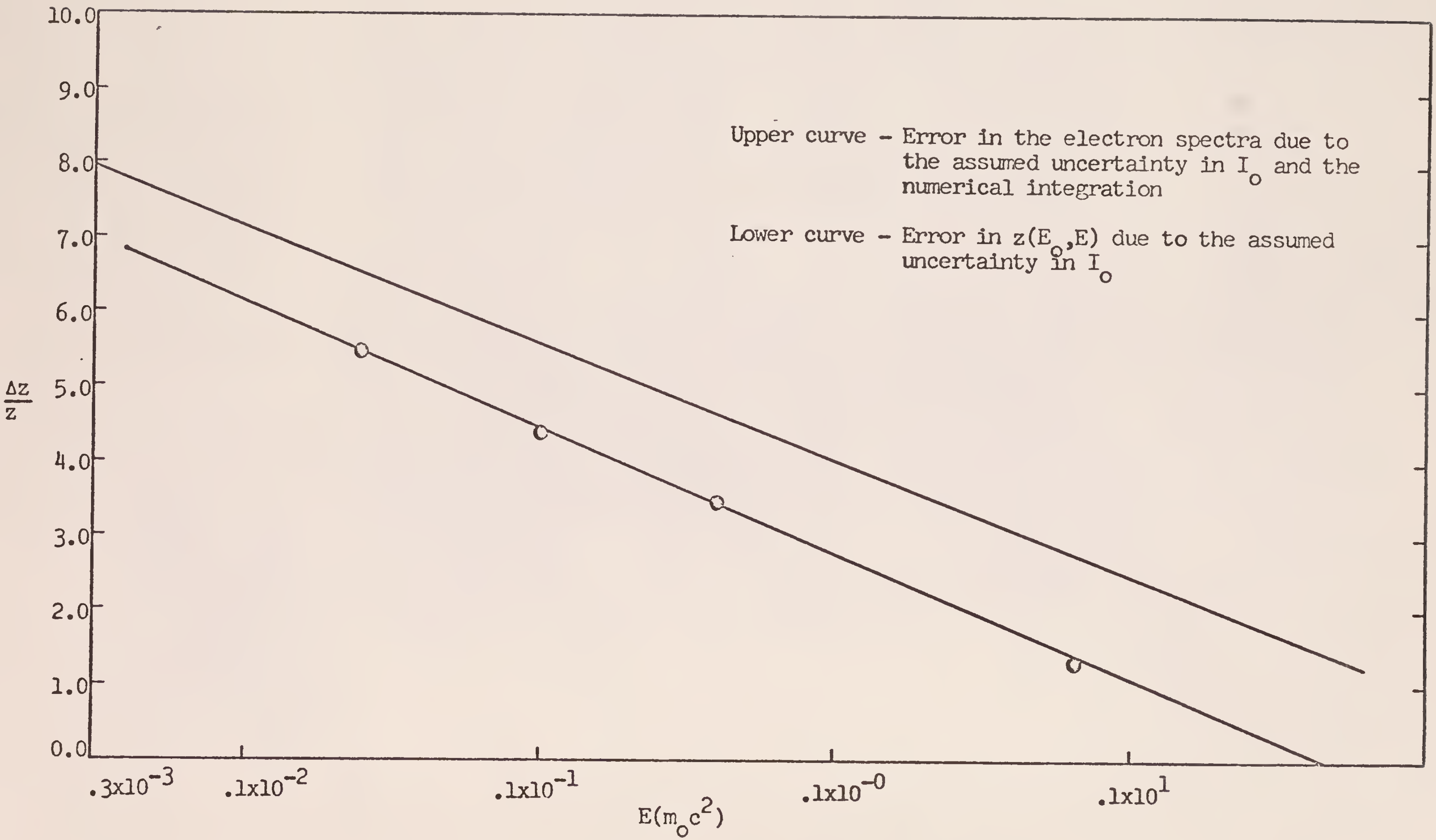

Fig. 4. Percent Uncertainty in $z(E_o,E)$ and $y(E)$ vs. E

Table III. Calculated Results for $z(E_o,E)((m_oc^2)^{-1}cm^{-1})$ for Various Values of E_o and E in m_oc^2 Units for I_o = 65.1 ev

$E_o \rightarrow$ / $E \downarrow$ m_oc^2	8.127	5.119	3.225	2.0314	1.2799	.8063	.5080	.3200	.20159	.12699	.0800
6.450	.2581										
4.063	.2614	.2679									
2.560	.2709	.2660	.2727								
1.612	.2808	.2668	.2619	.2685							
1.015	.2888	.2634	.2501	.2457	.2518						
.6400	.2943	.2553	.2325	.2208	.2171	.2224					
.4031	.2996	.2450	.2116	.1926	.1831	.1802	.1845				
.2539	.3080	.2368	.1923	.1656	.1507	.1434	.1412	.1447			
.1600	.3219	.2343	.1787	.1442	.1239	.1127	.1074	.1057	.1084		
.1007	.3431	.2391	.1725	.1305	.1049	.0899	.0817	.07785	.0766	.07871	
.0634	.3724	.2518	.1741	.1246	.0936	.0748	.0640	.05810	.0552	.05439	.05593
.0400	.4103	.2722	.1829	.1255	.0892	.0666	.0530	.04511	.04083	.03875	.03811
.0251	.4578	.30003	.1982	.1324	.0903	.06377	.0473	.03740	.03170	.02857	.02704
.0158	.5166	.3368	.2201	.1446	.0961	.06520	.0458	.03378	.02654	.02232	.02001

Table III. (continued)

$E_o \rightarrow$ / $E \downarrow$ / m_oc^2	8.127	5.119	3.225	2.0314	1.2799	.8063	.5080	.3200	.20159	.12699	.0800
.0100	.5897	.3833	.2491	.1622	.1062	.07029	.0474	.03323	.02430	.01895	.01581
.00629	.6819	.4426	.2870	.1860	.1208	.07883	.05202	.03499	.02438	.01880	.01368
.00396	.8012	.5197	.3367	.2178	.1408	.09122	.05942	.03913	.02623	.01820	.01320
.00250	.9605	.6229	.4033	.2607	.1683	.1086	.07030	.04574	.03009	.02011	.01389
.00157	1.182	.7669	.4964	.3208	.2070	.1334	.08616	.0556	.03624	.02381	.01587
.000992	1.510	.9797	.6343	.4100	.2644	.1704	.1098	.07092	.04585	.02985	.01962
.000625	2.039	1.322	.8566	.5535	.3572	.2302	.1483	.0956	.06182	.04011	.02605
.000393	3.021	1.959	1.269	.8204	.5293	.3412	.2199	.1417	.0916	.05934	.03847
.000248	5.460			1.483	.9571	.6170	.3976	.2565	.1657	.1072	.06968

Table III. (continued)

$E_o \rightarrow$ / $E \downarrow$ $m_o c^2$	.0504	.03174	.02000	.0126	.00793	.005	.003149	.001984	.001250	.000787	.000496
.0400	.03926										
.0251	.02656	.02743									
.0158	.01887	.01851	.01916								
.0100	.01408	.01322	.01295	.01344							
.00629	.01131	.01000	.009343	.009129	.009513						
.00396	.01003	.008213	.007194	.006678	.006508	.006811					
.00250	.01001	.007509	.006076	.005267	.004854	.004713	.004959				
.00157	.01091	.007813	.005780	.004616	.003953	.003610	.003490	.003697			
.000992	.01302	.008928	.006348	.004627	.003642	.003075	.002777	.002668	.002852		
.000625	.01711	.01129	.007727	.005465	.003927	.003042	.002527	.002249	.002141	.002325	
.000393	.02512	.01649	.01088	.007305	.005148	.003671	.002796	.002278	.001991	.001870	.002086
.000248	.04528	.02963	.01938	.01286	.008575	.005707	.004254	.003112	.002484	.002119	.001943

3.3 Results, Discussion and Conclusions of the Electron Spectrum Resulting From Co^{60} Irradiation

The differential cross section for the production of electrons between E and E + dE by Co^{60} gamma rays is given in Fig. 5. Tabular values for various sources are given in Table IV. These results are in excellent agreement with those given by Johns and Laughlin (14).

The electron energy spectrum listed in Table V and plotted in Fig. 6 is in close agreement with that computed by Harder (12); Table VI gives a comparison between several values given by Harder (12) and those obtained in this work. The spectrum obtained by Harder (12) used a somewhat different approach than that used for this work. The spectrum was also calculated using continuous slowing theory with the results listed in Table V and plotted in Fig. 6. The spectrum of Fig. 6 is normalized to 2 photons/ cm^2sec (one photon of energy 1.173 and the other of 1.332 Mev). If one chooses to normalize the spectrum to 1 rad/hr, the values listed must be multiplied by 2.33×10^5.

Inaccuracies in $y_g(E)$ $S_e^g(E_o)$, $z(E_o,E)$ would be inherent inaccuracies in the numerical integration and uncertainties in I_o. Since changing the number of integration points from 30 to 50 changed the results beyond the second place, 50 points were used. One percent error was assumed to be due to the numerical scheme. The most error one could expect in $y_g(E)$ is a 1 percent error superimposed on the error in $z(E_o,E)$. This error is presented in the upper curve in Fig. 4.

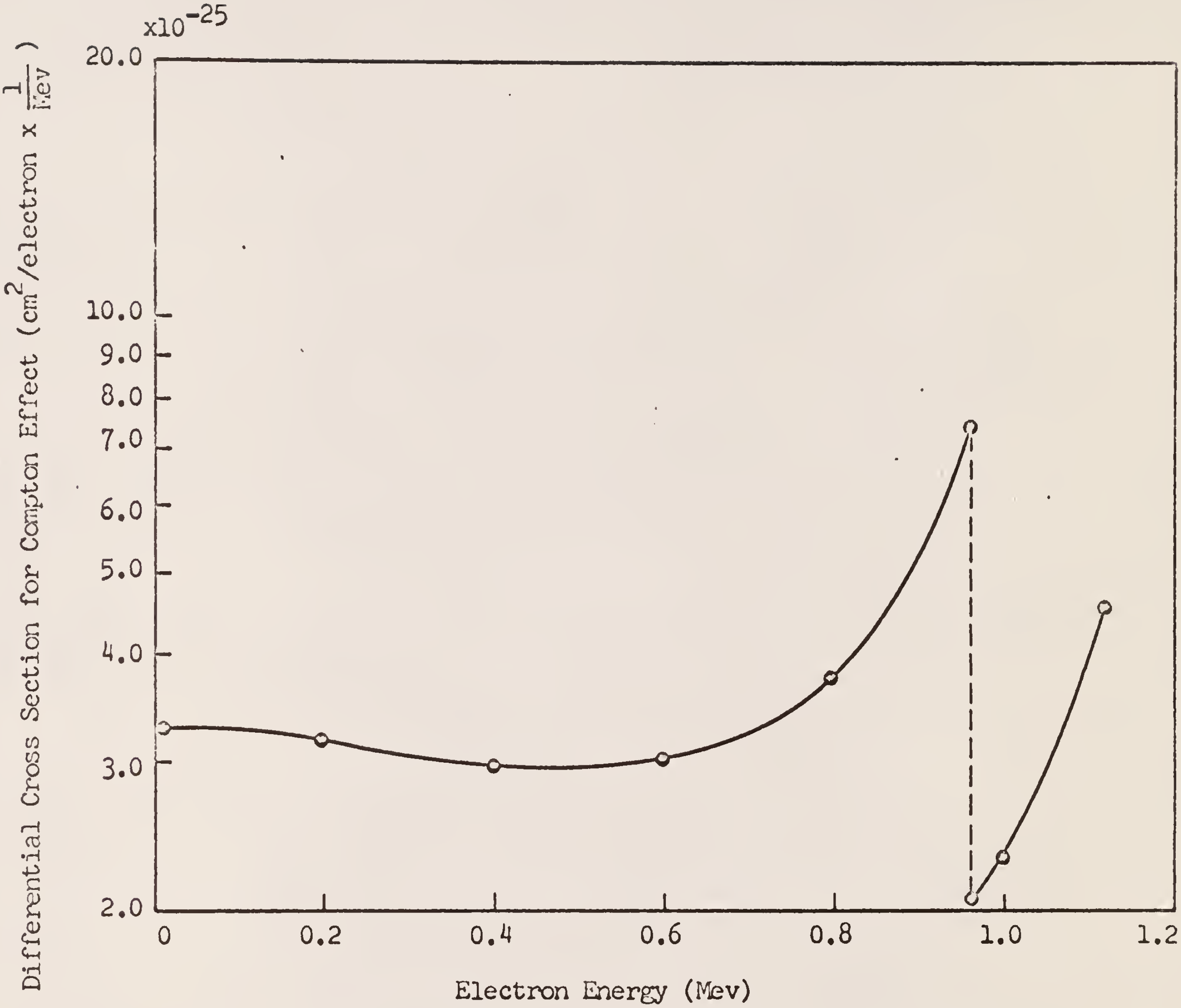

Fig. 5. Plot of the Total Differential Cross Section for the Production of Electrons of Energy E vs. Electron Energy for Co^{60} Irradiation

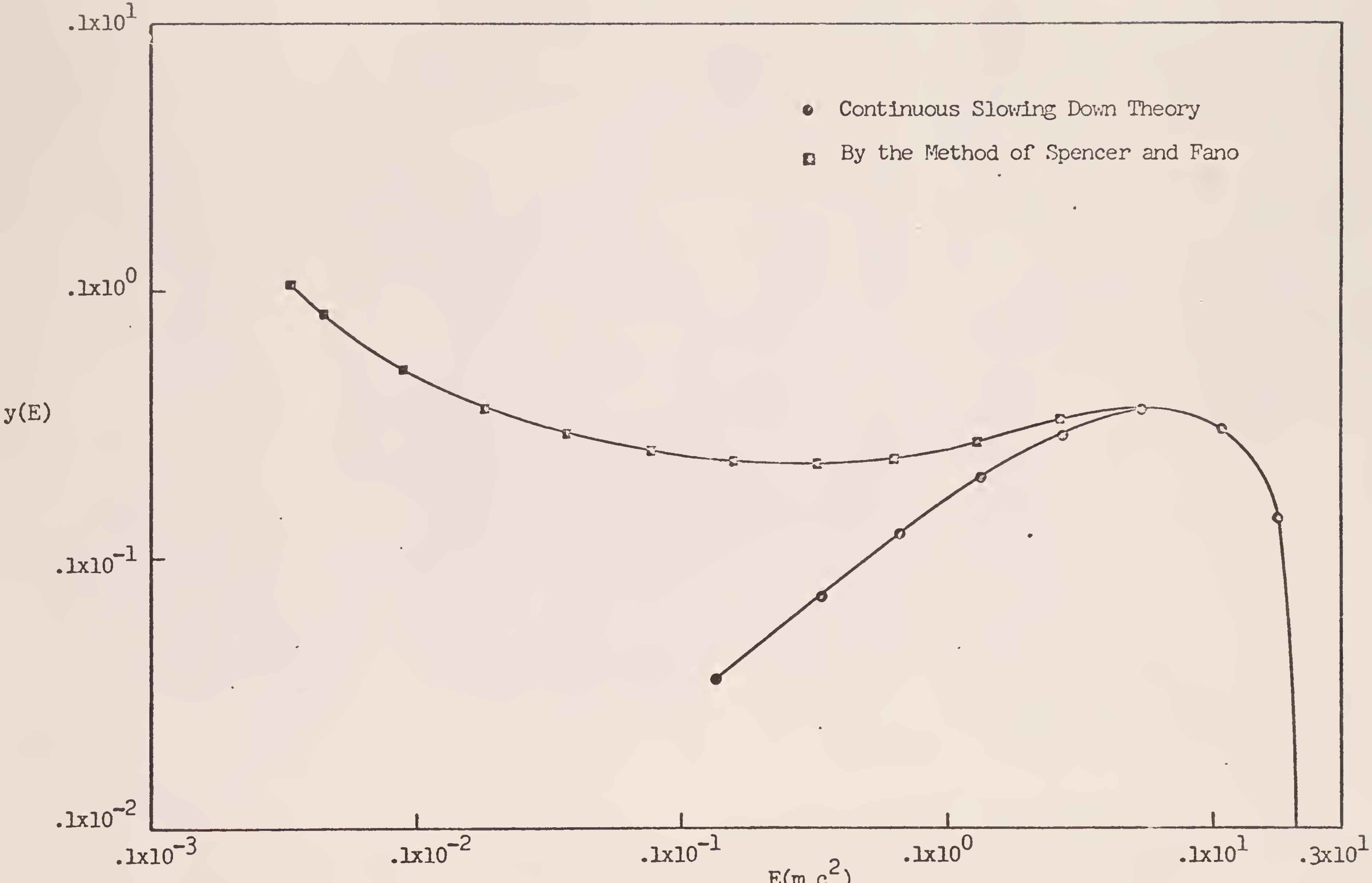

Fig. 6. Differential Electron Flux ($cm^{-2}sec^{-1}(m_oc^2)^{-1}$) vs. Electron Energy ($m_oc^2$) Resulting From Co^{60} Irradiation

Table IV. Differential Cross Section, $d_e\sigma(E)/dE$, for the Number of Electrons with Kinetic Energies Between E and E + dE Scattered per Electron for Monoenergetic Photon Sources of 1.17 and 1.33 Mev

E(Mev)	$d_e\sigma(E)/dE$ (cm^2 $electron^{-1}$ Mev^{-1})$x10^{-25}$ 1.17 Mev Photon	1.33 Mev Photon
0	1.858	1.438
0.10	1.791	1.398
0.20	1.731	1.303
0.30	1.682	1.333
0.40	1.650	1.313
0.50	1.648	1.307
0.60	1.703	1.323
0.70	1.871	1.376
0.80	2.306	1.499
0.90	3.502	1.765
0.96	5.359	2.062
1.00		2.376
1.10		4.063
1.116		4.585

Table V. Electron Energy Spectra Resulting From Co^{60} Irradiation Calculated by the Method of Spencer and Fano $y_g(E)$ and by the Method of Continuous Slowing-Down Theory $y_g^{SP}(E)$ Listed with the Electron Energy E in m_oc^2 Units

$E(m_oc^2)$	$y_g(E)(cm^{-2}sec^{-1}(m_oc^2)^{-1})$	$y_g^{SP}(E)(cm^{-2}sec^{-1}(m_oc^2)^{-1})$
0.2184E + 01	0.0000E - 99	0.0000E - 99
0.1733E + 01	0.1464E - 01	0.1432E - 01
0.1375E + 01	0.2538E - 01	0.2497E - 01
0.1092E + 01	0.3129E - 01	0.3082E - 01
0.8667E + 00	0.3485E - 01	0.3417E - 01
0.6879E + 00	0.3665E - 01	0.3562E - 01
0.5460E + 00	0.3720E - 01	0.3552E - 01
0.4333E + 00	0.3664E - 01	0.3421E - 01
0.3439E + 00	0.3541E - 01	0.3201E - 01
0.2730E + 00	0.3368E - 01	0.2925E - 01
0.2166E + 00	0.3178E - 01	0.2622E - 01
0.1719E + 00	0.2983E - 01	0.2312E - 01
0.1365E + 00	0.2801E - 01	0.2012E - 01
0.1083E + 00	0.2640E - 01	0.1733E - 01
0.8599E - 01	0.2505E - 01	0.1480E - 01
0.6825E - 01	0.2397E - 01	0.1255E - 01
0.5417E - 01	0.2318E - 01	0.1060E - 01
0.4299E - 01	0.2265E - 01	0.8919E - 02

Table V. (continued)

$E(m_oc^2)$	$y_g(E)(cm^{-2}sec^{-1}(m_oc^2)^{-1})$	$y_g^{SP}(E)(cm^{-2}sec^{-1}(m_oc^2)^{-1})$
0.3412E - 01	0.2237E - 01	0.7483E - 02
0.2708E - 01	0.2232E - 01	0.6269E - 02
0.2149E - 01	0.2249E - 01	0.5247E - 02
0.1706E - 01	0.2286E - 01	0.4391E - 02
0.1354E - 01	0.2342E - 01	0.3676E - 02
0.1074E - 01	0.2416E - 01	0.3081E - 02
0.8531E - 02	0.2510E - 01	0.2586E - 02
0.6771E - 02	0.2624E - 01	0.2175E - 02
0.5374E - 02	0.2759E - 01	0.1833E - 02
0.4265E - 02	0.2919E - 01	0.1550E - 02
0.3385E - 02	0.3108E - 01	0.1316E - 02
0.2687E - 02	0.3331E - 01	0.1121E - 02
0.2132E - 02	0.3595E - 01	0.9610E - 03
0.1692E - 02	0.3911E - 01	0.8281E - 03
0.1343E - 02	0.4295E - 01	0.7185E - 03
0.1066E - 02	0.4867E - 01	0.6287E - 03
0.8464E - 03	0.5364E - 01	0.5558E - 03
0.6718E - 03	0.6133E - 01	0.4977E - 03
0.5332E - 03	0.7156E - 01	0.4529E - 03
0.4232E - 03	0.8596E - 01	0.4212E - 03
0.3359E - 03	0.1074E - 01	0.4034E - 03

Table VI. Comparison of y(E) Calculated in This Work and y(E) Obtained by Harder With the Spectra Normalized to a Photon Absorbed Dose Rate of 1 rad/sec

E(Mev)	y(E) - Harder	y(E) - This Work
1.00	$0.56x10^{7}$	$0.5x10^{7}$
0.20	$2.9x10^{7}$	$3.1x10^{7}$
0.10	$2.7x10^{7}$	$2.6x10^{7}$
0.02	$1.8x10^{7}$	$1.9x10^{7}$
0.01	$1.8x10^{7}$	$1.9x10^{7}$

3.4 Results, Discussion and Conclusions of the Determination of the Electron Energy Spectra Resulting From Fast Neutron Irradiation

The electron sources resulting from the slowing down of alpha particles and protons, as determined from the program described in section 6.4, are listed in Table VII and plotted in Figs. 7 and 8. The resulting electron energy spectra, $y_a(E)$ and $y_p(E)$, are listed in Tables VIII and IX and plotted in Figs. 8 and 10.

The electron energy spectrum resulting from the proton source was not obtained for electron energies below .000972, but calculations for a paper by Faw and Miller (7) using a slightly different model suggested that further calculations were unnecessary. Calculations for $y_a^{SP}(E)$ and $y_p^{SP}(E)$ using continuous slowing down theory are listed in Tables VIII and IX. The results were not plotted since the results were very close to those obtained by the method of Spencer and Fano (22).

Errors would be only a result of the numerical integrations, added to the uncertainty in $z(E_o,E)$. No appreciable change in the results were obtained above 30 integration points. Therefore, it was assumed that the error associated with the numerical integration was approximately 1 percent. This one percent error, superimposed on the lower curve in Fig. 4 was the maximum error that could be associated with the spectra $y_a(E)$ and $y_p(E)$.

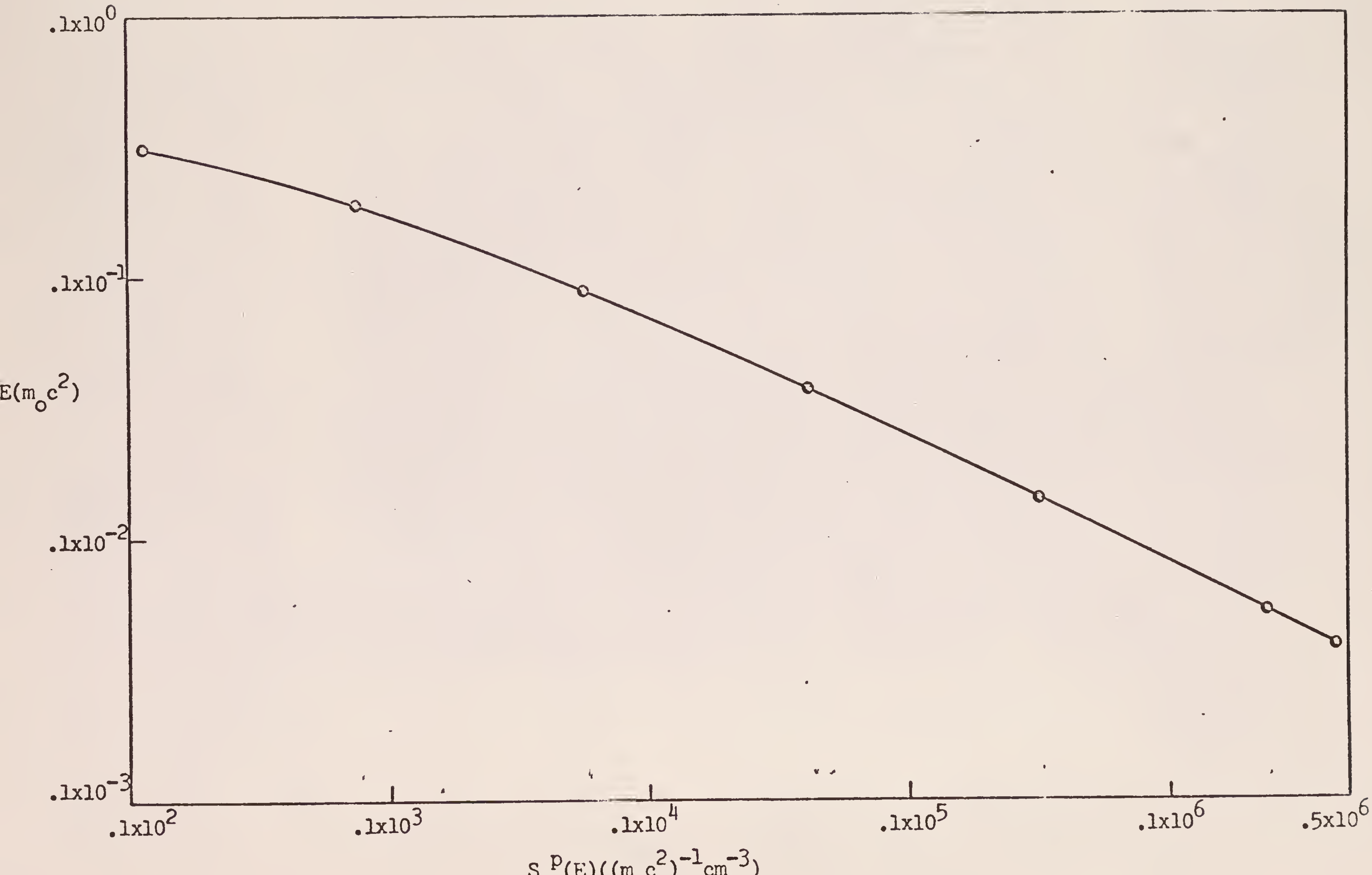

Fig. 7. Plot of the Electron Energy in m_oc^2 Units vs. the Electron Source Resulting From a Given Proton

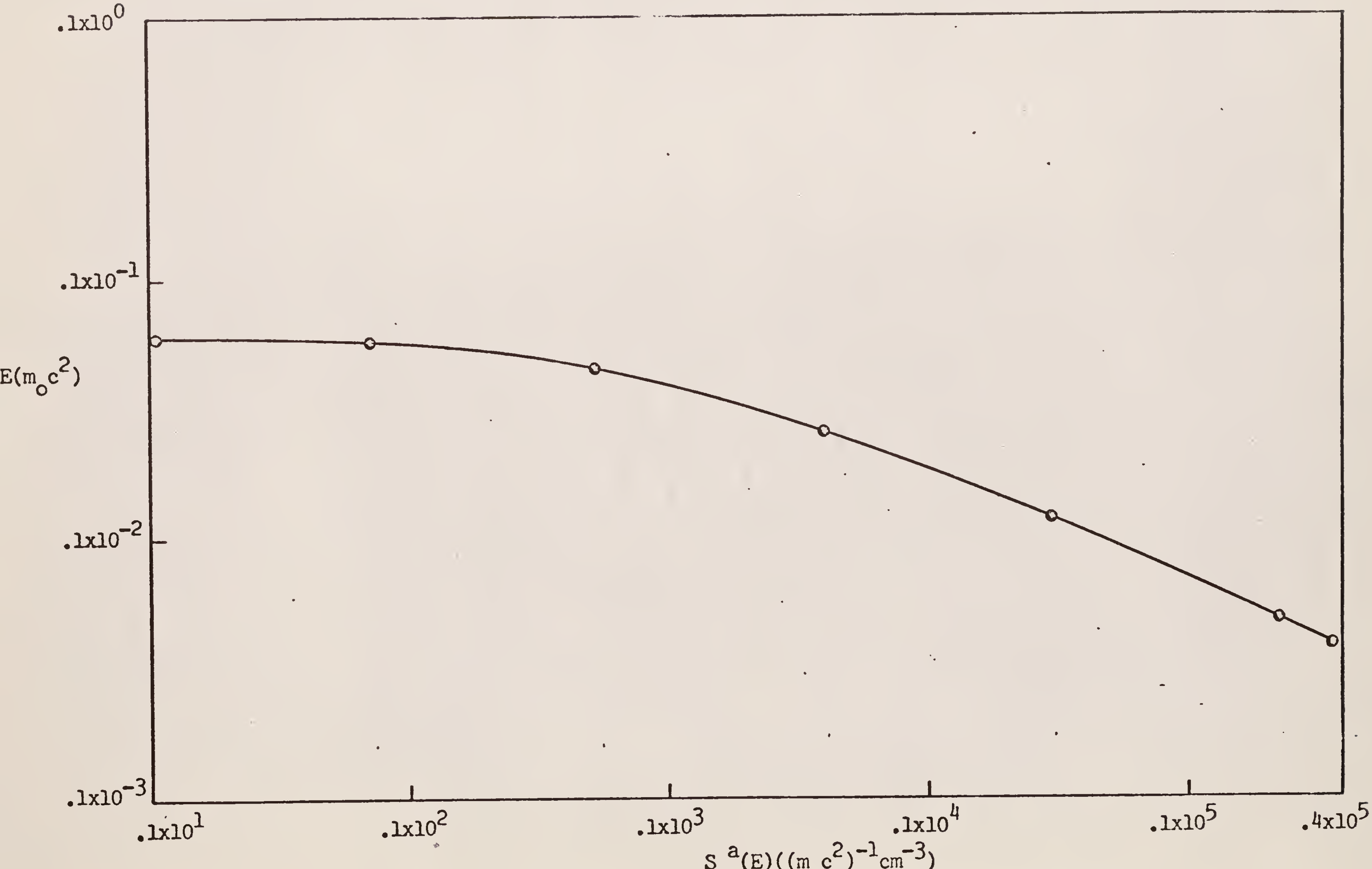

Fig. 8. Plot of the Electron Energy in Units of m_oc^2 vs. the Electron Source Resulting From a Given Alpha Particle Flux

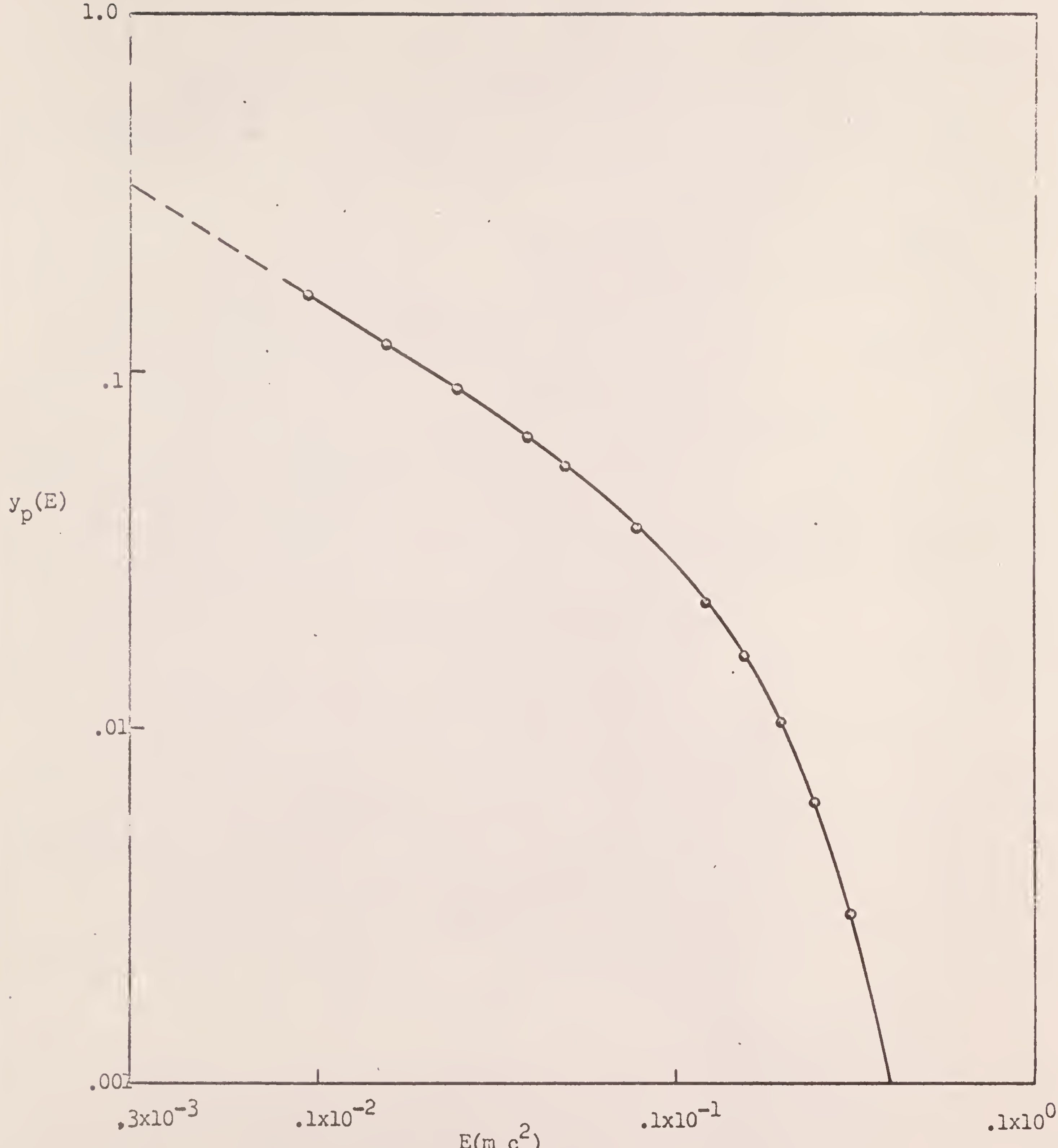

Fig. 9. Plot of the Electron Energy Spectrum $y_p(E)(cm^{-2}sec^{-1}(m_oc^2)^{-1})$ Resulting From Proton Irradiation vs. Electron Energy in m_oc^2 Units

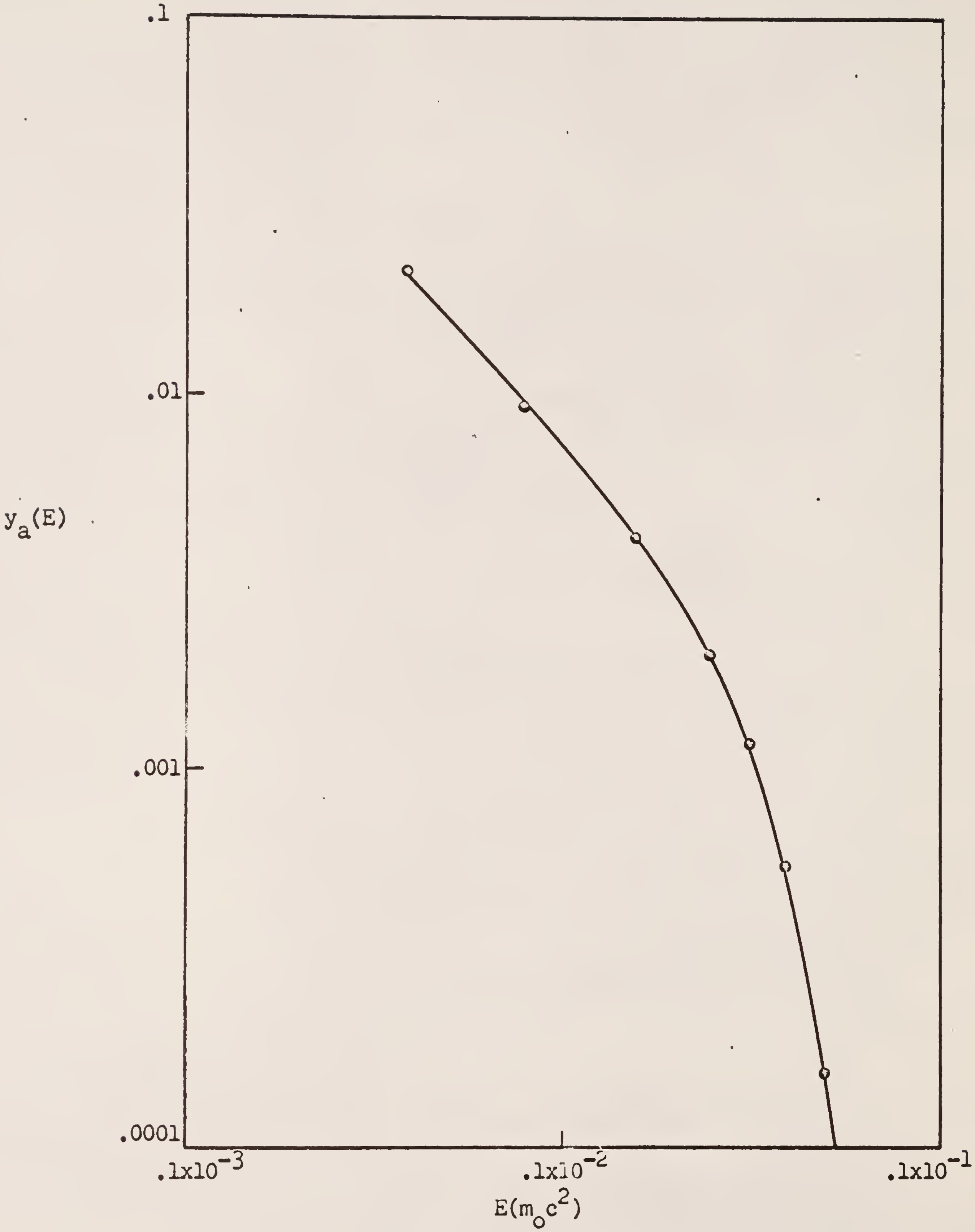

Fig. 10. Plot of the Electron Energy Spectrum $y_a(E)(cm^{-2}sec^{-1}(m_oc^2)^{-1})$ Resulting from Alpha Particle Irradiation vs. Electron Energy in m_oc^2 Units

Table VII. Initial Electron Sources Resulting From Alpha and Proton Irradiation

$E(m_oc^2)$	$S_e^a(E)$	$E(m_oc^2)$	$S_e^p(E)$
.622E-02	.521E-02	.622E-01	.203E-04
.586E-02	.663E 01	.558E-01	.155E-00
.553E-02	.146E 02	.501E-01	.729E-00
.521E-02	.243E 02	.450E-01	.189E 01
.491E-02	.359E 02	.404E-01	.385E 01
.463E-02	.496E 02	.362E-01	.689E 01
.437E-02	.658E 02	.325E-01	.113E 02
.412E-02	.849E 02	.292E-01	.176E 02
.388E-02	.107E 03	.262E-01	.263E 02
.366E-02	.133E 03	.235E-01	.383E 02
.345E-02	.164E 03	.211E-01	.543E 02
.325E-02	.199E 03	.190E-01	.756E 02
.307E-02	.240E 03	.170E-01	.103E 03
.289E-02	.288E 03	.153E-01	.139E 03
.273E-02	.343E 03	.137E-01	.186E 03
.257E-02	.406E 03	.123E-01	.247E 03
.242E-02	.480E 03	.110E-01	.324E 03
.228E-02	.564E 03	.994E-02	.434E 03
.215E-02	.661E 03	.893E-02	.552E 03
.203E-02	.772E 03	.801E-02	.714E 03
.191E-02	.900E 03	.719E-02	.919E 03

Table VII. (continued)

$E(m_oc^2)$	$S_e^a(E)$	$E(m_oc^2)$	$S_e^p(E)$
.180E-02	.104E 04	.646E-02	.117E 04
.170E-02	.121E 04	.580E-02	.150E 04
.160E-02	.140E 04	.520E-02	.192E 04
.151E-02	.162E 04	.467E-02	.245E 04
.142E-02	.187E 04	.419E-02	.311E 04
.134E-02	.216E 04	.376E-02	.394E 04
.127E-02	.248E 04	.338E-02	.499E 04
.119E-02	.286E 04	.303E-02	.630E 04
.112E-02	.328E 04	.272E-02	.795E 04
.105E-02	.377E 04	.244E-02	.100E 05
.100E-02	.433E 04	.219E-02	.126E 05
.946E-03	.496E 04	.197E-02	.158E 05
.892E-03	.569E 04	.177E-02	.199E 05
.841E-03	.652E 04	.159E-02	.249E 05
.793E-03	.746E 04	.142E-02	.313E 05
.747E-03	.854E 04	.128E-02	.392E 05
.705E-03	.977E 04	.115E-02	.491E 05
.664E-03	.111E 05	.103E-02	.615E 05
.626E-03	.127E 05	.927E-03	.770E 05
.590E-03	.146E 05	.832E-03	.963E 05
.557E-03	.166E 05	.747E-03	.120E 06

Table VII. (continued)

$E(m_oc^2)$	$S_e^a(E)$	$E(m_oc^2)$	$S_e^p(E)$
.525E-03	.190E 05	.671E-03	.150E 06
.495E-03	.217E 05	.602E-03	.188E 06
.467E-03	.248E 05	.540E-03	.234E 06
.440E-03	.284E 05	.485E-03	.293E 06
.415E-03	.324E 05	.435E-03	.355E 06
.391E-03	.370E 05	.391E-03	.457E 06

Table VIII. Energy Spectra of Electrons Resulting from Alpha Irradiation Calculated by the Method of Spencer and Fano $y_a(E)$, and by the Method of Continuous Slowing-Down Theory $y_a^{SP}(E)$, Listed with the Electron Energy E in m_oc^2 Units

$E(m_oc^2)$	$y_a(E)(cm^{-2}sec^{-1}(m_oc^2)^{-1})$	$y_a^{SP}(E)(cm^{-2}sec^{-1}(m_oc^2)^{-1})$
0.6223E - 02	0.0000E - 99	0.000E - 99
0.4939E - 02	0.1541E - 03	0.150E - 03
0.3920E - 02	0.5665E - 03	0.556E - 03
0.3111E - 02	0.1190E - 02	0.118E - 02
0.2469E - 02	0.2018E - 02	0.201E - 02
0.1960E - 02	0.3015E - 02	0.302E - 02
0.1555E - 02	0.4235E - 02	0.424E - 02
0.1234E - 02	0.5634E - 02	0.566E - 02
0.9801E - 03	0.7387E - 02	0.736E - 02
0.7779E - 03	0.9451E - 02	0.941E - 02
0.6174E - 03	0.1223E - 01	0.119E - 01
0.4900E - 03	0.1556E - 01	0.152E - 01
0.3889E - 03	0.2103E - 01	0.197E - 01

Table IX. Energy Spectra of Electrons Resulting from Proton Irradiation Calculated by the Method of Spencer and Fano $y_p(E)$, and by the Method of Continuous Slowing-Down Theory $y_p^{SP}(E)$, Listed with the Electron Energy E in m_oc^2 Units

$E(m_oc^2)$	$y_p(E)(cm^{-2}sec^{-1}(m_oc^2)^{-1})$	$y_p^{SP}(E)(cm^{-2}sec^{-1}(m_oc^2)^{-1})$
0.6223E - 01	0.0000E - 99	0.000E - 99
0.4939E - 01	0.1709E - 03	0.170E - 03
0.3920E - 01	0.1045E - 02	0.104E - 02
0.3111E - 01	0.3001E - 02	0.303E - 02
0.2469E - 01	0.6183E - 02	0.623E - 02
0.1960E - 01	0.1045E - 01	0.106E - 01
0.1555E - 01	0.1589E - 01	0.161E - 01
0.1234E - 01	0.2206E - 01	0.225E - 01
0.9801E - 02	0.2925E - 01	0.297E - 01
0.7779E - 02	0.3696E - 01	0.377E - 01
0.6174E - 02	0.4570E - 01	0.464E - 01
0.4900E - 02	0.5486E - 01	0.558E - 01
0.3889E - 02	0.6531E - 01	0.660E - 01
0.3087E - 02	0.7637E - 01	0.771E - 01
0.2450E - 02	0.8924E - 01	0.892E - 01
0.1944E - 02	0.1032E - 00	0.102E - 00
0.1543E - 02	0.1201E - 00	0.117E - 00
0.1225E - 02	0.1390E - 00	0.135E - 00
0.9724E - 03	0.1632E - 00	0.155E - 00

3.5 Results, Discussion and Conclusions of the Determination of a Low Energy Cross Section and Low Energy Stopping Power for Water

The parameters AKT, a and b are plotted in Figs. 11, 12 and 13, respectively, for the energy range that $k_M(E,\tau)$ is valid; a straight line extrapolation is shown for lower energies. The parameters AKT, a and b are listed in Table X. It was first attempted to determine the behavior of a and b at energies below 2 Kev by making a linear extrapolation for AKT on a log-log plot and calculating a and b, utilizing the program listed in section 6.5.2. However, a and b diverged. L(E) is not valid below 2 Kev, so those numbers were disregarded.

Due to the linear behavior of these parameters between $.002mc^2$ and $0.1mc^2$, it is assumed they are linear below $0.1mc^2$ and the approximation is reasonably accurate to at least 400 ev. AKT, a and b were approximated by straight lines over the entire energy range of interest for simplicity of calculation. The error in fitting the curve resulted in, at most, a 1 percent error.

The stopping power calculated with the sythesized cross section is compared to the analytic formula (3) in Fig. 15.

In the energy range where the Moller formula is accurate, this synthesized cross section is an improvement on the Moller formula, since the synthesized cross section takes into account the small energy losses to within the uncertainty of the experimental data.

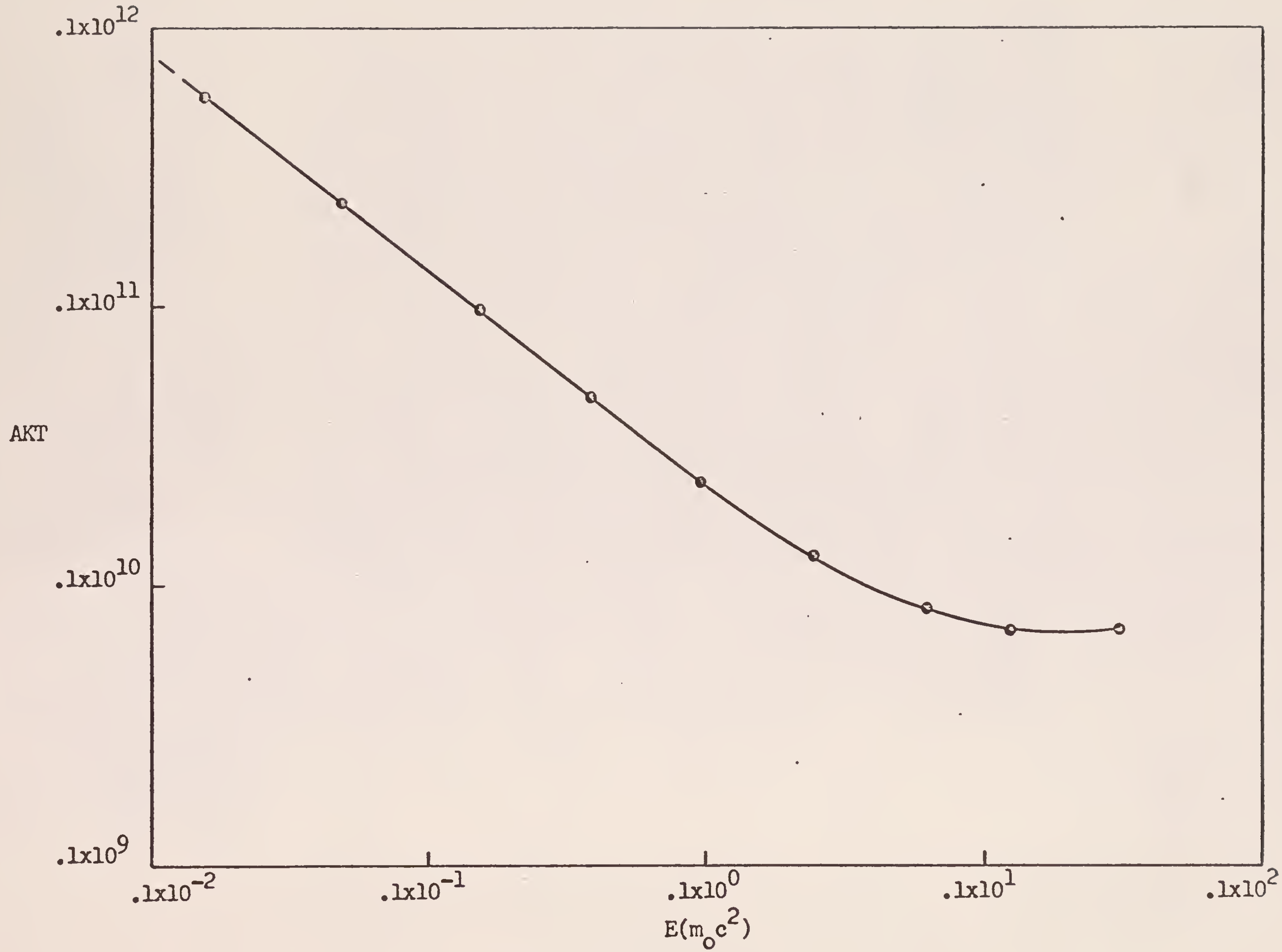

Fig. 11. Plot of AKT vs. Electron Energy

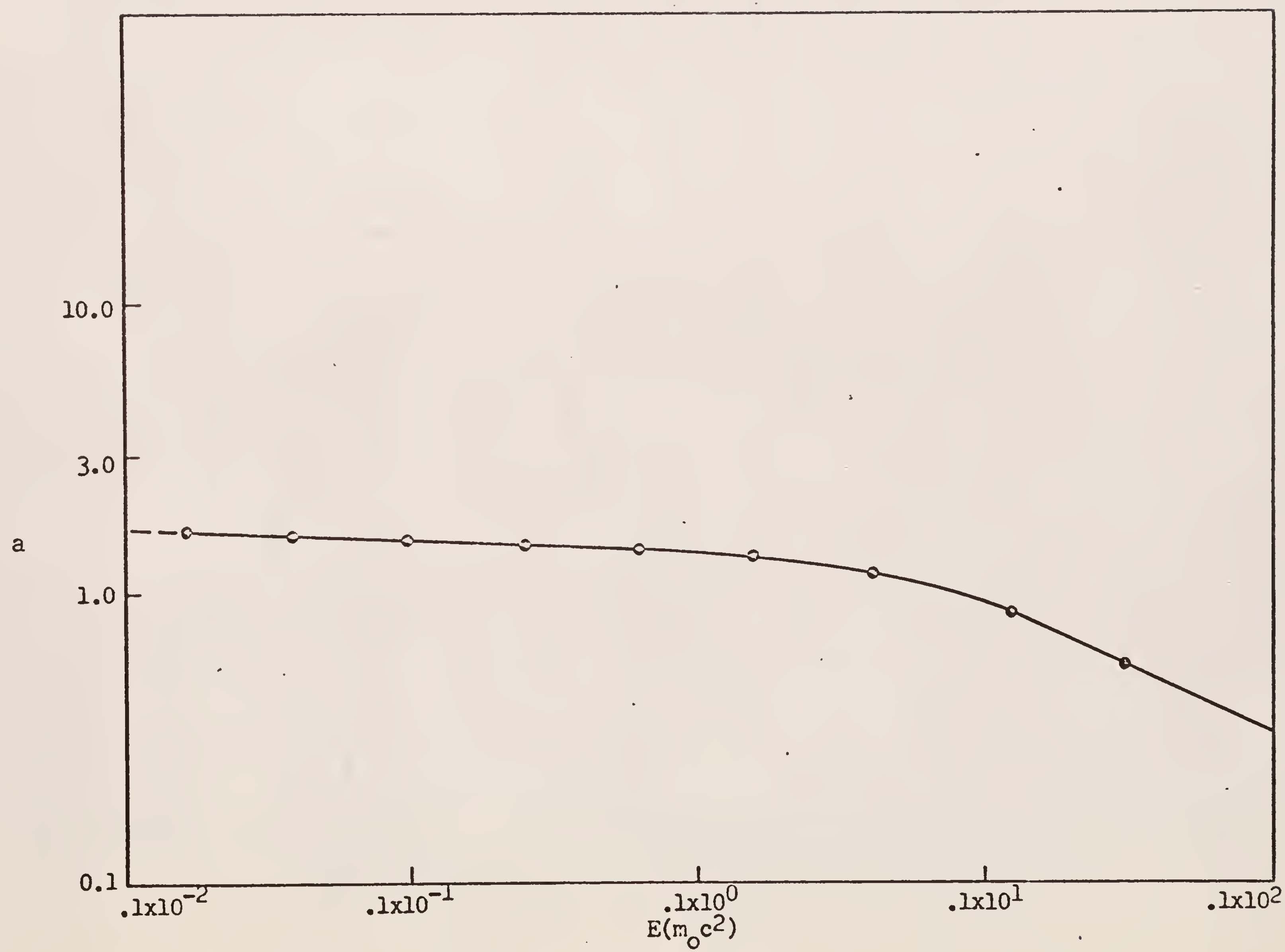

Fig. 12. Plot of Parameter a vs. Electron Energy

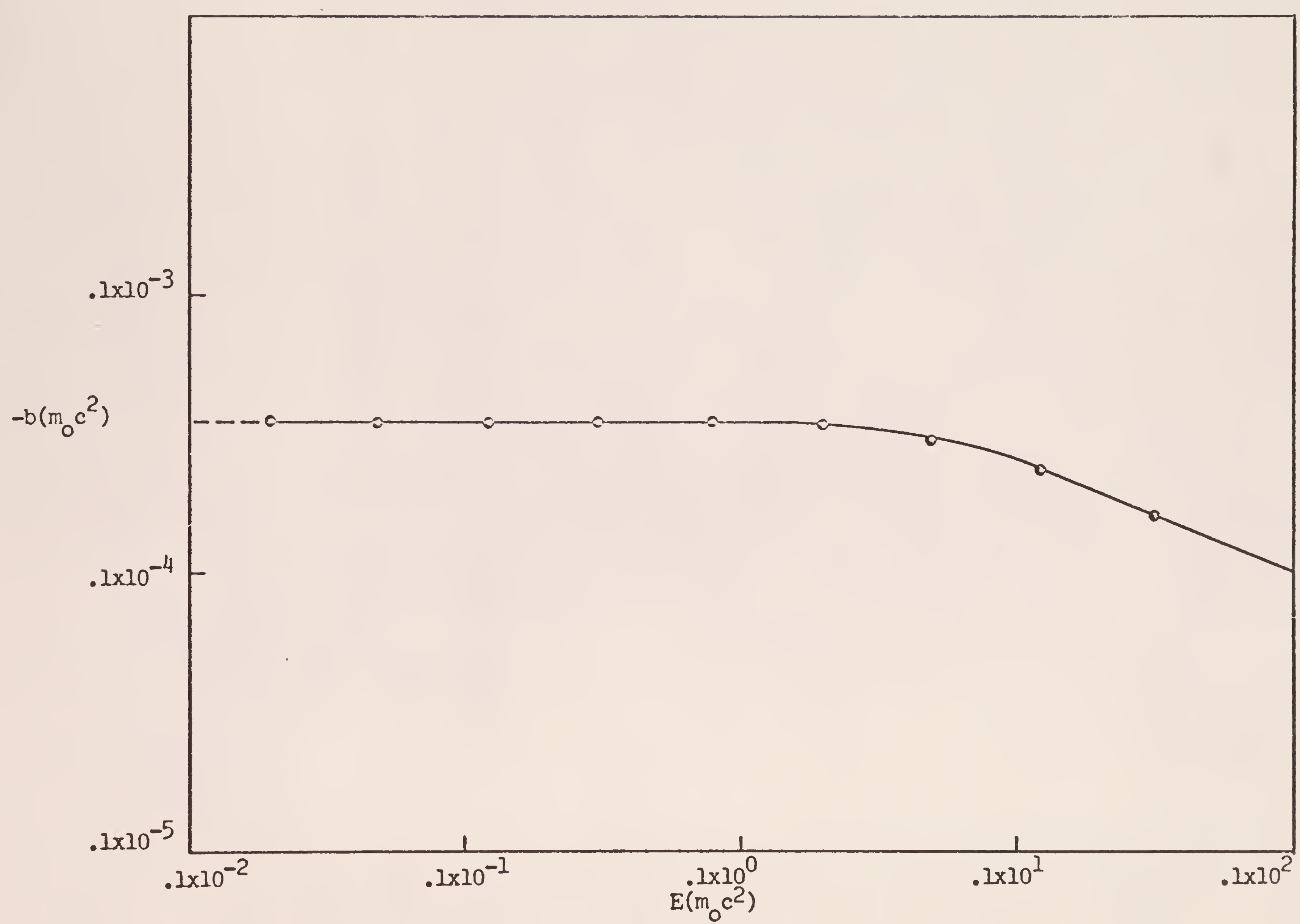

Fig. 13. Plot of Parameter b vs. Electron Energy

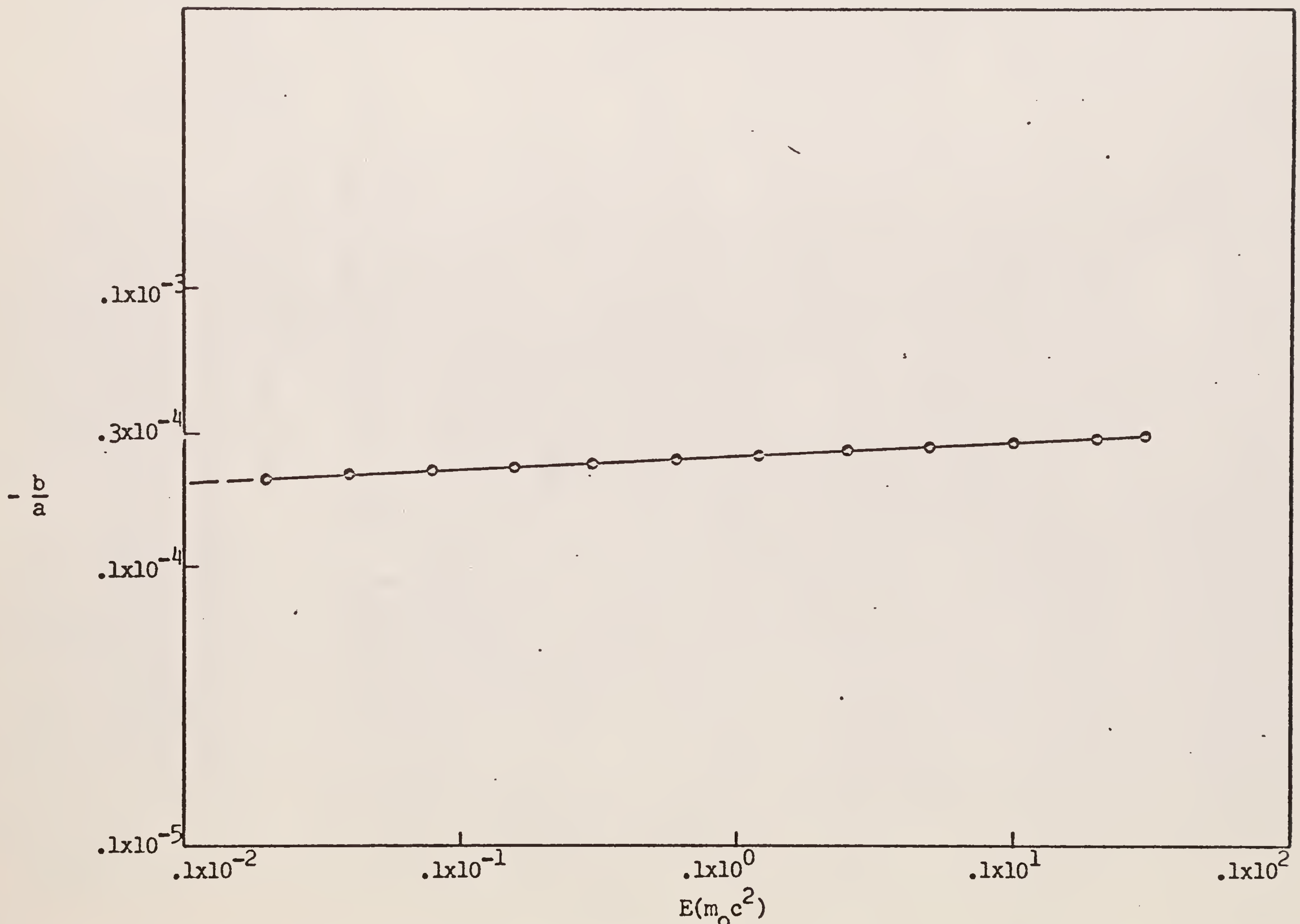

Fig. 14. Plot of $\frac{b}{a}$ vs. Electron Energy

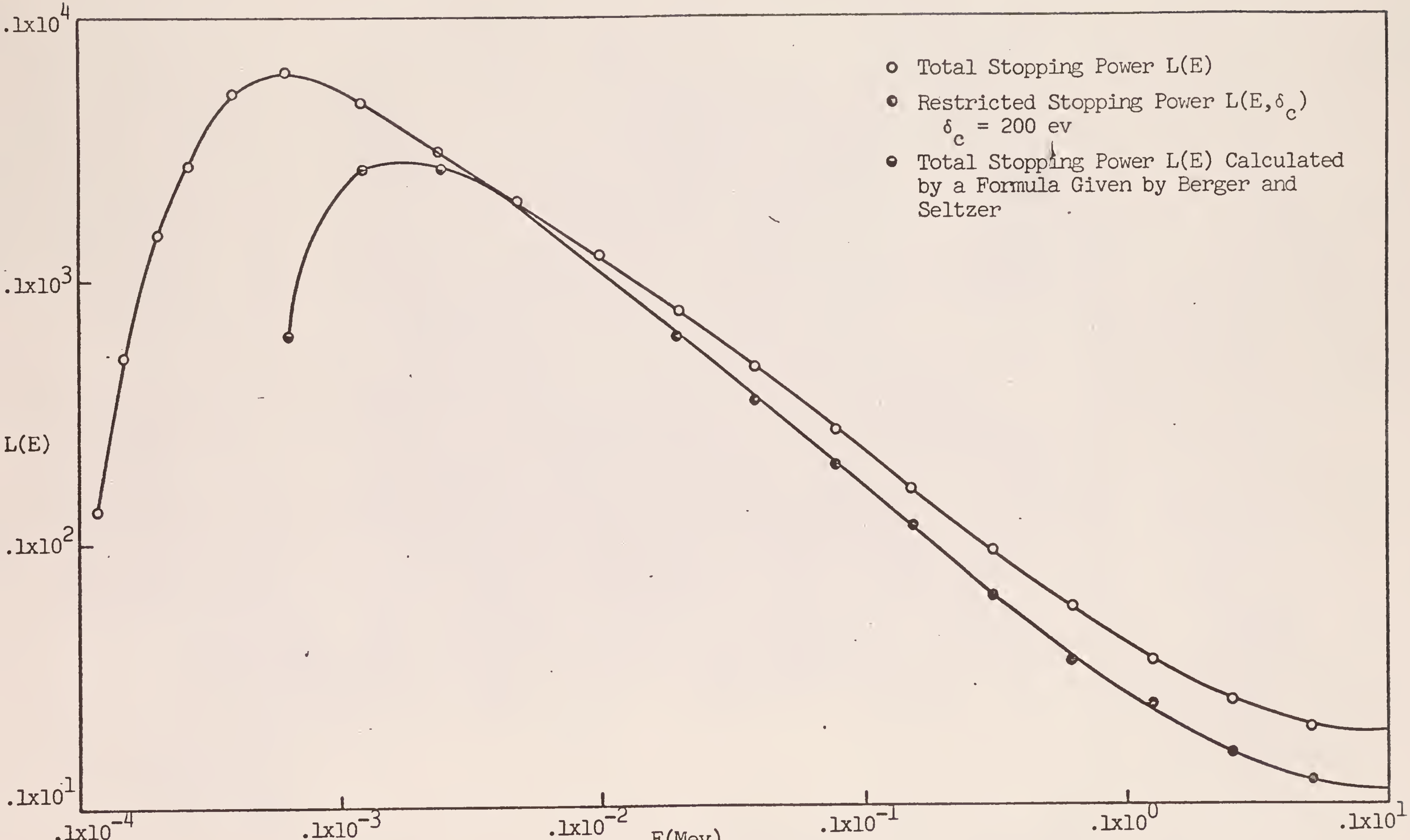

Fig. 15. Stopping Power Calculated From the Synthesized Cross Section Compared to Results Obtained From a Formula Given by Berger and Seltzer.

Table X. Results for AKT, a and b at Various Electron Energies

E	AKT	a	b	b/a
.320E 01	.680E 09	.571E-00	-.164E-04	-28.7E-04
.253E 01	.671E 09	.632E-00	-.181E-04	-28.6E-04
.201E 01	.670E 09	.698E-00	-.198E-04	-28.4E-04
.160E 01	.675E 09	.766E-00	-.215E-04	-28.05E-04
.126E 01	.691E 09	.836E-00	-.233E-04	-27.82E-04
.100E 01	.717E 09	.906E-00	-.251E-04	-27.7E-04
.800E 00	.757E 09	.975E-00	-.268E-04	-27.5E-04
.634E 00	.812E 09	.104E 01	-.284E-04	-27.3E-04
.503E 00	.885E 09	.110E 01	-.299E-04	-27.2E-04
.400E 00	.981E 09	.116E 01	-.312E-04	-26.8E-04
.317E 00	.110E 10	.121E 01	-.323E-04	-26.6E-04
.251E 00	.125E 10	.125E 01	-.333E-04	-26.5E-04
.200E 00	.144E 10	.129E 01	-.340E-04	-26.4E-04
.158E 00	.168E 10	.132E 01	-.346E-04	-26.1E-04
.125E 00	.196E 10	.135E 01	-.350E-04	-25.9E-04
.100E 00	.232E 10	.138E 01	-.353E-04	-25.6E-04
.793E-01	.275E 10	.140E 01	-.355E-04	-25.3E-04
.629E-01	.327E 10	.141E 01	-.355E-04	-25.05E-04
.500E-01	.390E 10	.143E 01	-.355E-04	-24.8E-04
.396E-01	.467E 10	.144E 01	-.353E-04	-24.6E-04
.314E-01	.559E 10	.145E 01	-.352E-04	-24.2E-04

Table X. (continued)

E	AKT	a	b	b/a
.250E-01	.670E 10	.146E 01	-.349E-04	-23.8E-04
.198E-01	.804E 10	.147E 01	-.347E-04	-23.6E-04
.157E-01	.965E 10	.148E 01	-.344E-04	-23.3E-04
.125E-01	.115E 11	.149E 01	-.342E-04	-22.9E-04
.992E-02	.139E 11	.150E 01	-.340E-04	-22.7E-04
.787E-02	.166E 11	.151E 01	-.339E-04	-22.5E-04
.625E-02	.200E 11	.153E 01	-.339E-04	-22.2E-04
.496E-02	.240E 11	.155E 01	-.341E-04	-21.9E-04
.393E-02	.288E 11	.158E 01	-.344E-04	-21.78E-04
.312E-02	.346E 11	.161E 01	-.350E-04	-21.7E-04
.248E-02	.415E 11	.165E 01	-.357E-04	-21.5E-04
.196E-02	.493E 11	.168E 01	-.361E-04	-21.4E-04

3.6 Results, Discussion and Conclusions Concerning the Determination of the Weighted Average Spur Size

According to Magee (18), any reasonable estimate of the average energy loss for the low energy spectrum should be near 40 ev. Results obtained herein are 38.4, 43.0 and 44.0 ev for electron spectra with initial energies of 1.116 Mev, 31.8 Kev and 3.18 Kev for δ_c equal to 200. ev, E_{min} = 200. ev and δ_{min} = 2.0 ev. This would suggest that the average spur size is weakly dependent on the electron energy. This effect could be investigated but was not considered important when this work was outlined.

The average spur size was found to be strongly dependent on the maximum spur size (δ_c) and weakly dependent on the minimum spur size for δ_{min} below 12 ev. Neither of these parameters were accurately known. Bruce, Pearson and Freedhoff (4) suggest δ_c could be between 100 ev and 500 ev. The minimum energy required to create a radical pair is 6.5 ev; however, 7.4 ev (the lowest allowed electronic level) allows the H atom to recoil one or two molecular diameters from its OH partner, according to Hochanadel (13).

During the process of testing the program explained in section 6.6, calculations were made for δ_{min} equal to 2, 8 and 12 ev. The calculations were made using the proton spectrum and E_{min} = 2 ev. An expression for $y_p(E)$, E<400 ev, was obtained graphically. The absolute values of these results were not considered to be valid since E_{min} was equal to 2 ev. Even so, the relative increase of $\langle\bar{\tau}\rangle$ due to increasing δ_{min} should be close. For ranges of δ_c of interest, $\langle\bar{\tau}\rangle$ was raised by 1.5 to 4 ev when δ_{min} was increased from 2 to 8 ev. When δ_{min} was increased from 8 ev to 12 ev, $\langle\bar{\tau}\rangle$ increased between 1 ev to 3 ev. Therefore, it is reasonable to assume that the results listed and plotted in this work are 1 to 4 ev too low, probably about 3 ev too low since δ_{min} should be near 7.4 ev.

Since calculations were completed with $\delta_{min} = 2$ ev before it was noted that 2 ev was too low for δ_{min} and the change was not significant when compared to the change incurred by a change in the upper limit δ_c, the results listed were not recomputed. With $E_{min} = 200$ ev, $\delta_{min} = 2$ ev, the following results were obtained for the spectra $y_g(E)$, $y_p(E)$, $y_a(E)$ from Figs. 17, 18 and 19:

δ_c	$y_g - \langle\bar{\tau}\rangle$	$y_p - \langle\bar{\tau}\rangle$	$y_a(E) - \langle\bar{\tau}\rangle$
100 ev	25 ± 5 ev	29 ± 5 ev	30 ± 6 ev
200 ev	39 ± 7 ev	43 ± 8 ev	44 ± 8 ev
500 ev	66 ± 12 ev	74 ± 14 ev	67 ± 12 ev

The combination of these results is plotted in Fig. 16. The distribution of spur sizes, $G(\tau)$, is plotted in Figs. 20, 21 and 22 for the electron spectra $y_g(E)$, $y_p(E)$ and $y_a(E)$. The values used in plotting Figs. 17, 18 and 19 are listed in Tables XI, XII and XIII.

The error estimates for the above numbers were obtained by assuming 10 percent error in the hypothesized cross section and 5 percent error in the electron flux. A 1 percent error was superimposed on each numerical integration. As a result, 18.5 percent was estimated to be the uncertainty associated with $\langle\bar{\tau}\rangle$.

Both the uncertainty in the hypothesized cross section and in $z(E_o,E)$ were not accurately known and both functions were somewhat inadequate. However, it was felt that a reasonable maximum uncertainty incurred by the hypothesized cross section would be 10 percent and one incurred by the uncertainty in the electron spectra would be 5 percent. Errors due to multiplication and division were obtained by the square root of the sum of the squared errors, for each integration, and a 1 percent error was superimposed due to the numerical integration. Uncertainties listed for the above numbers were obtained by rounding off to the nearest ev.

From the results listed, it appears that the average spur size is somewhat dependent on the nature of the electron spectra. For the electron spectra resulting from fast neutron irradiation, a graphical extrapolation and one performed by subroutine INTER gave different answers with E_{min} = 2 ev. This indicates that for very small E_{min}, $\langle\bar{\tau}\rangle$ is quite sensitive to y(E).

According to Burch (5), experimental results from the Fricke dosimeter indicate $\bar{\varepsilon}$ is somewhat less than 21 ev/(radical pair) and theory indicates it could be greater than 28 ev/(radical pair). If $\bar{\varepsilon}$ is taken to be 20 ev/(radical pair) and $\langle\bar{\tau}\rangle$ = 45 ev, $N_o = 4.5 \frac{\text{radicals}}{\text{spur}}$. An average over the distribution given by Kupperman (16) results in $4.9 \frac{\text{radicals}}{\text{spur}}$.

From the above discussion and calculated results, it is concluded that 45 ± 8 ev would be a reasonable value for $\langle\bar{\tau}\rangle$ for a wide range of LET and any electron spectra if δ_c is considered to be 200 ev.

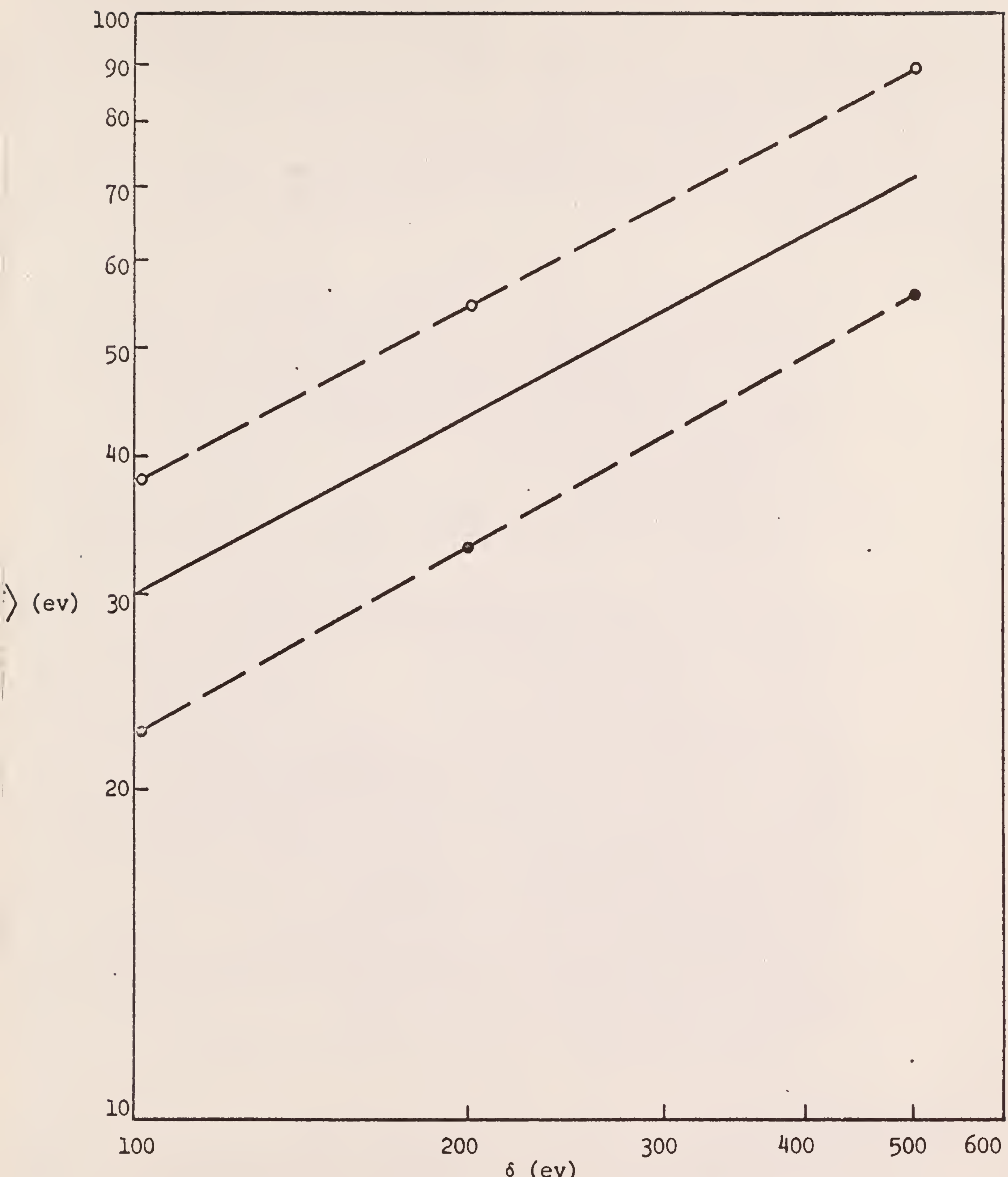

Fig. 16. Plot of $\langle\overline{\tau}\rangle$ (ev) vs. δ_c(ev). The dotted lines were obtained by the maximum or minimum value associated with the three electron spectra calculated and considering the 18.5 percent uncertainty associated with each weighted average spur size ($\langle\overline{\tau}\rangle$). δ_c is the effective maximum spur size. The solid line is an estimate based on the values reported on page 104

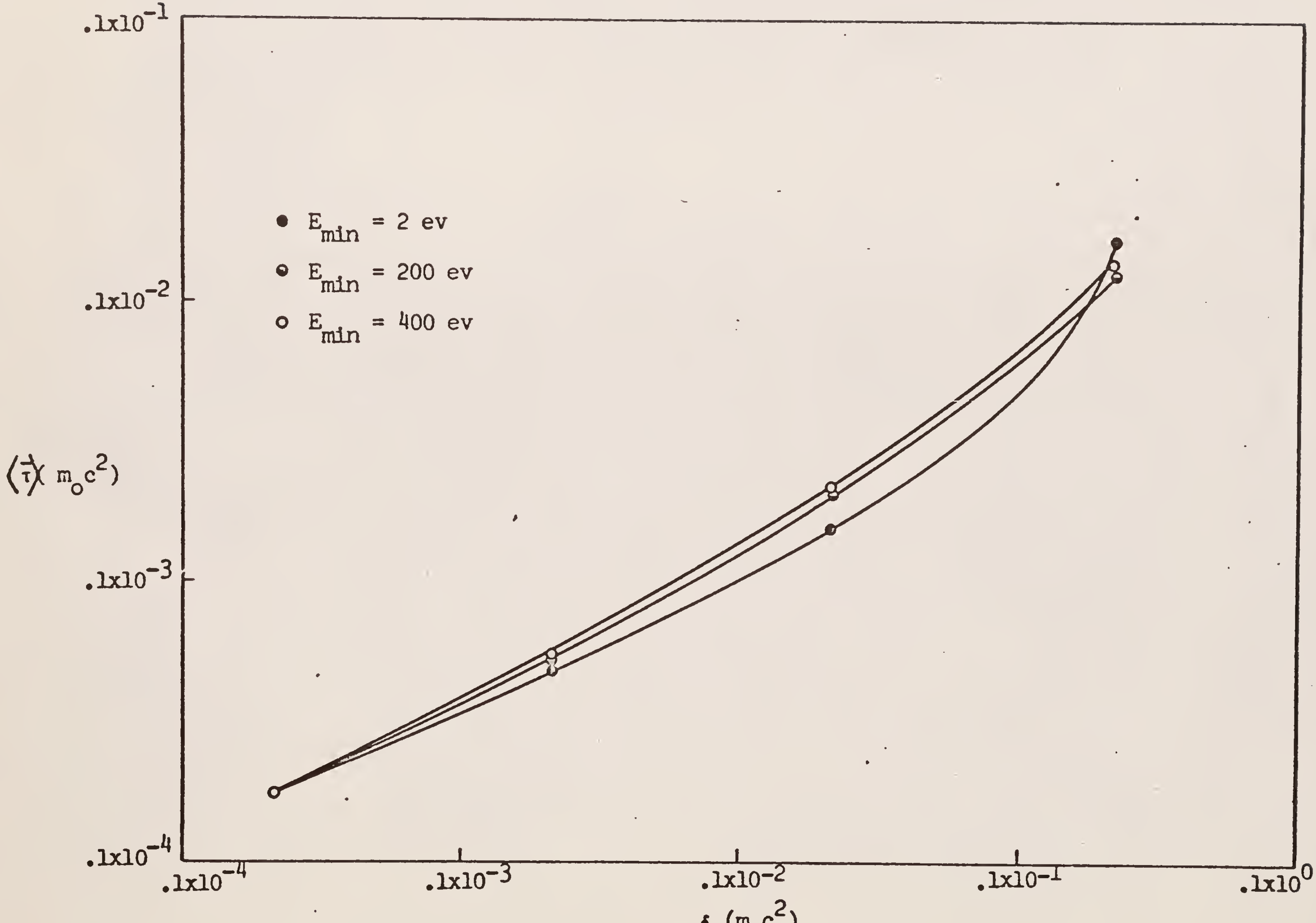

Fig. 17. Plot of $\langle \bar{\tau} \rangle$ (m_oc^2) vs. $\delta_c(m_oc^2)$ for the Electron Spectra Resulting From Co^{60} Irradiation for Various E_{min}

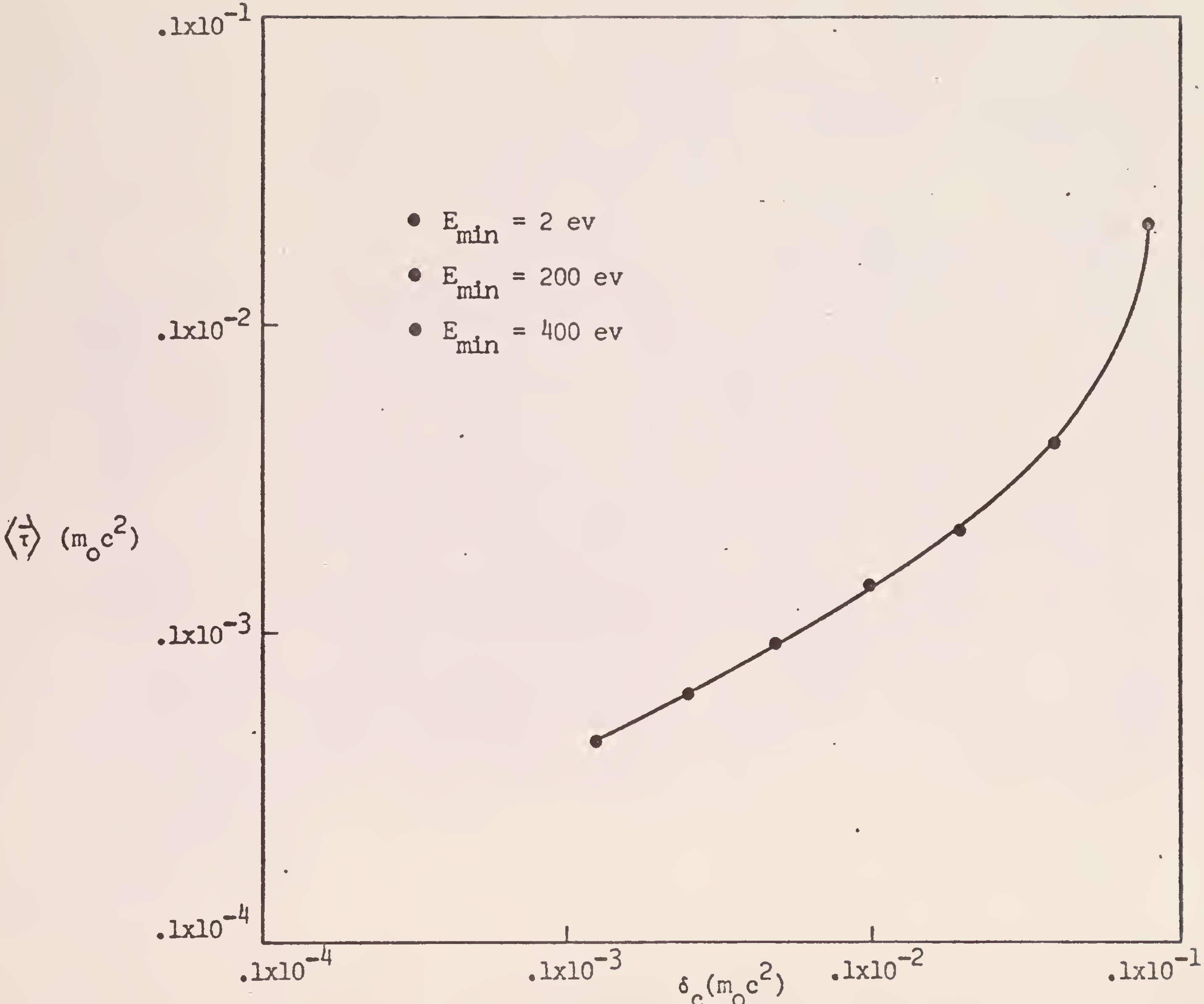

Fig. 18. Plot of $\langle\bar{\tau}\rangle$ vs. $\delta_c(m_oc^2)$ for the Electron Spectra Resulting From the Proton Source for Various E_{min}

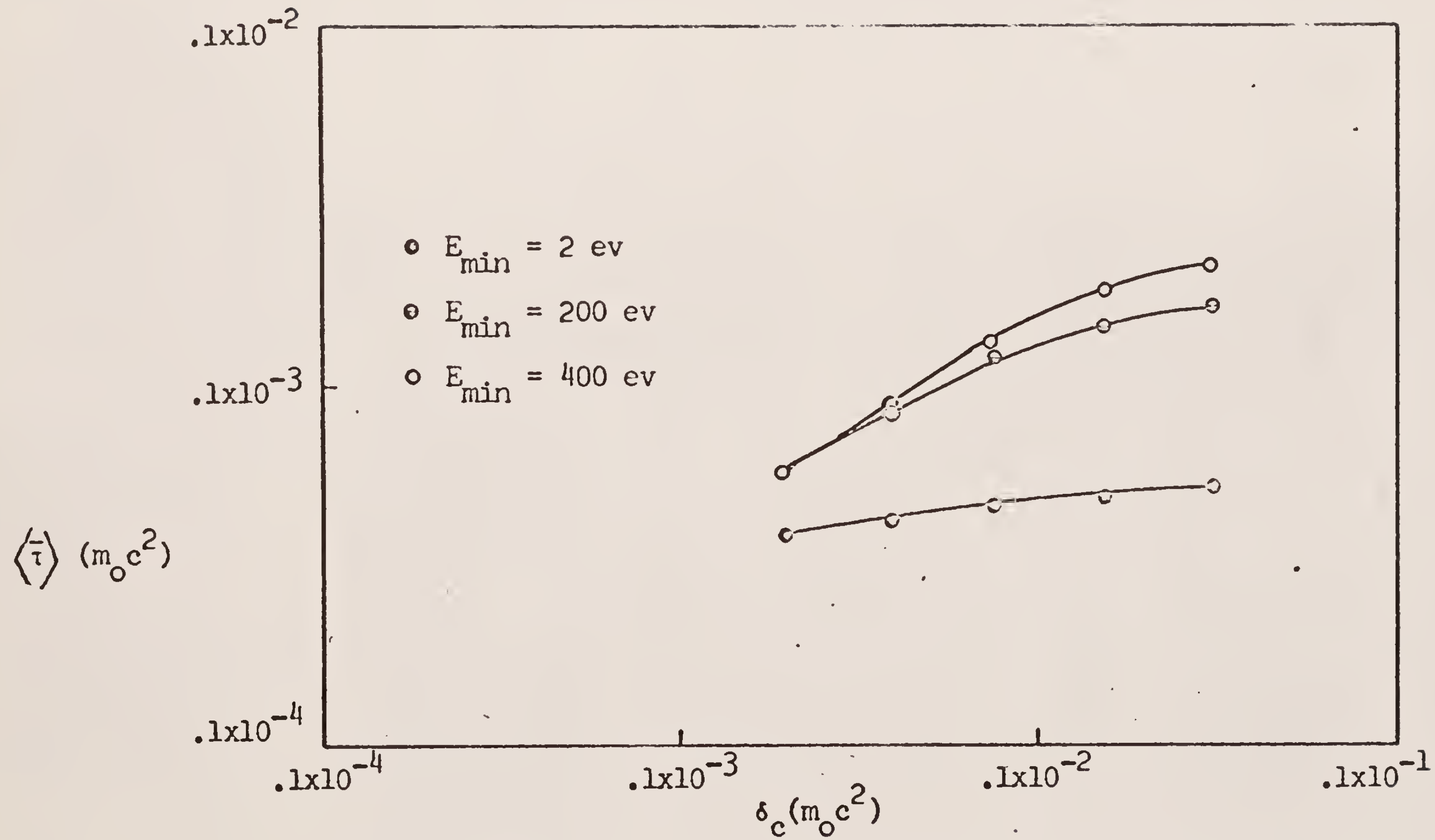

Fig. 19. Plot of $\langle\bar{\tau}\rangle$ vs. $\delta_c(m_oc^2)$ for the Electron Spectra Resulting From the Alpha Particle Source for Various E_{min}

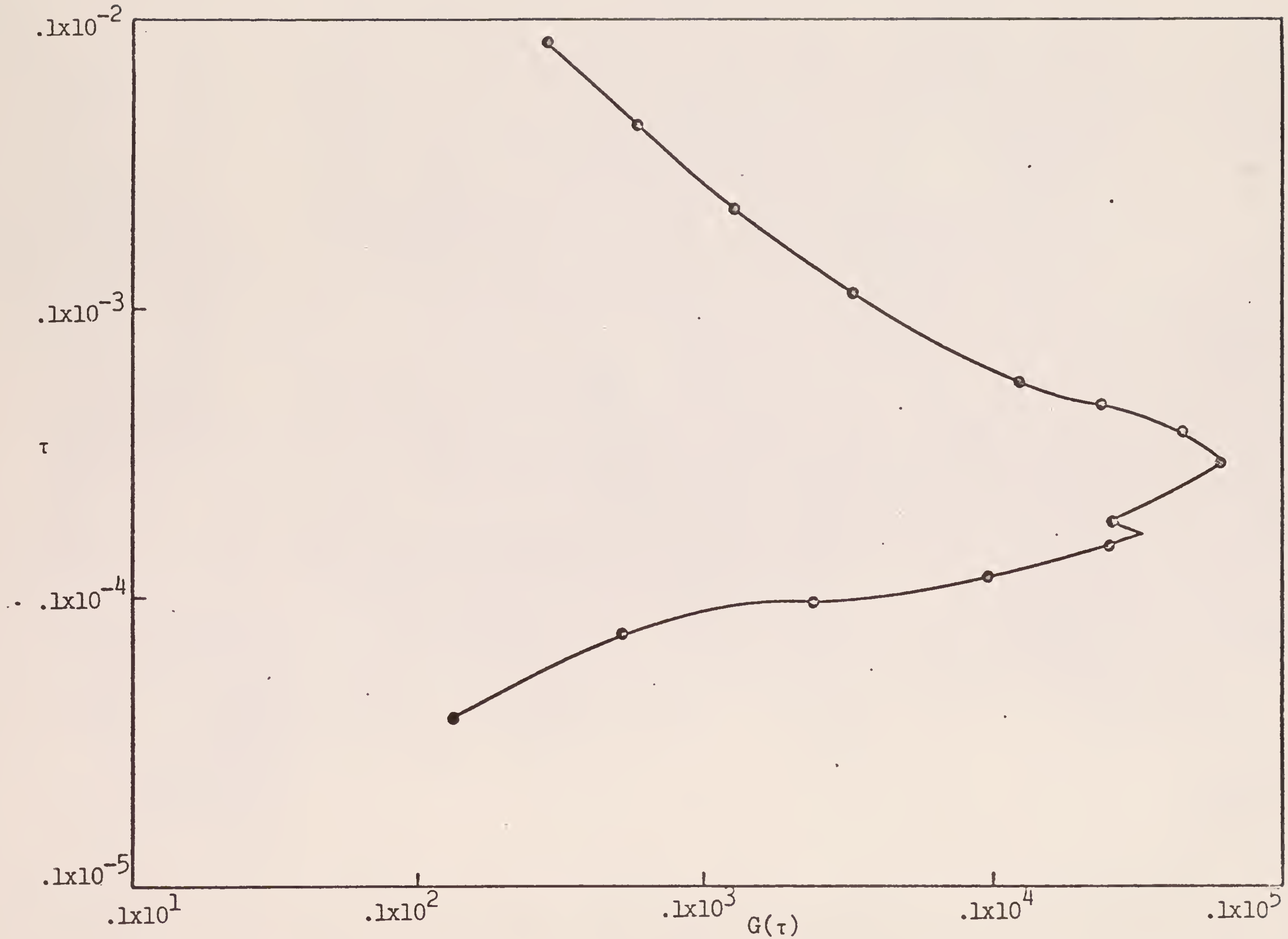

Fig. 20. Plot of the Spur Size $\tau(m_o c^2)$ vs. $G(\tau)(cm^{-3}sec^{-1})$ for the Electron Spectrum Resulting From Co^{60} Irradiation for E_{min} = 400 ev

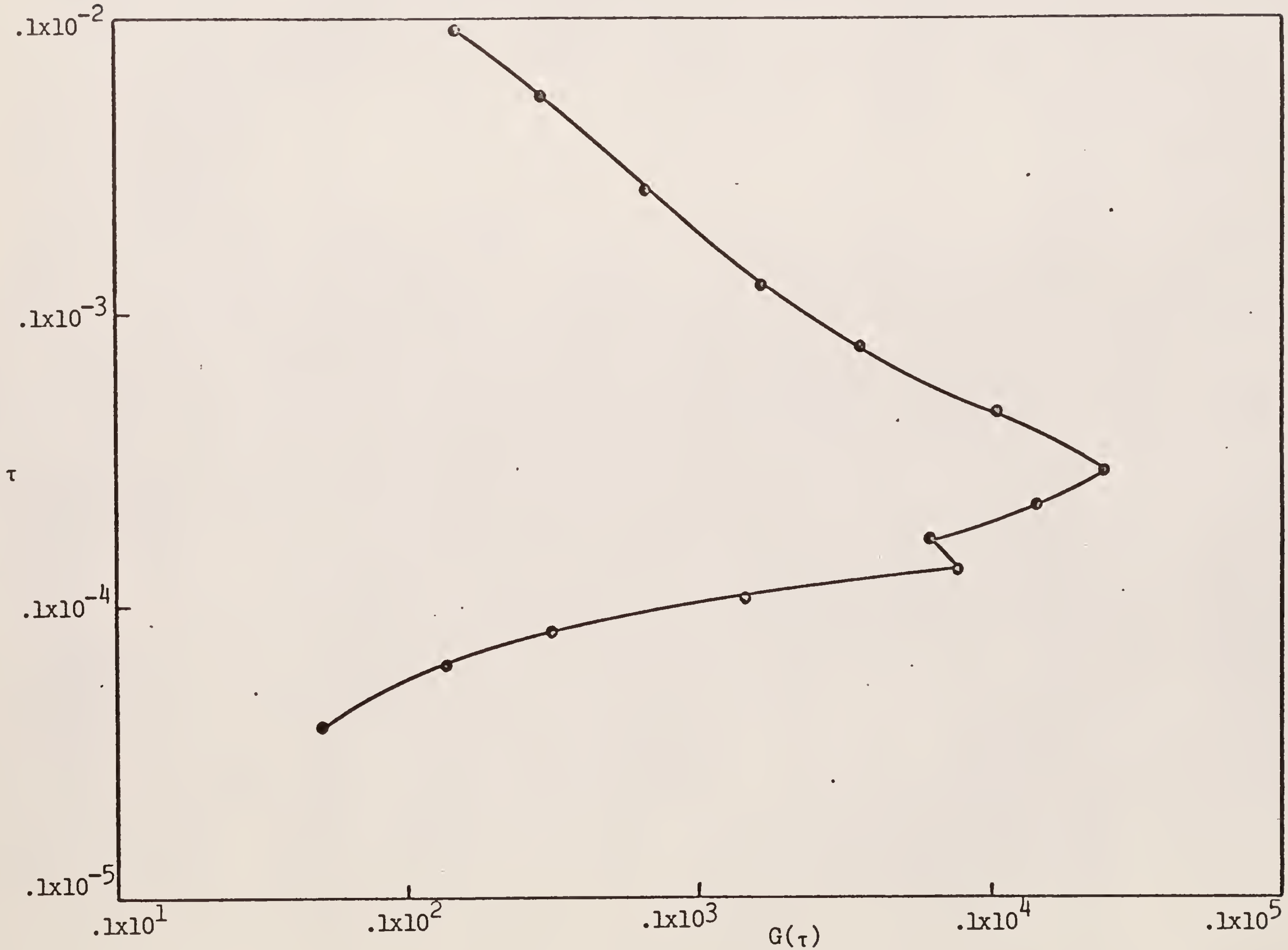

Fig. 21. Plot of the Spur Size $\tau(m_o c^2)$ vs. $G(\tau)(cm^{-3}sec^{-1})$ for the Electron Spectrum Resulting From the Proton Source for E_{min} = 400 ev

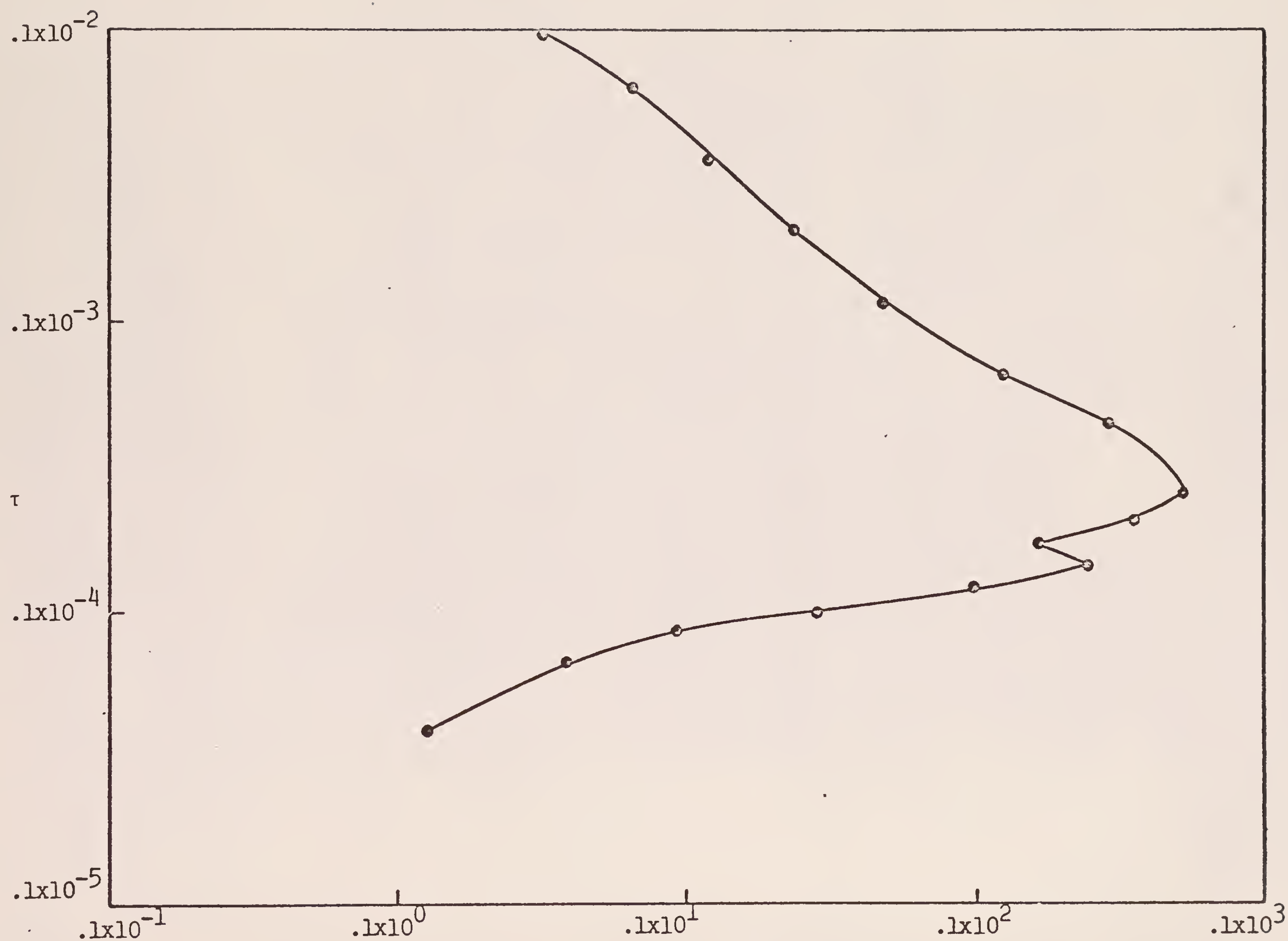

Fig. 22. Plot of the Spur Size $\tau(m_o c^2)$ vs. $G(\tau)(cm^{-3}sec^{-1})$ for the Electron Spectrum Resulting From the Alpha Particle Source for E_{min} = 400 ev.

Table XI. Results for the Weighted Average Energy Loss at Various E_{min} and δ_c Considering the Electron Spectrum Resulting from the Gamma Source

	$\langle\bar{\tau}\rangle$ (mc^2)		
$\delta_c(mc^2)$	E_{min} = 2 ev	E_{min} = 20 ev	E_{min} = 200 ev
.218E-04	.172E-04	.175E-04	.175E-04
.218E-03	.483E-04	.502E-04	.529E-04
.218E-02	.151E-03	.159E-03	.207E-03
.218E-01	.163E-02	.172E-02	.228E-02
.218E-00	.254E-01	.264E-01	.326E-01
$\delta_c(mc^2)$	E_{min} = 400 ev	E_{min} = 800 ev	E_{min} = 1600 ev
.218E-04	.175E-04	.175E-04	.175E-04
.218E-03	.522E-04	.517E-04	.513E-04
.218E-02	.214E-03	.217E-03	.215E-03
.218E-01	.239E-02	.248E-02	.256E-02
.218E-00	.338E-01	.347E-01	.356E-01

Table XII. Results for the Weighted Average Energy Loss at Various E_{min} and δ_c Considering the Electron Spectrum Resulting from the Proton Source

	$\langle \Delta_\tau \rangle$ (mc^2)		
$\delta_c (mc^2)$	E_{min} = 2 ev	E_{min} = 20 ev	E_{min} = 200 ev
.121E-03	.445E-04	.442E-04	.446E-04
.243E-03	.619E-04	.614E-04	.617E-04
.486E-03	.925E-04	.916E-04	.917E-04
.972E-03	.146E-03	.145E-03	.145E-03
.194E-02	.214E-03	.212E-03	.212E-03
.388E-02	.405E-03	.401E-03	.401E-03
.777E-02	.215E-02	.214E-02	.214E-02
.155E-01	.389E-02	.387E-02	.387E-02
.311E-01	.566E-02	.563E-02	.563E-02

$\delta_c (mc^2)$	E_{min} = 400 ev	E_{min} = 800 ev
.121E-03	.447E-04	.442E-04
.243E-03	.618E-04	.606E-04
.486E-03	.920E-04	.898E-04
.972E-03	.144E-03	.143E-03
.194E-02	.209E-03	.234E-03
.388E-02	.390E-03	.505E-03
.777E-02	.208E-02	.264E-02
.155E-02	.378E-02	.460E-02
.311E-01	.551E-02	.660E-02

Table XIII. Results for the Weighted Average Energy Loss at Various E_{min} and δ_c Considering the Electron Spectrum Resulting from the Alpha Source

	$\langle \bar{\tau} \rangle$ (mc^2)		
$\delta_c(mc^2)$	E_{min} = 2 ev	E_{min} = 20 ev	E_{min} = 200 ev
.194E-03	.395E-04	.452E-04	.595E-04
.388E-03	.437E-04	.503E-04	.877E-04
.777E-03	.472E-04	.548E-04	.120E-04
.155E-02	.500E-04	.583E-04	.144E-03
.311E-02	.517E-04	.603E-04	.158E-03
$\delta_c(mc^2)$	E_{min} = 400 ev	E_{min} = 800 ev	E_{min} = 1600 ev
.194E-03	.585E-04	.575E-04	.565E-04
.388E-03	.856E-04	.837E-04	.819E-04
.777E-03	.133E-03	.130E-03	.127E-03
.155E-02	.185E-03	.215E-03	.209E-03
.311E-02	.214E-03	.294E-03	.443E-03

3.7 Results, Discussion and Conclusions Concerning the Determination of the Average Spur Separation Distance

A comparison is made between $\overline{Y}_{RS}$ and $Y_{RS}(\overline{\ell})$. The weighted average spur separation distance $\langle \ell' \rangle$ is related to the parameter ℓ by $\ell = \frac{\ell'}{2r_o}$. Therefore, $\overline{\ell} = \frac{\langle \ell' \rangle}{2r_o}$. The four methods used in determining $\langle \ell' \rangle$ are described in section 2.7 of the theory. Using a 10 point Gaussian quadrature integration, by hand, $\overline{Y}$ is found to be 0.92, 0.85 and 0.68 for the electron energy spectra $y_g(E)$, $y_p(E)$ and $y_a(E)$. The following reaction parameters are used:

$$\langle \tau \rangle = 45 \text{ ev}, \qquad \overline{\varepsilon} = 20 \frac{\text{ev}}{\text{radical pair}}, \qquad k_{RR} = .4\text{x}10^{10} \left(\frac{\text{moles}}{\text{liter}}\right)^{-1} (\text{sec})^{-1}$$

$$k_{RS} = 2.0\text{x}10^{10} \left(\frac{\text{moles}}{\text{liter}}\right)^{-1} (\text{sec})^{-1}, \qquad \delta_c = 200 \text{ ev}, \qquad r_o = 1.5\text{x}10^{-7}\text{cm}$$

$$D = 4.5\text{x}10^{-5} \frac{\text{cm}^2}{\text{sec}}, \qquad N_o = 4.5 \frac{\text{radical}}{\text{spur}}, \qquad C_S = 5\text{x}10^{-4} \left(\frac{\text{moles}}{\text{liter}}\right).$$

Using $Y(\overline{\ell})$, the following results are obtained with $E_{min} = 200$ ev in each case (These results were taken from Figs. 25, 26 and 27):

	$Y(\overline{\ell}) - y_g(E)$	$Y(\overline{\ell}) - y_p(E)$	$Y(\overline{\ell}) - y_a(E)$
Case 1	.92	.88	.72
Case 2	.92	.83	.59
Case 3	.92	.88	.75
Case 4	.92	.82	.56

From the results, it is apparent that substituting a weighted average spur separation distance into the yield expression is not a satisfactory method of finding the average chemical yield. The upper curve is obtained from values listed by Hochanadel (13) and the lower curve is obtained from this work by taking $\langle \bar{\tau} \rangle$ = 45 ev.

The spur separation distance as a function of energy is given in Fig. 23. When the spur separation distance is less than or equal to r_o it is assumed that the track model is valid. Therefore, the transition of the curve for $Y_{RS}(\infty)$ from the spur model to the track model in Fig. 34 is begun at a slightly higher energy than that corresponding to spur separation distance r_o.

The upper curve in Fig. 24 is obtained by values given by Hochanadel (13) and the lower curve is given by $\langle \bar{\tau} \rangle$ /LET. If it is assumed that the solid line in Fig. 16 is indeed a reasonable estimate of the average spur size as a function of maximum spur size, a maximum spur size on the order of 900 ev would be required to match the curves in Fig. 24. A maximum spur size near 400 ev would match the curves in Fig. 23. However, Hochanadel (13) does not say how these values for Figs. 23 or 24 were obtained. Therefore, the upper curves are probably not very accurate.

Figures 25, 26 and 27 present a weighted average spur separation distance for the three electron spectra previously described. The following four cases are considered for each spectra:

$$\langle \ell' \rangle_1 = \frac{\displaystyle\int_{E_{min}}^{E_{max}} y(E) \frac{L(E,\delta_c)}{L(E)} \ell'(E,\delta_c)dE}{\displaystyle\int_{E_{min}}^{E_{max}} y(E) \frac{L(E,\delta_c)}{L(E)} dE} \qquad (154)$$

$$\langle \ell' \rangle_2 = \frac{\int_{E_{min}}^{E_{max}} y(E)L(E,\delta_c)\ell'(E,\delta_c)dE}{\int_{E_{min}}^{E_{max}} y(E)L(E,\delta_c)dE} \tag{155}$$

$$\langle \ell' \rangle_3 = \frac{\int_{E_{min}}^{E_{max}} y(E)\ell'(E,\delta_c)dE}{\int_{E_{min}}^{E_{max}} y(E)dE} \tag{156}$$

$$\overline{LET} = \frac{\int_{E_{min}}^{E_{max}} y(E) \frac{L(E,\delta_c)}{L(E)} L(E,\delta_c)dE}{\int_{E_{min}}^{E_{max}} y(E) \frac{L(E,\delta_c)}{L(E)} dE} \tag{157}$$

$$\langle \ell' \rangle_4 = \frac{\langle \overline{\tau} \rangle}{\overline{LET}} . \tag{158}$$

Since neither the stopping power nor the electron flux is accurately known for low energy electrons, the weighted average spur separation distance is plotted as a function of E_{min} in Figs. 25, 26 and 27. These figures are based on an average energy loss of 43.5 ev.

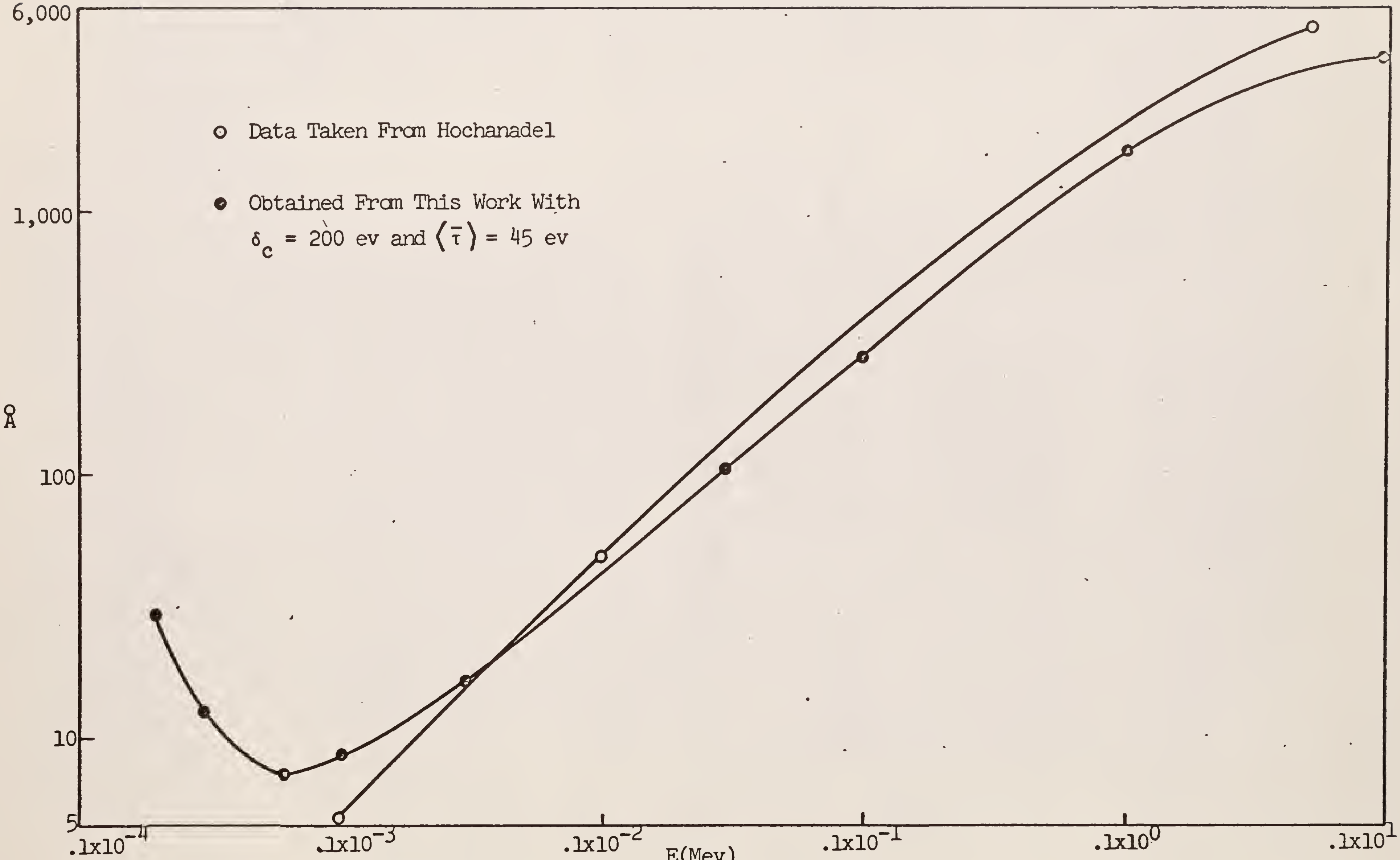

Fig. 23. Plot of the Spectrum of Spur Separation Distances in Å vs. Electron Energy E(Mev) as Determined From the Synthesized Cross Section Compared to Data Given by Hochanadel

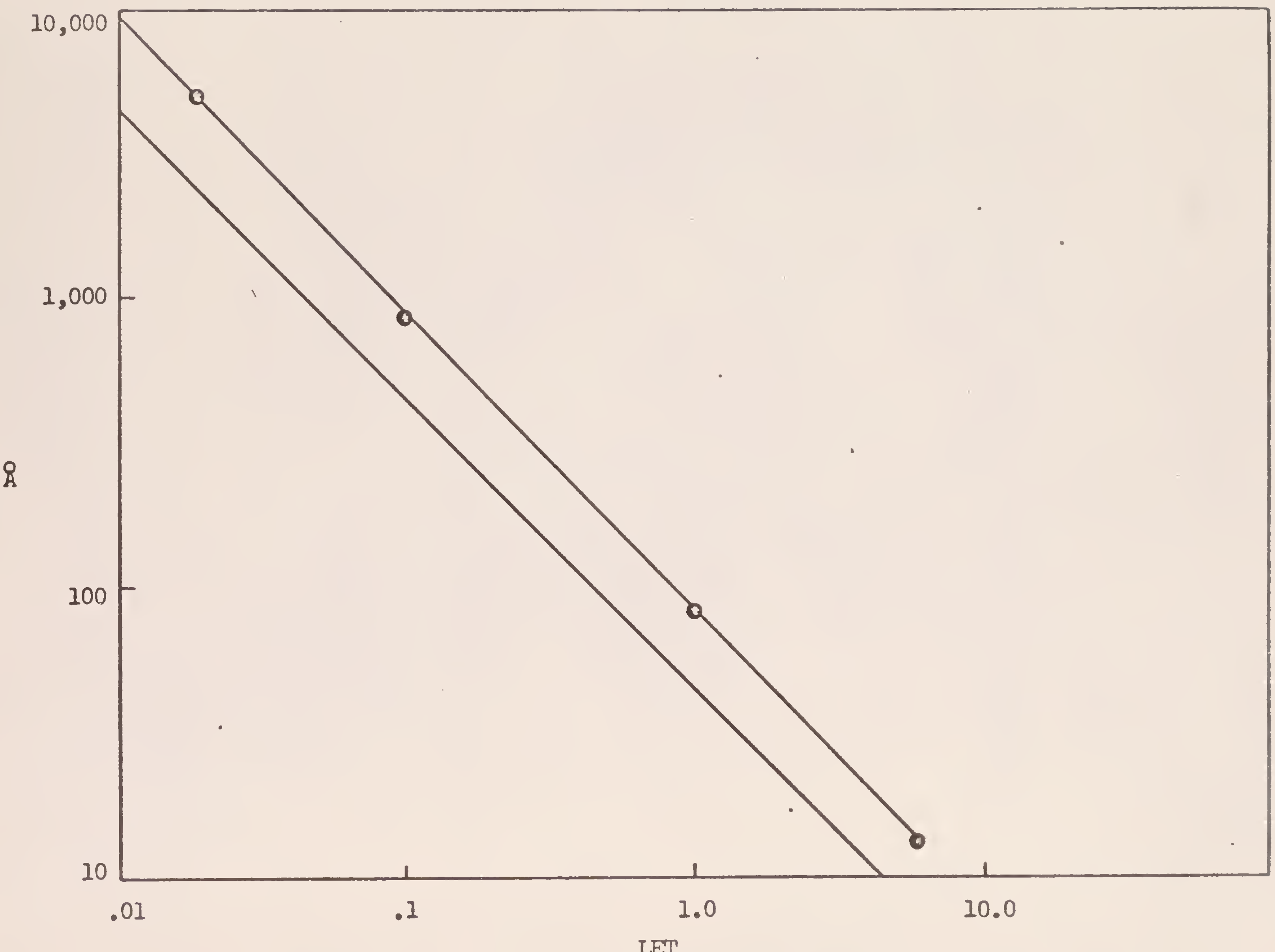

Fig. 24. Plot of the Spur Separation Distance in Å vs. LET(mev/cm). The upper curve is obtained from data from Hochanadel (13) and the lower curve is obtained by dividing the weighted average spur size $\langle \bar{\tau} \rangle$ by the LET where $\langle \bar{\tau} \rangle$ was chosen to be 45 ev.

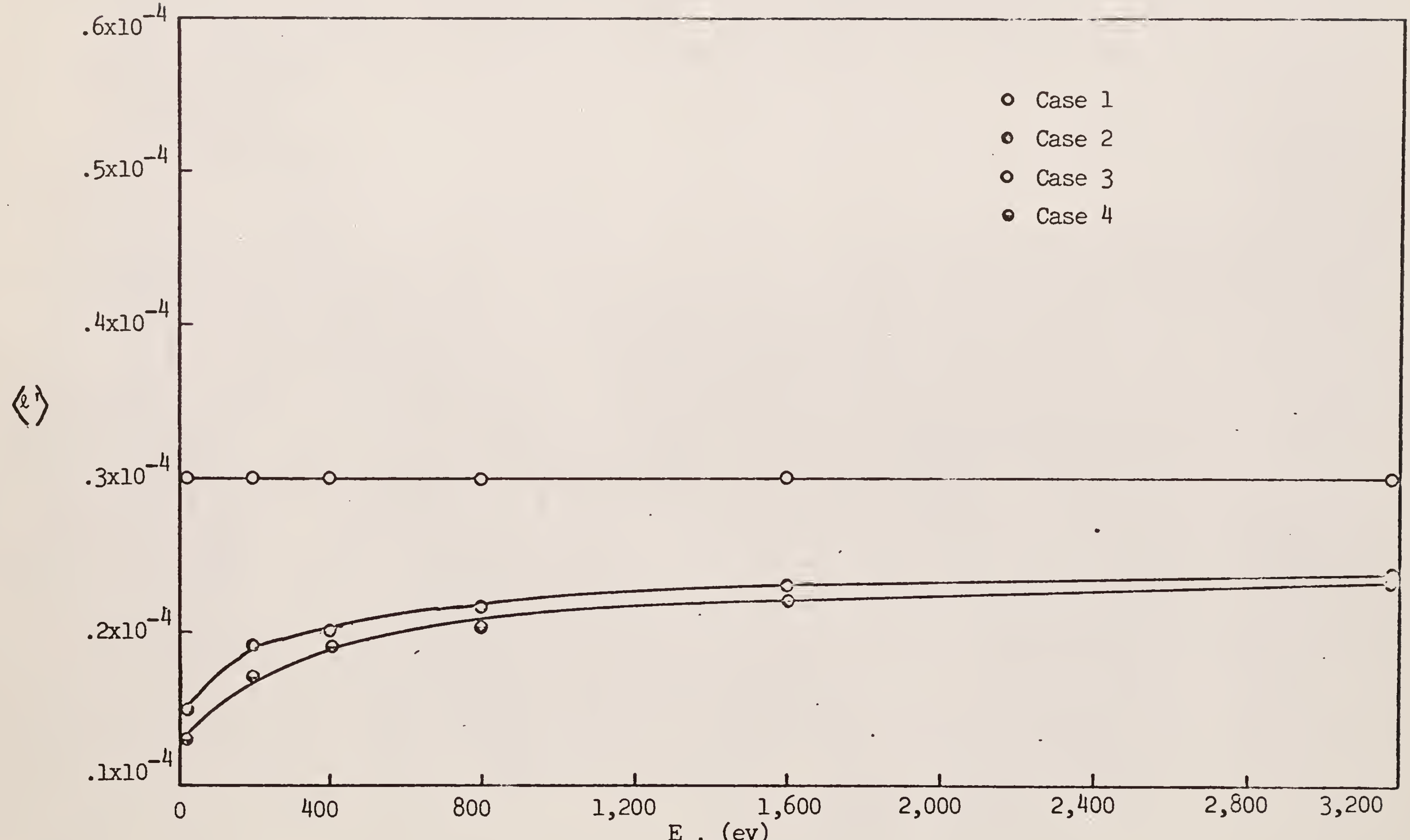

Fig. 25. Plot of the Weighted Average Spur Separation Distance vs. E_{min}(ev) for the Electron Spectrum Resulting From Co^{60} Irradiation with $\langle \tau \rangle = 43.5$ ev

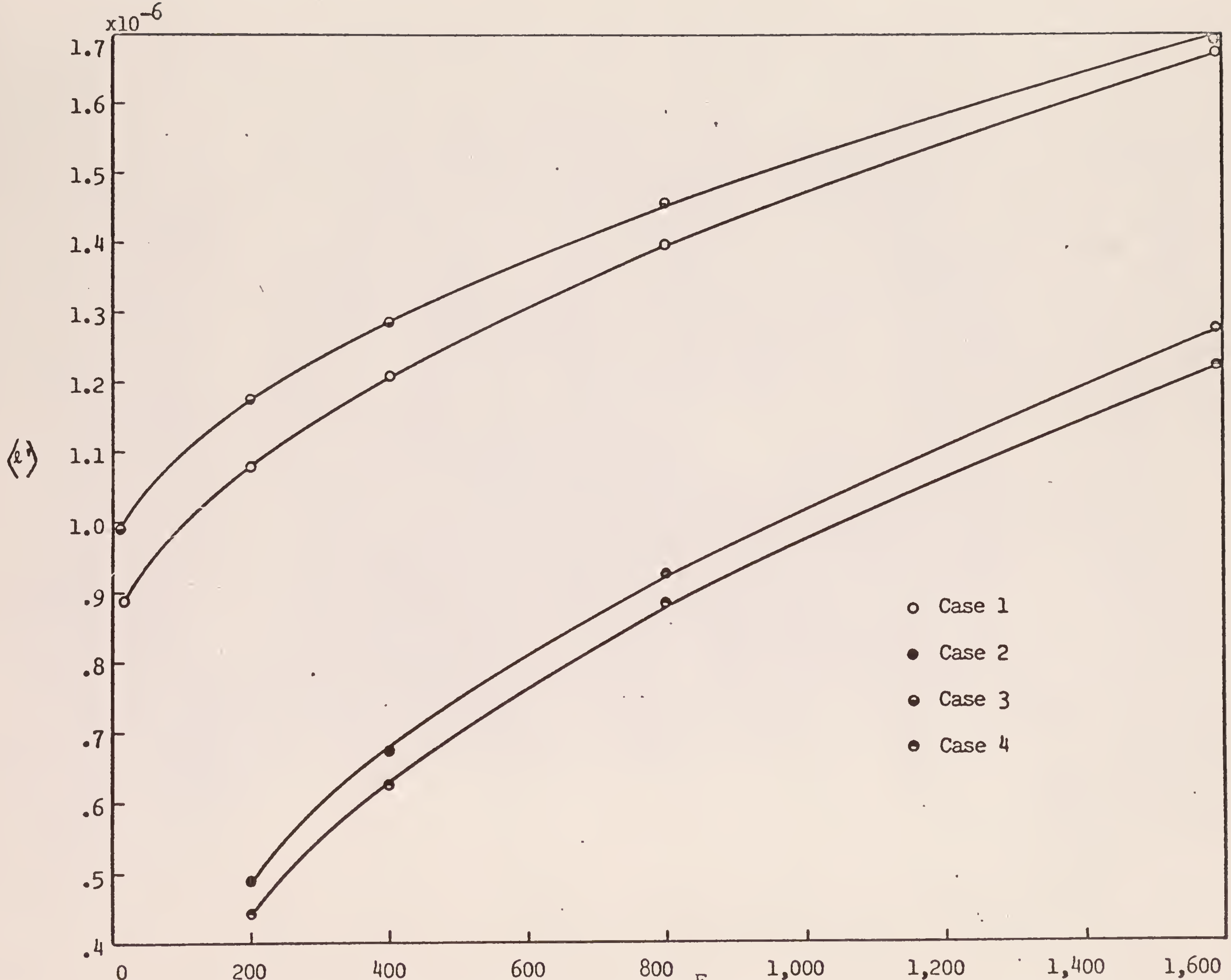

Fig. 26. Plot of the Weighted Average Spur Separation Distance vs. E_{min}(ev) for the Electron Spectrum Resulting From the Proton Source

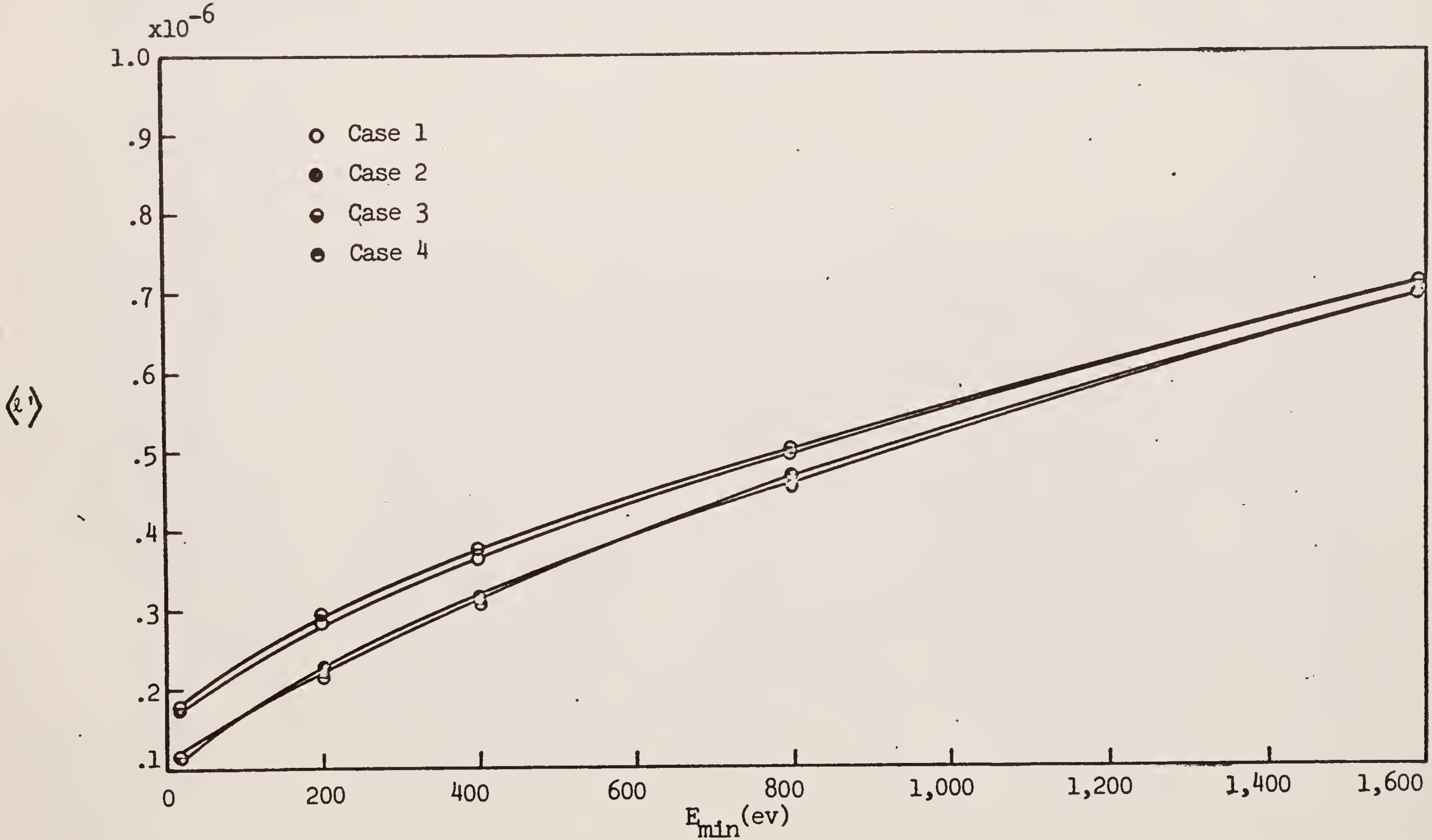

Fig. 27. Plot of the Weighted Average Spur Separation Distance vs. E_{min}(ev) for the Electron Spectrum Resulting From the Alpha Particle Source With $\langle \tau \rangle$ = 43.5 ev

3.8 Results, Discussion and Conclusions Concerning the Energy Balance

The dose rate expressions given in section 2.8 are:

$$\underline{\text{Dose 1}} = \int_{E_{min}}^{E_{max}} S(E')(E' - E_{min})dE'' \tag{160}$$

$$\underline{\text{Dose 2}} = \int_{E_{min}}^{E_{max}} S(E')E'dE' \tag{161}$$

$$\underline{\text{Dose 3}} = \int_{E_{min}}^{E_{max}} y(E')L_s(E')dE' \tag{162}$$

$$\underline{\text{Dose 4}} = \int_{E_{min}}^{E_{max}} y(E')L_s(E',\delta_c)dE'. \tag{163}$$

$L_s(E)$ and $L_s(E,\delta_c)$ are the total and restricted stopping powers obtained from the synthesized cross section with δ_c = 200 ev. For the electron spectrum resulting from gamma irradiation, Dose 2 was obtained analytically.

Evaluated with $E_{min} \leq 200$ ev, Dose 2 represents the total energy released as kinetic energy of secondary electron delta rays arising from proton and alpha particle collisions. Energy losses of less than 200 ev are treated as local losses along the tracks of protons and alpha particles. According to continuous slowing-down theory,

$$y(E) = \frac{1}{L_s(E)} \int_{E}^{E_{max}} S(E')dE'. \tag{192}$$

Substitution of this expression into the equation for Dose 3 shows that, under the continuous slowing-down approximation, Dose 3 is equal to Dose 1 for all $E_{min} \geq 200$ ev. As shown in Tables V, VIII and IX, the electron spectra computed according to the method of Spencer and Fano exceed the spectra based on continuous slowing-down over the greater part of the energy range of interest. This is due to the production of secondary electrons. The former method was used to compute the y(E) used in the integration for Dose 3. Thus, Dose 3 would be expected to slightly exceed Dose 1. Dose 4 would be expected to be less than Dose 3 simply because of the use of restricted instead of total stopping power. These effects are exhibited in Figs. 28, 29 and 30.

Dose 3 and Dose 4 exceed the total input energy, D_2, for small E_{min} in Figs. 28 and 30. This means that a linear extrapolation for y(E) on a log-log plot overestimates the electron flux for low energies. The stopping power obtained from the synthesized cross section may also be overestimated but this is doubtful when considered in the light of Fig. 23. The fact that, in Fig. 30, Dose 3 and Dose 4 far exceed Dose 2 for small E_{min} explains why the average energy loss $\langle\bar{\tau}\rangle$ obtained for $E_{min} = 2$ ev is far too small.

The energy balance results indicate that the electron spectra have been determined fairly accurately down to 200 ev, and have been overestimated in calculations at lower energies. Therefore, the results obtained for $E_{min} < 200$ ev involving y(E) are overweighted at low energies.

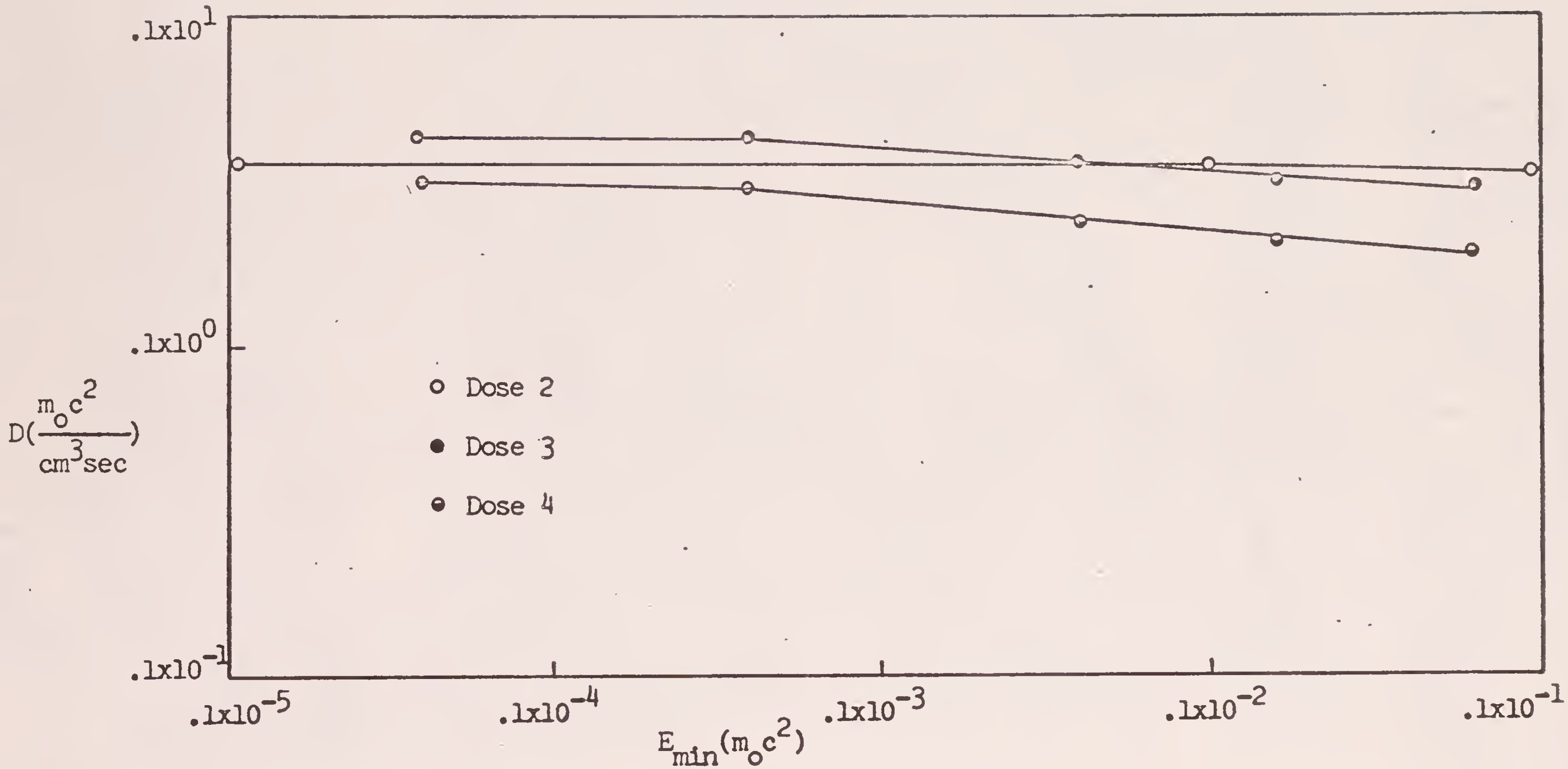

Fig. 28. Plot of Several Electron Spectrum Dose Rates vs. E_{min} for the Electron Spectrum Resulting From Co^{60} Irradiation

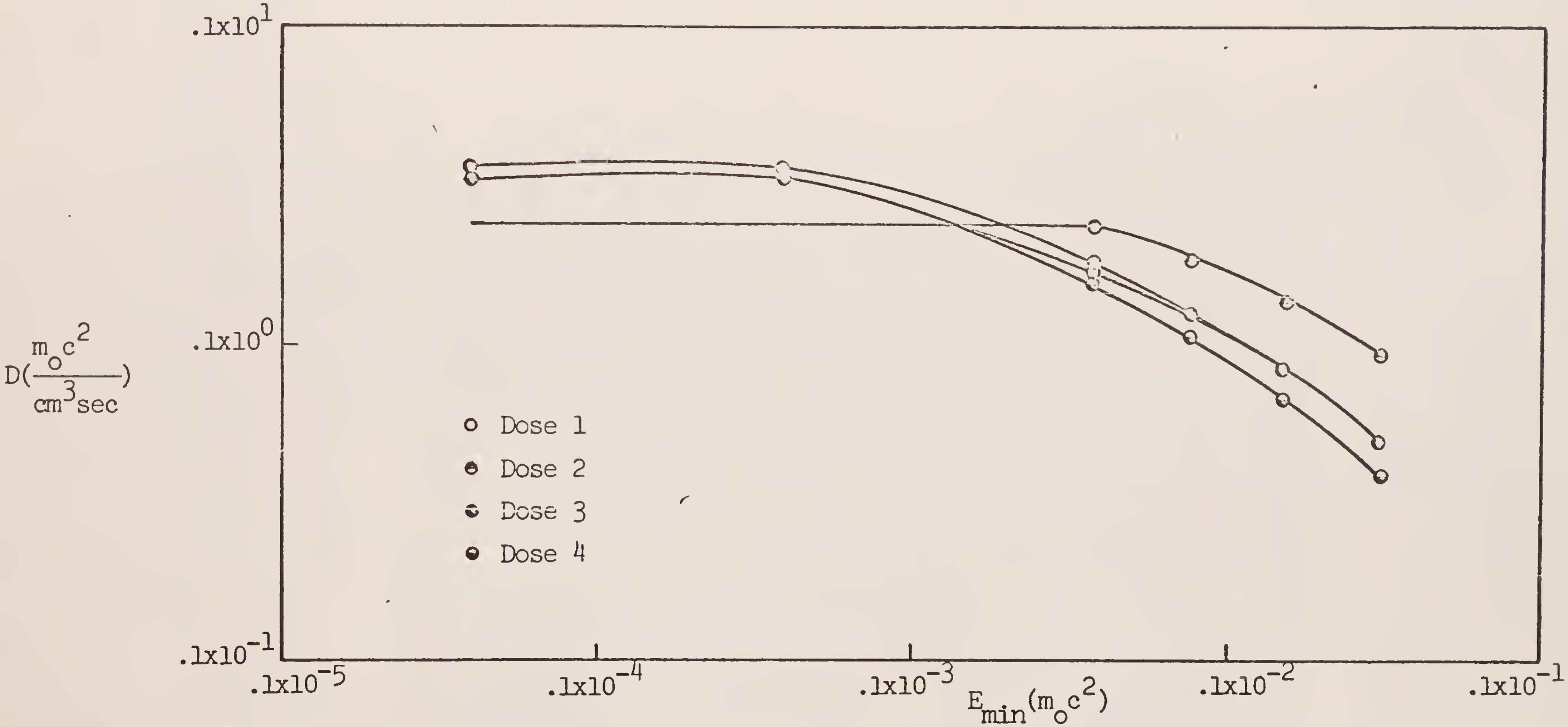

Fig. 29. Plot of Several Electron Spectrum Dose Rates vs. E_{min} for the Electron Spectrum Resulting From the Proton Source

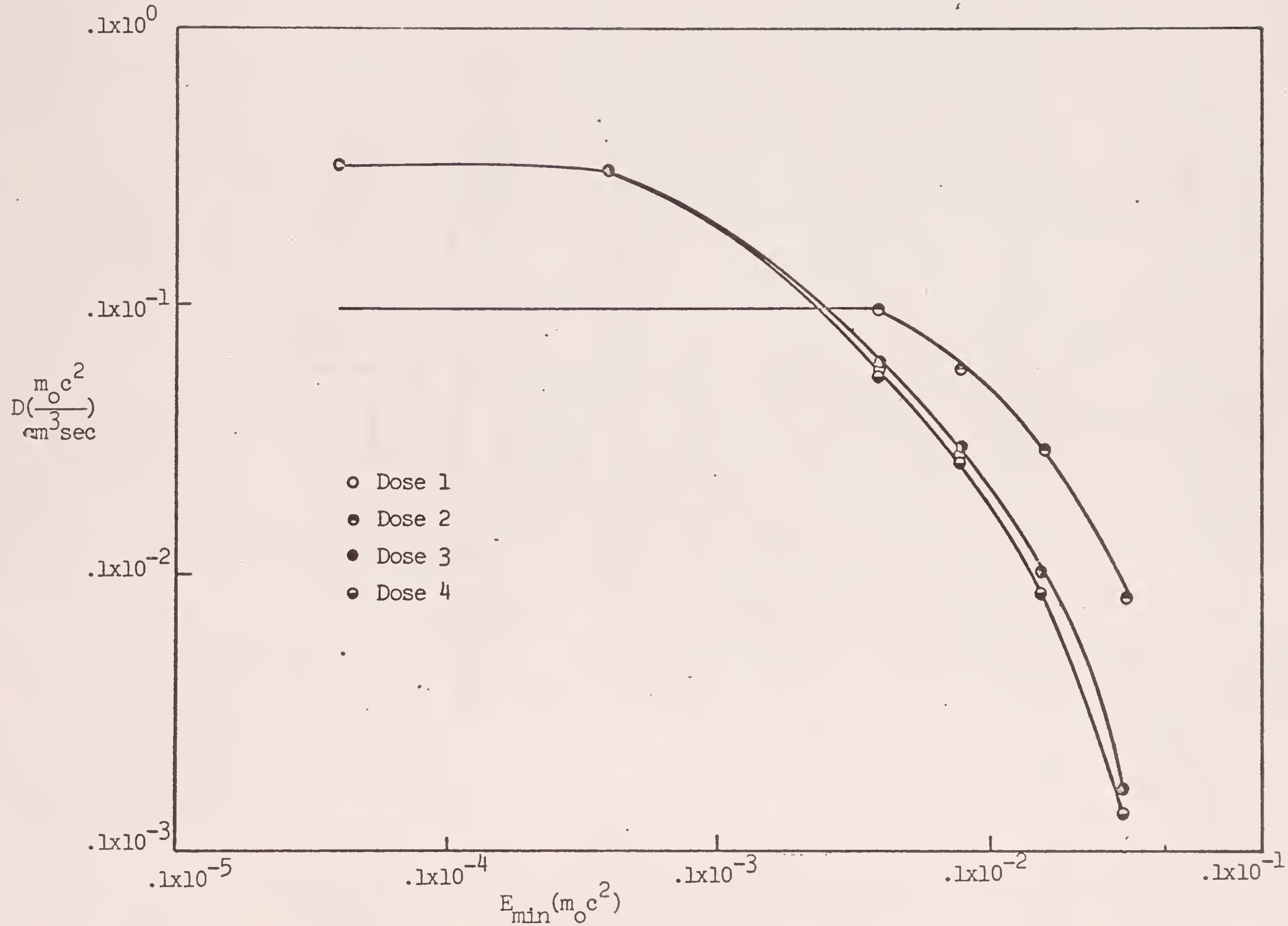

Fig. 30. Plot of Several Electron Spectrum Dose Rates vs. E_{min} for the Electron Spectrum Resulting From the Al ha Particle Source

3.9 Results, Discussion and Conclusions of Prediction of G-Values

The theoretical prediction of absolute G values is very sensitive to the average energy required to create a radical pair. According to Burch (5), the energy required to create a radical pair could be slightly below 20 ev to nearly 30 ev for water. Predictions for G values were made using several expressions to give an indication of the validity of the one radical model.

For the case not considering the back reaction,

$$Fe^{+3} + H \rightarrow Fe^{+2} + H^{+},$$

and considering equal production of H_2, H_2O_2 and H_2O, the following table compares these predictions with experimental values given by Hochanadel (13).

Initial LET	Experimental G	Theoretical G
0.01	8.2	9.7
0.1	7.9	9.6
0.3	7.0	9.3
1.0	5.8	8.6
2.0	5.4	7.7

If the fraction of H_2O_2 produced from the radical-radical reaction is taken to be that suggested by experimental G values in Hochanadel (13) (namely .115) and the back reaction is not considered, the following results are obtained:

Initial LET	Experimental G	Theoretical G
0.01	8.2	9.3
0.1	7.9	9.1
0.3	7.0	8.6
1.0	5.8	6.7
2.0	5.4	4.7

These experimental and theoretical G values are normalized and plotted in Fig. 36.

From the third approximation described in section 2.9 the following results are given:

Initial LET	Experimental G	Theoretical G
0.01	8.2	8.2
0.1	7.9	8.0
0.3	7.0	7.5
1.0	5.8	5.9
2.0	5.4	4.3

Figure 32 was taken from a paper by Faw and Miller (7) while Figs. 33 and 34 were obtained from results and techniques described in the aforementioned paper. Figure 31 was obtained from results listed in section 3.1 and additional calculations. Figure 35 was obtained using a 10 point Gaussian quadrature integration (performed by hand) to evaluate the following integral

$$\overline{Y}_{RS} = \frac{\int_{E_{min}}^{E_o} Y_{RS}(E)\ell'(E,\delta_c)z(E_o,E)dE}{\int_{E_{min}}^{E_{max}} z(E_o,E)\ell'(E,\delta_c)dE}$$

to evaluate the average chemical yield as a function of initial LET which is plotted in Fig. 35.

The yield ($Y_{RS}(E)$) obtained in Fig. 34 for the track model is somewhat uncertain since identical reaction parameters are used for the spur and the track model. In reality, r_o should probably be smaller for the track model.

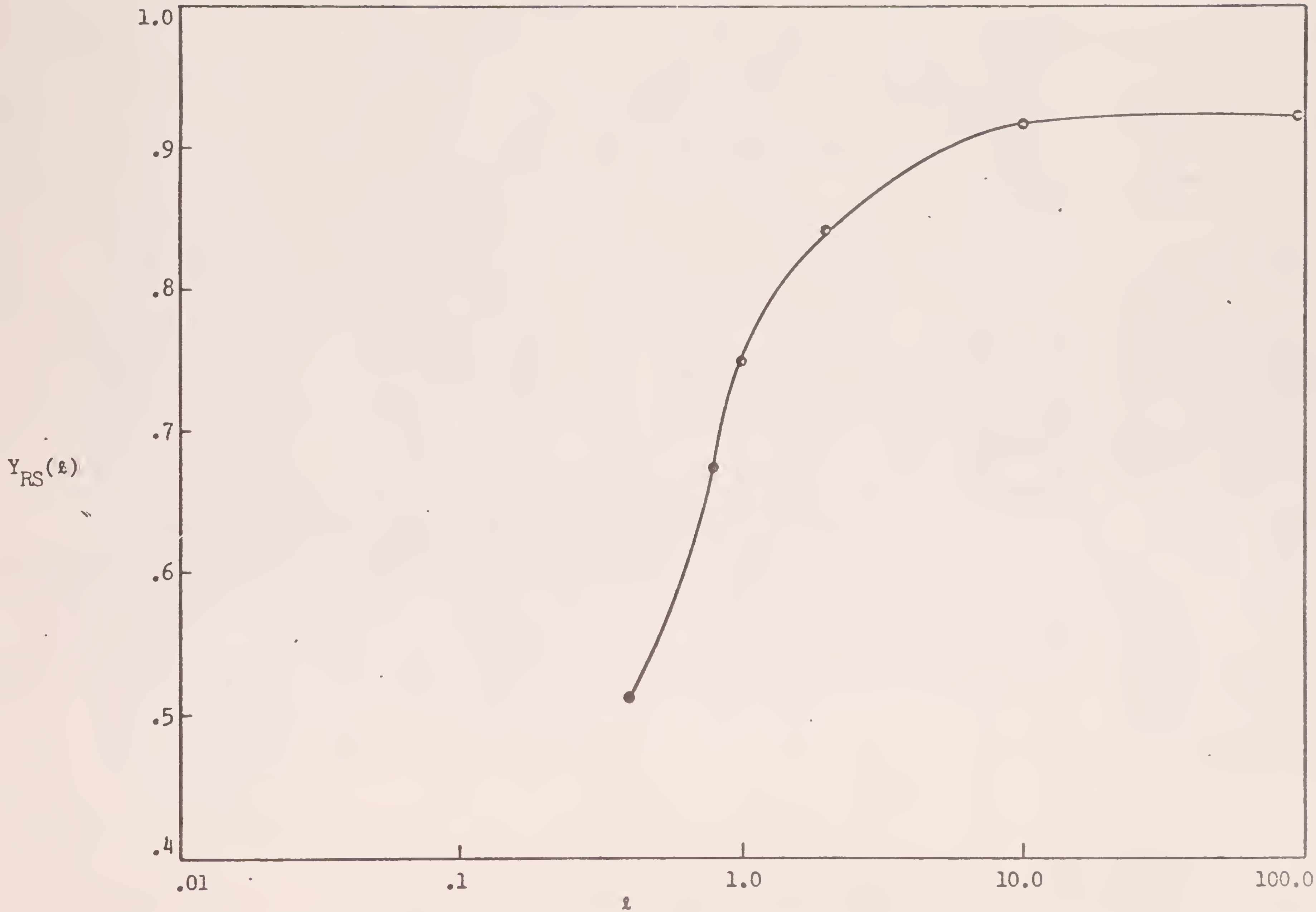

Fig. 31. Plot of the Fractional Chemical Yield $Y_{RS}(\ell)$ vs. ℓ for A = .0995, B = .00324 in which $\ell = \ell'/2r_o$

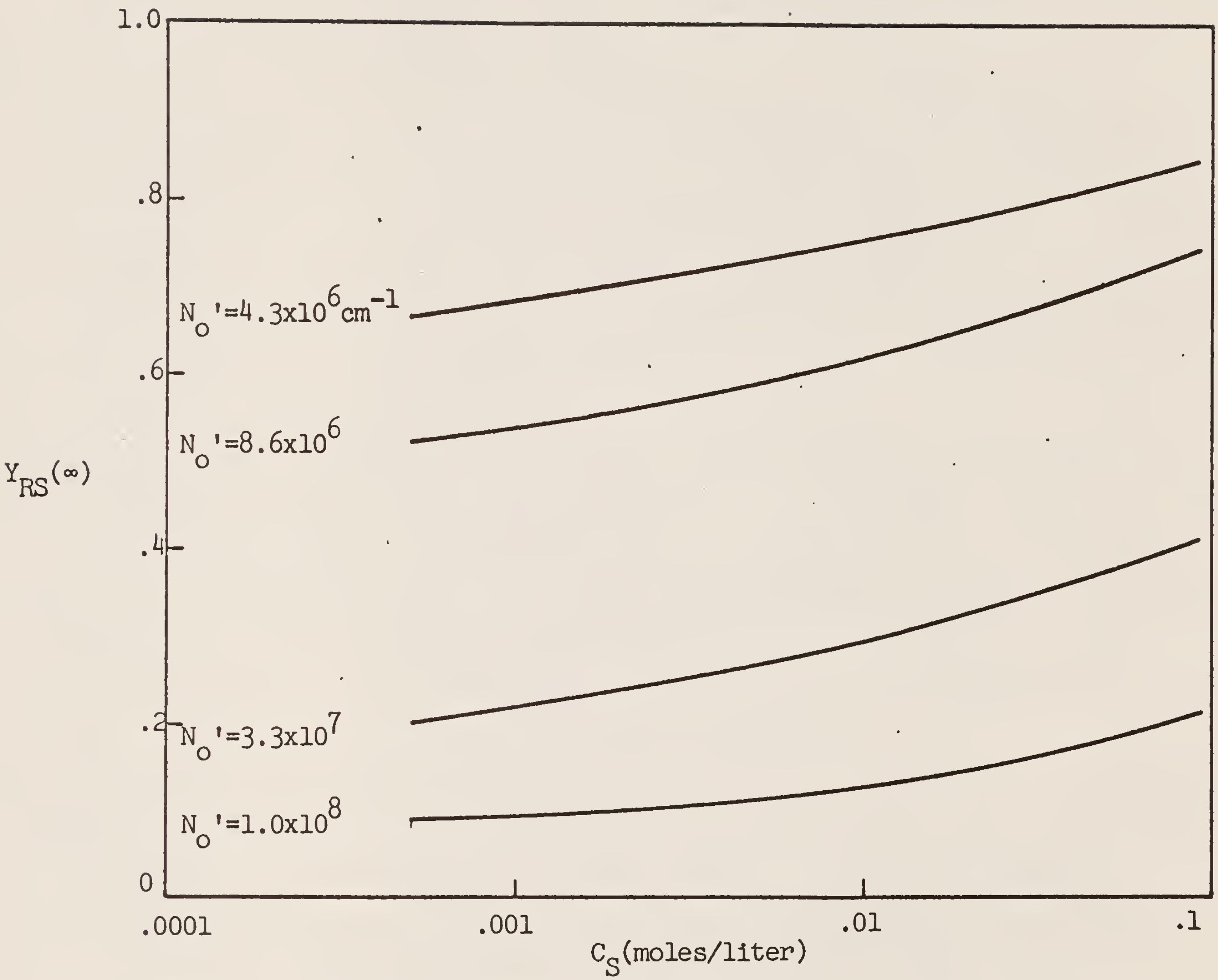

Fig. 32. Plot of the Fractional Chemical Yield Y_{RS} vs. the Solute Concentration C_S With the Number of Radicals Produced per Centimeter Along Cylindrical Tracks (N_o') as a Parameter (This Figure is Taken From a Paper by Faw and Miller (10)

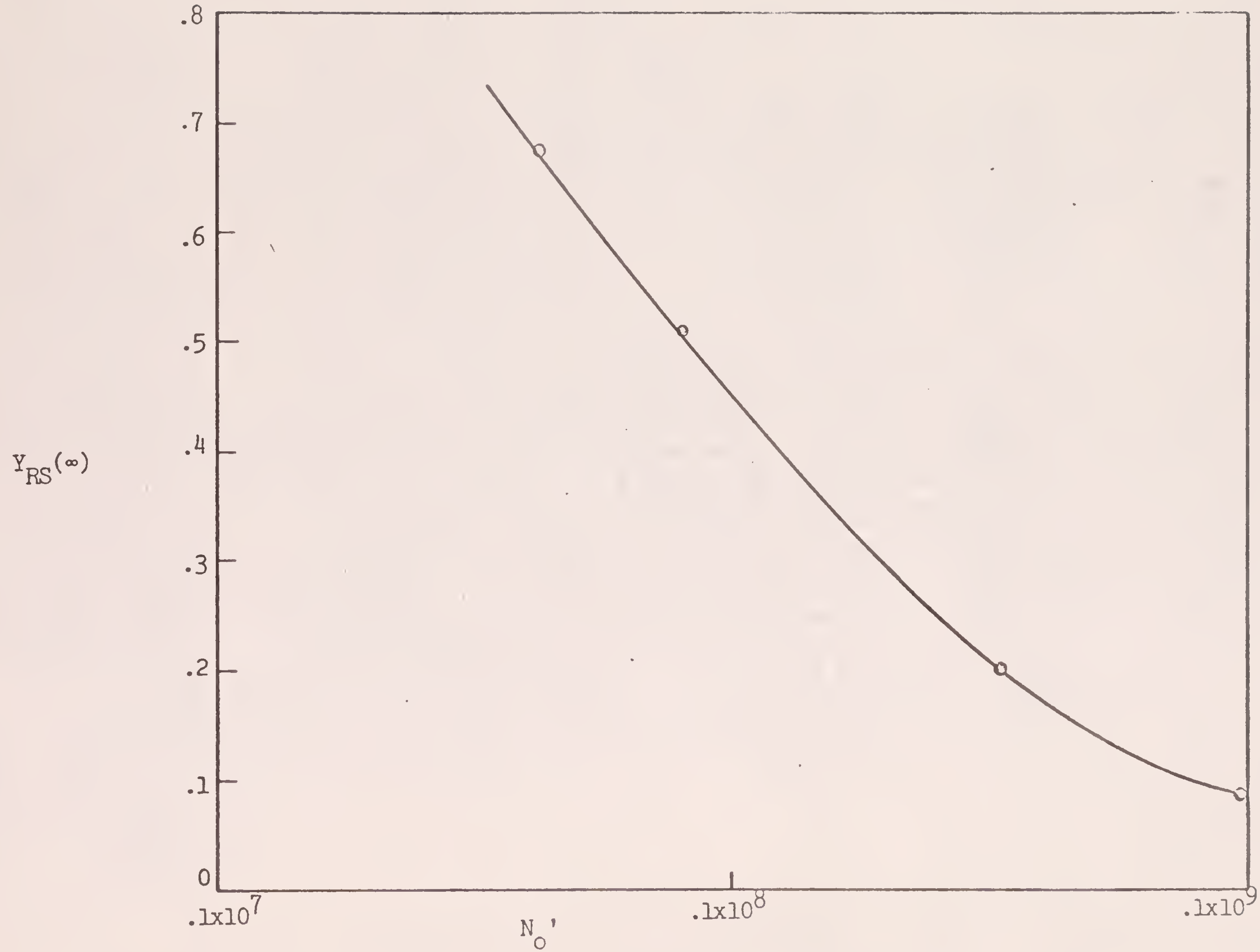

Fig. 33. Plot of the Fractional Chemical Yield Y_{RS} for Cylindrical Tracks vs. the Number of Radicals Produced per Centimeter (N_o') With C_S=.0005

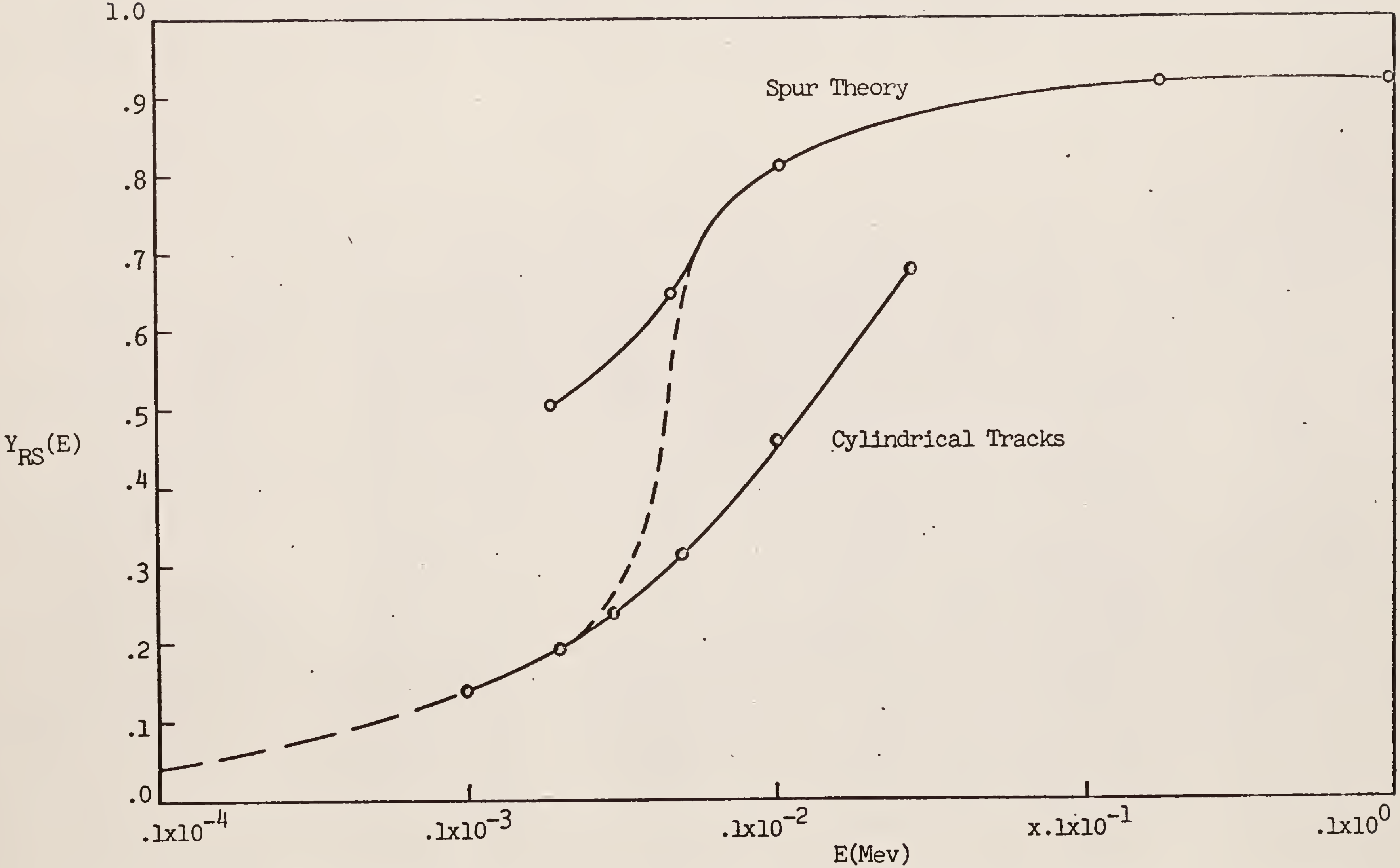

Fig. 34. Plot of the Fractional Chemical Yield Y_{RS} vs. Electron Energy Making Use of Both the Spur and Cylindrical Track Models

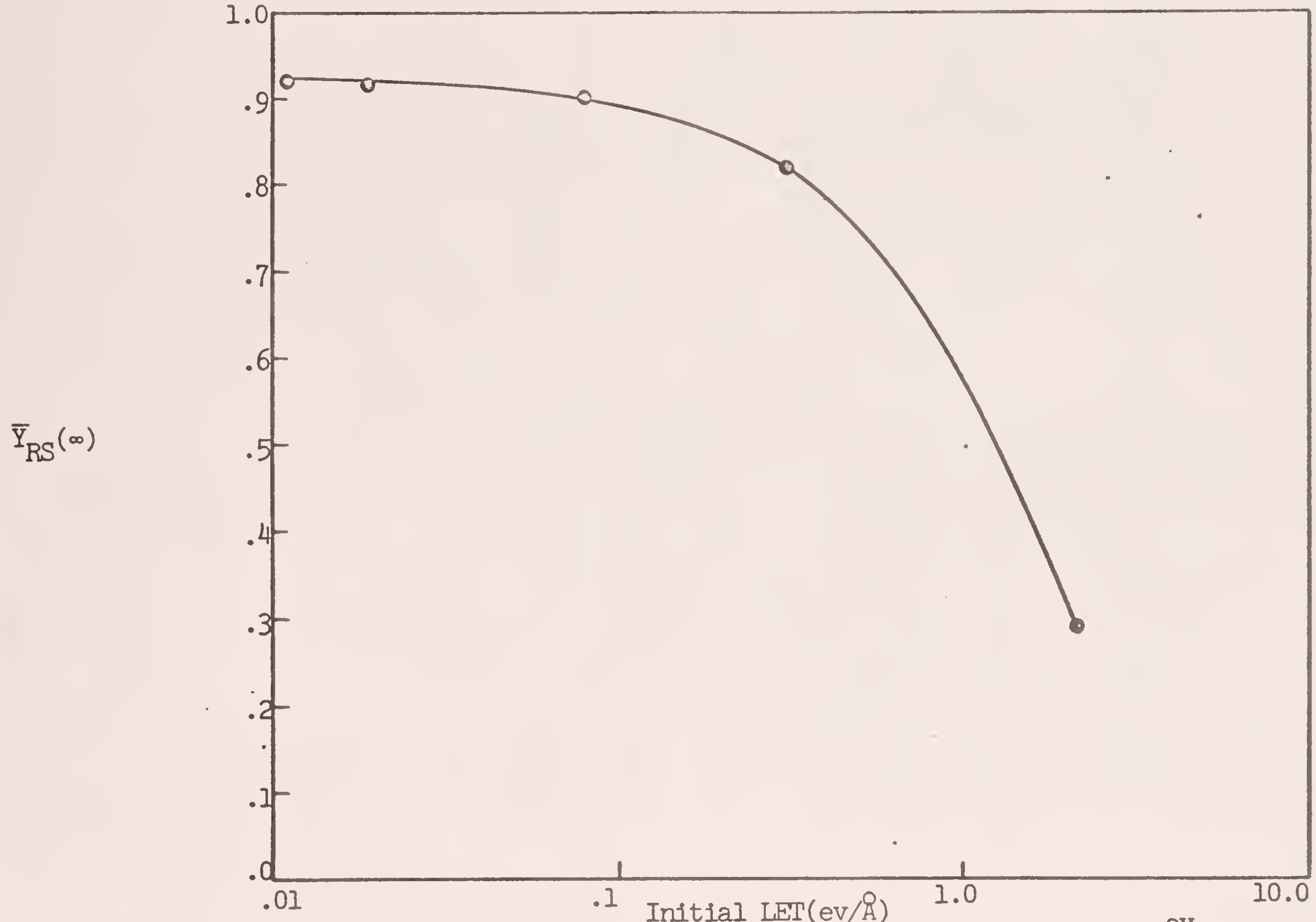

Fig. 35. Plot of the Average Chemical Yield vs. Initial LET $(\frac{ev}{Å})$

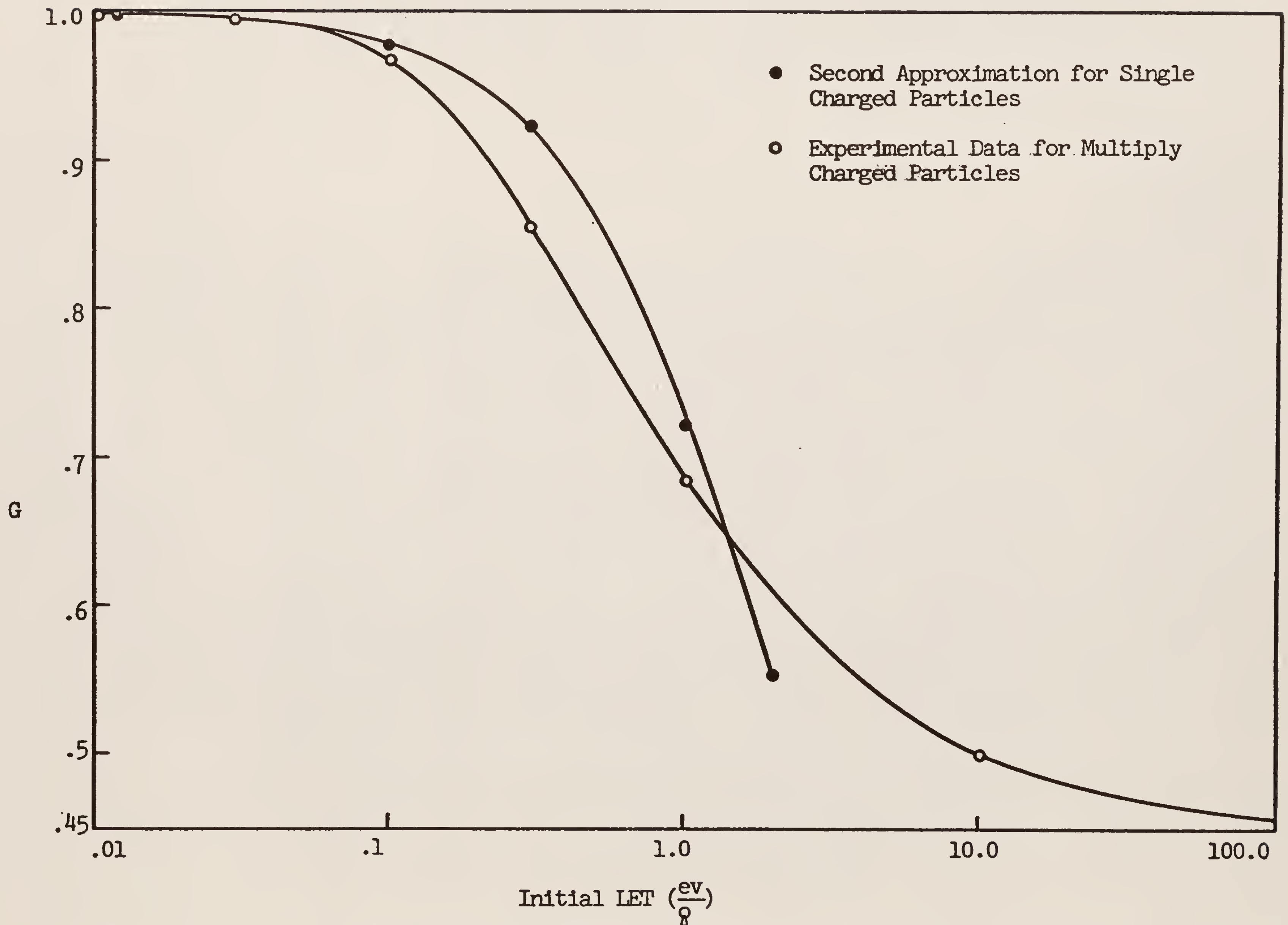

Fig. 36. Plot of Experimental and Theoretical G Values (Normalized to 1.0) vs. Initial LET. The Theoretical G Values Were Obtained From the Second Approximation Described in Section 2.9

3.10 Suggestions for Further Work

Much work has yet to be done in the field of Radiation Chemistry. Therefore, only those subjects of interest to the author are discussed here. Before accurate predictions of chemical yield induced by ionizing radiation for practical conditions can be made, it will be necessary to predict yields for complex reaction mechanisms. This accomplishment will require considerably better computing facilities than those presently available at Kansas State University.

There are a number of parameters associated with the mathematical model presented in section 2.1, for which the chemical yield is sensitive, that need to be determined accurately. Much of the limitation of accurate theoretical predictions is due to the lack of knowledge of the electron-electron collision cross sections for low energy electrons and for small energy losses. This cross section is given fairly accurately by the Moller cross section for electron energies above 2 Kev and for energy losses above 100 ev. Due to the complexity of this problem, it would be advisable to solve the problem experimentally. Extended experimental data could be utilized in the manner described in section 2.5.

Upon solution of the cross section problem, electron energy spectra could be obtained for low energy electrons. This would require a slight modification of the theory presented in section 2.2. The spectrum of spur separation distances would easily be obtained if the cross section problem were solved.

Determination of the average spur size depends strongly upon the effective maximum spur size. If this and the electron-electron cross section were known accurately, the average spur size could be obtained accurately. Rather than average the local energy loss over the entire energy spectrum, it would be more rigorous to find the average energy loss as a function of electron energy and, in turn, average this spectrum over the fractional chemical yield. This average energy loss should be essentially independent of energy down to a few Kev.

The effective maximum spur size could be approximated by considering the range of the delta ray in conjunction with the localization of the energy loss as obtained by the uncertainty principle. An energy loss as large as 400 ev is quite well localized. However, the resulting delta ray could lose its energy in such a manner that the entire 400 ev would result in one spur. For accurate determination of the effective maximum energy loss, one would need accurate range-energy information obtained from the low energy cross section.

For this work, the initial distribution of radicals is assumed to be Gaussian, it is also assumed that the Gaussian form is maintained as the spur expands. This assumption can be checked by direct numerical integration of the diffusion kinetics equation. The initial distribution, according to Hochanadel (13),is a function of LET and is not exactly Gaussian. It would be possible to carry out a full parametric study to indicate the importance of each parameter. Other ramifications of the associated subject matter may be investigated if the reader desires.

4.0 ACKNOWLEDGMENT

The author is grateful for support given by the National Science Foundation through a Research Initiation Grant. Appreciation goes to the staff of the Computing Center at Kansas State University for computing time on the IBM 1410 computer.

The author sincerely appreciates the extensive technical assistance and encouragement given by Dr. Richard E. Faw. Sincere gratitude is also given to Dr. William R. Kimel for making this study possible. The assistance of Dr. J. O. Mingle is also gratefully acknowledged.

5.0 REFERENCES

1. Abramowitz, Milton and Irene A. Stegun
   Handbook of Mathematical Functions With Formulas, Graphs and Mathematical Tables, National Bureau of Standards Applied Mathematics Series 55, (1965).

2. Bame, S. J., E. Hadded, J. E. Perry and R. K. Smith
   Absolute Determination of Monoenergetic Neutron Flux in the Energy Range 1 to 30 Mev, Rev. Sci. Instr. 28, 997-1006, (1957).

3. Berger, Martin J. and Stephen M. Seltzer
   Tables of Energy Losses and Ranges of Electrons and Positrons, National Aeronautics and Space Administration, (1964).

4. Bruce, W. R., M. L. Pearson and Helen S. Freedhoff
   The Linear Energy Transfer Distributions Resulting from Primary and Scattered X-Rays and Gamma Rays with HVL's 1.25 mm Cu to 11 mm Pb, Radiation Research 19, 606-620, (1963).

5. Burch, P. R.
   A Theoretical Interpretation of the Effect of Radiation Quality on Yield in the Ferrous and Ceric Sulfate Dosimeters, Radiation Research 11, 481-497, (1959).

6. Burch, P. R.
   Calculations of Energy Dissipation Characteristics in Water for Various Radiations, Radiation Research 6, 289-301, (1957).

7. Faw, R. E. and L. F. Miller
   Charged Particle Slowing-Down Spectra for Fast Neutron Irradiation of Water, Trans. Amer. Nuclear Soc., November, 1965 (in press).

8. Faw, R. E.
   Charged Particle Slowing-Down Spectra and Energy Loss Distribution for Fast Neutron Irradiation of Water, submitted to Radiation Research.

9. Faw, R. E.
   Spur Coalescence in Radiation Chemistry, Kansas Engineering Experiment Station, Special Report Number 44, Manhattan, Kansas, (1963).

10. Faw, R. E. and L. F. Miller
    Track Effects in Radiation-Induced Chemical Reactions, Proceedings of the A.I.Ch.E. Symposium on Photoreactor Design, February, 1966 (in press).

11. Grodstein, Gladys White
X-Ray Attentuation Coefficients From 10 Mev to 100 Mev, National Bureau of Standards Circular 583, (1957).

12. Harder, Von Dietrich
Physikalische Grundlagan zur Relativen Biologischen Wirksamkeit, Biophysik 1, 225-258, (1964).

13. Hochanadel, C. J.
Radiation Chemistry of Water, in "Comparative Effects of Radiation", M. Burton, J. S. Kirby-Smith and L. L. Magee (eds), Wiley, New York, (1960).

14. Johns, H. E. and I. S. Laughlin
Interaction of Radiation with Matter, in "Radiation Dosimetry", Hine and Brownell (eds.) Academic Press, New York (1956).

15. Kalos, M. H., H. Goldstein and S. Ray
Revised Cross Sections for Neutron Interactions with Oxygen and Deuterium, UNC-5038, (1962).

16. Kupperman, A.
Diffusion Kinetics in Radiation Chemistry, in "The Chemical and Biological Action of Radiation", Vol. V. Haissinsky (ed.), Academic Press, London, (1961).

17. Lassettre, Edwin N. and Stanley A. Francis
Inelastic Scattering of 390-V Electrons by Helium, Hydrogen, Methane, Ethane, Cyclohexane, Ethylene and Water, Journal of Chemical Physics, Volume 40, Number 5, 1208-1217, (1963).

18. Magee, J. L.
Radiation Chemistry, Annual Review of Physical Chemistry, 12, 389, (1961).

19. Mathews, Jon and R. L. Walker
Mathematical Methods of Physics, W. A. Benjamin, Inc., New York, New York, (1954).

20. McGinnies, Rosemary T.
Energy Spectrum Resulting from Electron Slowing Down, Natinnal Bureau of Standards Circular 597, (1959).

21. Rossi, Bruno
High-Energy Particles, Prentice-Hall, Inc., Englewood Cliffs, N. J., (1952).

22. Spencer, L. V. and U. Fano
Energy Spectrum Resulting from Electron Slwoing Down, Phys. Rev. 93, 1172-1181, (1954).

6.0 EXPLANATION OF THE COMPUTER PROGRAMS USED IN THIS WORK

6.1 Integration of the Chemical Yield Expression

The yield expression

$$Y_{RS}(\theta) = \int_0^{\theta} \frac{e^{-\tau} d\tau}{1 + A\, e^{B} \sqrt{B}\, K(\tau,B,n,\ell)} \tag{73}$$

in which

$$K(\tau,B,n,\ell) = \int_B^{B+\tau} \frac{e^{-t''} dt''}{(t'')^{3/2}} \left[\frac{1}{2} + \sum_{m=1}^{n-1} \frac{n-m}{n}\, e^{-\ell^2 m^2 B/t''} \right] \tag{74}$$

was not difficult to program for numerical integration. However, the calculations were rather time-consuming to obtain accurate results if B and ℓ were small and a large number of spurs were considered for a chain. Therefore, several integration schemes were employed. The first method utilized a subroutine "BATES" to generate the weights for integration points chosen on a logarithmic scale. Consistent results were obtained when more than 10 integration points were used for the main integration and more than 15 for evaluating the function $K(\tau,B,n,\ell)$.

It was found that Gaussian quadrature integration was more efficient for calculating the yield as a function of the upper limit θ, defined in section 2.1 of the theory.

To evaluate the yield for infinite time, which corresponds to infinite θ, integration utilizing the weights and roots of Laguerre polynomials was found to be most efficient. Laguerre integration was very useful for this case since the interval of orthogonality of Laguerre polynomials is zero to infinity.

As a result, the yield calculations for the parameters A,B,n,ℓ and θ were performed using Gaussian quadrature integration and those for θ equal to infinity were performed using Laguerre integration. The program utilizing the subprogram BATES was used to cross-check the results of each.

A very important point to take into consideration was that the integrand in the first term on the right-hand side of Eq. (74) behaved very badly if B became small. A Taylor's expansion of the second term about B illustrated that it was well-behaved for all B of interest. Therefore, it proved quite benefical to evaluate

$$A\, e^B \sqrt{B} \int_B^{B+\tau} \frac{dt''\, e^{-t''}}{(t'')^{3/2}} ,$$

analytically in terms of error functions. According to reference (1), error functions are defined as

$$\mathrm{erf}(x) = \frac{2}{\sqrt{\pi}} \int_0^x e^{-t^2} dt. \tag{193}$$

One can then integrate the above ill-behaved expression by parts with the result:

$$A\, e^B \sqrt{B} \int_B^{B+\tau} \frac{dt''\, e^{-t''}}{(t'')^{3/2}} = A \left\{1 - \frac{\sqrt{B}\, e^{-\tau}}{\sqrt{B+\tau}}\right.$$

$$\left. - e^B \sqrt{B}\, \sqrt{\pi}\, (\mathrm{erf}(\sqrt{B+\tau} - \mathrm{erf}\,(\sqrt{B})\right\} \tag{194}$$

A polynomial approximation from reference (1) was used to evaluate the error function for the programs in which Eq. (194) was used.

6.1.1 Method Using the Subprogram BATES to Generate the Weight Factors for Numerical Integration

To make possible logarithmic steps of integration, a change of variable was made for τ,

$$\tau = \tau' - \eta \tag{195}$$

thus giving the following expression when substituted into Eq. (73):

$$Y_{RS}(\theta) = e^{\eta} \int_{\eta}^{\eta + \theta} \frac{e^{-\tau'} d\tau}{1 + A \sqrt{B}\, e^{B} K(\tau' - \eta, B, n, \ell)} . \tag{196}$$

Since $K(\tau - \eta, B, n, \ell)$ was used as a FUNCTION statement, the main program evaluated the following sum:

$$Y_{RS}(\theta) = e^{\eta} \sum_{i=1}^{NWT} \frac{e^{-\tau_i'} W_i}{1 + A e^{B} \sqrt{B}\, K(\tau_i' - \eta, B, n, \ell)} . \tag{197}$$

The FUNCTION statement for $K(\tau_i - \eta, B, n, \ell)$ evaluated the following expression:

$$K(\tau_i - \eta, B, n, \ell) = \sum_{j=1}^{NWT} \frac{e^{-t_j''}}{(t_j'')^{3/2}} \left[\frac{1}{2} + \sum_{m=1}^{n-1} \frac{(n-m)}{n} e^{-\ell^2 m^2 B / t_j''} \right] W_j . \tag{198}$$

The t_j'' points are chosen between B and $B + \tau_i' - \eta$ with a geometric progression of NWT points. In terms of the maximum and minimum points on the interval for NWT points, the ratio between terms was chosen by

$$\xi = \left[\frac{x_{NWT}}{x_1} \right]^{\frac{1}{NWT - 1}} . \tag{199}$$

The variables (A, B, n, ℓ, θ and η) used for this formulation were respectively given by (A,B,AN,AL,THETA and ADD) in the program listing. Other program variables should be self-explanatory. Logic diagrams are given for the main program and also for the subprogram AK in this section.

The subprograms used for this program were:

FUNCTION AK(THETA1,B,N,L)

SUBROUTINE BATES (IWT,NWT,WTAB,WATES).

The subprogram BATES was explained in section 6.8.1.

LOGIC DIAGRAM FOR THE COMPUTER PROGRAM DESCRIBED IN SECTION 6.1.1

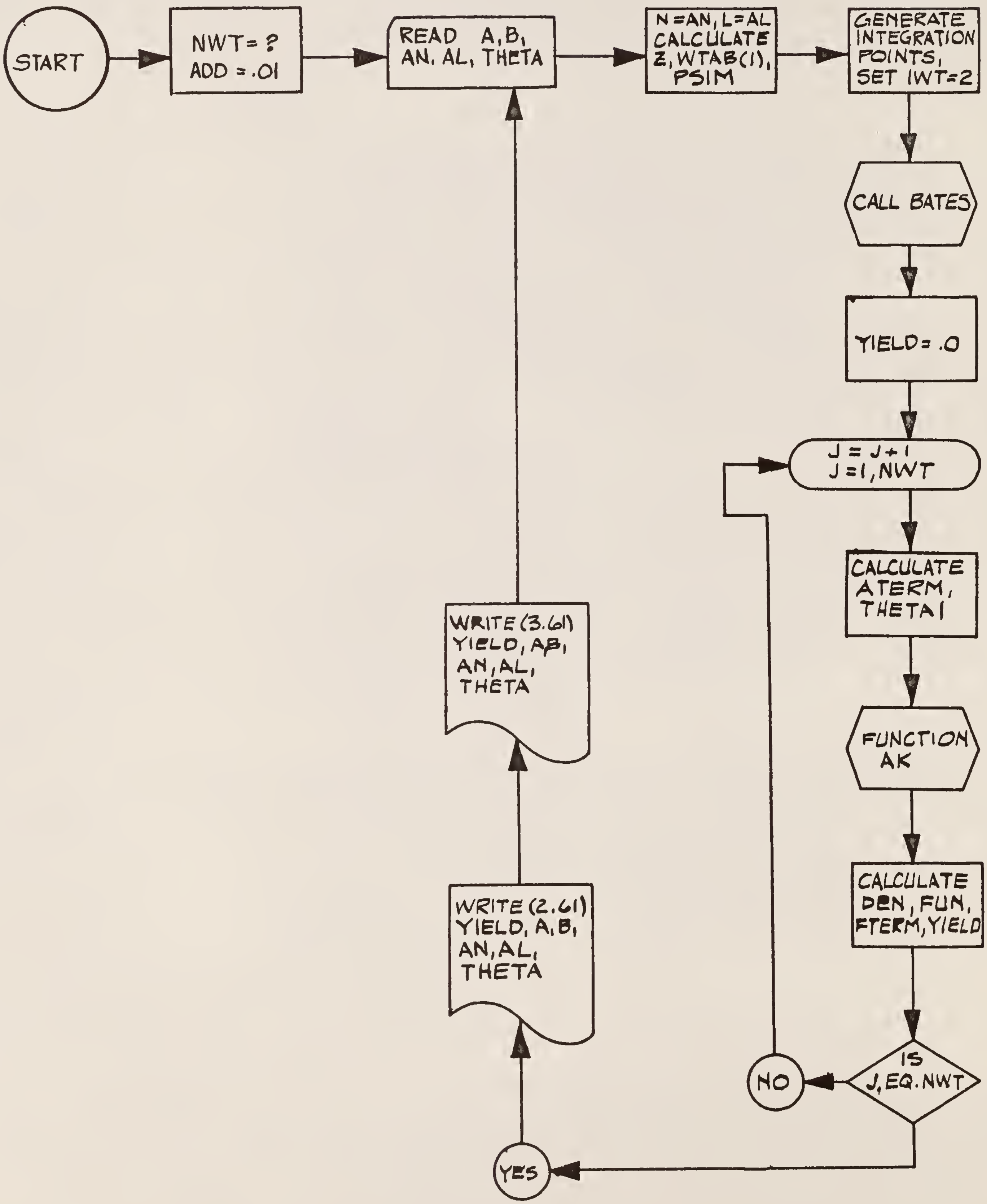

LOGIC DIAGRAM FOR THE FUNCTION STATEMENT DESCRIBED IN SECTION 6.1.1

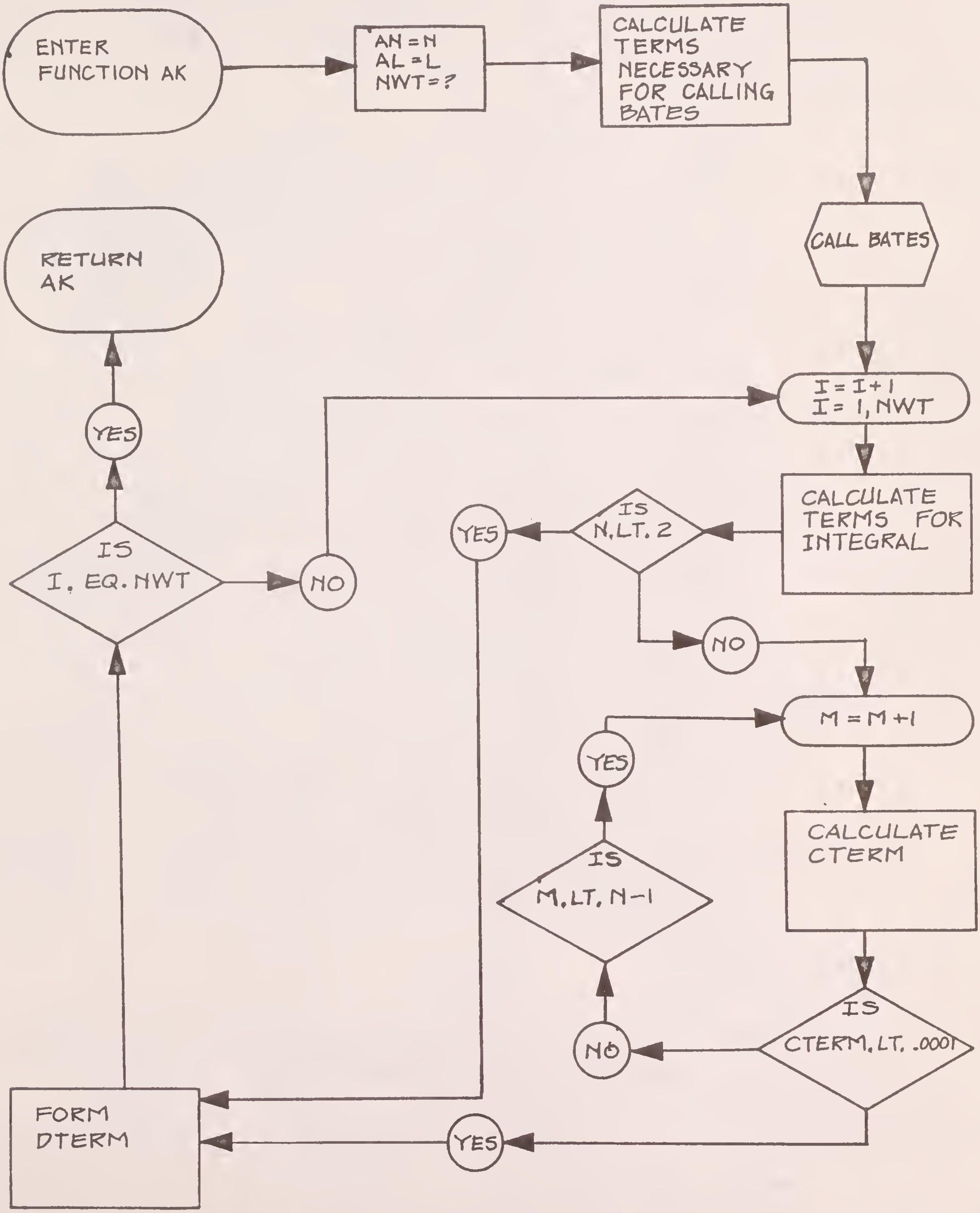

```
MON$$      JOB
MON$$      COMT 15,1, LAURENCE F. MILLER DEPT OF NUCLEAR ENG
MON$$      ASGN MJB,12
MON$$      ASGN MGO,16
MON$$      MODE GO,TEST
MON$$      EXEQ FORTRAN,,,,,,,YIFLDI1
      DIMENSION WTAB(100),WATES(100)
   60 FORMAT(1HK,6E14.8)
   61 FORMAT(6E10.4)
   70 FORMAT(5E10.5)
      NWT=7
      ADD=.01
   25 READ(1,70)A,B,AN,AL,THETA
      N=AN
      L=AL
      Z=A*SQRT(B)*EXP(B)
      WTAB(1)=THETA+ADD
      PSIM=(ADD/(ADD+THETA))**(1./FLOAT(NWT-1))
      DO 101 JA=2,NWT
  101 WTAB(JA)=WTAB(JA-1)*PSIM
      IWT=2
      CALL RATES(IWT,NWT,WTAB,WATES)
      YIELD=.0
      DO 50 J=1,NWT
      ATERM=EXP(-WTAB(J))
      THETA1=WTAB(J)-ADD
      DEN=1.+Z*AK(THETA1,B,N,L)
      FUN=ATERM/DEN
      ETERM=FUN*WATES(J)
   50 YIELD=YIELD+ETERM
      YIELD=YIELD*EXP(ADD)
      WRITE(2,61)YIELD,A,B,AN,AL,THETA
      WRITE(3,60)YIELD,A,B,AN,AL,THETA
      GO TO 25
      END
```

```
MON$$      EXEQ FORTRAN
      FUNCTION AK(THETA1,B,N,L)
      DIMENSION WTAB(100),WATES(100)
      AN=N
      AL=L
C  B CAN NOT BE ZERO
      NWT=9
      PSI=(B/(B+THETA1))**(1./(FLOAT(NWT-1)))
      WTAB(1)=B+THETA1
      DO 5 JF=2,NWT
    5 WTAB(JF)=WTAB(JF-1)*PSI
      IWT=2
      CALL BATES(IWT,NWT,WTAB,WATES)
      BSUM=.0
      DO 80 I=1,NWT
      Y=WTAB(I)
      BTERM=1./Y**1.5
      IF(N.LT.2)GO TO 12
      M=0
      ASUM=.0
   20 M=M+1
      AM=M
      R=AL*AL*AM*AM
      IF(N.LT.200)CTERM=EXP(-R*B/Y)*(AN-AM)/AN
      IF(N.GT.200)CTERM=EXP(-R*B/Y)
      ASUM=ASUM+CTERM
      IF(CTERM.LT..0001)GO TO 12
      IF(M.LT.N-1)GO TO 20
   12 CONTINUE
      DTERM=BTERM*EXP(-Y)*(.5+ASUM)
   80 BSUM=BSUM+DTERM*WATES(I)
      AK=BSUM
      RETURN
      END
```

6.1.2 Method Using Gaussian Quadrature

Since Gaussian quadrature integration was found to be a very common integration scheme, the method of obtaining the associated weights and roots from the polynomials is not given. When the upper and lower limits were not +1 and -1, the following change of variable was made:

$$\int_a^b f(x)dx = \frac{b - a}{2} \int_{-1}^{+1} dy\ g(y) \tag{200}$$

in which

$$g(y) = f(x)\Big|_{x = \frac{(a + b)}{2} + \frac{(b - a)}{2} y} . \tag{201}$$

The weights and roots listed for Gaussian quadrature integration are defined such that

$$\int_{-1}^{+1} dy\ g(y) = \sum_{j=1}^{NWT} W_j\ g(y_j). \tag{202}$$

Since the limits on Eqs. (73) and (74) do not correspond to the interval of orthogonality of the polynomials from which the weights and roots were obtained, the following changes of variable were needed:

$$t'' = B + \tau/2\ (1 + \xi) \tag{203}$$

and

$$\tau = \theta/2\ (1 + \gamma). \tag{204}$$

Making these changes resulted in:

$$Y_{RS}(\theta) = \frac{\theta}{2} \int_{-1}^{+1} \frac{e^{-\frac{\theta}{2}(1 + \gamma)_d}}{1 + A\sqrt{B}\ e^{B} \frac{(1 + \gamma)}{4} K(\gamma,B,n,\ell)} \tag{205}$$

$$K(\gamma,B,n,\ell) = \int_{-1}^{+1} \frac{dt'' \, e^{-t''}}{(t'')^{3/2}} \left[\frac{1}{2} + \sum_{m=1}^{n-1} \left(\frac{n-m}{n}\right) e^{-\ell^2 m^2 B/t''} \right] \qquad (206)$$

Written in the form of finite sums, this gave:

$$Y_{RS}(\theta) = \frac{\theta}{2} \sum_{i=1}^{NWTL} \frac{e^{-\frac{\theta}{2}(1+\gamma_i)} W_i}{1 + A\sqrt{B}\, e^{B} \frac{\theta(1+\gamma_i)}{4} K(\gamma_i,B,n,\ell)} \qquad (207)$$

in which

$$K(\gamma_i,B,n,\ell) = \sum_{j=1}^{NWTG} \frac{1}{t_{ji}^{3/2}} e^{-t_{ji}''} \left[\frac{1}{2} + \sum_{m=1}^{n-1} \left(\frac{n-m}{n}\right) e^{-\ell^2 m^2 B/t_{ji}''} \right] W_j . \qquad (208)$$

The t_{ji}'' points were given by

$$t_{ji}'' = B + \frac{\theta}{4}(1+\gamma_i) + \frac{\theta}{4}(1+\gamma_i)\xi_j \qquad (209)$$

where γ_i and ξ_j were the roots for the outer and inner sums, respectively. The Gaussian quadrature weights and roots for the outer sum (indexed by i) were given respectively by WATESL and WTABL.

The variables A,B,n,ℓ and θ are given by A,B,AN,AL and THETA in the program listing. Logic diagrams are given in this section for the main program and subprogram AK.

The subprograms used were:

FUNCTION AK(TAP,B,N,AL)

FUNCTION ERF(X).

Subprogram ERF(X) is self-explanatory. The left-hand portion of the inner sum in the denominator was evaluated by error functions.

LOGIC DIAGRAM FOR THE COMPUTER PROGRAM
DESCRIBED IN SECTION 6.1.2

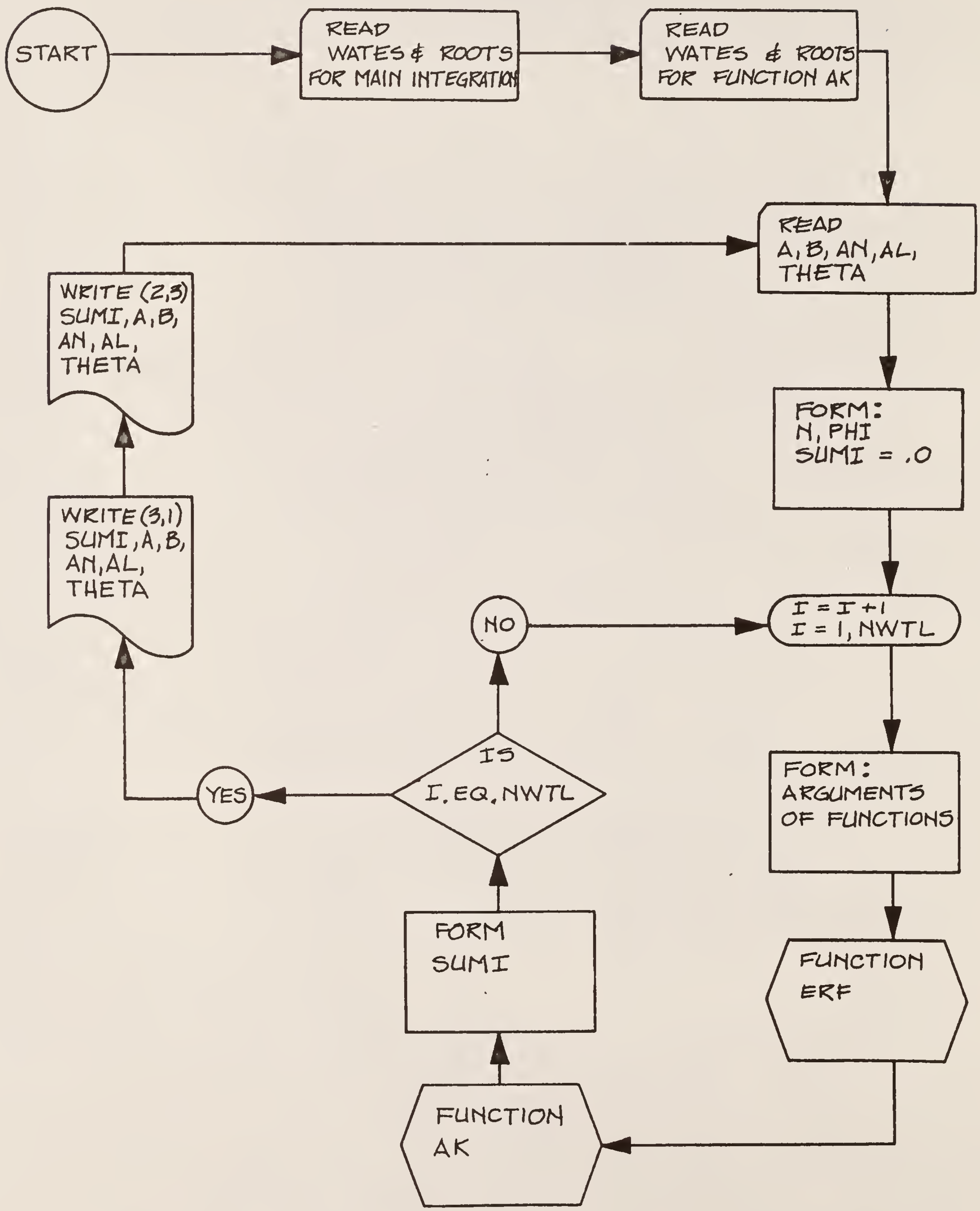

LOGIC DIAGRAM FOR THE FUNCTION STATEMENT DESCRIBED IN SECTION 6.1.2

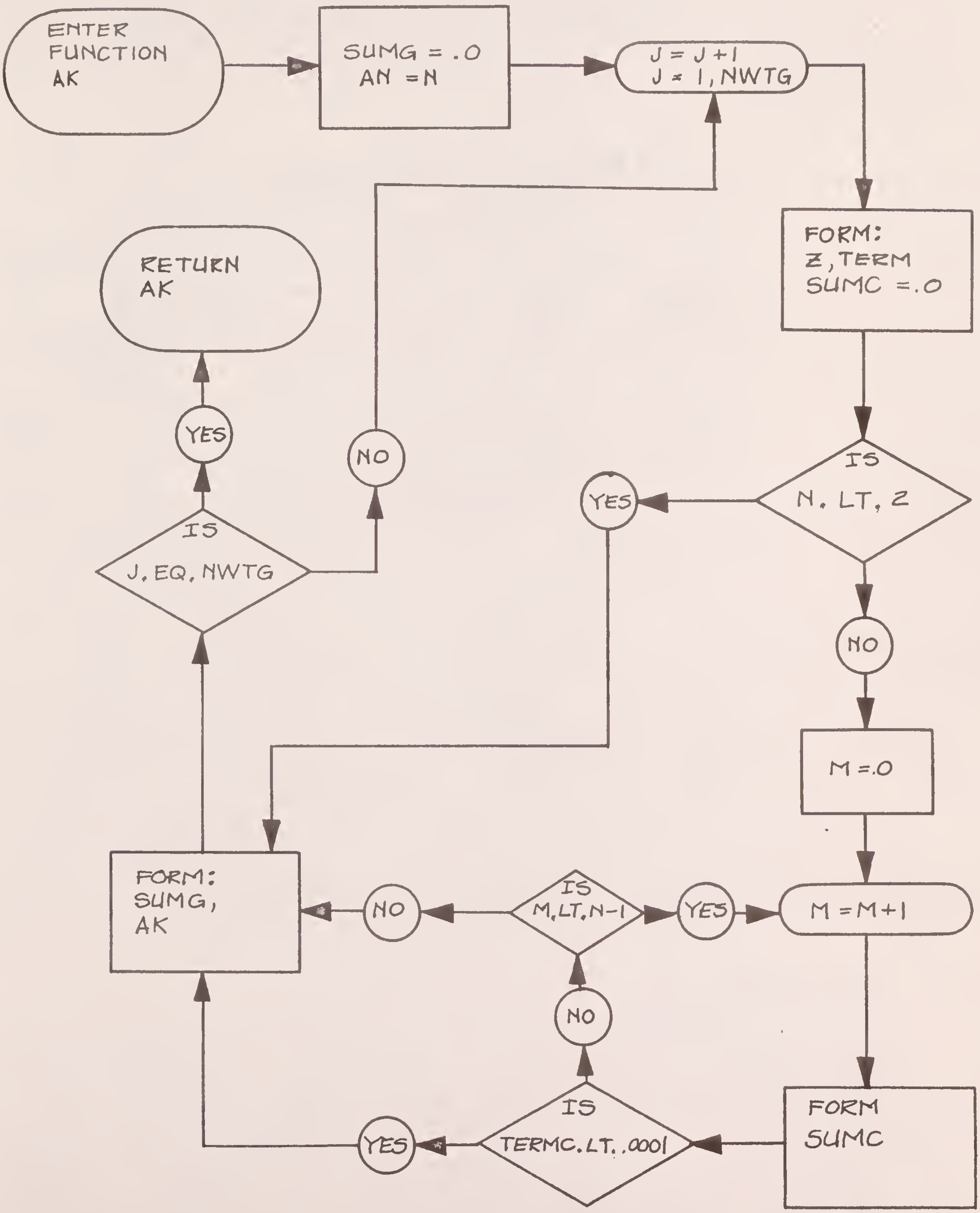

```
MON$$     JOB
MON$$     COMT 25MINUTES,2PAGES L.F. MILLER N.E.
MON$$     ASGN MJB,12
MON$$     ASGN MGO,16
MON$$     MODE GO,TEST
MON$$     EXEQ FORTRAN,,,12,,,,COMB
      COMMON WTABL(20),WATESL(20),WTABG(20),WATESG(20),NWTG
    1 FORMAT(1HK,6E14.6)
    2 FORMAT(I5/(2F20.16))
    3 FORMAT(6E14.6)
   61 FORMAT(6E10.4)
   70 FORMAT(5F10.5)
      READ(1,2)NWTL,(WTABL(K),WATESL(K),K=1,NWTL)
      READ(1,2)NWTG,(WTABG(N),WATESG(N),N=1,NWTG)
   25 READ(1,70)A,B,AN,AL,THETA
      N=AN
      PHI=A*SQRT(B)*EXP(B)
      SUM1=.0
      DO 20 I=1,NWTL
      XG=THETA/2.*(1.+WTABL(I))
      TAP=XG/2.
      AIONF=A*(1.-EXP(-XG)*SQRT(B/(B+XG))-EXP(B)*SQRT(B*3.1416)*(ERF
     1(SQRT(B+XG))-ERF(SQRT(B))))
      TERM1=EXP(-XG)*WATESL(I)/(1.+PHI*AK(TAP,B,N,AL)+AIONF)
      SUM1=TERM1+SUM1
   20 CONTINUE
      SUM1=SUM1*THETA/2.
      WRITE(3,1)SUM1,A,B,AN,AL,THETA
      WRITE(2,3)SUM1,A,B,AN,AL,THETA
      GO TO 25
      END
```

```
MON$$      EXEQ FORTRAN,,,12
      FUNCTION AK(TAP,B,N,AL)
      COMMON WTABL(20),WATESL(20), TABG(20),WATEG(20),NWT
      SUMG=.
      AN=N
      DO 10 J=1,NWTG
      Z=TAP*(1.+XTABG(J))+B
      TERM=EXP(-Z)/(Z*SQRT(Z))
      SUMC=0.
      IF(N.LT.2)GO TO 12
      M=0
   11 M=M+1
      AM=M
      R=AL*AL*AM*AM
      TERMC=(AN-AM)/AN*EXP(-R*B/Z)
      SUMC=SUMC+TERMC
      IF(TERMC.LT..0001)GO TO 12
      IF(M.LT.N-1)GO TO 11
   12 CONTINUE
      TERMG=TERM*SUMC*WATEG(J)
   10 SUMG=SUMG+TERMG
      AK=SUMG*TAP
      RETURN
      END
```

```
MON$$      EXEQ FORTRAN,,,12,,,,YTAB
      FUNCTION ERF(X)
      A1=.254829592
      A2=-.284496736
      A3=1.421413741
      A4=-1.453152027
      A5=1.061405429
      P=.3275911
      T=1./(1.+P*X)
      ERF=1.-(A1*T+A2*T*T+A3*T*T*T+A4*T*T*T*T+A5*T*T*T*T*T)*EXP(-X*
      RETURN
      END
```

6.1.3 Method Using a Combination of Laguerre and Gaussian Quadrature Integration

The weights and roots of Laguerre polynomials were defined in such a way that the following expression was true:

$$\int_0^\infty e^{-x} f(x)dx = \sum_{j=1}^{NWT} W_j \; f(x_j). \tag{210}$$

To use Laguerre integration for finite limits, a change of variable was made. The following equation illustrates this point:

$$\int_0^\theta e^{-x} f(x)dx = \int_0^\infty e^{-x} f(x)dx - e^{-\theta} \int_0^\infty e^{-x} f(x + \theta)dx. \tag{211}$$

Beginning with the chemical yield expression for the RS species, Eqs. (73) and (74), let $t'' = B + \frac{\tau}{2}(1 + y)$ and consider θ as infinite.

$$Y_{RS}(\infty) = \int_0^\infty \frac{e^{-\tau} d\tau}{1 + A\sqrt{B}\; e^{B}\; K(\tau,B,n,\ell)} \tag{212}$$

and

$$K(\tau,B,n,\ell) = \frac{\tau}{2} \int_{-1}^{+1} \frac{dy \; e^{-(B + \frac{\tau}{2}(1 + y))}}{\left[-1 \; B + \frac{\tau}{2}(1 + y)\right]^{3/2}}$$

$$\times \left[.5 + \sum_{m=1}^{n-1} \frac{n-m}{n} \exp\left\{-\ell^2 m^2 B/(B + \frac{\tau}{2}(1 + y)\right\}\right] . \tag{213}$$

The rewriting of Eq. (212) with finite sums gives

$$Y_{RS}(\infty) = \sum_{i=1}^{NWTL} \frac{W_i}{1 + A\sqrt{B}\ e^{B}\ K(\tau_i,B,n,\ell)} \tag{214}$$

in which NWTL was the number of points for the Laguerre integration and τ_i were the roots of the Laguerre polynomials. The function $K(\tau_i,B,n,\ell)$ was calculated by Gaussian quadrature integration,

$$K(\tau_i,B,n,\ell) = \frac{\tau_i}{2} \sum_{j=1}^{NWTG} \left[\frac{w_G(j) \exp\{-(B + \frac{\tau_i}{2}(1 + y_j))\}}{\left[B + \frac{\tau_i}{2}(1 + y_j)\right]^{3/2}} \times \left[.5 + \sum_{m=1}^{n-1} \left(\frac{n-m}{n}\right) \exp \quad -\ell^2 m^2 B/(B + \frac{\tau_i}{2}(1 + y_j))\right]\right] . \tag{215}$$

However, the first section was evaluated with error function called AIONE in the program. Therefore, the subprogram for $K(\tau_i,B,n,\ell)$ evaluated the following expression:

$$K(\tau_i,B,n,\ell) = \frac{\tau_i}{2} \sum_{j=1}^{NWTG} \frac{w_G(j)\ e^{-t_{ij}''}}{(t_{ij}'')^{3/2}} \sum_{m=1}^{n-1} \frac{n-m}{n}\ e^{-\ell^2 m^2 B/t_{ij}''} . \tag{216}$$

In the above Eq. (216), $t_{ij}'' = B + \frac{\tau_i}{2}(1 + y_j)$, and the y_j's were used as the roots for the Gaussian quadrature.

The Laguerre weights and roots were given by WATESL and WTABL, respectively in the program listing. The Gaussian quadrature weights and roots were given by WATESG and WTABG, respectively. Logic diagrams for the main program and subprogram AK are given in this section. The subprograms used were:

FUNCTION AK(THETA1,B,N,AL)

FUNCTION ERF(X).

Subprogram ERF(X) is considered self-explanatory. The parameters A,B,n and ℓ were given by A,B,AN and AL in the program listing.

LOGIC DIAGRAM FOR THE COMPUTER PROGRAM DESCRIBED IN SECTION 6.1.3

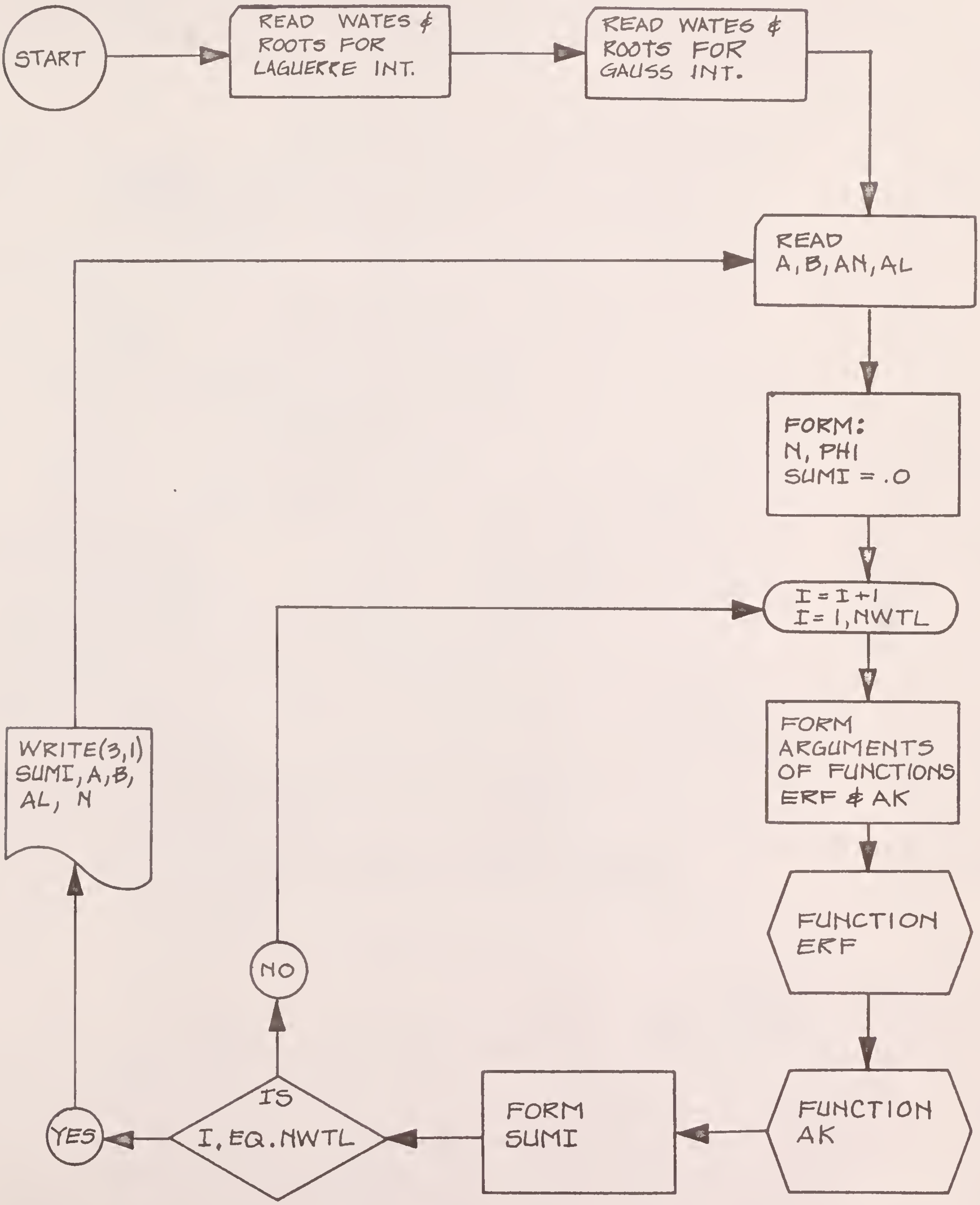

LOGIC DIAGRAM FOR THE FUNCTION STATEMENT DESCRIBED IN SECTION 6.1.3

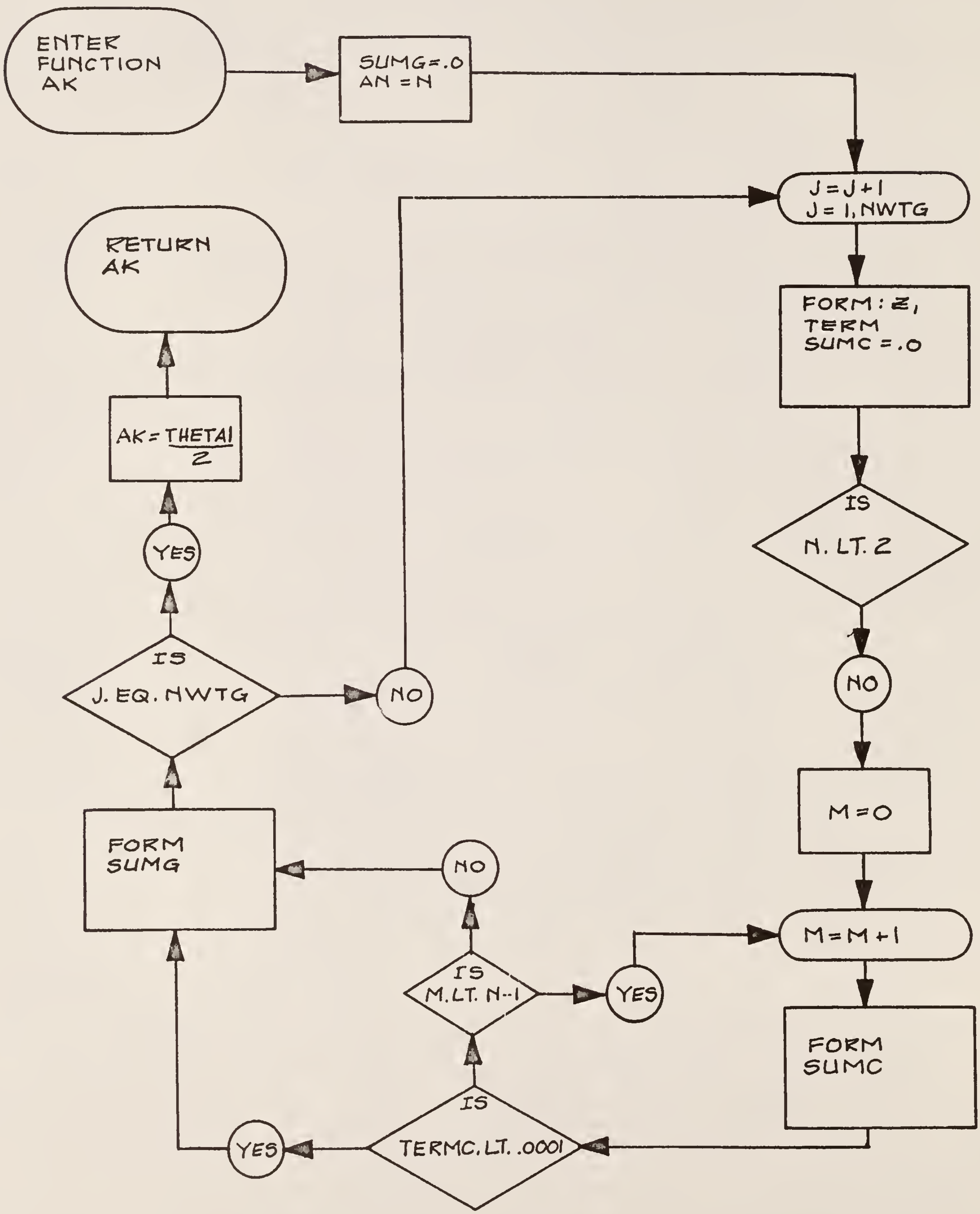

```
MON$$      JOB
MON$$      COMT 25MINUTES,2PAGES L.F. MILLER N.E.
MON$$      ASGN MJB,12
MON$$      ASGN MGO,16
MON$$      MODE GO,TEST
MON$$      EXEQ FORTRAN,,,12,,,,COMB
      COMMON WTABL(20),WATESL(20),WTABG(20),WATESG(20),NWTG
    1 FORMAT(1HK,7HYIELD =,F10.5,3HA =,F10.5,3HB =,F10.5,4HAL =,F10.5
     13HN =,I5)
    2 FORMAT(I5/(2F20.16))
   61 FORMAT(6E10.4)
   70 FORMAT(5F10.5)
      READ(1,2)NWTL,(WTABL(K),WATESL(K),K=1,NWTL)
      READ(1,2)NWTG,(WTABG(N),WATESG(N),N=1,NWTG)
   25 READ(1,70)A,B,AN,AL
      N=AN
      PHI=A*SQRT(B)*EXP(B)
      SUM1=.0
      DO 20 I=1,NWTL
      XG=WTABL(I)
      AIONE=A*(1.-EXP(-XG)*SQRT(B/(B+XG))-EXP(B)*SQRT(B*3.1416)*(ERF
     1(SQRT(B+XG))-ERF(SQRT(B))))
      TERM1=WATESL(I)/(1.+PHI*AK(XG,B,N,AL)+AIONE)
      SUM1=TERM1+SUM1
   20 CONTINUE
      WRITE(3,1)SUM1,A,B,AL,N
      GO TO 25
      END
```

```
MON$$     EXEC FORTRAN,,,12
      FUNCTION AK(THETA1,B,N,AL)
      COMMON WTABL(20),WATESL(20),WTABG(20),WATESG(20),NWTG
      SUMG=.0
      AN=N
      DO 10 J=1,NWTG
      Z=THETA1/2.*(1.+WTABG(J))+B
      TERM=EXP(-Z)/(Z*SQRT(Z))
      SUMC=.0
      IF(N.LT.2)GO TO 12
      M=0
   11 M=M+1
      AM=M
      R=AL*AL*AM*AM
      TERMC=(AN-AM)/AN*EXP(-R*B/Z)
      SUMC=SUMC+TERMC
      IF(TERMC.LT..0001)GO TO 12
      IF(M.LT.N-1)GO TO 11
   12 CONTINUE
      TERMG=TERM*SUMC*WATESG(J)
   10 SUMG=SUMG+TERMG
      AK=SUMG*THETA1/2.
      RETURN
      END
```

```
MON$$     EXEC FORTRAN,,,12,,,,YTAB
      FUNCTION ERF(X)
      A1=.254829592
      A2=-.284496736
      A3=1.421413741
      A4=-1.453152027
      A5=1.061405429
      P=.3275911
      T=1./(1.+P*X)
      ERF=1.-(A1*T+A2*T*T+A3*T*T*T+A4*T*T*T*T+A5*T*T*T*T*T)*EXP(-X*X)
      RETURN
      END
```

6.2 Explanation of the Computer Program Which Calculates the Electron Spectrum Resulting from a Monoenergetic Electron Source

It was shown in section 2.2 that the following expression represents the differential electron flux at energy E_n resulting from a monoenergetic source of electrons at energy E_o:

$$z(E_o,E_n) = \left[\frac{\left[1 + \sum\limits_{j=1}^{n-p} w_j z(E_o,E_j) K_S(E_j,E_n) - \sum\limits_{i=n-p}^{n-1} w_i z(E_o,E_i) K_c(E_i,E_n)\right]}{F(E_o,E_n) - \left[\dfrac{4C(E_n + 1)w_n}{E_n(E_n + 2)^2} + \sum\limits_{i=n-p}^{n-1} w_i \bar{K}_c(E_i,E_n)\right]} \right] \qquad (116)$$

in which

$$K_S(E_j,E_n) = \frac{2C}{(\beta_j)^2} \left[\frac{1}{E_n} - \frac{1}{E_j - E_n} - \left[\frac{2 + \frac{1}{E_j}}{(E_j + 1)^2}\right] \ln\left[\frac{E_j - E_n}{E_n}\right] + \frac{E_j/2 - E_n}{(E_j + 1)^2} \right] \qquad (94)$$

$$K_C(E_i,E_n) - K_S(E_k,E_n) \qquad (217)$$

$$\bar{K}_c(E_i,E_n) = \frac{2C}{(\beta_n)^2} \left[\frac{1}{E_i - E_n} - \frac{1}{E_n} - \left[\frac{2 + \frac{1}{E_n}}{(E_n + 1)^2}\right] \ln\left[\frac{E_n}{E_i - E_n}\right] + \frac{(E_n - E_i/2)}{(E_n + 1)^2} \right] \qquad (98)$$

and

$$F(E_o,E_n) = \frac{2C}{(\beta_n)^2}\left[1 + \ln\left(\frac{\Delta}{\bar{Q}}\right) - \frac{\Delta}{E_n} - \frac{(2E_n + 1)}{E_n(E_n + 1)^2}\,\Delta\left(1 + \ln\left(\frac{E_n}{\Delta}\right)\right.\right.$$

$$\left. + \frac{1}{4}\,\Delta\,\frac{(2E_n - \Delta)}{(E_n + 1)^2}\right] \tag{102}$$

in which

$$\Delta = \begin{cases} E_n & \text{for } 2E_n \leq E_o \\ E_o - E & \text{for } 2E > E_o \end{cases}$$

$\bar{Q}$, C and B are defined in section 2.2.

This program evaluated the electron slowing down spectrum resulting from a unit monoenergetic source. Results are listed in section 3.2. The only required input data were: p, the number of points chosen to reduce the energy by 1/2 on a logrithmic scale; I_o, the mean ionization potential; Z/A, the ratio of atomic number to atomic weight; and E_o, the source energy. The entire program except subprogram BATES is listed in this section but a logic diagram is given only for the main program since the FUNCTION subprograms are considered self-explanatory and subroutine BATES is explained in section 6.8.1.

The functions $K_s(E_j,E_n)$, $K_c(E_i,E_n)$, $\bar{K}_c(E_i,E_n)$ and $F(E_o,E_n)$ were given in the program by:

```
FUNCTION XKS(E1,E)
FUNCTION XKC(E1,E)
FUNCTION XKCB(E1,E)
FUNCTION XFC(E)
```

Several program variables are defined in Tible XIV.

Table XIV. Input Data and Selected Variables

Symbol	Explanation
C	1/2 the Moller Formula Coefficient
QB	$\bar{Q}$, defined in section 2.2
BETA	β, ratio of the velocity of the electron to the velocity of light
MP	p, defined in section 2.2 (input data)
PSI	Ratio for the geometric progression
EZERO	Source energy, E_o (input data)
NMAX	Number of points needed for the iteration

LOGIC DIAGRAM FOR THE COMPUTER PROGRAM DESCRIBED IN SECTION 6.2

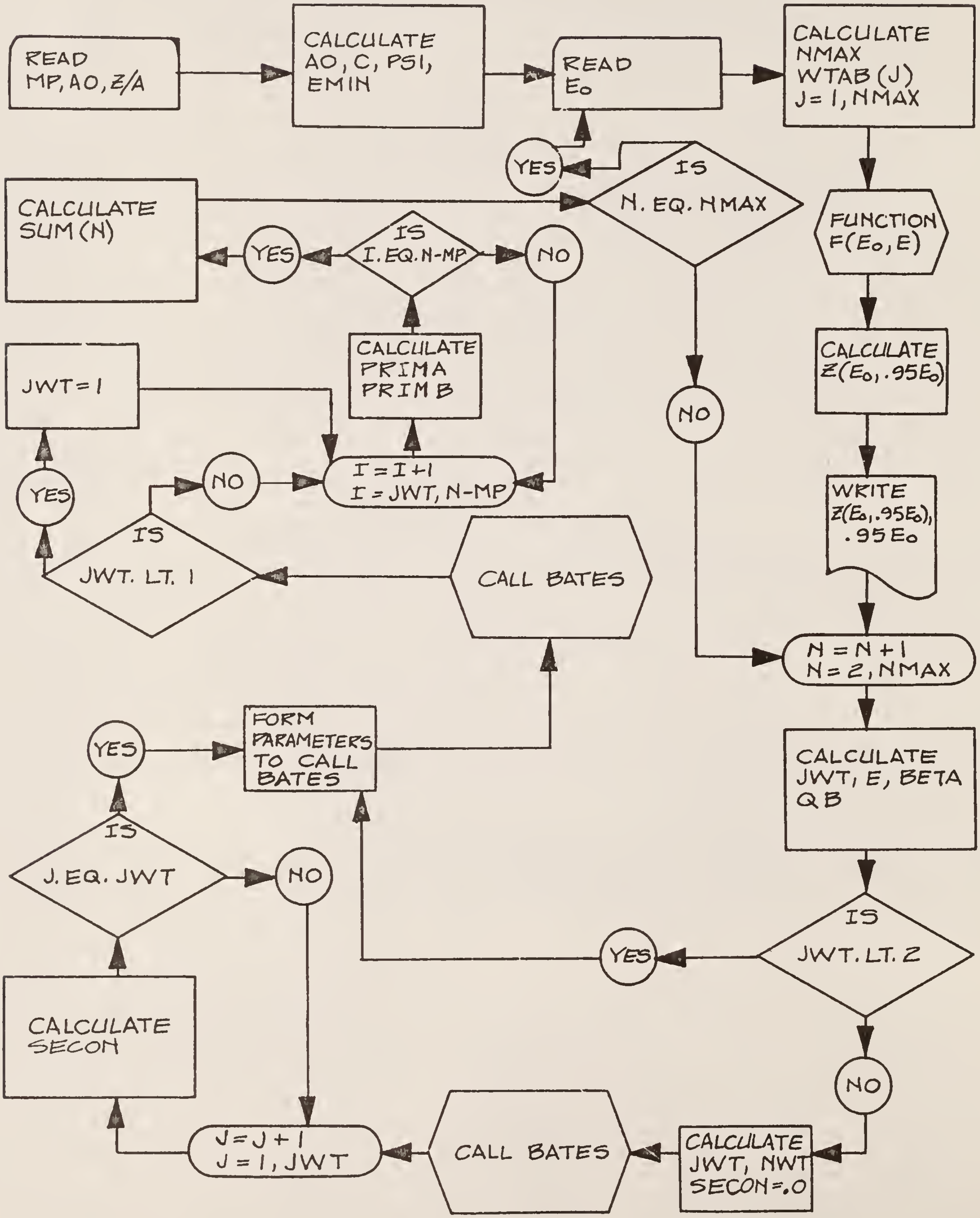

```
MON$$      JOB
MON$$      COMT 15MINUTES,5PAGES     LARRY   MILLER
MON$$      ASGN MJB,12
MON$$      ASGN MGO,16
MON$$      MODE GO,TEST
MON$$      EXEQ FORTRAN,,,,,,,SPECTRUM
      DIMENSION SUM(100),WTAB(100),WATES(100)
      COMMON C,QB,BETA,EZERO
    1 FORMAT(I5,2E14.8)
    2 FORMAT(F12.6)
    3 FORMAT(1HK,2E14.8)
   14 FORMAT(1HS,I5)
      READ(1,1)MP,AO,ZOVERA
      AO=AO/.51097
      C=.15*ZOVERA
      PSI=.5**(1./FLOAT(MP))
      EMIN=.0002/.51097
   21 READ(1,2)EZERO
      EZERO=EZERO/.51097
      NMAX=ALOG(EMIN/EZERO)/ALOG(PSI)+1.
      WRITE(3,14)NMAX
      WTAB(1)=EZERO
      SUM(1)=.0
      DO 8 IK=2,NMAX
      SUM(IK)=.0
    8 WTAB(IK)=WTAB(IK-1)*PSI
      E=.95*EZERO
      BETA=SQRT(E*(E+2.))/(E+1.)
      QB=AO*AO*EXP(BETA*BETA)/(E*(E+2.))*.5
      AFC=XFC(E)
      A=1./AFC
      SUM(1)=A*(1.-(3.14159**2/6.)/((AFC*BETA*BETA/(2.*C))**2))
      WRITE(3,3)SUM(1),E
      DO 7 N=2,NMAX
      JWT=N-MP
      E=WTAB(N)
      BETA=SQRT(E*(E+2.))/(E+1.)
      QB=AO*AO*EXP(BETA*BETA)/(E*(E+2.))*.5
      IF(JWT.LT.2)GO TO 5
      SECON=.0
      IWT=2
      NWT=JWT
      CALL WATES(IWT,NWT,WTAB,WATES)
```

```
      DO 4 J=1,JWT
      TERM=WATES(J)*SUM(J)*XKS(WTAB(J),E)
    4 SECON=SECON+TERM
    5 CONTINUE
      NWT=N
      IWT=2
      CALL WATES(IWT,NWT,WTAB,WATES)
      JWT=N-1
      PRIMA=.0
      PRIMB=.0
      IF(JWT.LT.1)JWT=1
      DO 6 I=JWT,IWT
      TERM=WATES(I)*SUM(I)*XKC(WTAB(I),E)
      PRIMA=PRIMA+TERM
      TERM=WATES(I)*XKCB(WTAB(I),E)
    6 PRIMB=PRIMB+TERM
      TERM=XFC(E)-C*4.*(E+1.)/(E*E*(E+2.)*(E+2.))*WATES(NWT)-PRIMB
      SUM(N)=(1.+SECON-PRIMA)/TERM
      WRITE(3,3)SUM(N),WTAB(N)
    7 CONTINUE
      IF(EZERO.GT..1)GO TO 21
      STOP
      END

     MON$$      EXEQ FORTRAN
      FUNCTION XFC(E)
      COMMON C,QB,BETA,EZERO
      COFC=2.*C/(BETA*BETA)
      DELTA=E
      IF(E.GT.EZERO/2.)DELTA=EZERO-E
      TMFC=(1.+ALOG(DELTA/QB)-DELTA/E-((2.+1./E)/(E+1.)**2)*
     1DELTA*(1.+ALOG(E/DELTA))+1./(E+1.)**2*(DELTA/2.)*(E-DELTA/2.))
      XFC=COFC*TMFC
      RETURN
      END
     MON$$      EXEQ FORTRAN
      FUNCTION XKC(E1,E)
      COMMON C,QB,BETA,EZERO
      T1=E1
      IF(E1.GE.2.*E)XKC=.0
      IF(E1.GE.2.*E)GO TO 913
      IF(E1.LE.E+QB)T1=E+QB
      BETA1=SQRT(T1*(T1+2.))/(T1+1.)
      COKC=2.*C/(BETA1*BETA1)
      TMKC=((T1-E)**(-1)-E**(-1)-((2.+T1**(-1))/(T1+1.)**2)*
     1ALOG(E/(T1-E))+((T1+1.)**(-2))*(E-T1/2.))
      XKC=COKC*TMKC
  913 RETURN
      END
```

```
      MON$$      EXEQ FORTRAN
      FUNCTION XKCB(E1,E)
      COMMON C,QB,BETA,EZERO
      T1=E1
      IF(E1.GE.2.*E)XKCB=.0
      IF(E1.GE.2.*E)GO TO 914
      IF(E1.LE.E+QB)T1=E+QB
      COKCB=2.*C/(BETA*BETA)
      TMKCB=((T1-E)**(-1)-E**(-1)-((2.+E**(-1))/(E+1.)**2)*
     1ALOG(E/(T1-E))+((E+1.)**(-2))*(E-T1/2.))
      XKCB=COKCB*TMKCB
  914 RETURN
      END


      MON$$      EXEQ FORTRAN
      FUNCTION XKS(E1,E)
      COMMON C,QB,BETA,EZERO
      T=E
      T1=E1
      IF(E1.GT.2.*E)GO TO 111
      XKS=0.0
      GO TO 95
  111 BETA1=SQRT(T1*(T1+2.))/(T1+1.)
      COKS=2.*C/(BETA1*BETA1)
      TMKS=(1.0/T-1./(T1-T)-((2.+1./T1)/(T1+1.)**2)*
     1ALOG((T1-T)/T)+(T1+1.)**(-2)*(T1/2.-T))
      XKS=TMKS*COKS
   95 RETURN
      END
```

6.3 Program to Calculate the Electron Spectrum Resulting from Co^{60} Irradiation of Water

This program calculated the electron energy spectrum resulting from Co^{60} irradiation of water. To find the resulting spectrum, the following integral was evaluated:

$$y_g(E) = \int_E^Q z(E_o,E)S_e{}^g(E_o)dE_o. \tag{122}$$

For input data, the spectra $z(E_o,E)$ resulting from a number of monoenergetic sources were needed and were obtained from the program described in section 6.2.

The subprograms required for this code were:

FUNCTION SPECT(TI)

SUBROUTINE INTER(N,M,X,Y,CHECK)

SUBROUTINE BATES(IWT,NWT,WTAB,WATES)

FUNCTION Y(T)

FUNCTION ZEE(TI,T)

Logic diagrams for the main program and the subprogram SPECT were given in this section. An explanation of input data and variables of interest is given in Table XV.

FUNCTION SPECT(TI) utilized Eq. (123) to determine the initial electron source from Co^{60} irradiation. The electron source resulting from the two gamma rays were obtained by superposition of the individual source terms. The index for the DO loop was obtained by comparing the electron energy under consideration to the maximum energy electron produced by the lower energy gamma ray.

Table XV. Explanation of Computer Program Variables

Symbol	Explanation
NCOLM	Number of $z(E_o,E)$ spectra
EZ(K)	Source Energy E_o
Q2	Point of discontinuity in the initial electron spectra
Q	Maximum energy electron resulting from Co^{60} irradiation
ANECC	(Electrons per cm^3)$*10^{-25}$
COB	$(\bar{r}_o{}^2) \times 10^{+25}$
PSI	Geometric progression ratio

LOGIC DIAGRAM FOR THE COMPUTER PROGRAM DESCRIBED IN SECTION 6.3

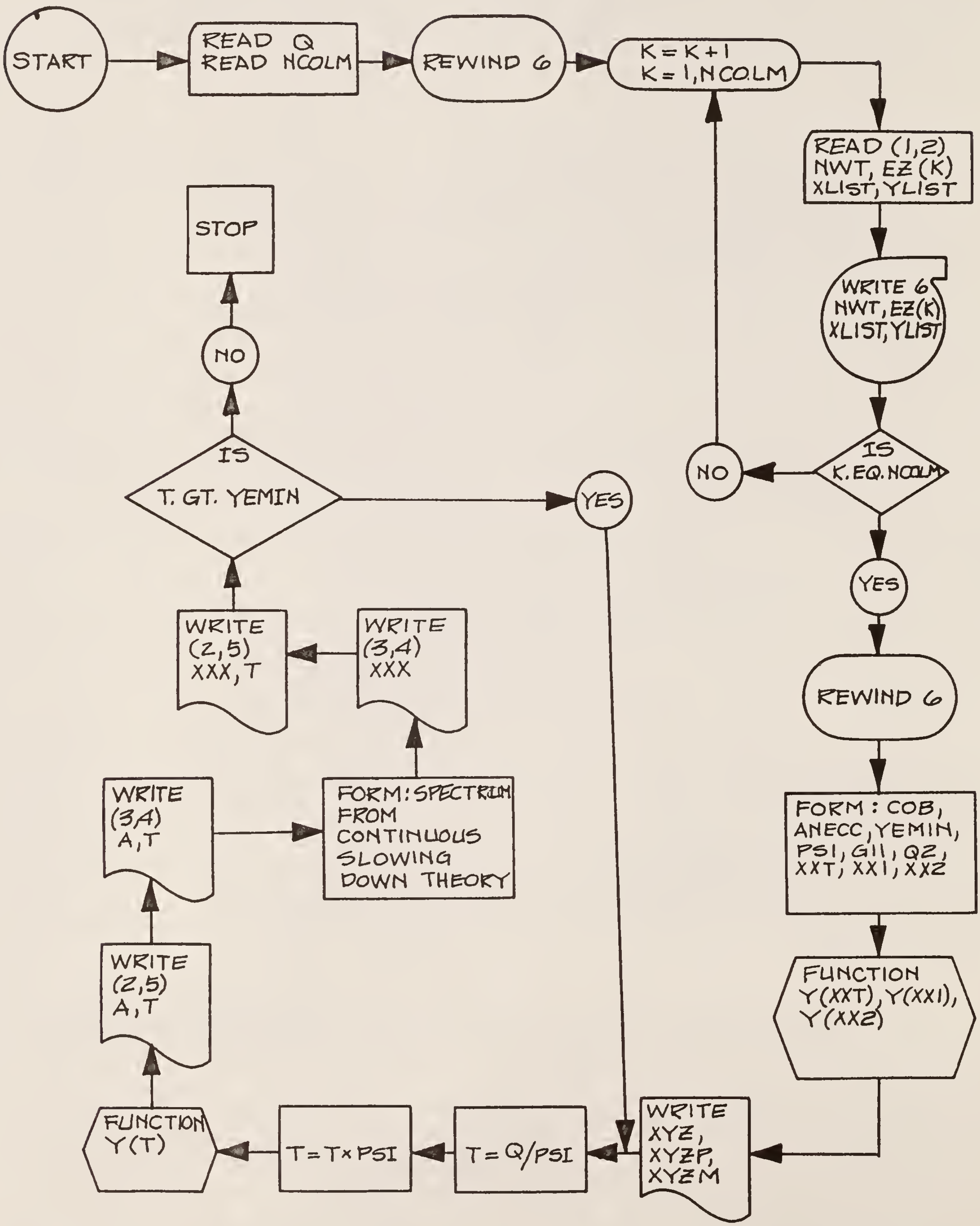

LOGIC DIAGRAM FOR THE FUNCTION SPECT(TI) DESCRIBED IN SECTION 6.3

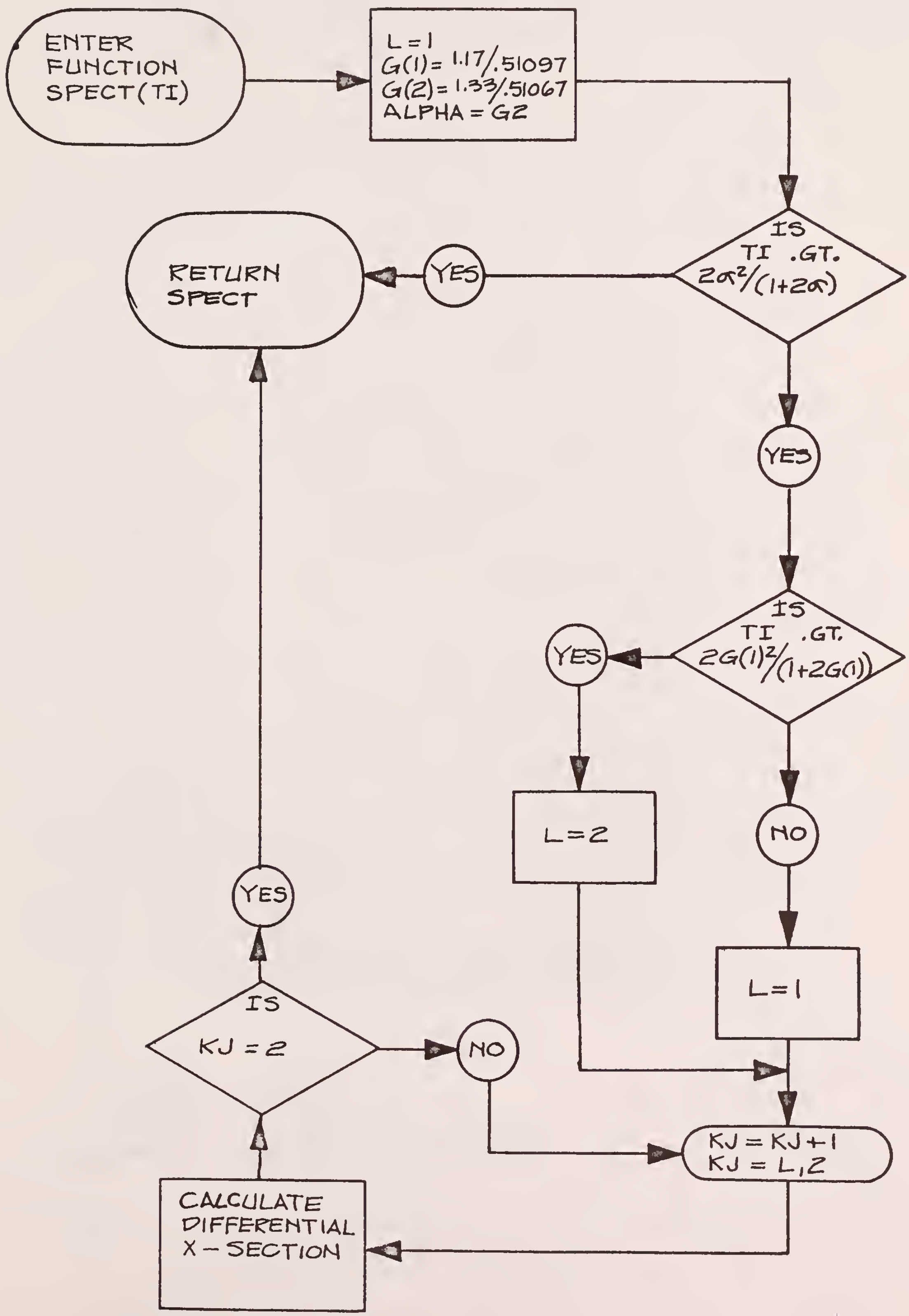

```
MONS$       JOB
MONS$       COST 15.1, LAURENCE F. MILLER DEPT OF NUCLEAR ENG
MONS$       ASGN MJF,12
MONS$       ASGN MGO,16
MONS$       MODE GO,TEST
MONS$       EXEC FORTRAN,,,,,,,,ANSW
      COMMON XLIST(49),YLIST(49),DELY(100),FZ(25),ROW(25),COR,WTAB(50),
     1WATES(50),ICET,NCOLM,Q,ZHECK,Q2,XYZ,XSPEC(40),YSPEC(40),NPTS
    1 FORMAT(1HK,I5)
    2 FORMAT(1HK,I5,F12.6/(1X,2F12.6))
    3 FORMAT(1HK,I5,F12.6,I5/(1X,2F12.6))
    4 FORMAT(1HK,6HY(T) =,F12.6,5X,3HT =,F12.6)
    5 FORMAT(2E14.8)
    8 FORMAT(I5/(2F10.5))
    9 FORMAT(1HK,E14.8)
   28 FORMAT(1HK,3E14.8)
      REWIND 6
      READ(1,1)NCOLM
      DO 10 K=1,NCOLM
      READ(1,2)(NWT,FZ(K),(XLIST(J),YLIST(J),J=1,NWT))
   10 WRITE(6)(NWT,FZ(K),(XLIST(J),YLIST(J),J=1,NWT))
      REWIND 6
      COR=.31415*2.8178*2.8178
      ANECC=.6023*.9/16.
      MEMIN=200.*10.**(-6)/.51097
      PSI=.5**(1./3.)
      Q=1.116/.51097
      G11=1.17/.51097
      Q2=2.*G11*G11/(1.+2.*G11)
      XXT=Q2+.001
      XX1=XXT+.001
      XX2=XXT-.001
      XYZ=Y(XXT)
      XYZP=Y(XX1)
      XYZM=Y(XX2)
      WRITE(3,28)XYZ,XYZP,XYZM
      T=Q/PSI
   11 CONTINUE
      T=T*PSI
      A=Y(T)*ANECC
      WRITE(2,5)A,T
      WRITE(3,4)A,T
```

```
      DEL=.0
      C=.15*.5555
      BETA=SQRT(T*(T+2.))/(T+1.)
      COF=2.*C/(BETA*BETA)
      ZI=.00C6651/.51097
      TTERM=1.-BETA*BETA+(T*T/8.-(2.*T+1.)*ALOG(2.))/((T+1.)*(T+1.))
      BTERM=ALOG(T*T*(T+2.)/(2.*ZI*ZI))
      TSP=COF*(TTERM+BTERM-DEL)
      TPRI=T*.51097
      WRITE(3,5)TSP,TPRI
      XXX=ZHECK/TSP*ANECC
      WRITE(3,9)XXX
      WRITE(2,5)XXX,T
      IF(T.GT.YEMIN)GO TO 11
      STOP
      END


    MON$$      EXEQ FORTRAN
      FUNCTION SPECT(TI)
      DIMENSION G(2)
      COMMON XLIST(49),YLIST(49),DELY(100),EZ(25),ROW(25),COB,WTAB(50),
     1WATES(50),IOFT,NCOLM,Q,ZHECK,Q2,XYZ,XSPEC(40),YSPEC(40),NPTS
      L=1
      G(1)=1.17/.51097
      G(2)=1.33/.51097
      ALPHA=G(2)
      IF(TI.GT.2.*ALPHA**2/(1.+2.*ALPHA))SPECT=.0
      IF(TI.GT.2.*ALPHA**2/(1.+2.*ALPHA))GO TO 14
      IF(TI.GT.2.*G(1)**2/(1.+2.*G(1)))L=2
      SUM=.0
      DO 32 KJ=L,2
      ALPHA=G(KJ)
      XQZ=(ALPHA*ALPHA-ALPHA*TI-TI)/(ALPHA*ALPHA-TI*ALPHA)
      SIGC=COB*(1./(ALPHA*ALPHA))*(1.+TI+XQZ*XQZ-TI*XQZ)/.51
   32 SUM=SUM+SIGC
      SPECT=SUM
   14 RETURN
      END
```

6.4 Explanation of the Computer Programs Which Calculate the Electron Spectra Resulting From Fast Neutron Irradiation

The electron spectra resulting from given alpha and proton particle fluxes were determined by the programs described in this section. This required that the electron sources resulting directly from alpha and proton fluxes be determined first. The slowing down spectra were then calculated from the initial spectra.

Since several parameters associated with the determination of the electron sources required changing of a few Fortran statements, both of the main programs are listed. In each case, input data on the proton and alpha particle fluxes were required. These data were the proton and alpha particle fluxes, divided by their energy, corresponding to equally-spaced logarithmic intervals generated by the program. These data were plotted in Figs. 37 and 38, and listed in Table XVII. Twenty-two sets of $z(E_o,E)$ data were also required.

Eqs. (136) and (137), given in section 2.4 of the theory, reduced to:

$$S_e^p(E) = \frac{39.98}{E^2}\left(1 - \frac{E}{2}\right)\int_{459.1E}^{14.6/.51047} dE'Q(E') \tag{218}$$

and

$$S_e^a(E) = \frac{159.9}{E^2}\left(1 - \frac{E}{2}\right)\int_{1824.E}^{5.8/.51047} dE'V(E') \tag{219}$$

in which

$$Q(E') = \frac{\phi_p(E')}{E'} \tag{220}$$

and

$$V(E') = \frac{\phi_a(E')}{E'} \ . \qquad (221)$$

Since the programs were very similar, one logic diagram was considered sufficient. The subprograms used were:

```
FUNCTION ZEE(TI,T)
SUBROUTINE BATES(IWT,NWT,WTAB,WATES)
SUBROUTINE INTER(N,M,X,Y,CHECK)
FUNCTION Y(T)
FUNCTION SPECT(TI)
```

All of the above subprograms except SPECT(TI) are given in section 6.8. Table XVI explains several computer program variables associated with the main program.

Table XVI. Explanation of Computer Program Variables

Symbol	Explanation
PIT	Geometric progression ratio to generate the abcissa points associated with the input data of alpha or proton flux
NPTS	Number of data points chosen for alpha or proton flux
COB	$(\pi \bar{r}_o^{\,2})$ x10^{+25}
YEMIN	200 ev, lowest electron energy considered
ANN	Geometric progression ratio to obtain initial electron spectrum
Q	Maximum energy of electrons in the spectrum

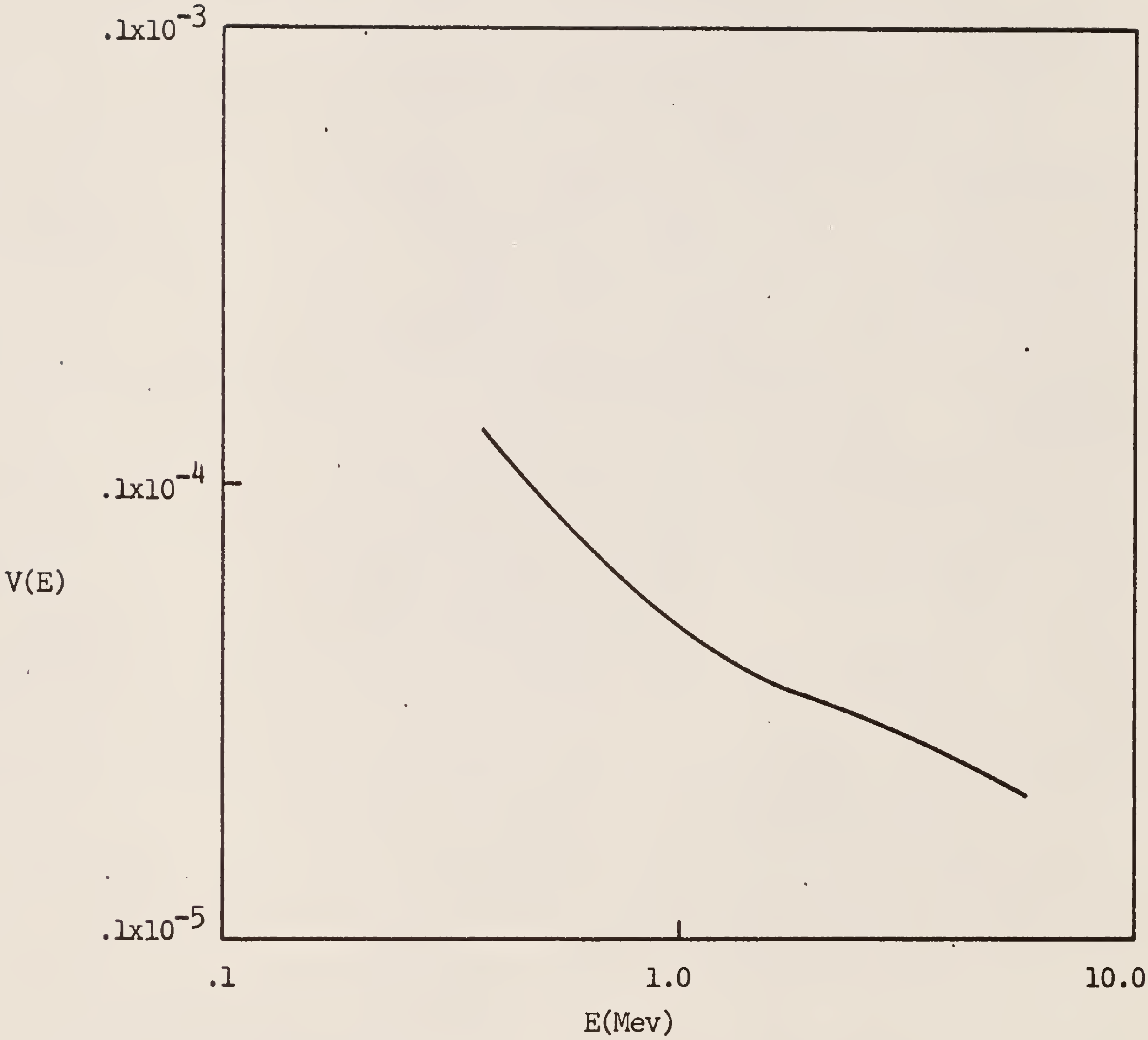

Fig. 37. Plot of V(E) vs. E

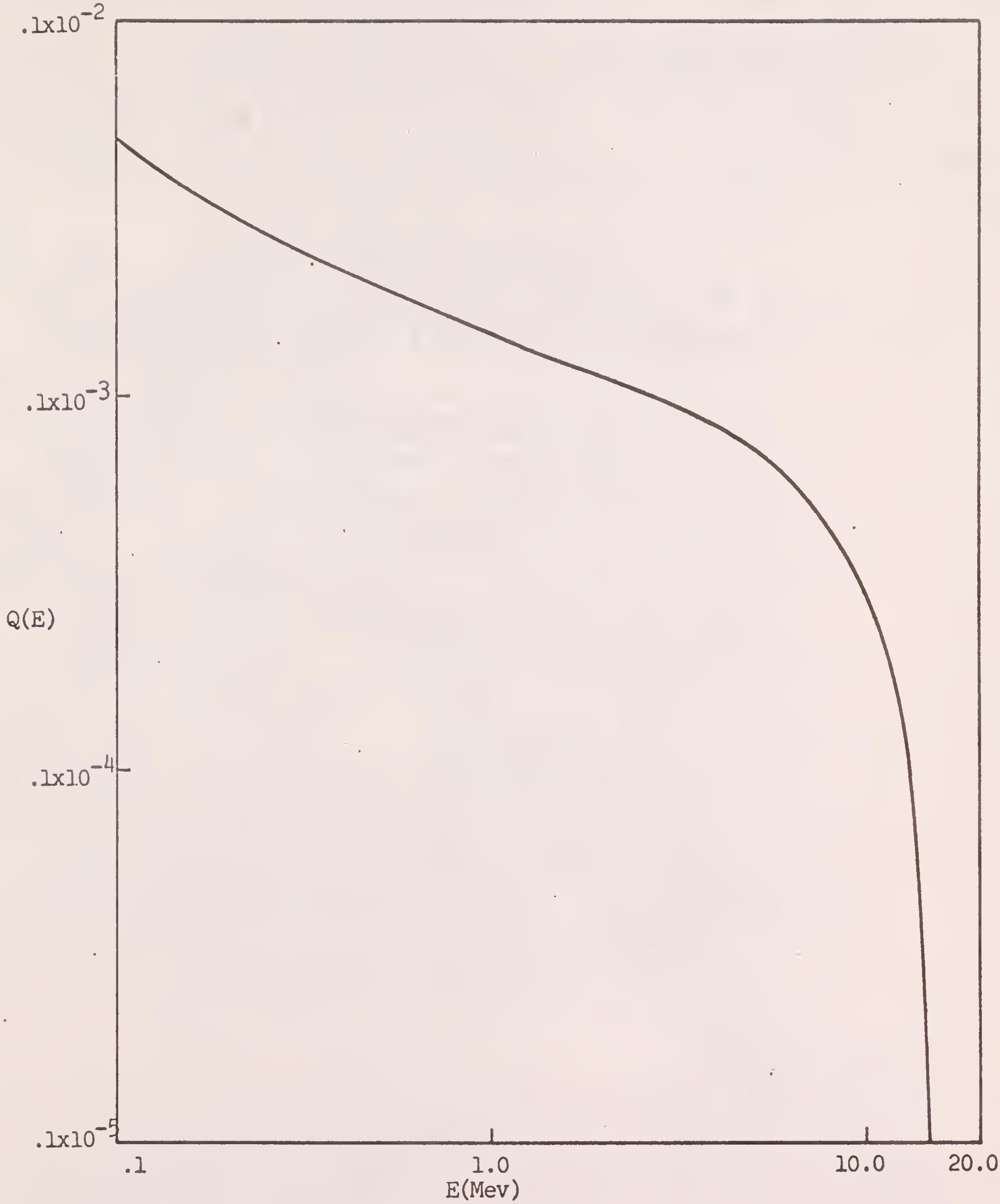

Fig. 38. Plot of Q(E) vs. E

Table XVII. Listing of Q(E) and V(E) Chosen at Equally Spaced Logarithmic Intervals of Energy E in Figs. 37 and 38

Q(E)	V(E)
.100E-09	.768E-04
.450E-02	.540E-04
.540E-02	.400E-04
.460E-02	.340E-04
.370E-02	.275E-04
.280E-02	.260E-04
.220E-02	.260E-04
.160E-02	.310E-04
.120E-02	.442E-04
.100E-02	.550E-04
.840E-03	.700E-04
.780E-03	.900E-04
.860E-03	.110E-03
.110E-02	.140E-03
.150E-02	.180E-03
.190E-02	.230E-03
.230E-02	.280E-03
.300E-02	.350E-03
.380E-02	.440E-03
.470E-02	.560E-03

Table XVII. (continued)

Q(E)	V(E)
.600E-02	.700E-03
.740E-02	.875E-03
.960E-02	
.120E-01	
.150E-01	
.190E-01	
.234E-01	

LOGIC DIAGRAM FOR THE COMPUTER PROGRAM DESCRIBED IN SECTION 6.4

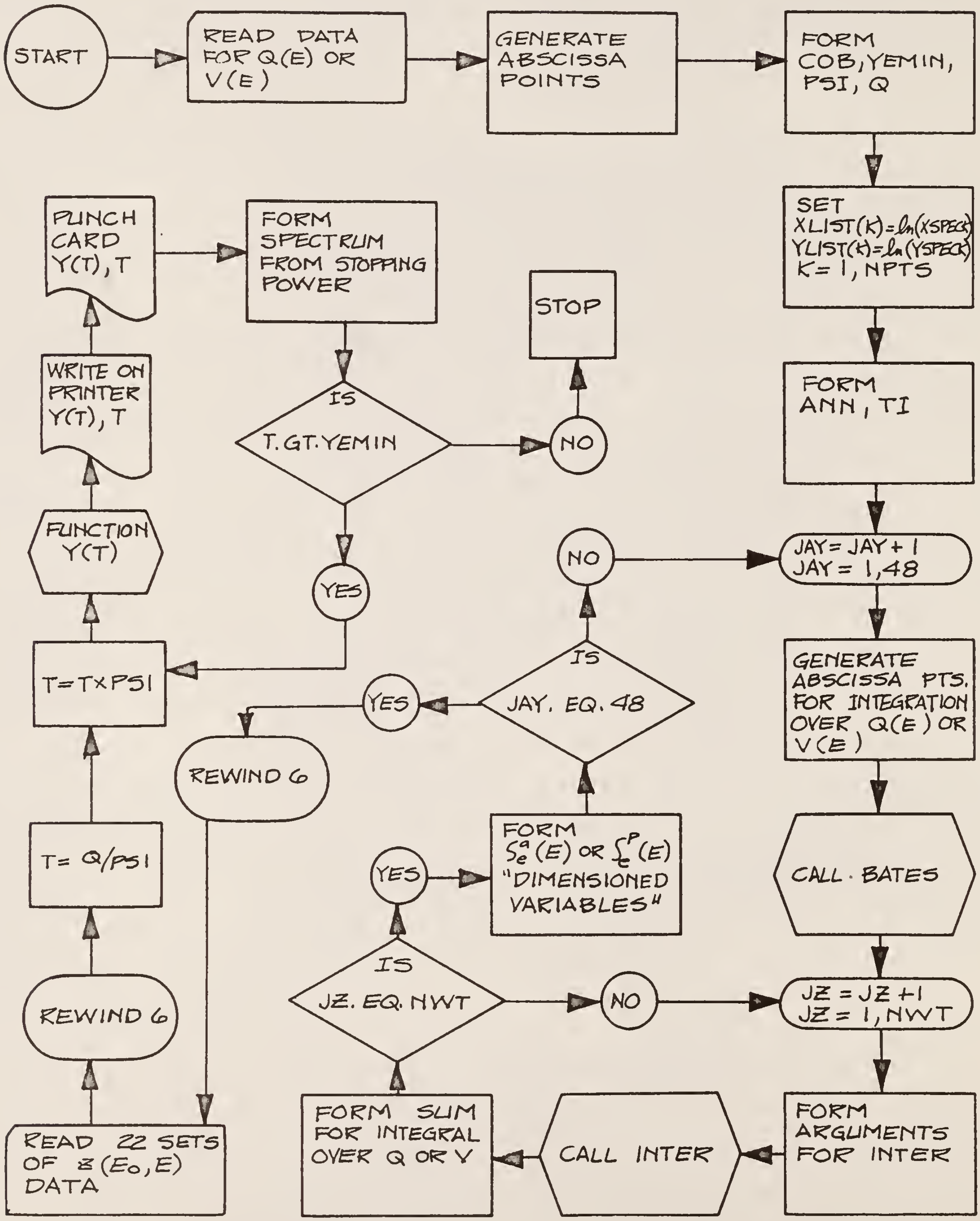

LOGIC DIAGRAM FOR THE FUNCTION SPECT(TI) DESCRIBED IN SECTION 6.4

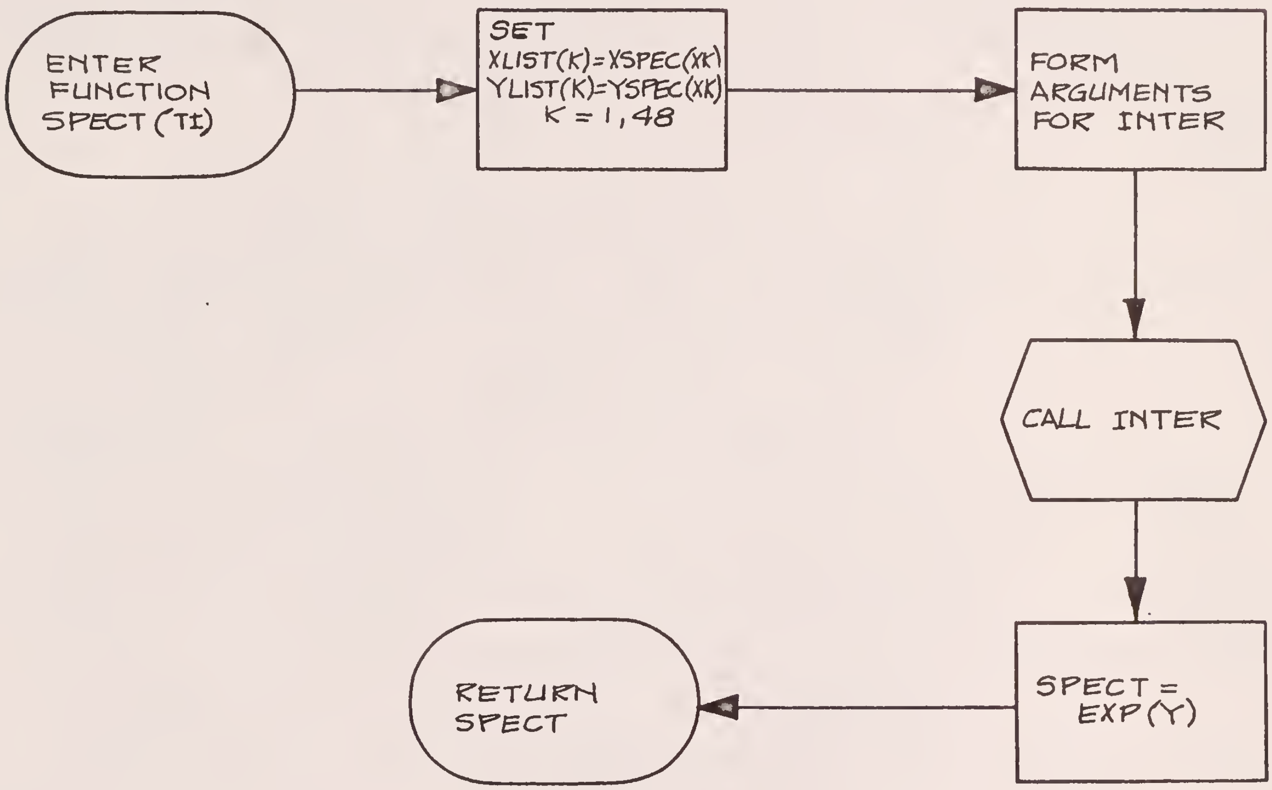

This program calculates the electron spectrum resulting from the proton source

```
MONSS      JOB     ELECTRON SPECTRUM
MONSS      CONT 15MINUTES,5PAGES LARRY MILLER  DEPT OF ME
MONSS      ASGN MJB,12
MONSS      ASGN MGO,16
MONSS      MODE GO,TEST
MONSS      EXEQ FORTRAN,,,,,,,,ANSW
   COMMON XLIST(49),YLIST(49),DELY(2 ),LZ(25),ROW(25),COL,WTAB(50),
  1NATES(5 ),IOPT,NCOLM,N,ZHECK,Q2,XYZ,XSPEC(50),YSPEC(50),NPTS,NPZ
 1 FORMAT(1HK,I5)
 2 FORMAT(1HK,I5,F12.6/(1X,2F12.6))
 3 FORMAT(1HK,I5,F12.6,I5/(1X,2F12.6))
 4 FORMAT(1HK,6HY(T) =,F12.6,5X,3HT =,F12.6)
 5 FORMAT(2F14.8)
 6 FORMAT(I5/(F14.8))
 7 FORMAT(1HK,11HINTEGRAL =,F14.8,17HELECTRON SOURCE =,E14.8,
  11HENERGY =,F14.8)
 8 FORMAT(I5/(2F10.5))
 9 FORMAT(1HK,E14.8)
   READ(1,6)NPTS,(YSPEC(J),J=1,NPTS)
   PIT=(.09182/14.5)**(1./FLOAT(NPTS-1))
   XSPEC(1)=14.5/.51097
   DO 12 IT=2,NPTS
12 XSPEC(IT)=XSPEC(IT-1)*PIT
   COP=.31415*2.8178*2.8178
   YEMIN=200.*10.**(-6)/.51097
   PSI=.5**(1./3.)
   Q=31.6*10.**(-3)/.51097
   DO 15 JF=1,NPTS
   XLIST(JF)=ALOG(XSPEC(JF))
15 YLIST(JF)=ALOG(YSPEC(JF))
   ANN=(YEMIN/Q)**(1./47.)
   TI=Q/ANN
   DO 70 JAY=1,48
   TI=TI*ANN
   NWT=30
   PSJ=(TI*459.1/(14.6/.51097))**(1./FLOAT(NWT-1))
   WTAB(1)=14.6/.51097
   DO 16 JQ=2,NWT
16 WTAB(JQ)=WTAB(JQ-1)*PSJ
   IWT=2
   CALL RATES(IWT,NAT)
   M=NPTS
   N=2
   SUM=.0
```

```
      DO 17 JZ=1,NWT
      X=ALOG(ETA (JZ))
      CALL INTER(N,M,X,Y,CHECK)
      AE=EXP(Y)
      TERM=AE*RATES(JZ)
      IF(JZ.EQ.1)TERM=.0
17    SUM=SUM+TERM
      XXXXX=SUM*(1.-TI/2.)*39.98/(TI*TI)
      WRITE(3,7)SUM,XXXYX.TI
      XSPEC(JAY)=TI
7     YSPEC(JAY)=XXXXX
      WRITE(2,5)(XSPEC(K),YSPEC(K),K=1,48)
      DO 72 JKY=1,48
      IF(XSPEC(JKY).EQ..0)GO TO 72
      IF(YSPEC(JKY).EQ..0)GO TO 72
      XSPEC(JKY)=ALOG(XSPEC(JKY))
      YSPEC(JKY)=ALOG(YSPEC(JKY))
72    CONTINUE
      REWIND 6
      READ(1,1)NCOLM
      DO 10 K=1,NCOLM
      READ(1,2)(NWT,EZ(K),(XLIST(J),YLIST(J),J=1,NWT))
10    WRITE(6)(NWT,EZ(K),(XLIST(J).YLIST(J),J=1,NWT))
      REWIND 6
      T=Q/PSI
11    CONTINUE
      T=T*PSI
      A=Y(T)
      WRITE(2,5)A,T
      WRITE(3,4)A,T
      DEL=.0
      C=.15*.5555
      BETA=SQRT(T*(T+2.))/(T+1.)
      COF=2.*C/(BETA*BETA)
      ZI=.00 651/.51097
      TTERM=1.-BETA*BETA+(T*T/8.-(2.*T+1.)*ALOG(2.))/((T+1.)*(T+1.))
      BTERM=ALOG(T*T*(T+2.)/(2.*ZI*ZI))
      TSP=COF*(TTERM+BTERM-DEL)
      TPRI=T*.51097
      WRITE(3,5)TSP,TPRI
      XXX=ZHECK/TSP
      WRITE(3,9)XXX
      IF(T.GT.YEMIN)GO TO 11
      STOP
      END
```

This program calculates the electron spectrum resulting from the alpha source.

```
MONITR      JOB     ELECTRON SPECTRUM                                      J
MONITR      COMT 15MINUTES,5PAGES LARRY MILLER  DEPT OF NE
MONITR      ASGN MJB,12
MONITR      ASGN MGO,16
MONITR      MODE GO,TEST
MONITR      EXEC FORTRAN,,,,,,,ANSW
      COMMON XLIST(49),YLIST(49),DELY(20),EZ(25),ROW(25),COB,WTAB(50),
     1WATES(50),IOFT,NCOLM,Q,ZHECK,Q2,XYZ,XSPEC(50),YSPEC(50),NPTS,NPZ
    1 FORMAT(1HK,I5)
    2 FORMAT(1HK,I5,F12.6/(1X,2F12.6))
    3 FORMAT(1HK,I5,F12.6,I5/(1X,2F12.6))
    4 FORMAT(1HK,6HY(T) =,F12.6,5X,3HT =,F12.6)
    5 FORMAT(2E14.8)
    6 FORMAT(I5/(E14.8))
    7 FORMAT(1HK,10HINTEGRAL =,E14.8,17HELECTRON SOURCE =,E14.8,
     18HENERGY =,E14.8)
    8 FORMAT(I5/(2F10.5))
    9 FORMAT(1HK,E14.8)
      READ(1,6)NPTS,(YSPEC(J),J=1,NPTS)
      PIT=(.37/5.8)**(1./FLOAT(NPTS-1))
      XSPEC(1)=5.8/.51097
      DO 12 IT=2,NPTS
   12 XSPEC(IT)=XSPEC(IT-1)*PIT
      COB=.31415*2.8178*2.8178
      YEMIN=200.*10.**(-6)/.51097
      PSI=.5**(1./3.)
      Q=3.18*10.**(-3)/.51097
      DO 15 JF=1,NPTS
      XLIST(JF)=ALOG(XSPEC(JF))
   15 YLIST(JF)=ALOG(YSPEC(JF))
      ANN=(YEMIN/Q)**(1./47.)
      TI=Q/ANN
      DO 70 JAY=1,48
      TI=TI*ANN
      NWT=30
      PSJ=(TI*1824./(5.8/.51097))**(1./FLOAT(NWT-1))
      WTAB(1)=5.8/.51097
      DO 16 JQ=2,NWT
   16 WTAB(JQ)=WTAB(JQ-1)*PSJ
      IWT=2
      CALL RATES(IWT,NWT)
      M=NPTS
      N=2
      SUM=.0
```

```
      DO 17 JZ=1,NWT
      X=ALOG(ETAM(JZ))
      CALL INTERP(N,M,X,Y,CHECK)
      AF=EXP(Y)
      TERM=AF*WATES(JZ)
      IF(JZ.EQ.NWT)TERM=.1311*10.**(-4)*WATES(JZ)
   17 SUM=SUM+TERM
      XXXXX=SUM*(1.-TI/2.)*159.9/(TI*TI)
      WRITE(3,7)SUM,XXXXX,TI
      XSPEC(JAY)=TI
    7 YSPEC(JAY)=XXXXX
      WRITE(2,5)(XSPEC(K),YSPEC(K),K=1,48)
      DO 72 JKY=1,48
      IF(XSPEC(JKY).EQ..0)GO TO 72
      IF(YSPEC(JKY).EQ..0)GO TO 72
      XSPEC(JKY)=ALOG(XSPEC(JKY))
      YSPEC(JKY)=ALOG(YSPEC(JKY))
   72 CONTINUE
      REWIND 6
      READ(1,1)NCOLM
      DO 10 K=1,NCOLM
      READ(1,2)(NWT,EZ(K),(XLIST(J),YLIST(J),J=1,NWT))
   10 WRITE(6)(NWT,EZ(K),(XLIST(J),YLIST(J),J=1,NWT))
      REWIND 6
      T=0/PSI
   11 CONTINUE
      T=T*PSI
      A=Y(T)
      WRITE(2,5)A,T
      WRITE(3,4)A,T
      DEL=.0
      C=.15*.5555
      BETA=SQRT(T*(T+2.))/(T+1.)
      COF=2.*C/(BETA*BETA)
      ZI=.00  651/.51097
      TTERM=1.-BETA*BETA+(T*T/8.-(2.*T+1.)*ALOG(2.))/((T+1.)*(T+1.))
      RTERM=ALOG(T*T*(T+2.)/(2.*ZI*ZI))
      TSP=COF*(TTERM+RTERM-DEL)
      TPRI=T*.51097
      WRITE(3,5)TSP,TPRI
      XXX=ZHECK/TSP
      WRITE(3,9)XXX
      IF(T.GT.YEMIN)GO TO 11
      STOP
      END
```

```
 $ONS$     EXEQ FORTRAN
      FUNCTION SPECT(TI)
      COMMON XLIST(49),YLIST(49),DELY(25),EZ(25),ROW(25),COB,WTAB(50),
     1WATES(50),ICFT,NCOLM,Q,ZHECK,Q2,XYZ,XSPEC(50),YSPEC(50),NPTS,NPZ
      IF(TI.GE.Q)SPECT=.0
      IF(TI.GE.Q)GO TO 61
      DO 28 JDS=1,48
      XLIST(JDS)=XSPEC(JDS)
   28 YLIST(JDS)=YSPEC(JDS)
      M=48
      N=2
      X=ALOG(TI)
      CALL INTER(N,M,X,Y,CHECK)
      SPECT=EXP(Y)
   61 RETURN
      END
```

6.5 Explanation of Programs Used to Synthesize an Electron-Electron Cross Section and a Program to Calculate the Stopping Power of Water Using the Synthesized Cross Section

6.5.1 Program for Evaluating the Parameters a, b and AKT in the Energy Region Where the Moller Formula is Valid

Evaluation of the parameters a, b and AKT, as associated with the hypothesized cross section developed in section 2.4 of the theory, was accomplished by an iterative procedure. From the boundary conditions given in section 2.4, the following expressions for a and b were obtained:

$$a = \pm \left[\sqrt{\frac{\kappa(E)}{k_m(E,\delta_2)}} - \sqrt{\frac{\kappa(E)}{\mathrm{AKT}\ k_{ex}(\delta_1)}} \right] \Big/ (\delta_2 - \delta_1) \tag{145}$$

$$b = \pm \left[\delta_2 \sqrt{\frac{\kappa(E)}{\mathrm{AKT}\ k_{ex}(\delta_1)}} - \delta_1 \sqrt{\frac{\kappa(E)}{k_m(E,\delta_2)}} \right] \Big/ (\delta_2 - \delta_1). \tag{146}$$

Note that δ_2 is the value of τ at which one chooses to match the hypothesized cross section to the Moller cross section, that δ_1 is the largest energy loss for which inelastic collision cross section data are available and that $\kappa(E) = \frac{2C}{E}$.

The subprograms used for this code were:

```
FUNCTION PROBT(T,TAU)
FUNCTION SMALL(TAU)
FUNCTION AMOLIN(T,DELTA)
FUNCTION AINEX(DELTA)
SUBROUTINE BATES(IWT,NWT,WTAB,WATES)
```

All of these subprograms are explained in section 6.8. A logic diagram is given for the main program in this section.

LOGIC DIAGRAM FOR THE COMPUTER PROGRAM DESCRIBED IN SECTION 6.5.1

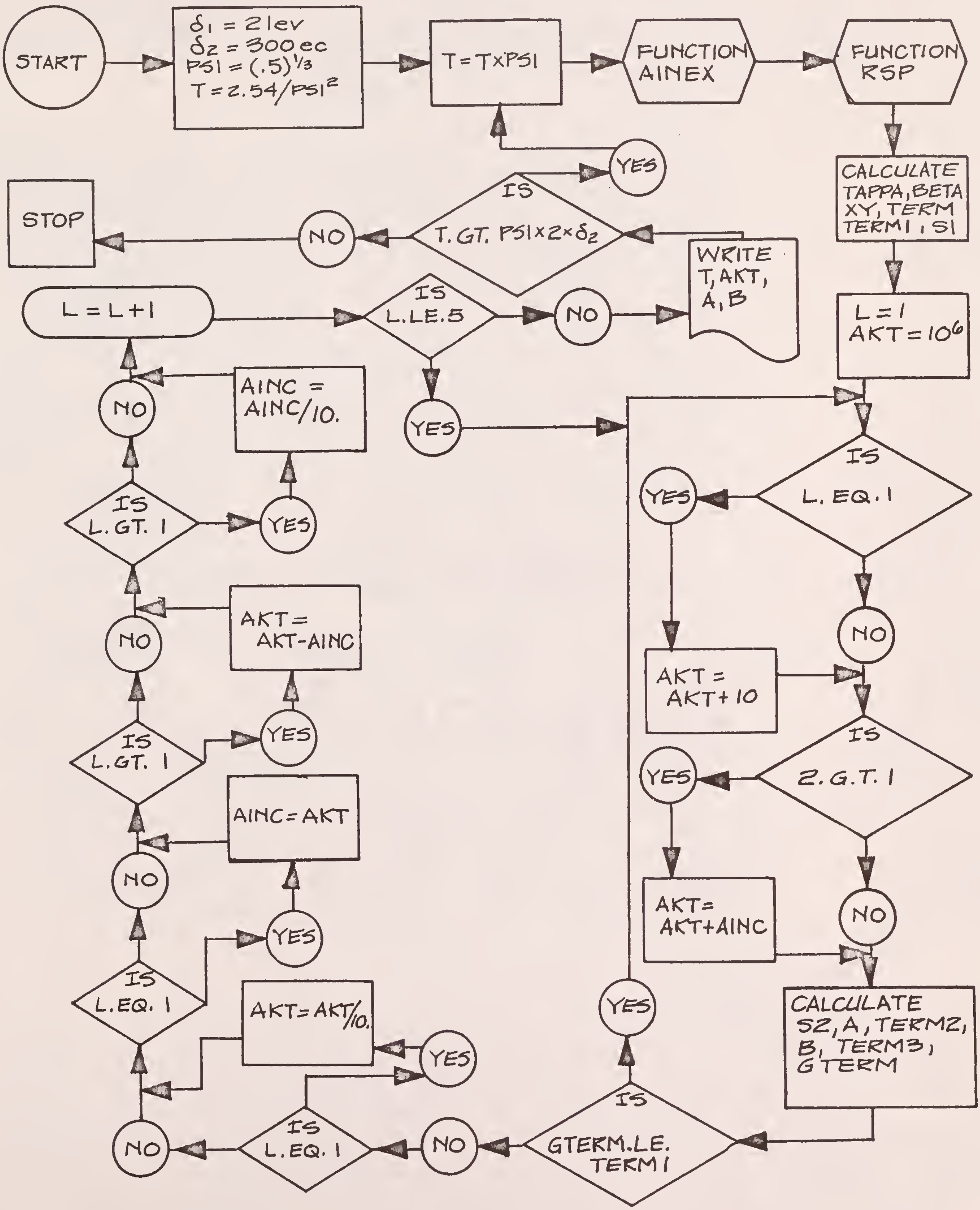

```
MON$$       JOB         KAPIT    MILLER                                   J
MON$$       CONT  ...  L.F.  MILLER R.L.
MON$$       ASGN   JR.12
MON$$       ASGN   MGO.16
MON$$       MODE   GO.TEST
MON$$       EXT    FORTRAN........KAPIT
   COMMON   TAR(10)...(10)..BETA,COF,AKT,DELTA1,DELTA2,QB
 7 FORMAT(1HK,10F12.6)
 8 FORMAT(1HK,2F14.8)
 9 FORMAT(1HK,4F14.8)
   C=.15*.5555
   DELTA1=21.*10.**(-6)/.51097
   DELTA2=300.*10.**(-6)/.51097
   PSI=.5**(1./2.)
   XY=AINMX(DELTA1)
   T=2.54/(PSI*PSI)
10 T=T*PSI
   KAPPA=2.*C/T
   BETA=SQRT(T*(T+2.))/(T+1.)
   COF=2.*C/(BETA*BETA)
   TERM1=AMOLIN(T,DELTA2)
   S1=SQRT(KAPPA/PR...T(T,DELTA2))
   L=1
   AKT=10.**6
12 CONTINUE
   IF(L.EQ.1)AKT=AKT*10.
   IF(L.GT.1)AKT=AKT+AINC
   S2=SQRT(KAPPA/(...))
   A=(S2-S1)/(DELTA1-DELTA2)
   TERM2=AKT*XY
   B=(DELTA1*S1-DELTA2*S2)/(DELTA1-DELTA2)
   TERM3=KAPPA/(2*A)*(.../(...)-.../(A*DELTA1+B))+ALOG(SQRT(AKT*
  1SMALL(DELTA1)/PROB(T,DELTA2))))
   GTERM=TERM2+TERM3
   IF(GTERM.LE.TERM1)GO TO 12
   IF(L.EQ.1)AKT=AKT/10.
   IF(L.EQ.1)AINC=AKT
   IF(L.GT.1)AKT=AKT-AINC
   IF(L.GT.1)AINC=AINC/10.
   L=L+1
   IF(L.LE.5)GO TO 12
   WRITE(2,9)T,AKT,A,B
   WRITE(3,9)T,AKT,A,B
   IF(T.GT.PSI*1.*DELTA2)GO TO 10
   STOP
   END
```

6.5.2 Explanation of the Program Used to Investigate the Behavior of a and b by Assuming AKT to be Proportional to a Constant Power of E

This program was written mostly for the sake of curiosity. If AKT were assumed to be known, a and b could be evaluated directly in terms of AKT. One would need only to match the synthesized and experimental cross sections. If the stopping power of water for low energy electrons were known, one might extract some useful information from the procedure. Since the stopping power was under estimated by an integral over the Moller cross section or by conventional stopping power formulas, the parameters a and b were, as a result, too large. Therefore, meaningful results were not obtained. The program listing and logic diagram for the program explained in section 6.5.1 was considered sufficient for the interpretation of the program listed in this section. The subprograms required were:

FUNCTION AKTG(E)

FUNCTION SMALL(TAU)

FUNCTION AMOLIN(T,DELTA)

FUNCTION AINEX(DELTA)

SUBROUTINE BATES(IWT,NWT,WTAB,WATES)

Subprogram AKTG(E) is a straight line fit of Fig. 11. The other subprograms are explained in section 6.8.

```
 MONT$      JOB    DATAFIT    MILLER                                          J
 MON$$      COMT 25MINUTES,10PAGES  L.F. MILLER N.F.
 MON$$      ASGN MJB,12
 MON$$      ASGN MGO,16
 MON$$      MODE GO,TEST
 MON$$      EXEQ FORTRAN,,,,,,,DATAFIT
      COMMON WTAB(100),WATES(100),DEL,BETA,COF,AKT,DELTA1,DELTA2,QB
    7 FORMAT(1HK,10E12.6)
    8 FORMAT(1HK,2E14.8)
    9 FORMAT(1HK,4E14.8)
    6 FORMAT(1HK,5E14.8)
      DEL=.0
      C=.15*.5555
      DELTA1=21.*10.**(-6)/.51097
      DELTA2=3  .*10.**(-6)/.51097
      PSI=.5**(1./3.)
      T=2.*DELTA2/PSI
   10 T=T*PSI
      DELTA2=T/2.
      TAPPA=2.*C/T
      BETA=SQRT(T*(T+2.))/(T+1.)
      COF=2.*C/(BETA*BETA)
      XY=AINEX(DELTA1)
      TERM1=AMOLIN(T,DELTA2)
      AKT=AKTG(T)
      TERM2=AKT*XY
      L=1
      A=1.4
      ADD=0.1
   12 CONTINUE
      IF(L.EQ.1)A=A+ADD
      IF(L.GT.1)A=A+AINC
      B=-A*DELTA1+SQRT(TAPPA/(AKT*SMALL(DELTA1)))
      XGZ=SQRT(TAPPA/(AKT*SMALL(DELTA1)))
      TERM=TAPPA/(A*A)*(B/(A*DELTA2+B)-B/(A*DELTA1+B)+ALOG((A*DELTA2+B)
     1/XGZ))
      GTERM=TERM2+TERM
      IF(GTERM.GE.TERM1)GO TO 12
      IF(L.EQ.1)A=A-ADD
      IF(L.EQ.1)AINC=ADD/10.
      IF(L.GT.1)A=A-AINC
      IF(L.GT.1)AINC=AINC/10.
      L=L+1
      IF(L.LE.3)GO TO 12
      WRITE(3,6)T,AKT,A,B,TERM1
      IF(T.GT.3.*DELTA1)GO TO 10
      STOP
      END
```

```
$IBFTC MONSS     EXEQ FORTRAN
      FUNCTION AKTG(E)
      IF(E.LT..05)AKTG=3.8*10.**(8)*E**(-ALOG(12.61)/ALOG(25.))
      IF(E.LT..05)GO TO 26
      IF(E.LT..3)AKTG=4.8*10.**8*E**(-ALOG(3.8/1.1)/ALOG(6.))
      IF(E.LT..3)GO TO 26
      IF(E.LT.1.)AKTG=7.1*10.**8*E**(-ALOG(1.1/.717)/ALOG(1./.3))
      IF(E.LT.1.)GO TO 26
      IF(E.LT.5.)AKTG=7.1*10.**8*E**(-ALOG(7.17/6.32)/ALOG(3.2/1.008))
   26 RETURN
      END
```

6.5.3 Explanation of the Program Used to Calculate the Stopping Power of Water From the Synthesized Cross Section

This program calculated the stopping power using the synthesized cross section and for comparison, using an analytic expression obtained from Berger and Seltzer (3). The subprograms TSP and RSP were the total and restricted stopping power formulas. The subprogram SPRS calculated the stopping power using the synthesized cross section. The subprograms used for this program were:

```
FUNCTION TSP(T)
FUNCTION RSP(T)
FUNCTION SMALL(TAU)
FUNCTION SPRS(E,DELTA2)
SUBROUTINE BATES(IWT,NWT,WTAB,WATES)
FUNCTION AINEXD(E,O,DELTA1)
FUNCTION AINGS(E,DELTA1,DELTA2)
```

The subprograms not listed in this section are given in section 6.8. The program was quite simple so the listing was considered sufficient for understanding the program.

```
MONS$       JOB   LOW ENERGY STOPPING POWER                                    J
MONS$     . CONT 15MINUTES,10PAGES   L.F. MILLER N.E.
MONS$       ASGN MJB,12
MONS$       ASGN MGO,16
MONS$       MODE GO,TEST
MONS$       EXEQ FORTRAN,,,,,,,SYNTH
  COMMON MTAF(100),MATES(100),BETA,COF,DEL
 5 FORMAT(1H1,5X,10HTAU(MC**2),7X,7HTAU(EV),6X,8HT(MC**2),8X,6HT(MEV)
  1,4X,10HRSP(MC**2),6X,8HRSP(MEV),4X,10HTSP(MC**2),6X,8HTSP(MEV),7X,
  17HRSP/TSP,//)
 6 FORMAT(1H ,9E14.4)
   C=.15*.5555
   DEL=.0
   TAU=25.*10.**(-6)/.51097
   TAU=TAU/2.
   DO 14 JJ=1,6
   TAU=TAU*2.
   IJM=1
   T=2.
   T=T/.51097
13 T=T*.5
   TAPPA=2.*C/T
   BETA=SQRT(T*(T+2.))/(T+1.)
   COF=2.*C/(BETA*BETA)
   IJM=IJM+1
   TTSP=TSP(T)
   IF(IJM.EQ.2)WRITE(3,5)
   TRSP=RSP(T,TAU)
   TTEST=TRSP/TTSP
   TRSPM=.51097*TRSP
   TTSPM=.51097*TTSP
   EMEV=T*.51097
   TAUEV=TAU*.51097*10.**6
   WRITE(3,6)TAU,TAUEV,T,EMEV,TRSP,TRSPM,TTSP,TTSPM,TTEST
   TT=T/2.
   TTSP=SPRS(T,TT)
   TRSP=SPRS(T,TAU)
   TTEST=TRSP/TTSP
   TRSPM=.51097*TRSP
   TTSPM=.51097*TTSP
   EMEV=T*.51097
   TAUEV=TAU*.51097*10.**6
   WRITE(3,6)TAU,TAUEV,T,EMEV,TRSP,TRSPM,TTSP,TTSPM,TTEST
   IF(T*.5.GT.TAU)GO TO 13
14 CONTINUE
   STOP
   END
```

```
MON$$      EXEQ FORTRAN
 FUNCTION RSP(T,DELTA2)
 COMMON WTAB(100),WATES(100),BETA,COF,DEL
 ZI=.0000651/.51097
 ATERM=ALOG((2.*(T+2.))/(ZI*ZI))
 FTERM=-1.-BETA*BETA+ALOG((T-DELTA2)*DELTA2)+T/(T-DELTA2)+(DELTA2*
1DELTA2/2.+(2.*T+1.)*ALOG(1.-DELTA2/T))/((T+1.)*(T+1.))
 RSP=(ATERM+FTERM-DEL)*COF
 RETURN
 END
```

```
MON$$      EXEQ FORTRAN
 FUNCTION TSP(T)
 COMMON WTAB(100),WATES(100),BETA,COF,DEL
 ZI=.0000651/.51097
 TTERM=1.-BETA*BETA+(T*T/8.-(2.*T+1.)*ALOG(2.))/((T+1.)*(T+1.))
 BTERM=ALOG(T*T*(T+2.)/(2.*ZI*ZI))
 TSP=COF*(TTERM+BTERM-DEL)
 RETURN
 END
```

6.6 Explanation of the Program Used to Calculate the Weighted Average Spur Size

This program calculated the average spur size from a known electron energy spectrum. From section 2.6 of the theory, it was evident that the following integrals needed to be evaluated:

$$G(\tau)\; d\tau = \tau d\tau \int_{E_{min}}^{E_{max}} y(E)\; k_H(E,\tau)\; dE \qquad (150)$$

$$\langle\bar{\tau}\rangle = \frac{\displaystyle\int_{\delta_{min}}^{\delta_c} \tau G(\tau) d\tau}{\displaystyle\int_{\delta_{min}}^{\delta_c} G(\tau) d\tau} \qquad (151)$$

The subprograms used for this code were:

FUNCTION VALUE(T,TAU)

FUNCTION SMALL(TAU)

FUNCTION G(TAU)

FUNCTION SPECY(E)

SUBROUTINE BATES(IWT,NWT,WTAB,WATES)

SUBROUTINE INTER(N,M,X,Y,CHECK)

FUNCTION PROBT(T,TAU)

Subprograms BATES, INTER, SMALL and PROBT were explained in section 6.8. The subprogram VALUE(T,TAU) evaluated $k_H(E,\tau)$ for any given energy and energy loss; G(TAU) evaluated $G(\tau)$; SPECY(E) interpolated for the electron flux from data read in as XLIST and YLIST.

Table XVIII describes variables and input data associated with this computer program.

Table XVIII. Explanation of Computer Program Variables

Symbol	Explanation
JWT	Number of points at which $G(\tau)$ is evaluated
DELTA1	δ_c (input data)
EMAX	E_{max} (input data)
EMIN	E_{min}
TAUMIN	δ_{min}
NSPEC	Number of data points of the electron spectrum (input data)
ZETA	Geometric progression ratio

LOGIC DIAGRAM FOR THE COMPUTER PROGRAM DESCRIBED IN SECTION 6-6

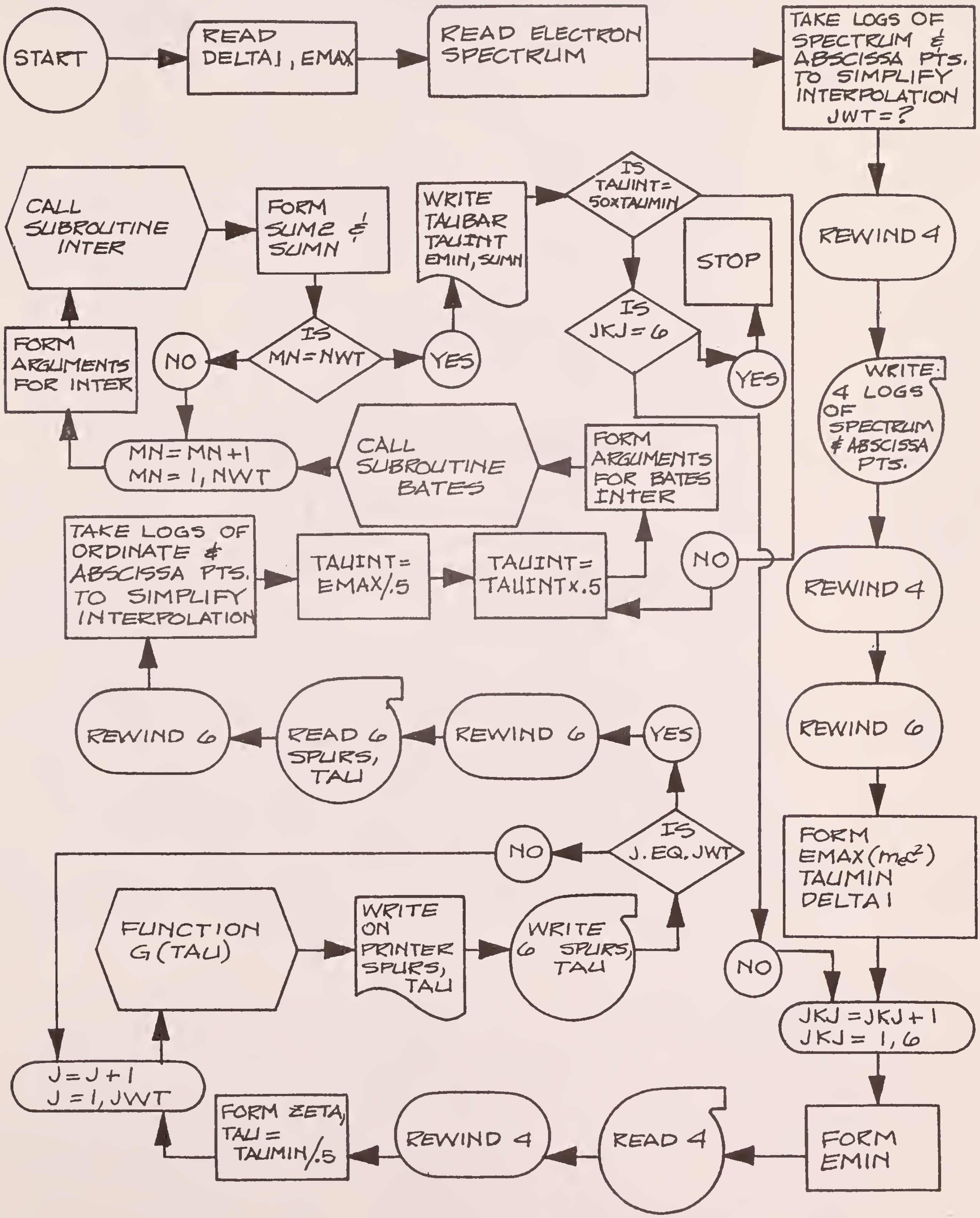

LOGIC DIAGRAM FOR THE FUNCTION VALUE (T, TAU) DESCRIBED IN SECTION 6.6

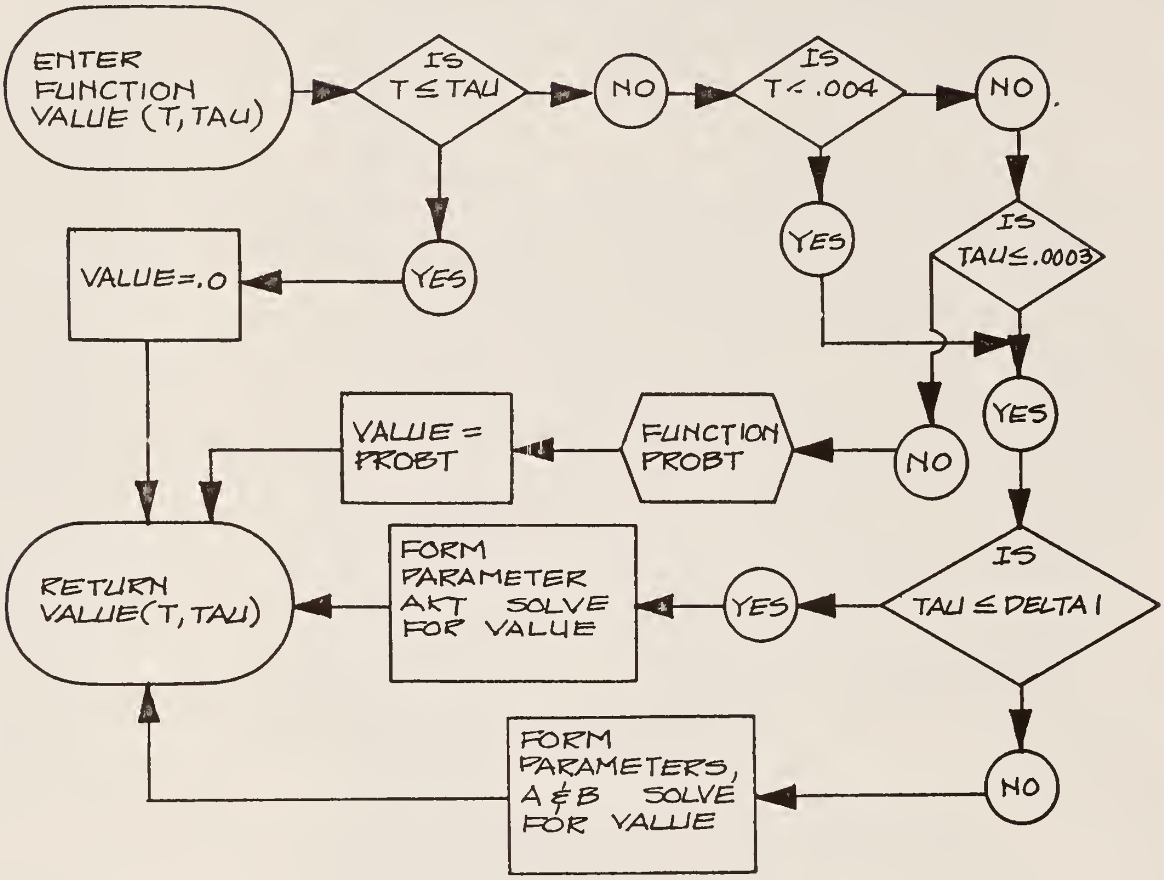

LOGIC DIAGRAM FOR THE FUNCTION SPECY (E) DESCRIBED IN SECTION 6.6

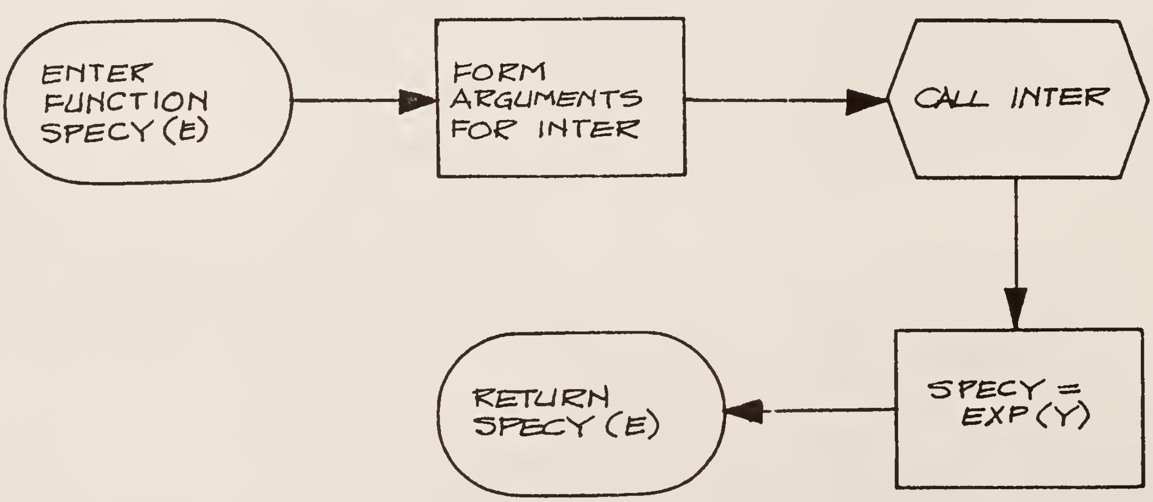

LOGIC DIAGRAM FOR THE FUNCTION G(TAU) DESCRIBED IN SECTION 6.6

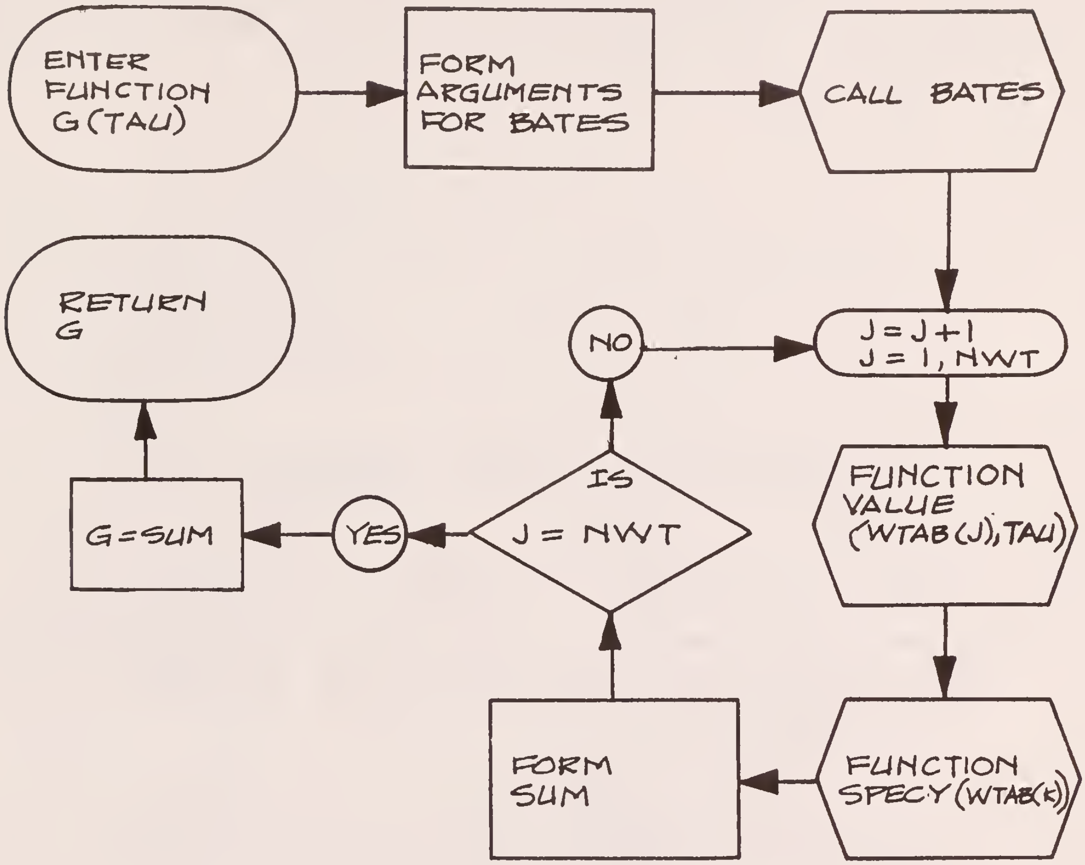

```
MON$$      JOB   SPUR SIZE DISTRIBUTION                                    J
MON$$      COMT 15MINUTES,10PAGES  L.F. MILLER  N.E.
MON$$      ASGN MJB,12
MON$$      ASGN MGO,16
MON$$      MODE GO,TEST
MON$$      EXEQ FORTRAN,,,,,,,SPURSIZE
      COMMON WTAB(50),WATES(50),XLIST(50),YLIST(50),DELY(10),EMAX,
     1DELTA1,DELTA2,NSPEC,EMIN,J
    1 FORMAT(I5)
    3 FORMAT(2E14.8)
    5 FORMAT(1HK,2E14.8)
    7 FORMAT(1HK,20X,E14.8)
    9 FORMAT(1HK,8HTAUBAR =,E14.8,10X,8HTAUINT =,E14.8,10X,6HEMIN =,E14.
     18)
      JWT=40
      READ(1,3)DELTA1,EMAX
      READ(1,1)NSPEC
      READ(1,3)(YLIST(K),XLIST(K),K=1,NSPEC)
      XLIST(1)=ALOG(XLIST(1))
      YLIST(1)=-10.
      DO 28 JN=2,NSPEC
      XLIST(JN)=ALOG(XLIST(JN))
   28 YLIST(JN)=ALOG(YLIST(JN))
      REWIND 4
      WRITE(4)(XLIST(KM),YLIST(KM),KM=1,NSPEC)
      REWIND 4
      REWIND 6
      EMAX=EMAX/.51097
      TAUMIN=2.*10.**(-6)/.51097
      DELTA1=DELTA1/.51097
C  ***  TAPE 4 STORES LOG OF ELECTRON SPECTRUM
      TAUMAX=EMAX
      DO 77 JKJ=1,6
      IF(JKJ.EQ.1)EMIN=TAUMIN
      IF(JKJ.EQ.2)EMIN=TAUMIN*10.
      IF(JKJ.EQ.3)EMIN=TAUMIN*100.
      IF(JKJ.GT.3)EMIN=EMIN*2.
      READ(4)(XLIST(KJ),YLIST(KJ),KJ=1,NSPEC)
      REWIND 4
      ZETA=(TAUMIN/TAUMAX)**(1./FLOAT(JWT-1))
      TAU=TAUMAX/ZETA
      DO 11 J=1,JWT
      TAU=TAU*ZETA
      SPURS=G(TAU)
      WRITE(3,5)SPURS,TAU
      WRITE(6)SPURS,TAU
   11 CONTINUE
```

```
C   ***  TAPE 6 STORES THE SPUR SIZE DISTRIBUTION
      REWIND 6
      READ(6)(YLIST(K),XLIST(K),K=1,JWT)
      REWIND 6
      IF(YLIST(1).EQ..0)YLIST(1)=-10.
      IF(YLIST(1).GT..0)YLIST(1)=ALOG(YLIST(1))
      XLIST(1)=ALOG(XLIST(1))
      DO 15 MQ=2,JWT
      YLIST(MQ)=ALOG(YLIST(MQ))
   15 XLIST(MQ)=ALOG(XLIST(MQ))
      NWT=50
      TAUINT=EMAX/.5
   29 TAUINT=TAUINT*.5
      PSI=(TAUMIN/TAUINT)**(1./FLOAT(NWT-1))
      WTAB(1)=TAUINT
      DO 12 N=2,NWT
   12 WTAB(N)=WTAB(N-1)*PSI
      IWT=2
      CALL BATES(IWT,NWT)
      M=JWT
      N=2
      SUMN=.0
      SUM2=.0
      DO 14 MN=1,NWT
      X=ALOG(WTAB(MN))
      CALL INTER(N,M,X,Y,CHECK)
      TERM=EXP(Y)*WATES(MN)
      TERM2=TERM*WTAB(MN)
      SUM2=SUM2+TERM2
   14 SUMN=SUMN+TERM
      TAUBAR=SUM2/SUMN
      WRITE(3,9)TAUBAR,TAUINT,EMIN
      WRITE(3,7)SUMN
      IF(TAUINT.GT.50.0*TAUMIN)GO TO 29
   77 CONTINUE
      STOP
      END
```

```
MONS$       EXEQ FORTRAN
      FUNCTION VALUE(T,TAU)
      COMMON WTAB(50),WATES(50),XLIST(50),YLIST(50),DELY(10),EMAX,
     1DELTA1,DELTA2,NSPEC,EMIN,J
      IF(T.LE.TAU)VALUE=.0
      IF(T.LE.TAU)GO TO 27
      E=T
      IF(T.LT..004)GO TO 22
      IF(TAU.LE..0003)GO TO 22
      VALUE=PROBT(T,TAU)
      GO TO 27
   22 CONTINUE
      IF(TAU.LE.DELTA1)GO TO 25
      IF(E.LT..1)A=1.29*E**(-ALOG(1.88/1.29)/ALOG(10000.))
      IF(E.LT..1)GO TO 16
      IF(E.LT..32)A=1.1*E**(-ALOG(1.4/1.1)/ALOG(10.))
      IF(E.LT..32)GO TO 16
      IF(E.LT.1.)A=.94*E**(-ALOG(1.7/.94)/ALOG(10.))
      IF(E.LT.1.)GO TO 16
      A=.94*E**(-ALOG(.94/.335)/ALOG(10.))
   16 CONTINUE
      IF(E.LT..2)B=-.35*10.**(-4)
      IF(E.LT..2)GO TO 17
      IF(E.LT.1.)B=-.255*10.**(-4)*E**(-ALOG(.398/.255)/ALOG(10.))
      IF(E.LT.1.)GO TO 17
      B=-.255*10.**(-4)*E**(-ALOG(.255/.1)/ALOG(10.))
   17 CONTINUE
      C=.15*.555
      TAPPA=2.*C/T
      VALUE=TAPPA/((TAU*A+B)*(TAU*A+B))
      IF(TAU.GT.DELTA1)GO TO 27
   25 CONTINUE
      IF(T.LE..15)AKT=3.8*10.**8*E**(-ALOG(210.6)/ALOG(1000.))
      IF(T.LE..15)GO TO 24
      IF(T.LE..5)AKT=6.*10.**8*E**(-ALOG(11.65)/ALOG(100.))
      IF(T.LE..5)GO TO 24
      IF(T.LE.1.3)AKT=7.2*10.**8*E**(-ALOG(3.61)/ALOG(100.))
      IF(T.LE.1.3)GO TO 24
      AKT=6.75*10.**8
   24 CONTINUE
      VALUE=AKT*SMALL(TAU)
   27 RETURN
      END
```

```
 MON$$      EXEQ FORTRAN
      FUNCTION G(TAU)
      COMMON WTAB(50),WATES(50),XLIST(50),YLIST(50),DELY(10),EMAX,
     1DELTA1,DELTA2,NSPEC,EMIN
      NWT=50
      IF(EMIN.GE.TAU)PSI=(EMIN/EMAX)**(1./FLOAT(NWT-1))
      IF(EMIN.LT.TAU)PSI=(TAU/EMAX)**(1./FLOAT(NWT-1))
      WTAB(1)=EMAX
      DO 81 J=2,NWT
   81 WTAB(J)=WTAB(J-1)*PSI
      IWT=2
      CALL BATES(IWT,NWT)
      SUM=.0
      DO 82 K=1,NWT
      XTEST=VALUE(WTAB(K),TAU)
      TERM=SPECY(WTAB(K))*XTEST*TAU*WATES(K)
   82 SUM=SUM+TERM
      G=SUM
      RETURN
      END


 MON$$      EXEQ FORTRAN
      FUNCTION SPECY(E)
      COMMON WTAB(50),WATES(50),XLIST(50),YLIST(50),DELY(10),EMAX,
     1DELTA1,DELTA2,NSPEC
   22 CONTINUE
      X=ALOG(E)
      M=NSPEC
      N=2
      IF(E.LT..001)N=1
      CALL INTER(N,M,X,Y,CHECK)
      SPECY=EXP(Y)
   23 RETURN
      END
```

6.7 Explanation of the Program Used to Calculate the Weighted Average Spur Separation Distance

The spur separation distance, $\ell'(E,\delta_c)$ was given in terms of the elementary cross section $k_H(E,\tau)$, as follows:

$$\ell'(E,\delta_c) = \frac{\langle\bar{\tau}\rangle}{\int_0^{\delta_c} k_H(E,\tau)\tau d\tau} . \tag{159}$$

The maximum spur size was δ_c and the weighted average spur size was $\langle\bar{\tau}\rangle$.

Four forms were chosen to investigate the possibility of determining a weighted average spur separation distance. The forms were:

Case 1: (weighting by the electron spectrum and the relative local energy loss)

$$\langle\ell\rangle_1 = \frac{\int_{E_{min}}^{E_{max}} y(E) \frac{L(E,\delta_c)}{L(E)} \ell'(E,\delta_c)dE}{\int_{E_{min}}^{E_{max}} y(E) \frac{L(E,\delta_c)}{L(E)} dE} \tag{154}$$

Case 2: (weighting by the local energy loss)

$$\langle\ell\rangle_2 = \frac{\int_{E_{min}}^{E_{max}} y(E)L(E,\delta_c)\ell'(E,\delta_c)dE}{\int_{E_{min}}^{E_{max}} y(E)L(E,\delta_c)dE} \tag{155}$$

Case 3: (weighting by the electron spectrum)

$$\langle \ell' \rangle_3 = \frac{\int_{E_{min}}^{E_{max}} y(E)\,\ell'(E,\delta_c)\,dE}{\int_{E_{min}}^{E_{max}} y(E)\,dE} \tag{156}$$

Case 4: (The definition of the average linear energy transfer ($\overline{LET}$) is taken from a paper by Burch (6))

$$\overline{LET} = \frac{\int_{E_{min}}^{E_{max}} y(E)\,\frac{L(E,\delta_c)}{L(E)}\,L(E,\delta_c)\,dE}{\int_{E_{min}}^{E_{max}} y(E)\,\frac{L(E,\delta_c)}{L(E)}\,dE} \tag{157}$$

$$\langle \ell \rangle_4 = \frac{\langle \bar{\tau} \rangle}{\overline{LET}} \; . \tag{158}$$

$L(E)$ and $L(E,\delta_c)$ were the total the restricted stopping powers.

To check the accuracy of the numerical scheme and to estimate the accuracy of a linear extrapolation for $y(E)$, ($E<400$ ev), several dose rates were calculated. They were:

$$\underline{\text{Dose 1}} = \int_{E_{min}}^{E_{max}} S(E')(E' - E_{min})\,dE'' \tag{160}$$

$$\underline{\text{Dose 2}} = \int_{E_{min}}^{E_{max}} S(E')E'\,dE' \tag{161}$$

$$\underline{\text{Dose 3}} = \int_{E_{min}}^{E_{max}} y(E')L(E')dE' \tag{162}$$

$$\underline{\text{Dose 4}} = \int_{E_{min}}^{E_{max}} y(E')L(E',\delta_c)dE'. \tag{163}$$

The subprograms used by this code were:

FUNCTION SOURCE(T)

FUNCTION SPECY(E)

FUNCTION SPRS(E,DELTA2)

FUNCTION AINEXD(T,BLIMIT,TAU)

FUNCTION SMALL(TAU)

FUNCTION AINGS(T,DELTA1,TAU)

SUBROUTINE BATES(IWT,NWT,WTAB,WATES)

SUBROUTINE INTER(N,M,X,Y,CHECK).

Only SPECY(E) and SOURCE(T) are listed in this section since the rest are used in other programs and explained in section 6.8. Subprogram SOURCE(T) evaluated S(E) and subprogram SPECY(E) evaluated the electron spectrum. Dose 1 and Dose 2 were not obtained numerically for Co^{60} irradiation since they could be obtained analytically. Only Dose 2 was calculated.

Table XIX gives an explanation of variables associated with the code.

Table XIX. Explanation of Computer Program Variables

Symbol	Explanation
CUTOFF	δ_c, maximum spur size
EMAX	E_{max}, maximum energy of electrons in the given spectrum
TAUBAR	$\langle\bar{\tau}\rangle$, weighted average spur size
NSPEC	Number of data cards for the electron spectrum
NSOUR	Number of data cards for the initial electron spectrum
BLIMIT	E_{min}

LOGIC DIAGRAM FOR THE COMPUTER PROGRAM DESCRIBED IN SECTION 6.7

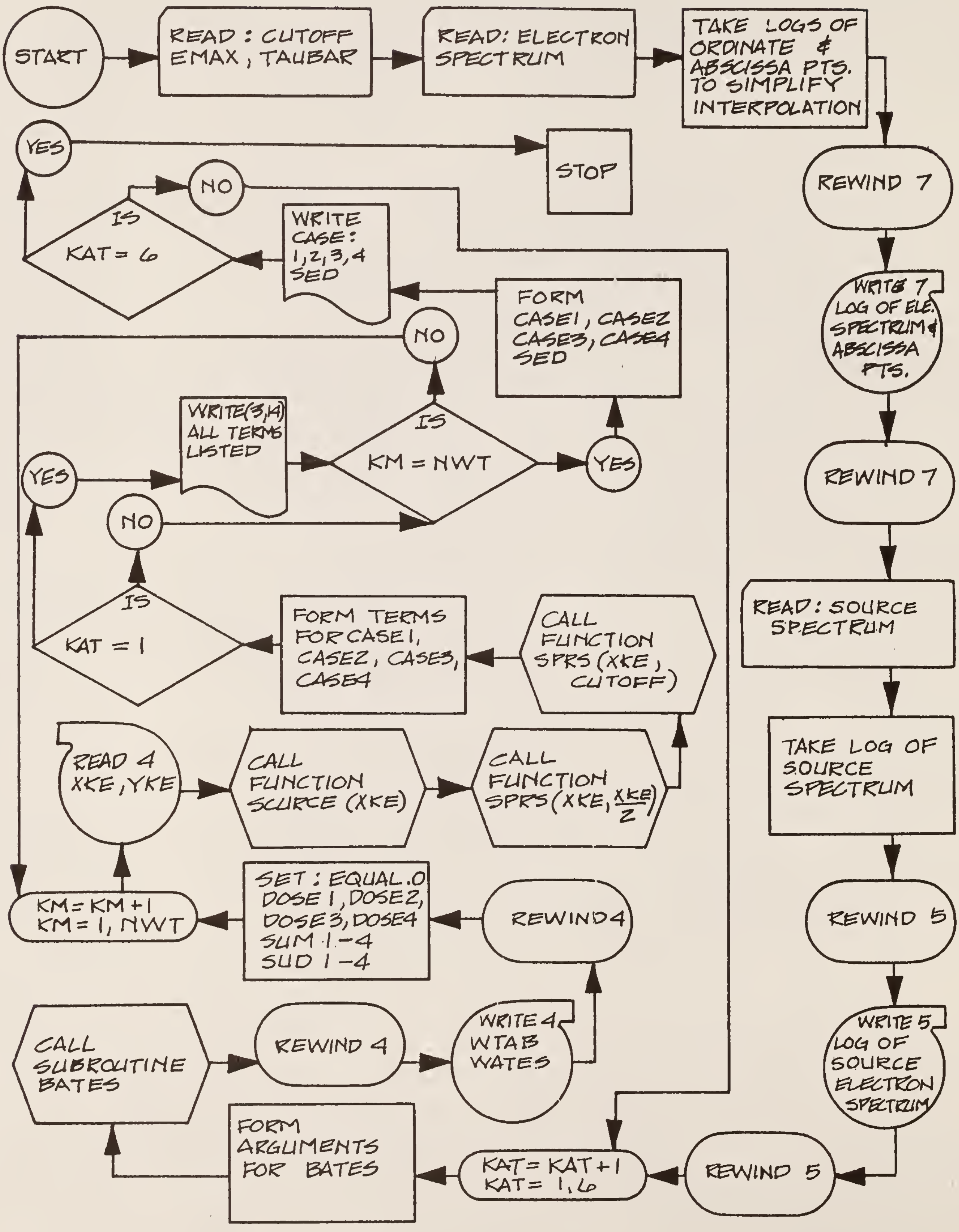

LOGIC DIAGRAM FOR THE FUNCTION SPECY(E) DESCRIBED IN SECTION 6.7

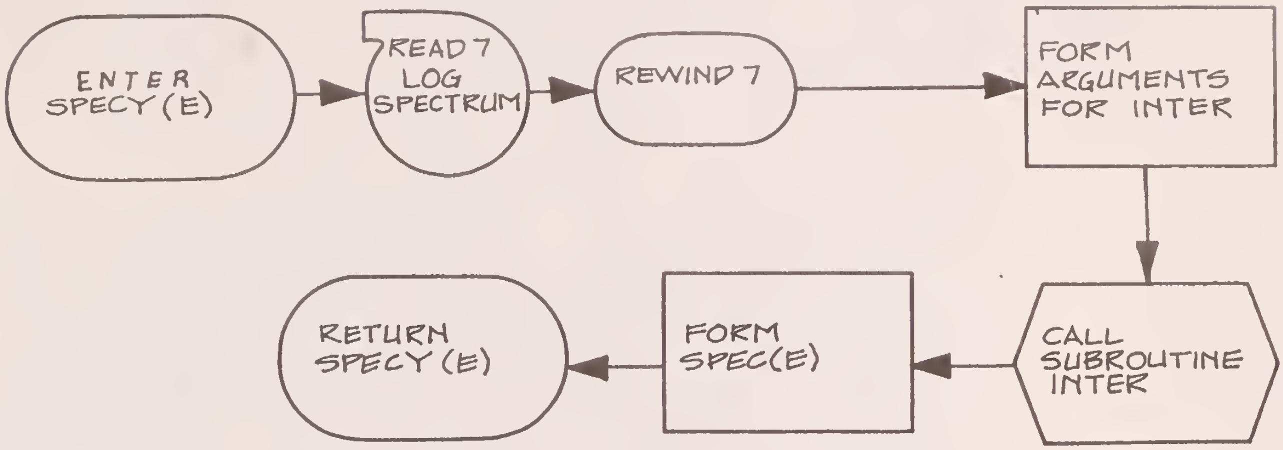

LOGIC DIAGRAM FOR THE FUNCTION SOURCE(E) DESCRIBED IN SECTION 6.7

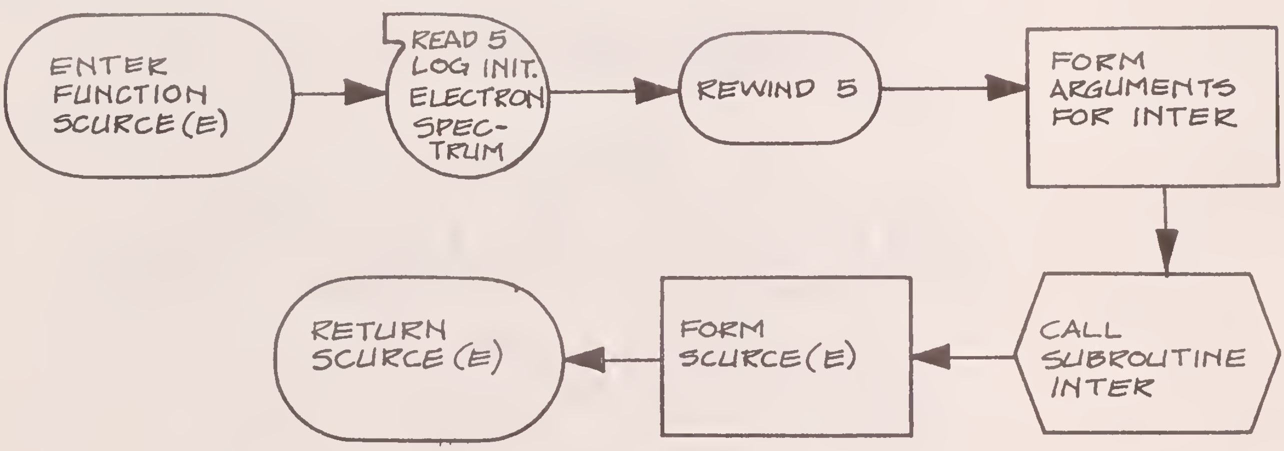

```
MON$$      JOB   SPUR SEPARATION DISTANCE          MILLER                    J
MON$$      CONT 15 MINUTES, 5 PAGES  L.F. MILLER
MON$$      ASGN MJB,12
MON$$      ASGN MGO,16
MON$$      MODE GO,TEST
MON$$      EXEQ FORTRAN,,,,,,,SSD
      COMMON WTAB(50),WATES(50),XLIST(50),YLIST(50),DELY(10),JK,NSOUR,
     1NSPEC
    1 FORMAT(I5)
    3 FORMAT(2E14.8)
    2 FORMAT(5E14.8)
    5 FORMAT(1HK,5E14.8)
   14 FORMAT(1H ,14E9.3)
      READ(1,2)AO,CUTOFF,BLIMIT,EMAX,TAUBAR
      BLIMIT=BLIMIT/.51097
      CUTOFF=CUTOFF/.51097
      READ(1,1)NSPEC
      READ(1,3)(YLIST(KK),XLIST(KK),KK=1,NSPEC)
      YLIST(1)=-10.
      XLIST(1)=ALOG(XLIST(1))
      DO 88 KKK=2,NSPEC
      XLIST(KKK)=ALOG(XLIST(KKK))
   88 YLIST(KKK)=ALOG(YLIST(KKK))
      REWIND 7
      WRITE(7)(XLIST(K),YLIST(K),K=1,NSPEC)
      REWIND 7
      READ(1,1)NSOUR
      READ(1,3)(XLIST(KK),YLIST(KK),KK=1,NSOUR)
      DO 89 KQ=1,NSOUR
      XLIST(KQ)=ALOG(XLIST(KQ))
   89 YLIST(KQ)=ALOG(YLIST(KQ))
      REWIND 5
      WRITE(5)(XLIST(K),YLIST(K),K=1,NSOUR)
      REWIND 5
      DO 93 KAT=1,6
      IF(KAT.EQ.1)BLIMIT=2.*10.**(-6)/.51097
      IF(KAT.EQ.2)BLIMIT=BLIMIT*10.
      IF(KAT.EQ.3)BLIMIT=BLIMIT*10.
      IF(KAT.GT.3)BLIMIT=BLIMIT*2.
      NWT=50
      IWT=2
      PSI=(BLIMIT/EMAX)**(1./FLOAT(NWT-1))
      WTAB(1)=EMAX
      DO 90 LCD=2,NWT
   90 WTAB(LCD)=WTAB(LCD-1)*PSI
      CALL BATES(IWT,NWT)
      REWIND 4
      DO 99 KE=1,NWT
      XKE=WTAB(KE)
      YKE=WATES(KE)
```

```
99 WRITE(4)XKE,YKE
   REWIND 4
   DOSE1=.0
   DOSE2=.0
   DOSE3=.0
   DOSE4=.0
   SUD1=.0
   SUD2=.0
   SUD3=.0
   SUD4=.0
   SUM1=.0
   SUM2=.0
   SUM3=.0
   SUM4=.0
   DO 91 KM=1,NWT
   READ(4)XKE,YKE
   TR1=SOURCE(XKE)
   TR2=SPECY(XKE)
   TR3=SPRS(XKE,XKE/2.)
   TR4=SPRS(XKE,CUTOFF)
   TERM1=TR1*(XKE-BLIMIT)*YKE
   TERM2=TR1*XKE*YKE
   DOSE1=DOSE1+TERM1
   DOSE2=DOSE2+TERM2
   TERM3=TR2*TR3*YKE
   TERM4=TR2*TR4*YKE
   DOSE3=DOSE3+TERM3
   DOSE4=DOSE4+TERM4
   RATIO=TR4/TR3
   TNUM1=TR2*YKE/TR3
   TDEM1=TR2*RATIO*YKE
   TNUM2=TR2*YKE
   TDEM2=TR2*TR4*YKE
   TNUM3=TR2/TR4*YKE
   TDEM3=TR2*YKE
   TNUM4=TR2*TR4*TR4/TR3*YKE
   TDEM4=TR2*TR4/TR3*YKE
   SUM1=SUM1+TNUM1
   SUD1=SUD1+TDEM1
   SUM2=SUM2+TNUM2
   SUD2=SUD2+TDEM2
   SUM3=SUM3+TNUM3
   SUD3=SUD3+TDEM3
   SUM4=SUM4+TNUM4
   SUD4=SUD4+TDEM4
```

```
      IF(KAT.EQ.1)WRITE(3,14)TR1,TR2,TR3,TR4,RATIO,SUM1,SUM2,SUM3,SUM4,
     1SUD1,SUD2,SUD3,SUD4,XKE
      IF(KAT.EQ.1)WRITE(3,5)DOSE1,DOSE2,DOSE3,DOSE4,XKE
   91 CONTINUE
      CASE1=SUM1/SUD1*TAUBAR
      CASE2=SUM2/SUD2*TAUBAR
      CASE3=SUM3/SUD3*TAUBAR
      CASE4=SUM4/SUD4
      SED=TAUBAR/CASE4
      WRITE(3,14)CASE1,CASE2,CASE3,CASE4,SED,DOSE1,DOSE2,DOSE3,DOSE4,
     1SLIMIT,EMAX,TAUBAR,CUTOFF,AO
   93 CONTINUE
      STOP
      END

     MON$$      EXEQ FORTRAN
      FUNCTION SPECY(E)
      COMMON WTAB(50),WATES(50),XLIST(50),YLIST(50),DELY(10),JK,NSOUR,
     1NSPEC
      READ(7)(XLIST(K),YLIST(K),K=1,NSPEC)
      REWIND 7
   22 CONTINUE
      X=ALOG(E)
      M=NSPEC
      N=2
      IF(E.LT..001)N=1
      CALL INTER(N,M,X,Y,CHECK)
      SPECY=EXP(Y)
   23 RETURN
      END

     MON$$      EXEQ FORTRAN
      FUNCTION SOURCE(T)
      COMMON WTAB(50),WATES(50),XLIST(50),YLIST(50),DELY(10),JK,NSOUR,
     1NSPEC
      READ(5)(XLIST(K),YLIST(K),K=1,NSOUR)
      REWIND 5
      X=ALOG(T)
      M=NSOUR
      N=2
      IF(T.LT..001)N=1
      CALL INTER(N,M,X,Y,CHECK)
      SOURCE=EXP(Y)
      RETURN
      END
```

6.8 Explanation of Subprograms Used in More Than One Code

6.8.1 Explanation of SUBROUTINE BATES

To use SUBROUTINE BATES, one needs to define the arguments IWT, NWT and WTAB. WTAB is a dimensioned variable and locates the abscissa points for the integration. NWT is the number of points and the value of IWT depends on the scale chosen for the integration points. If a linear scale is used, IWT must be defined as IWT 1; if logrithmic, IWT must be set equal to a number larger than 1.

The following statement-by-statement description of this subroutine was written by L. V. Spencer:

819 WTA = NWT

This order makes a floating point number equal to NWT, the number of points in the abscissa list.

IF(NWT-2GE.0)GO TO 39

19 WATES(1) = .0

GO TO 259

These orders take care of the case in which the list consists of only a single value. The integral in this case is zero, and control goes to 259, which will return control to the main program.

39 IF(IWT-2GE.0)GO TO 79

59 WTDEL = (WTAB(1)-WTAB(NWT))/(WTA-1.)

GO TO 99

The first order determines whether the list progression is linear or geometric. The second calculates the interval between points of the list for the linear case. This is only one of many ways for doing this.

```
79 WTDEL = LOG(WTAB(1)/WTAB(NWT))/WTA-1.)
99 IF(WTDEL.GE.0.)GO TO 990
119 WTDEL = -WTDEL
```

The first order calculates the factor between points if the interval changes geometrically. The last two orders make the interval size positive in all cases. This may or may not be desirable.

```
990 IF(NWT-2) 259,1190,139
1190 WATES(1) = .5*WTDEL
WATES(2) = WATES(1)
GO TO 199
```

This takes care of the case in which only two points are involved in the integration, which is then trapezoidal. The transfer to 199 permits either linear or geometric progression to be assumed. The two cases are not quite the same for two point integration, even though at first thought it would seem they should be.

```
139 NWTA = (WTA/2.+.1)
NWTB = (WTA/2.-.1)
NWTC = (WTA/4.+.1)
NWTD = (WTA/4.-.1)
```

These four orders generate parameters to be used in determining whether the number of weights is odd, divisible by 4, or even. WTA is numerically almost identical with NWT, differing at most in the 8'th significant figure. The orders are to construct integers from the number in paranthesis. The important thing is that the integer is always the <u>smaller</u> of the two numbers bracketing the floating point value. Thus, a number divisible by 2 will yield NWTA larger by unity than NWTB. A number not divisible by 2 will yield NWTA = NWTB. The same trick is used also for divisibility by 4.

```
WATES(1) = WTDEL/3.
WTC = WATES(1)
WATES(NWT) = WATES(1)
```

The first and last weights are given their proper value, and WTC, to be used later, is assigned its value.

```
DO 159 I=1, NWTB
WATES(I+1) = WTDEL + WTC
INDX = NWT-I
WATES(INDX) = WTDEL + WTC
159 WTC = -WTC
```

This group of orders assigns the bulk of the weights their 1,4,2,4,.... structure. Notice the symmetry between WATES(I+1) and WATES(NWT-I). NWTB will be a value such that NWTB = 1 is either the middle value or the lower of two middle values. In the latter case, after this set of orders, the two middle values are either 2*WTDEL/3, so that the middle interval is given incorrectly, or on the low side, or they are 4*WTDEL/3, so that the middle values are weighted too heavily. We must either subtract or add WTDEL/3 to establish weights which either neglect or add in twice the middle interval. Then we must add or subtract weights for the middle interval, which are WTDEL*(-1/24, 13/24, 13/24, -1/24), corresponding to approximating by a cubic, with integration only over the middle interval.

```
WTD = 1./24.
IF(NWTC-NWTD.2E.0)GO TO 1790
1590 WTD=- WTD
```

The first order establishes the divisor for the correction. The other two orders determine the sign of the correction for the middle interval, which depends on divisibility of NWT by 4.

```
1790 IF(NWTA-NWTB.LE.0)GO TO 194
179 WATES(NWTB) = WATES(NWTB)-WTD*WTDEL
WATES(NWTB+1) = WATES(NWTB+5.*WTD*WTDEL
WATES(NWTD+3) = WATES(NWTB)
WATES(NWTB+2) = WATES(NWTB+1)
```

These orders make the correction, which involves four middle values, when the number of points of integration is even (i.e., divisible by 2). When NWT is odd, the correction is bypassed.

```
199 IF(IWT-2.LT.0)GO TO 259
219 DO 239 I=1, NWT
239 WATES(I) = WATES(I)*WTAB(I)
259 RETURN
```

These orders complete the subroutine proper. The final modification which they make is multiplication by values of the abscissa for the case in which the mesh is geometric.

```
MONTT        EXEC FORTRAN,.,,,,,,WATES
      SUBROUTINE WATES(IWT,NWT)
      COMMON WTAB(50),WATES(50),XLIST(50),YLIST(50),DELY(10)
  819 WTA=NWT
      IF(NWT-2.GE.0)GO TO 39
   19 WATES(1)=0.
      GO TO 259
   39 IF(IWT-2.GE.0)GO TO 79
   59 WTDEL=(WTAB(1)-WTAB(NWT))/(WTA-1.)
      GO TO 99
   79 WTDEL=ALOG(WTAB(1)/WTAB(NWT))/(WTA-1.)
   99 IF(WTDEL.GE.0.)GO TO 990
  119 WTDEL=-WTDEL
  990 IF(NWT-2)259,1190,139
 1190 WATES(1)=.5*WTDEL
      WATES(2)=WATES(1)
      GO TO 199
  139 NWTA=(WTA/2.+.1)
      NWTB=(WTA/2.-.1)
      NWTC=(WTA/4.+.1)
      NWTD=(WTA/4.-.1)
      WATES(1)=WTDEL/3.
      WTC=WATES(1)
      WATES(NWT)=WATES(1)
      DO 159 I=1,NWTB
      WATES(I+1)=WTDEL+WTC
      INDX=NWT-I
      WATES(INDX)=WTDEL+WTC
  159 WTC=-WTC
      WTD=1./24.
      IF(NWTC-NWTD.LE.0)GO TO 1790
 1590 WTD=-WTD
 1790 IF(NWTA-NWTB.LE.0)GO TO 199
  179 WATES(NWTB)=WATES(NWTB)-WTD*WTDEL
      WATES(NWTB+1)=WATES(NWTB+1)+5.*WTD*WTDEL
      WATES(NWTB+3)=WATES(NWTB)
      WATES(NWTB+2)=WATES(NWTB+1)
  199 IF(IWT-2.LT.0)GO TO 259
  219 DO 239 I=1,NWT
  239 WATES(I)=WATES(I)*WTAB(I)
  259 RETURN
      END
```

6.8.2 Explanation of Subprogram Y(T)

This subprogram evaluated the following integral:

$$y(E) = \int_{E}^{E_{max}} z(E_o,E)S(E_o)dE_o \qquad (222)$$

The arguments of the integrand were obtained from FUNCTION subprograms. Table XX gives an explanation of several subprogram variables.

Table XX. Explanation of Subprogram Variables

Symbol	Explanation
PSI	Geometric progression ratio
Q2	Point of discontinuity in the initial electron spectrum from Co^{60} irradiation
Q	Maximum electron source energy
XYZ	Electron energy spectrum at Q2 divided by ANECC
DX	Integral over the initial electron spectrum above QZ
IOFT	Index to prevent duplication when calling ZEE

LOGIC DIAGRAM FOR THE FUNCTION Y(T) DESCRIBED IN SECTION 6.8.2

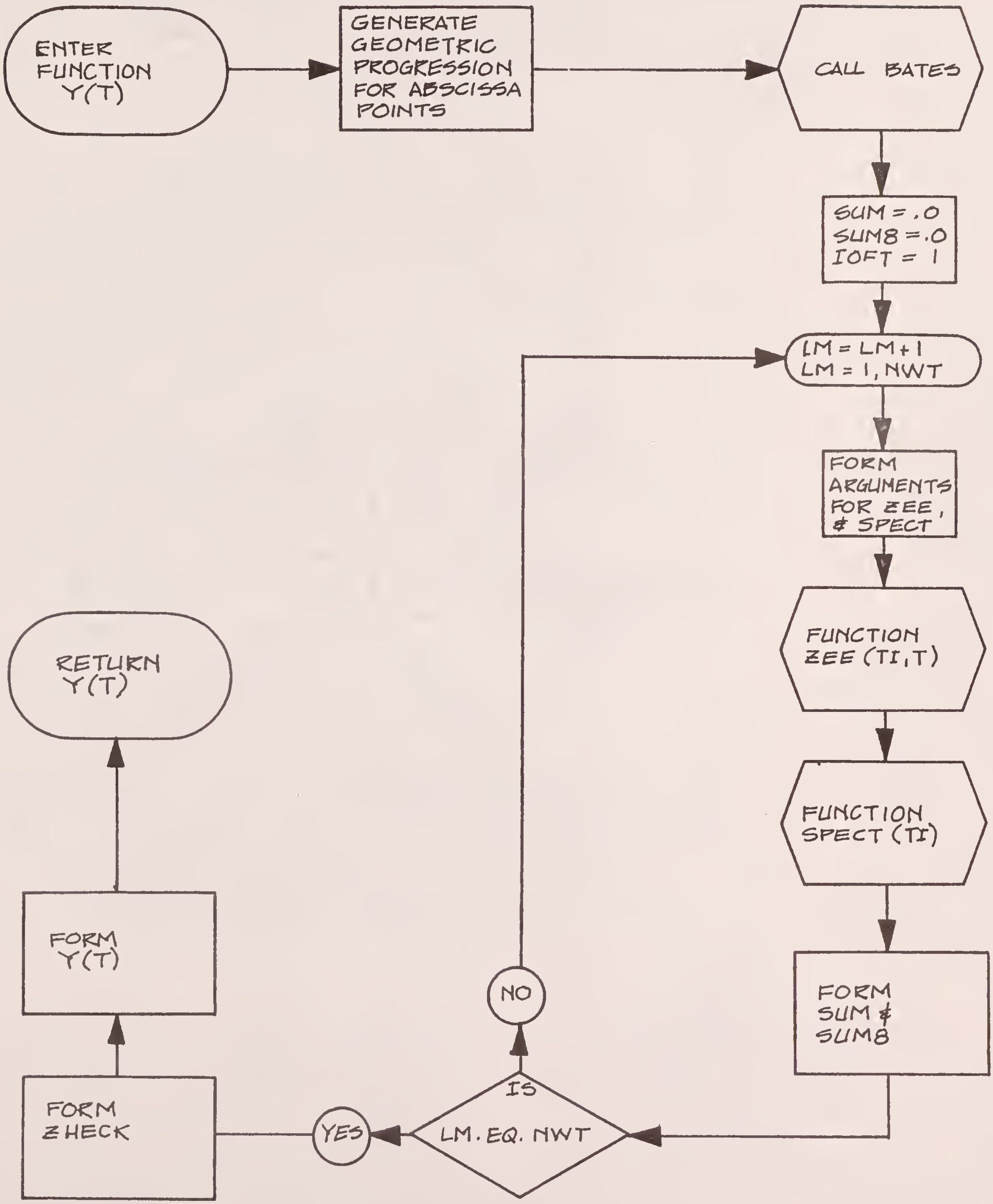

```
MON$$      EXEQ FORTRAN
       FUNCTION Y(T)
       COMMON XLIST(49),YLIST(49),DELY(100),EZ(25),ROW(25),COB,WTAB(50),
      1WATES(50),IOFT,NCOLM,G,ZHECK,Q2,XYZ,XSPEC(40),YSPEC(40),NPTS
       NWT=50
       IF(T.GE.Q2)PSI=(T/Q)**(1./FLOAT(NWT-1))
       IF(T.LT.Q2)PSI=(T/Q2)**(1./FLOAT(NWT-1))
       IF(T.GE.Q2)WTAB(1)=Q
       IF(T.LT.Q2)WTAB(1)=Q2
       DO 29 JM=2,NWT
    29 WTAB(JM)=WTAB(JM-1)*PSI
       IWT=2
       CALL BATES(IWT,NWT)
       SUM=.0
       SUM8=.0
       IOFT=1
       DO 30 LM=1,NWT
       TI=WTAB(LM)
       ABC=ZEE(TI,T)
       ABCD=SPECT(TI)
       TERM=ABC*ABCD*WATES(LM)
       TERM8=ABCD*WATES(LM)
       SUM8=TERM8+SUM8
    30 SUM=SUM+TERM
       IF(T.EQ.Q2+.0001)DZ=SUM8
       IF(T.GE.Q2)ZHECK=SUM8
       IF(T.LT.Q2)ZHECK=SUM8+DZ
       IF(T.GT.Q2)Y=SUM
       IF(T.LE.Q2)Y=SUM+XYZ
       RETURN
       END
```

6.8.3 Explanation of Subprogram ZEE(TI,T)

This subprogram performed a double interpolation using a single interpolation subroutine. The data for $z(E_o,E)$ were equally spaced on a logrithmic scale; therefore, it was necessary that the interpolation subprogram INTER use a logarithmic argument for $z(E_o,E)$. Due to the large number of data points, the data for $z(E_o,E)$ were stored on magnetic tape. Table XXI describes several subprogram variables.

Table XXI. Explanation of Subprogram Variables

Symbol	Explanation
ICOL	Used as an index to determine the required number of the 22 sets of input, $z(E_o,E)$ data needed for the interpolation
NCOLM	Equals 22 and represents the total number of $z(E_o,E)$ data sets
NWT	Takes on the value of the length of the list of each spectrum
ROW	$z(E_o,T)$ data generated to perform double interpolation
TI	Source energy
T	Electron energy

LOGIC DIAGRAM FOR THE FUNCTION ZEE(TI,T) DESCRIBED IN SECTION 6.8.3

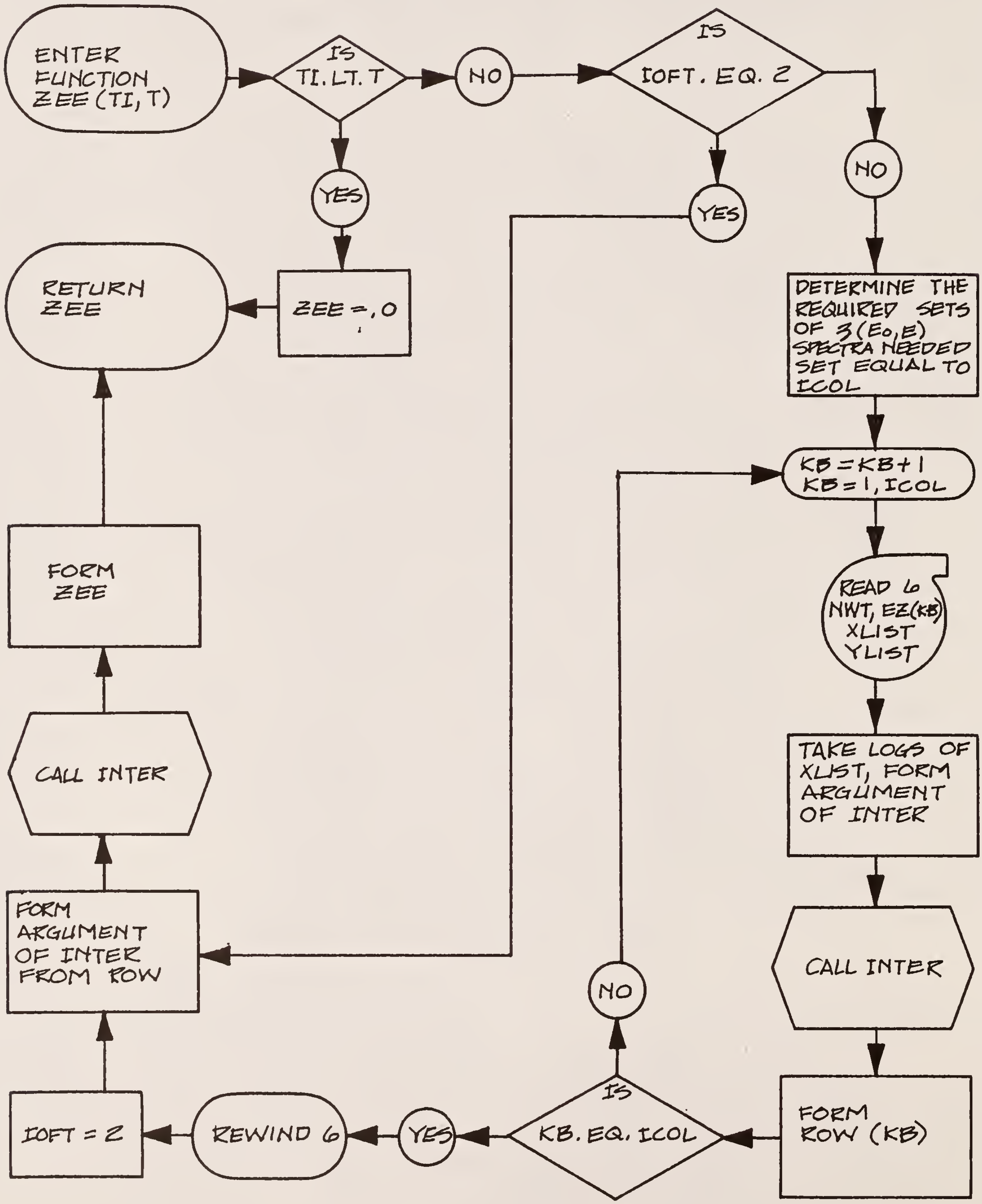

```
MON$1      EXEQ FORTRAN
 FUNCTION ZEE(TI,T)
 COMMON XLIST(49),YLIST(49),DFLY(100),FZ(25),ROW(25),COP,WTAB(50),
1WATES(50),IOFT,NCOLM,Q,ZHECK,Q2,XYZ,XSPEC(40),YSPEC(40),NPTS
 IF(TI.LT.T)ZEE=.0
 IF(TI.LT.T)GO TO 30
 IF(IOFT.EQ.2)GO TO 29
 ICOL=1
16 IF(T.LT.FZ(ICOL))ICOL=ICOL+1
 IF(ICOL.EQ.NCOLM)GO TO 17
 IF(T.LT.FZ(ICOL))GO TO 16
17 IF(T.GT.FZ(ICOL))ICOL=ICOL-1
 DO 27 KB=1,ICOL
 READ(6)(NWT,FZ(KB),(XLIST(J),YLIST(J),J=1,NWT))
 XLIST(1)=ALOG(FZ(KB))
 DO 25 J=2,NWT
25 XLIST(J)=ALOG(XLIST(J))
 X=ALOG(T)
 M=NWT
 N=2
 CALL INTER(N,M,X,Y,CHECK)
27 ROW(KB)=Y
 REWIND 6
 IOFT=2
29 X=ALOG(TI)
 DO 28 JK=1,ICOL
 YLIST(JK)=ROW(JK)
28 XLIST(JK)=ALOG(FZ(JK))
 M=ICOL
 N=2
 IF(N.EQ.0)N=1
 CALL INTER(N,M,X,Y,CHECK)
 ZEE=Y
30 RETURN
 END
```

6.8.4 Explanation of Subprogram INTER(M,N,X,Y,CHECK)

This subroutine was written by Merwin Brown under the supervision of Dr. J. O. Mingle. Only one statement in the program was changed for this work, but the arguments in the subroutine are different.

NAME: INTER

TYPE: PR-155 FORTRAN IV SUBROUTINE

PURPOSE: To interpolate values from a table of x and f(x) values using a Bessel's interpolation formula.

COMMONED VARIABLES: Dimensioned in common are:

XLIST(M), YLIST(M), DELY(N+1),

where XLIST(M) and YLIST(M) are x_i's and $f(x_i)$'s of a table of given values where i=1, M, M being the length of the table. DELY(N+1) is the central difference table variable and is required to dimension core storage area, where N is the order of fit. DELY(N+1) has no 'answer' value to the user.

ARGUMENTS: are N,M,X,Y

N is the desired order of the fitted polynomial - entered.

M is the length of the given table, *e.g.*, z_1, $f(x_1)$, x_2, $f(x_2),\ldots,x_M$, $f(x_M)$ - entered.

X is the arbitrary value at which interpolation is desired - entered.

Y is the corresponding interpolated f(x), *i.e.*, the answer - returned.

OTHER SUBPROGRAMS: None

WORK TAPES: None

STORAGE: 3536 excluding common area.

TIME: Roughly, 4 to 5 seconds for second order interpolation, less than half a minute for fifth order, for example.

THEORY: Uses a central divided difference Bessel interpolation formula (see NUMERICAL METHODS FOR SCIENCE AND ENGINEERING, Stanton, Ralph G., Prentice - Hall, Englewood Cliffs, New Jersey, 1961, pp. 39-41).

REMARKS: (1) Evenly spaced values of x should be used.

(2) If the order of fit specified by the user is too large for the table of values given, N is automatically set equal to the largest possible value for the given data and a message concerning this change is printed.

(3) If a value requires extrapolation, a message is printed warning the user. Extrapolated values should be used with scrutiny.

(4) The closer spaced the data and smoother the curve, the better the interpolation will be.

PROGRAMMER: Merwin Brown

DEPARTMENT: Nuclear Engineering

DATE: 7/2/65

```
 MONS$        EXEQ FORTRAN........,INTER
      SUBROUTINE INTER (N,M,X,Y,CHECK)
      COMMON WTAB(50),RATES(50),XLIST(50),YLIST(50),DELY(10)
    3 FORMAT(27H N TOO BIG - CHANGED TO MAX//)
    4 FORMAT(14H EXTRAPOLATING/)
C     N=ORDER OF FIT, M=LENGTH OF TABLE, XLIST1 IS THE FIRST X-VALUE,
C     DELX IS THE STEP INCREMENT OF THE X-VALUES, X IS THE VALUE AT WHIC
C     H INTERPOLATION IS DESIRED, Y IS THE INTERPOLATED ANSWER, CHECK IS
C     THE FRACTIONAL CHANGE IN THE ANSWER MADE BY THE LAST ADDITIONAL
C     CALCULATION, YLIST(M) IS THE F(X) ARRAY, DELY(N+1) IS CORE SPACE
C     SAVED FOR DIFFERENCE TABLE
      XLIST1=XLIST(1)
      DELX=XLIST(2)-XLIST(1)
      NA=(N/2)*2
      MM=M-1
      IF(NA.LT.MM)GO TO 11
      ME=(M/2)*2
      IF(ME.EQ.M)MM=M
      N=MM-1
      NA=(N/2)*2
   11 IA=1.+(X-XLIST1)/DELX
      XE=(XLIST1+FLOAT(M-1)*DELX-X)/DELX
      NH=(N+2)/2
      IF(XE.GE.0.0)GO TO 19
      IA=M-NH
      GO TO 22
   19 IF(IA.GT.0)GO TO 20
      IA=NH
      WRITE(3,4)
      GO TO 22
   20 IE=1.+XE
      IF(IA.LT.NH)IA=NH
      IF(NH.GE.IE)IA=M-NH
   22 M1=IA-N/2
      M2=IA+1
      DO 26 I=1,M2
      K=M1+I
   26 DELY(I)=YLIST(K)-YLIST(K-1)
      XIAL=XLIST1+FLOAT(IA-1)*DELX
      H=(X-XIAL)/DELX
      B=H-0.5
      ASU=(YLIST(IA+1)+YLIST(IA))*.5+B*DELY(NH)
      IF(NA.EQ.0)GO TO 58
      IF(N.EQ.NA)NA=NA-1
      SUM=0.0
      D=1.0
      C=1.0
```

```
      DO 56 I=1,NA
      NS=N2-I
      DO 38 J=1,NS
   38 DELY(J)=DELY(J+1)-DELY(J)
      IH=I/2
      IF(I.EQ.IH*2)GO TO 51
      K=(I+1)/2
      F=2.0*(FLOAT(K)-1.0)
      C=(2.0+F)*(1.0+E)*C
      D=(H+E/2. )*(H-FLOAT(K))*D
      COF=D/C
      NN=NH-K
      EVEN=(DELY(NN+1)+DELY(NN))*.5
      ODD=0.0
      GO TO 56
   51 Q=1.0/(1.0+FLOAT(I))
      NR=NH-IH
      ODD=Q*B*DELY(NR)
      EVEN=0.0
   56 SUM=(EVEN+ODD)*COF+SUM
      GO TO 59
   58 SUM=0.0
   59 Y=ASU+SUM
      CHECK=(EVEN+ODD)*COF/Y
      RETURN
      END
```

6.8.5 Explanation of Subprogram AINEXD(T,BLIMIT,TAU)

This subprogram performed the following integration:

$$\mathrm{AINEXD(T,BLIMIT,TAU)} = \int_{\mathrm{BLIMIT}}^{\mathrm{TAU}} \mathrm{AKT}\ k_{ex}(\tau)\tau d\tau. \quad (223)$$

AKT was a function of the electron energy T, and $k_{ex}(\tau)$ represented the inelastic collision cross section given by FUNCTION SMALL(TAU).

```
MONIT       EXEC FORTRAN
      FUNCTION AINEXD(T,BLIMIT,TAU)
      COMMON WTAB(50),WATES(50),XLIST(50),YLIST(50),DELY(10),JK
      IF(JK.GT.1)GO TO 25
      E=T
      NWT=30
      DEL=(TAU-BLIMIT)/FLOAT(NWT-1)
      DO 21 L=1,NWT
   21 WTAB(L)=DEL*FLOAT(L-1)+BLIMIT
      IWT=1
      CALL RATES(IWT,NWT)
      SUM=.0
      DO 22 KM=1,NWT
      TERM=SMALL(WTAB(KM))*WATES(KM)*WTAB(KM)
   22 SUM=SUM+TERM
   25 CONTINUE
      IF(T.LE..15)AKT=3.8*10.**8*E**(-ALOG(210.6)/ALOG(1000.))
      IF(T.LE..15)GO TO 24
      IF(T.LE..5)AKT=6.*10.**8*E**(-ALOG(11.65)/ALOG(100.))
      IF(T.LE..5)GO TO 24
      IF(T.LE.1.3)AKT=7.2*10.**8*E**(-ALOG(3.61)/ALOG(100.))
      IF(T.LE.1.3)GO TO 24
      AKT=6.75*10.**8
   24 CONTINUE
      AINEXD=SUM*AKT
      RETURN
      END
```

6.8.6 Explanation of Subprogram SMALL(TAU)

This subprogram evaluated the inelastic cross section data by a series of straight line approximations. Figure 28 illustrates the accuracy of the straight line fit.

```
MON$$       EXEC FORTRAN
      FUNCTION SMALL(TAU)
      F=1.
C     TAU CORRECTED TO UNITS OF ELECTRON VOLTS
      ATAU=TAU*10.**6*.51
      IF(ATAU.LT.4.)SMALL=F*(ATAU/36.)
      IF(ATAU.LT.4.)GO TO 199
      IF(ATAU.LT.6.)SMALL=F*(.33*ATAU-1.21)
      IF(ATAU.LT.6.)GO TO 199
      IF(ATAU.LT.7.48)SMALL=F*(1.482*ATAU-7.762)
      IF(ATAU.LT.7.48)GO TO 199
      IF(ATAU.LT.8.9)SMALL=F*(-1.015*ATAU+10.49)
      IF(ATAU.LT.8.9)GO TO 199
      IF(ATAU.LT.10.13)SMALL=F*(1.28*ATAU-9.98)
      IF(ATAU.LT.10.13)GO TO 199
      IF(ATAU.LT.12.)SMALL=F*(-0.1925*ATAU+4.97)
      IF(ATAU.LT.12.)GO TO 199
      IF(ATAU.LT.14.)SMALL=F*(0.67*ATAU-5.37)
      IF(ATAU.LT.14.)GO TO 199
      IF(ATAU.LT.16.)SMALL=F*(-.722*ATAU+14.1)
      IF(ATAU.LT.16.)GO TO 199
      IF(ATAU.LT.24.)SMALL=F*(-0.2*ATAU+5.756)
  199 RETURN
      END
```

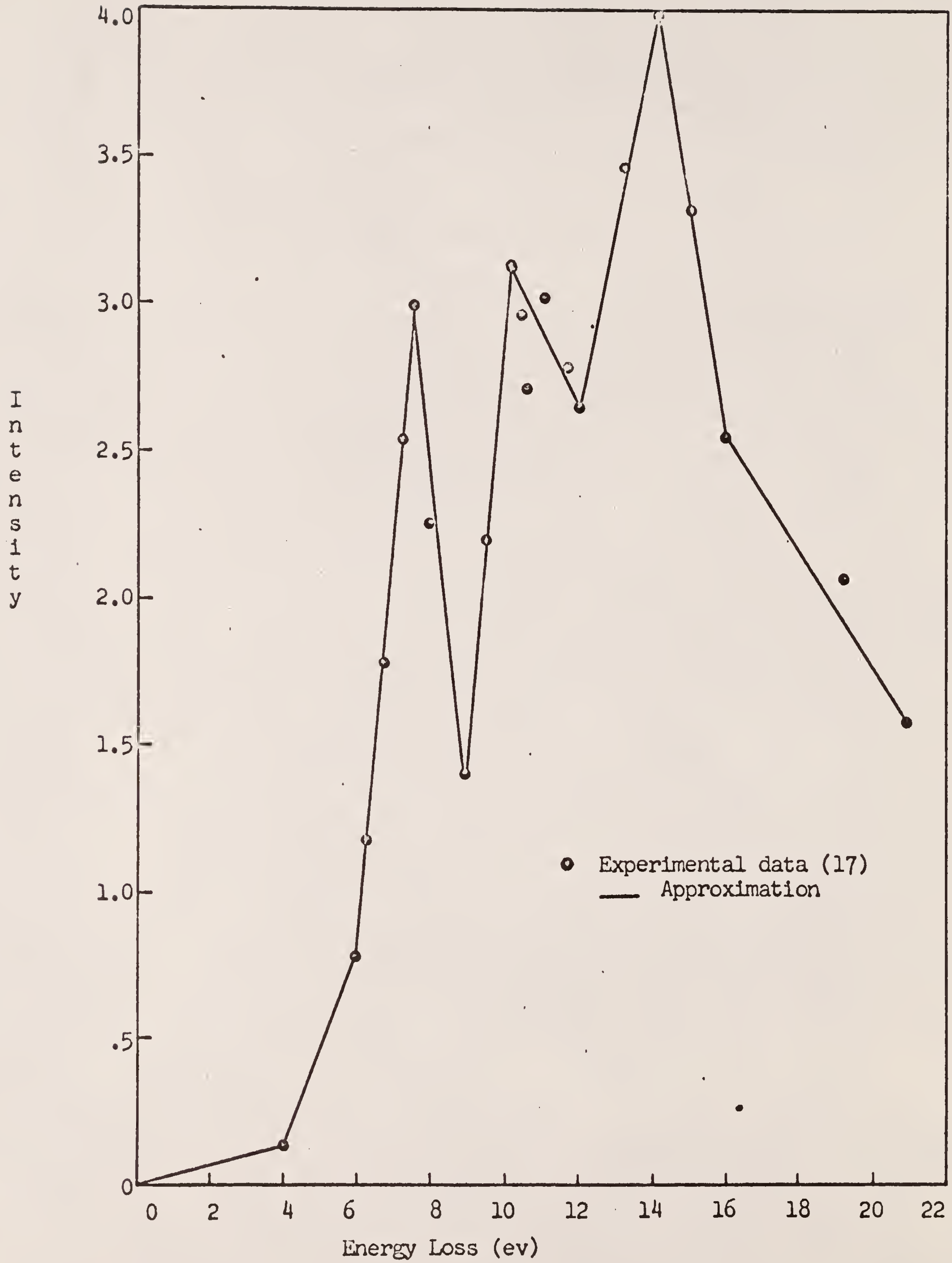

Fig. 39. Plot of the Straight Line Approximation for the Inelastic Collision Cross Section Data (Intensity vs. Energy Loss)

6.8.7 Explanation of the Subprogram AINGS(T,DELTA1,TAU)

This subprogram evaluated the following integral:

$$AINGS(T,DELTA1,TAU) = \int_{DELTA1}^{TAU} k_H(T,\tau)\tau d\tau. \quad (224)$$

Recall that

$$k_H(E,\tau) = k_m(E,\tau), \quad \tau>150 \text{ ev} \quad \text{and} \quad E>2 \text{ Kev} \quad (141)a$$

$$k_H(E,\tau) = \frac{\kappa(E)}{(a\tau + b)^2}, \quad \delta_1<\tau<150 \text{ ev} \quad \text{and} \quad E>0 \quad (141)b$$

$$k_H(E,\tau) = AKT\ k_{ex}(\tau), \quad 0<\tau<\delta_1 \quad \text{and} \quad E>0 \quad (141)c$$

in which a and b are given by A and B in this subprogram and C is defined in section 2.2.

```
MON$$      EXEQ FORTRAN
  FUNCTION AINGS(T,DELTA1,TAU)
  E=T
  IF(TAU.GE.T/2.)TAU=T/2.
  IF(E.LT..1)A=1.29*E**(-ALOG(1.88/1.29)/ALOG(10000.))
  IF(E.LT..1)GO TO 16
  IF(E.LT..32)A=1.1*E**(-ALOG(1.4/1.1)/ALOG(10.))
  IF(E.LT..32)GO TO 16
  IF(E.LT.1.)A=.94*E**(-ALOG(1.7/.94)/ALOG(10.))
  IF(E.LT.1.)GO TO 16
  A=.94*E**(-ALOG(.94/.335)/ALOG(10.))
16 CONTINUE
  IF(E.LT..2)B=-.35*10.**(-4)
  IF(E.LT..2)GO TO 17
  IF(E.LT.1.)B=-.255*10.**(-4)*E**(-ALOG(.398/.255)/ALOG(10.))
  IF(E.LT.1.)GO TO 17
  B=-.255*10.**(-4)*E**(-ALOG(.255/.1)/ALOG(10.))
17 CONTINUE
  C=.15*.5555
  TAPPA=2.*C/T
  AINGS=TAPPA/(A*A)*(B/(A*TAU+B)-B/(A*DELTA1+B)+ALOG((A*TAU+B)/
 1(A*DELTA1+B)))
  RETURN
  END
```

6.8.8 Explanation of FUNCTION PROBT(T,TAU)

The FUNCTION statement "PROBT(T,TAU)" evaluated the Moller formula, explicitly:

$$\mathrm{PROBT(T,TAU)} = k_m(T,\tau). \tag{225}$$

```
MON$$      EXEQ FORTRAN
      FUNCTION PROBT(T,TAU)
      COMMON WTAB(100),WATES(100),DEL,BETA,COF,AKT,DELTA1,DELTA2
      TERM=TAU**(-2)+(T-TAU)**(-2)-((2.+T**(-1))/((T+1.)**2))*(TAU**(-
     1)+(T-TAU)**(-1))+(T+1.)**(-2)
      PROBT=COF*TERM
   61 RETURN
      END
```

6.8.9 Explanation of FUNCTION AMOLIN(T,DELTA)

The FUNCTION statement AMOLIN(T,DELTA) evaluated the following integral:

$$\mathrm{AMOLIN(T,DELTA)} = \int_{\overline{Q}}^{\mathrm{DELTA}} \tau d\tau k_m(T,\tau). \tag{226}$$

```
MON$$      EXEC FORTRAN
 FUNCTION AMOLIN(T,DELTA)
 COMMON WTAB(100),WATES(100),DEL,BETA,COF,AKT,DELTA1,DELTA2,QB
 ZI=.000651/.51097
 QB=ZI*ZI*EXP(BETA*BETA)/(T*(T+2.))*.5
 CTERM=(2.+1./T)/((T+1.)*(T+1.))
 DTERM=1./((T+1.)*(T+1.))
 FTERM=ALOG(DELTA/QB)+T*(1./(T-DELTA)-1./(T-QB))+ALOG((T-DELTA)/
1(T-QB))*(1.+CTERM*T)+DTERM*(DELTA*DELTA-QB*QB)/2.
 AMOLIN=COF*FTERM
 RETURN
 END
```

6.8.10 Explanation of FUNCTION AINEX(DELTA)

This FUNCTION may be represented by

$$AINEX(DELTA) = \int_0^{DELTA} k_{ex}(\tau)\tau d\tau \qquad (227)$$

in which the inelastic collisions cross section data were given by FUNCTION SMALL(TAU).

```
MON1$      EXEQ FORTRAN
      FUNCTION AINEX(DELTA)
      COMMON WTAB(100),WATES(100),DEL,BLTA,COF,AKT,DELTA1,DELTA2
      NWT=50
      AINC=DELTA/FLOAT(NWT-1)
      DO 21 J=1,NWT
      AJ=J-1
   21 WTAB(J)=AINC*AJ
      IWT=1
      CALL RATES(IWT,NWT)
      SUM=.0
      DO 22 K=1,NWT
      XBY=SMALL(WTAB(K))
      TERM=XBY*WATES(K)*WTAB(K)
   22 SUM=SUM+TERM
      AINEX=SUM
      RETURN
      END
```

6.8.11 Explanation of FUNCTION SPRS(E,DELTA2)

This subprogram only called FUNCTION AINEXD(T,BLIMIT,TAU) and FUNCTION AINGS(T,DELTA1,TAU) for the appropriate arguments.

```
KON19       EXEC FORTRAN
      FUNCTION SPRS(E,DELTA2)
      IF(DELTA2.GE.E/2.)DELTA2=E/2.
      DELTA1=21.*10.**(-6)/.51097
      IF(DELTA1.GE.DELTA2)SPRS=AINEXD(E,.0,DELTA2)
      IF(DELTA1.LT.DELTA2)SPRS=AINEXD(E,.0,DELTA1)+AINGS(E,DELTA1,DEL
     1)
   14 RETURN
      END
```

EFFECTS OF RADIATION QUALITY
ON THE RADIOLYSIS OF WATER

by

LAURENCE FREDERICK MILLER

B. S., Kansas State University, 1964

AN ABSTRACT OF
A MASTER'S THESIS

submitted in partial fulfillment of the

requirements for the degree

MASTER OF SCIENCE

Department of Nuclear Engineering

KANSAS STATE UNIVERSITY
Manhattan, Kansas

1966

ABSTRACT

The objective of this work was the theoretical investigation of certain problems associated with the prediction of chemical reaction rates and yields of radiation-induced chemical reactions. All the problems considered were related to the assessment of the effects of radiation quality, that is, the effects of the energy and type of radiation. Particular emphasis was given to the determination of the energy spectra of electrons resulting from the irradiation of water by 14.6 Mev neutrons and by gamma rays of cobalt-60.

Slowing-down spectra for charged particles produced in radiolysis were computed. These spectra were used as a basis for models for the "spur" and "track" structure in irradiated water. Also involved in the establishment of the models were predictions of mean energy loss per spur and mean distance between spurs. These predictions, in turn, were based on empirical estimates of electron-scattering cross sections for low energy electrons and for small energy losses. Estimates of the yields of chemical reactions were based on approximate solutions of the partial differential equations describing simultaneous diffusion and chemical reaction along the tracks of charged particles. Yields were predicted for a simple chemical reaction and compared with experimental results taken from the literature.